Synthesis of monodisperse silver nanoparticles for antibacterial purposes

submitted by

Sarah Adam

In partial fulfilment of the requirements for the degree of

Master of Science in Engineering

Centre for Catalysis Research

c*change DST-NRF Centre of Excellence in Catalysis

Department of Chemical Engineering

University of Cape Town

Supervisor:

Professor Patricia Kooyman

Co-supervisors:

Dr Mariette Smart

Professor Sue Harrison

March 2018

“The universe is under no obligation to make sense to you.”

- Neil deGrasse Tyson

Declaration

I, Sarah Lynn Adam, know the meaning of plagiarism and declare that all the work herein is my own, except for what has been obtained from literature sources. All sources have been properly acknowledged and referenced.

Signed: Signed by candidate Date: 28 March 2018

Sarah Lynn Adam

Acknowledgements

The journey towards attaining a master's degree has been an unparalleled, extremely challenging but incredible rewarding, learning experience. It is also a journey that would not have been successful without a significant amount of help, advice and support from a numerous people, for which I am deeply grateful.

First and foremost, I am very thankful for the support my supervisor, Prof. Patricia Kooyman, provided. She allowed me to pursue my own research interests and, despite knowing that it would be a very difficult task to undertake, had complete faith in me and never once limited my thinking (although she gently steered me towards being realistic). I am grateful for the knowledge she imparted, the encouragement and support that she provided, the time she gave, and the enthusiasm with which she addressed every task.

I am indebted to Dr Mariette Smart for all her help (and patience) in the lab. I am immensely appreciative of the time and effort she invested in this research, the ideas that she contributed, and the role she played in completing this study. Thank you also to Prof. Sue Harrison who allowed me to make a temporary home in the CeBER group and to make use of the bioprocessing facilities.

I am thankful to Manju Bhamidipati at Delft University of Technology in The Netherlands who, in a collaboration forged by Prof. Andreas Schmidt-Ott and Prof. Patricia Kooyman, deposited silver nanoparticles on fibre filters for the antibacterial efficacy studies that were performed in this work.

My research group, the c*change DST-NRF Centre of Excellence in Catalysis hosted by the Centre for Catalysis Research, provided vital suggestions and asked thought-provoking questions that greatly assisted in the progress of this study. In this regard, I would particularly like to thank Prof. Michael Claeys, Assoc. Prof. Nico Fischer and Dr Jezreel Cloete. Thanks are also owed to Prof. Eric van Steen and Prof. Anja Olafsen Sjåstad who advised me on optimising the silver nanoparticle synthesis, and particularly the latter for the suggestion of pursuing a 'hot' injection method which proved invaluable.

For assistance in the Electron Microscope Unit, Mr Mohammed Jaffer, Dr Innocent Shuro and Mrs Miranda Waldron deserve a big thank you. Thank you also to Ms Ameerah Van Der Fort, Mr Lawrence Taderera, Mr Argon Poorun and Mr Heaven Nemaungane for their contributions towards SEM and TEM image analysis.

I gratefully acknowledge that this work was supported by the SARCHI Chair of Nanomaterials for Catalysis, National Research Foundation grant number 94878 and the c*change DST-NRF Centre of Excellence in Catalysis.

I am fortunate enough to have a very strong support system beyond the academic sphere and there are countless people to whom immeasurable gratitude is owed for their endless support and encouragement throughout this process, particularly Erin, Nicky and Alastair. I would not be where I am today without the kind words, the gentle pushes and the numerous distractions that were provided along the way.

Finally, and most importantly, my family has been indispensable in this journey. Thank you to James for always being willing to be a little ridiculous when I got too serious and for lending an ear whenever I needed it. Thank you to my dad for providing level-headed advice and for the constant care. Thank you to my mom for being my go-to person when things got tough and for teaching me to be kind to myself. I will never be able to fully express how much I value and appreciate their unwavering support.

Thank you.

Abstract

Safe drinking water is a scarcity for many in the developing world. Currently, 884 million people, 48% of whom live in sub-Saharan Africa, are without access to even basic drinking-water services (WHO/UNICEF Joint Monitoring Programme for Water Supply and Sanitation, 2017). This has a severe impact on the health of those living in such communities, which is why the universal access to safe and affordable drinking water has been made a priority by the United Nations. There is an undeniable need for change so that the lives of these many millions of people may be improved.

Silver nanoparticles have great potential in being used in water disinfection applications because of their high antibacterial activity and broad antimicrobial spectrum (Qu, Alvarez, & Li, 2013). Development in this area is critical, particularly in advancing technology to allow greater accessibility to clean drinking water for people in poor, rural areas in developing countries. Incorporating nanotechnology into current water disinfection systems, as well as developing new water treatment nanotechnology, shows promise in addressing this issue. However, much research needs to be done first before this can become a reality (Q. Li *et al*., 2008). There is particular concern about the toxicity aspects of silver nanoparticles, both in humans and towards the environment. Whilst the current study does not investigate their toxicity, it is important to highlight the need to fully understand the human and environmental impacts nanoparticles may have in assessing their applicability in microbial control.

Literature indicates that, although the role of silver nanoparticles themselves in the antibacterial mechanism cannot be excluded entirely, it is the silver ions that are mostly responsible for their antibacterial activity (Foldbjerg, Jiang, Miclăuş, et al., 2015; Le Ouay & Stellacci, 2015; Panacek et al., 2006; Xiu, Zhang, Puppala, Colvin, & Alvarez, 2012). Sotiriou & Pratsinis (2010) found that silver nanoparticles of smaller than 10 nm had a negligible antibacterial effect in comparison to the ions they released. Thus, to isolate just the effect of the released silver ions, it was desired to prepare uniformly sized particles of smaller than 10 nm. Controlling the size of the formed particles requires consideration of parameters that affect their nucleation and growth (Thanh *et al*., 2014). These can be thermodynamic, kinetic or stoichiometric parameters. It is on this basis that the work described herein was developed.

This study aimed to synthesise silver nanoparticles suitable for use in water disinfection applications by exploring how preparation conditions affect the particle size and distribution. To do this, two different aqueous chemical reduction preparation methods were performed and reaction conditions such as surfactant concentration, agitation rate, synthesis temperature, and method of chemical addition were varied to produce monodisperse silver nanoparticles with an average size of smaller than 10 nm. This study also aimed to investigate the antibacterial efficacy of silver nanoparticles deposited on quartz fibre filters against *E. coli*.

Two silver nanoparticle syntheses procedures were extensively investigated. Method One (AL-Thabaiti et al, 2008) uses ascorbic acid as the reducing agent and SDS (sodium dodecyl sulphate) as the surfactant whilst Method Two (Yang, Yin, Jia, & Wei, 2011) uses aniline as the reducing agent, DBSA (dodecylbenzenesulfonic acid) as the surfactant and NaOH (sodium hydroxide) as the ‘activating’ chemical. The surfactant concentrations, agitation rates, synthesis temperature, reducing agent

concentrations and methods of chemical addition were varied for each of these synthesis procedures and the effect thereof on particle size was investigated. Both synthesis methods produced fcc metallic silver nanoparticles with (111) and (200) lattice planes, confirmed by studying nanoparticle d-spacings. For Method One, the unaltered synthesis procedure produced the smallest particles with a number-based mean size of 3.6 ± 3.8 nm and a volume-based mean particle size of 15.4 ± 6.4 nm. For Method Two, which is performed at 90 °C, the 'hot' injection of NaOH into the system resulted in the production of the smallest nanoparticles with a number-based mean particle size of 6.7 ± 5.4 nm and a volume-based mean particle size of 22.3 ± 10.9. Removing excess surfactant and collecting these nanoparticles in powder form would facilitate antibacterial efficacy studies, however this proved to be difficult. Additionally, the presence of large nanoparticles in both samples, as evidenced from the volume-based size distributions, means that in assessing antibacterial activity of the nanoparticles, it will be difficult to interpret whether the bactericidal effect is due to silver ions or because of an interaction between the bacteria and the actual nanoparticles. Antibacterial efficacy studies were therefore not performed on these synthesised silver nanoparticles.

Silver nanoparticles deposited on quartz fibre filters via spark ablation were prepared at Delft University of Technology. SEM revealed that the deposited nanoparticles on the filters had a mean particle size ranging from 25 to 70 nm. Studies using *E. coli* (ATCC® 25922™) did not conclusively demonstrate antibacterial activity of the filters. It is believed the large particle size, and thus slow dissolution into silver ions, may be the reason for the lack of evidence of bactericidal activity over the 24-hour experimental period.

The results of this study indicate how small changes in synthesis parameters can have a significant effect on nanoparticle size and uniformity, morphology, and degree of agglomeration. This reveals the importance in specifying exact parameters used in nanoparticle preparation to allow for better reproducibility, including vessel size, mixing speed, and rate of chemical addition. This work also showed that it is important to quantify the release of silver ions from silver nanoparticles *before* performing antibacterial efficacy assessments. Since silver ions are the most important factor in the antibacterial action of silver nanoparticles, understanding their rate of release will allow for improved experimental design thus producing useful results. There is great potential for the use of silver nanoparticles for disinfection, as evidenced particularly by the antibacterial efficiency of Ag^+ against *E. coli* (ATCC® 25922™). However, improvements in both the synthesis of silver nanoparticles and methods of assessing their bactericidal efficacy are clearly necessary.

This study has highlighted the challenges that may be faced in the pursuit of efficiently and safely using silver nanoparticles for water treatment and disinfection. Numerous recommendations for future studies have been put forward. These include: further optimisation of the nanoparticle synthesis procedure so as to produce particles of the desired size and acquire them in powder form, performing a thermodynamic estimation of the equilibrium silver ion concentration as a function of silver nanoparticle size to quantify the effect nanoparticle size will have on bactericidal activity, and using more realistic water conditions for antibacterial efficacy experiments to simulate the environment in which silver nanoparticles will be applied.

Table of contents

List of tables

List of figures

Nomenclature

Abbreviations

Ag NPs – silver nanoparticles

BSE – backscattered electrons

CPC – condensation particle counter

CT – contact time

CVD – chemical vapour deposition

DAA – DBSA-aniline-$AgNO_3$ aqueous system

DBP – disinfection by-product

DBSA – dodecylbenzenesulfonic acid

DI – deionised

DMA – differential mobility analyser

fcc – face-centred cubic

FDA – fluorescein diacetate

FEG – field emission gun

FSP – flame spray pyrolysis

FWHM – full width at half maximum

ICP-OES – inductively coupled plasma optical emission spectroscopy

ISE – ion selective electrode

LB – lysogeny broth

MBC – minimum bactericidal concentration

MIC – minimum inhibitory concentration

MOPS – 4-morpholonepropanesulfonic acid

NOAEL – no observable adverse effect level

NOM – natural organic matter

NP – nanoparticle

PBS – phosphate buffered saline

PSD – particle size distribution

ROI – region of interest

SDG – sustainable development goal

SDS – sodium dodecyl sulphate

SE – secondary electrons

SEM – scanning electron microscope/microscopy

SMPS – scanning mobility particle sizer

SPR – surface plasmon resonance

TEM – transmission electron microscope/microscopy

TNTC – too numerous to count

UV – ultraviolet

UV-Vis – ultraviolet visible spectroscopy

XRD – x-ray diffraction

Chemical formulae

Ag – silver

$AgNO_3$ – silver nitrate

CdSe – cadmium selenide

Cu – copper

CuO – copper oxide

Fe_2O_3 – iron (III) oxide

H_2O_2 – hydrogen peroxide

KCl – potassium chloride

KH_2PO_4 – potassium phosphate

Na_2HPO_4 – disodium phosphate

NaCl – sodium chloride (salt)

NaOH – sodium hydroxide

SiO_2 – silica

TiO_2 – titanium dioxide

ZnO – zinc oxide

Chapter 1: Introduction

Potable water is a scarce resource for many in the developing world. Currently, 884 million people, 48% of whom live in sub-Saharan Africa, are without access to even a basic drinking-water service (WHO/UNICEF Joint Monitoring Programme for Water Supply and Sanitation, 2017). As a result, these communities face the risk of water-borne diseases, malnutrition and higher child mortality rates (UNICEF & World Health Organisation, 2015). Preventable diarrhoeal diseases, mainly caused by poor water quality and sanitation, are still the second leading cause of death among children under the age of five (Centers for Disease Control and Prevention, 2013). According to the WHO/UNICEF Joint Monitoring Programme for Water Supply and Sanitation (2017), a child dies every 90 seconds from a water-related disease. Furthermore, in low- and middle-income countries, a third of the healthcare facilities lack a safe water source. It is little wonder that one of the Sustainable Development Goals of the United Nations is to achieve universal access to safe and affordable drinking water for all (United Nations, 2016). There is an undeniable need for change so that the lives of these many millions of people may be improved.

Nanomaterials that can be used for small-scale, community-based water purification purposes provide a real solution to this severe problem. Some conventional chemical disinfection methods are known to form harmful by-products, many of which are carcinogenic (Q. Li *et al*., 2008). Additionally, most of the communities affected by a lack of potable water are in rural areas in poor, developing countries where there is little infrastructure available to address this issue. Using nanomaterials for the disinfection of water is an attractive option since this overcomes many of the drawbacks of traditional methods of water treatment, including allowing for a more decentralised treatment system i.e. a. point-of-use system (Liu, Tang, & Liu, 2014). Additionally, antibacterial nanomaterials have received much attention in the medical field recently due to the development of bacterial resistance to antibiotics. Nanomaterials are advantageous in applications such as water treatment because of their small size and large specific surface area, which aids surface interactions, and because their properties (physical, chemical and mechanical) can be adjusted by controlling their shape, size, surface and structure (R. Li, Zhang, & Wang, 2015).

One of the most commonly used antibacterial nanomaterials is silver because of its high bactericidal activity and broad antibacterial spectrum (Q. Li *et al*., 2008; Qu *et al*., 2013). These properties make nanosilver a promising and effective material for disinfection and microbial control. Silver nanoparticles have been used in medical supplies and devices and in consumer products available to the public (Tran, Nguyen, & Le, 2013; Prabhu & Poulose, 2012). For these reasons, there has been significant interest in silver with a particular focus on the material's antibacterial efficacy and toxicology (Foldbjerg, Jiang, Chen, Autrup, & Beer, 2015). There has also been much debate (and numerous contradictory studies have been published) regarding the antibacterial mechanism of silver nanoparticles, however, most of the evidence indicates that silver ions account for part of the toxicity (Foldbjerg, Jiang, Chen, Autrup, & Beer, 2015). Surprisingly, despite the increasing number of products and applications silver nanoparticles are being used in, there is still a lack of scientific understanding of the effects it may have on human health (Vrček et al., 2016). It is, therefore, critical that an understanding the cellular responses to silver ions and nanoparticles be developed.

Performing in-depth literature searches revealed that there is a lack of coherent information and systematic study in the field of nanotoxicology. This is true of nanoparticles, such as silver, that are used particularly for antibacterial purposes and of nanoparticles being used for other purposes that run the risk of being emitted into the environment. An editorial published in Nature Nanotechnology in 2012 highlighted this issue, suggesting that guidelines on the information required in research articles be put in place in an effort to "improve the quality and relevance of published papers" (Nature Nanotechnology, 2012). The overriding complaint in the editorial was that there are few studies that provide consistent and valuable data and that comparison of studies is difficult because inadequately characterised materials and arbitrary, ill-explained experimental conditions have been used (Nature Nanotechnology, 2012).

Because of the haphazard nature of the investigations into antibacterial nanomaterials and the difficulty in comparison of tested materials owing to the lack of relevant and valuable information, a more fundamental study on the synthesis of silver nanoparticles within a certain particle size distribution, for the purpose of use in antibacterial applications, will be performed. Two silver nanoparticle syntheses methods, both aqueous chemical reduction processes, will be extensively investigated by varying the surfactant concentrations and preparation conditions so as to obtain stable particles of the smallest achievable size. This study aims to synthesise monodisperse silver nanoparticles with an average particle size of less than 10 nm, thus making them suitable for antibacterial applications. The antibacterial efficacy of nanoparticles deposited on quartz fibre filters via spark ablation will be studied and compared to that of silver ions.

Chapter 2: Literature review

2.1 Antibacterial nanomaterials

In the face of rapid growth in the nanotechnology field, there has been significant interest in the environmental applications of nanomaterials, particularly in water treatment processes (Q. Li *et al*, 2008). Using nanomaterials as a method for water disinfection is advantageous in a number of ways. Intensive use of antibiotics has led to the development of bacterial resistance to antibacterial drugs, and antibacterial nanomaterials provide a good alternative option as such resistance in bacteria has not yet developed (Azócar *et al*., 2016; Dizaj *et al*., 2014; Hajipour *et al*., 2012). Additionally, it has been found that chemical disinfectants commonly used for water treatment, for example free chlorine, chloroamines and ozone, can result in the production of toxic disinfection by-products (DBPs), many of which are carcinogenic (Q. Li *et al*., 2008; Qu *et al*., 2013). Furthermore, morphology and physiochemical characteristics of bactericidal nanoparticles have an effect on their antibacterial activity (Dizaj, Lotfipour, Barzegar-Jalali, Zarrintan, & Adibkia, 2014). The shapes, size, surface and structure of nanoparticles can be controlled fairly easily, thus the physical and chemical properties that impact the antibacterial action of the particles can be adjusted (R. Li, Zhang, & Wang, 2015). Many nanomaterials, including silver nanoparticles, titanium dioxide, zinc oxide, copper, gold, silicon, magnesium oxide, calcium oxide and chitosan (obtained from arthropod shells), have been found to have antibacterial properties (Dizaj *et al*., 2014; Hajipour *et al*., 2012; Q. Li *et al*., 2008; Moritz & Geszke-Moritz, 2013; Qu *et al*., 2013). With regards to antibacterial nanomaterials, the focus in this literature review is on silver nanoparticles because they are the subject of this study. However, a brief introduction to copper as an antibacterial material is also given in this section because of its relevance to this investigation.

2.1.1 Antibacterial mechanisms

Numerous mechanisms for the interaction of bacteria with nanoparticles have been proposed but are still being investigated. Understanding the method of bacterial deactivation is important not only for the synthesis of nanoparticles for specific antibacterial purposes, but also to understand the potential impact such nanoparticles might have on both human and environmental health. The properties of bacteria, and therefore the way to kill them, are highly specific to the bacterial strain (Hajipour *et al*., 2012).

The bacterial cell wall provides strength and shape to the cell and protects it from physical damage (Hajipour *et al*., 2012). Bacteria can be divided into two broad categories based on the cell wall function and structure – Gram-negative and Gram-positive. The different cell wall structures of these bacteria types can be seen in Figure 2-1. The Gram-positive cell wall comprises a thick layer of peptidoglycan attached to teichoic acids, which are specific to Gram-positive bacteria (Hajipour *et al*, 2012; Harvey, Cornelissen, & Fisher, 2007). The Gram-negative cell wall is more complex and contains an outer membrane which covers the surface membrane. This outer membrane contains lipopolysaccharides which make the cell wall negatively charged and are necessary for the bacteria's structural integrity (Salton & Kim, 1996). Additionally, the peptidoglycan layer on Gram-negative bacteria is thinner than that of Gram-positive bacteria, making the cell more susceptible to physical damage (Harvey, Cornelissen, & Fisher, 2007).

Bacterial growth rate is another factor that has been found to influence the tolerance of bacteria to nanoparticles. Fast-growing bacteria are more susceptible to antibacterial nanoparticles and antibiotics than are slow-growing bacteria, possibly due to production of stress-response genes by the slow-growing bacteria (Hajipour *et al*, 2012). Additionally, antibiotics and antibacterial nanoparticles are less effective against bacteria which produce biofilms that protect the bacteria against attack (Hajipour *et al*, 2012). The interaction between biofilm and nanoparticles is influenced by the electrostatic properties of both materials. Because the antibacterial efficacy of nanoparticles is highly dependent on the specific bacterial strain, it is important to assess the bactericidal activity of these nanoparticles against a wide range of bacteria strains.

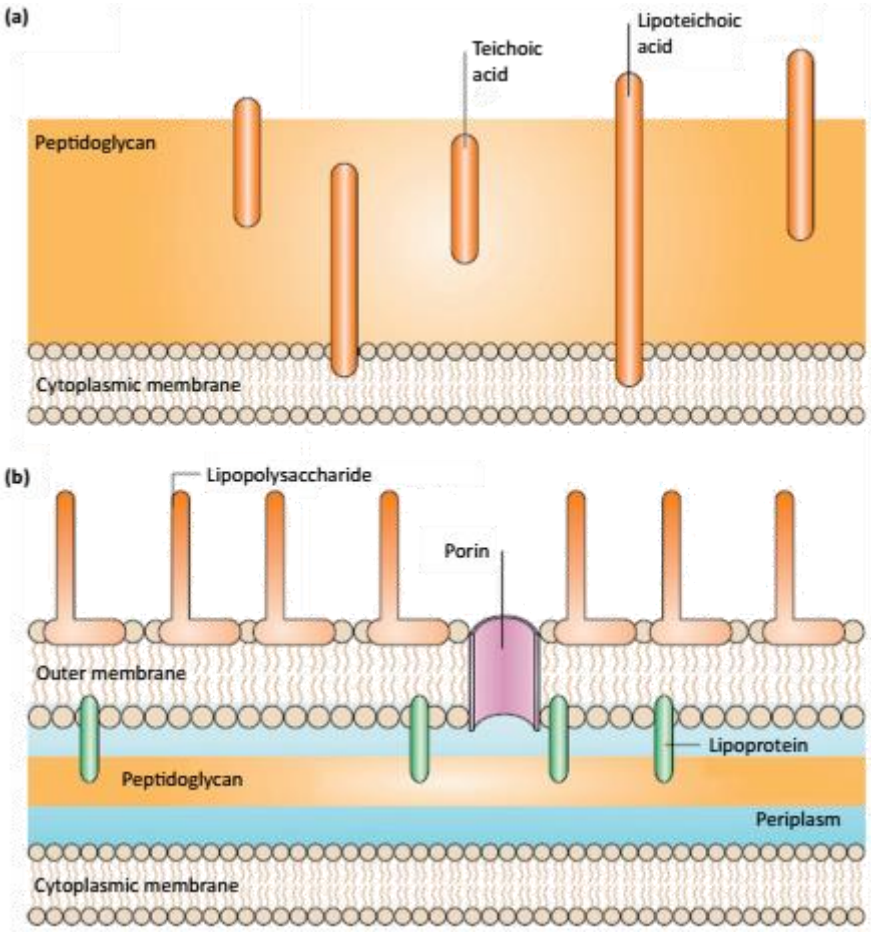

Figure 2-1: Cell wall structure of (a) Gram-positive and (b) Gram-negative bacteria. Reprinted, with permission, from Hajipour et al. (2012).

As mentioned, various antibacterial mechanisms have been suggested for different nanomaterials, however the exact mechanisms are not yet understood. Figure 2-2 shows several of these proposed mechanisms.

The nanoparticles either directly interact with the cell or produce secondary products that lead to cell damage. Proposed mechanisms involving cell wall interactions include positively charged materials (e.g. ions) attaching themselves to the negatively charged cell walls thereby causing increased membrane permeability, disruption of electron transport, and ultimately resulting in cell lysis (Cui *et al*., 2012; Dizaj *et al*., 2014; Q. Li *et al*., 2008; Marambio-Jones & Hoek, 2010; Ren *et al*., 2009). Suggested mechanisms

involving internal cell structures include antimicrobial action affecting respiratory enzymes and proteins and damage of cell DNA leading to its inability to replicate or repair itself (Mauter & Elimelech, 2008; Moritz & Geszke-Moritz, 2013; Pissuwan *et al*., 2010). It is also proposed that some of these nanomaterials catalyse the production of reactive oxygen species (ROS), including hydroxyl free radicals and hydrogen peroxide, that damage and kill bacteria (Azócar *et al*., 2016; Dizaj *et al*., 2014; Q. Li *et al*., 2008; Moritz & Geszke-Moritz, 2013; Qu *et al*., 2013). Additionally, it is known that heavy metal ions can damage bacterial cell walls (Ruparelia, Chatterjee, Duttagupta, & Mukherji, 2008).

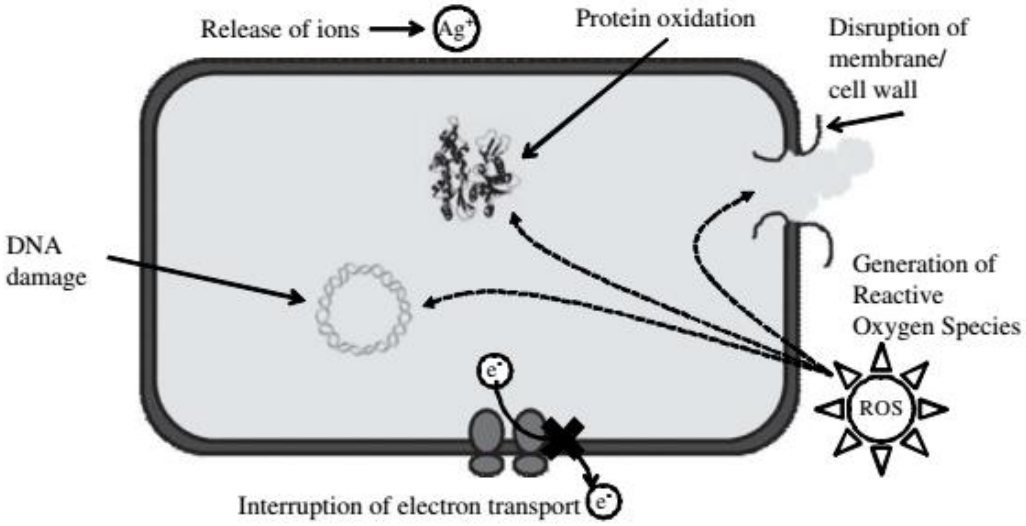

Figure 2-2: Antibacterial mechanisms of nanomaterials. Reprinted, with permission, from Q. Li et al. (2008)

2.1.2 Efficacy of antibacterial nanomaterials

In their review article on the antibacterial properties of nanoparticles, Hajipour *et al*. (2012) commented on the correlation of data on the antibacterial activity of nanoparticles reported in literature. The authors mention that, in performing experiments to test nanoparticles for bactericidal activity, many researchers select readily available nanoparticles and bacteria rather than targeting specific, desired nanoparticles or bacteria. Additionally, correlation of data is often difficult because nanoparticles in antibacterial studies are frequently not well characterised. Hajipour *et al*. (2012) suggest that, to systematically unravel the antibacterial properties of nanoparticles and the efficacy thereof, agreement on standard nanoparticles and bacteria as reference systems should be made. This position was echoed in an editorial published in Nature Nanotechnology (2012) which stated that there are not many studies offering consistent and valuable results and that comparison of studies is difficult because they are often performed using inadequately characterised nanomaterials and arbitrary experimental conditions. The publishers of the journal believe that materials characterisation should be performed based on relevance to the study, but several common parameters should be provided in all articles. These possible parameters include but are not limited to: particle size and distribution, composition, degree of aggregation or agglomeration under experimental conditions, morphology, surface area, and surface reactivity. Naturally, there are different opinions with regards to such a list but, for there to be progress in the field, some agreement must be reached (Nature Nanotechnology, 2012). It is necessary to define both the nanomaterial and the environment it is present in.

Despite this dialogue on the implementation of guidelines on the types of information required in nanotoxicology research articles "to improve the quality and relevance of published papers", little progress in this regard seems to have been made. Performing a literature search for this study showed that investigation into the antibacterial efficacy of nanomaterials has been haphazardly performed. Countless studies on the bactericidal nanoparticles have been undertaken, however there appears to be little evidence of a systematic approach.

For example, in an article that compared the antimicrobial activity of zinc oxide (ZnO), copper oxide (CuO) and iron (III) oxide (Fe_2O_3) it was concluded that ZnO has a higher bactericidal activity than CuO, which in turn has a higher bactericidal activity than Fe_2O_3 (Azam *et al.*, 2012). However, the particles produced for the study were of different sizes (with Fe_2O_3 > CuO > ZnO), which allowed for both size and nanomaterial variation to affect the experimental outcome. It is known that the antibacterial activity of nanoparticles is often related to their size, thus such a conclusion could not be definitively drawn. In other comparative studies of antibacterial nanomaterials, similar errors were made. To improve these studies, nanoparticles of the same sizes should be studied to allow for better comparison. Studying particles of the same size would mean a similar rate of dissolution would be observed, which means the comparison would truly be between the antibacterial efficacy of different materials (and not a combination of the material efficacy *and* the rate of ion release).

It was hoped that an application-based study, such as investigating surfaces coated with silver nanoparticles, could be undertaken. However, this did not prove feasible because of the lack of relevant and valuable information available. It is for this reason that a more fundamental study of the antibacterial action of silver nanoparticles will be performed.

2.1.3 Copper as an antibacterial material

Copper has been registered at the United States Environmental Protection Agency as the first solid antibacterial material (Grass, Rensing, & Solioz, 2014). Knowledge of the antibacterial capabilities of copper dates back to more than 2000 BC. In more recent history, it has been evaluated for use as a self-cleaning surface, particularly relevant in hospitals to limit the transfer of infections (Grass, Rensing, & Solioz, 2014). Bacteria and viruses that come into contact with metallic copper surfaces are rapidly killed, hence the term "contact killing" was coined (Grass, Rensing, & Solioz, 2014). Both copper and copper oxide (CuO) nanoparticles are effective in killing Gram-positive and Gram-negative bacteria (Ren et al., 2009; Ruparelia et al., 2008). However, the surface of Cu nanoparticles is rapidly oxidised in air and this limits their usage (Dizaj et al., 2014). Again, the antibacterial mechanism of copper oxide is still being investigated. One suggested mechanism is that the nanoparticles pass through the cell membrane and cause damage to the enzymes within the bacteria, causing cell death (Dizaj et al., 2014).

Experimental results in a study performed by Ren et al. (2009) indicated that CuO nanoparticles in suspension are active against a range of bacterial pathogens. The authors also found that, based on the minimum bactericidal concentration (MBC), CuO is more toxic to the bacteria tested than ZnO but less effective than nano Ag and nano Cu.

2.2 Using nanomaterials for water disinfection

It is predicted that antibacterial nanomaterials will, in the future, be used to address three major challenges in water and wastewater systems: disinfection, control of membrane biofouling and control of biofilms on surfaces such as pipes (Qu, Alvarez, & Li, 2013). Silver is currently one of the most widely used antimicrobial nanomaterials and already has applications in commercial home water purification

systems (Q. Li *et al*., 2008). The relative effectiveness of some antibacterial agents, including conventional disinfection chemicals, is presented in Table 2-1 (Q. Li *et al*., 2008). This review paper by Q. Li *et al*. (2008) is one of the few studies that have been found in the literature to compare the efficacy of traditional water disinfection methods to less common methods, such as using silver ions or TiO_2 nanoparticles. In Equation 2-1, *C* refers to the disinfectant concentration in mg/L and *T* refers to the contact time, in minutes, required to kill of 99% of an *E. coli* colony with a concentration of 10^6 cells/ml (Khan, 2005).

$$CT\ (mg.min.L^{-1}) = disinfectant\ concentration\ (mg.L^{-1}) \times contact\ time\ (mins) \qquad \textit{Equation 2-1}$$

Table 2-1: Relative effectiveness of various antimicrobial agents. Sourced from Q. Li et al. (2008).

Antibacterial agent	*CT*[1] *(mg.min/L or mJ/cm²)*
Chloroamine	95 – 180
Free chlorine	0.03 – 0.05
Ozone	0.0007 – 0.02
Chitosan	7.5 – 144
Fullerene (nC_{60})	100
Silver ions	0.075 – 26

Table 2-2: Relative effectiveness of UV as an antimicrobial agent. Sourced from Q. Li et al. (2008).

Antibacterial agent	*CT (mJ/cm²)*
UV-C (254 nm)	3.8 – 4.8
UV-A (300 – 400 nm)	16 000 – 20 000
TiO_2 (slurry) + UV (300 – 400 nm)	700 – 5000
TiO_2 (thin film) + UV (300 – 400 nm)	3600 – 8500
H_2O_2 + UV (315 – 400 nm)	66 – 89

The data shown in Table 2-1 are limited because the characteristics of the nanoparticles used in the study are not provided, however it does give some indication as to the bactericidal activity of some potential disinfection agents. Based on the comparison of the antibacterial efficacy of some common nanomaterials (TiO_2, chitosan, fullerene and Ag^+ which is released from Ag nanoparticles) to conventional chemical disinfectants (chloroamine, free chlorine, ozone) presented in Table 2-1, it can be said that there is great potential for nanomaterials to be used as water disinfectants. The similar or superior antibacterial activities mean these nanomaterials can be used to replace some chemical disinfectants or in conjunction with currently used technologies (such as UV treatment to which TiO_2 is well suited because of its photoactivity, as is seen by the data in Table 2-2) to enhance the antibacterial efficacy of the systems (Q. Li *et al*., 2008). Suggested ways in which nanomaterials may be used in water disinfection applications include surface coatings, filters and membranes.

As previously stated, DBP (disinfection by-products), many of which are considered possible carcinogens and mutagens, may be formed when using chlorine, chloroamines, chlorine dioxide and

[1] CT values are for 99% disinfection of *E. coli*. Units for CT values of all UV applications are mJ/cm^2 which is an expression of light energy

ozone to disinfect water (Hossain, Perales-Perez, Hwang, & Román, 2014). The formation of these DBPs is difficult to control and results from the reaction between natural organic matter and strongly oxidising disinfectants (Hossain *et al*., 2014). This has become more of a problem as the disinfection time and disinfectant concentration required to inactivate microbes in water increases (Hossain *et al*., 2014). Nanomaterials, in this instance, provide a distinct advantage as they have not yet been found to produce such DBPs. It is, however, necessary to highlight some of the potential limitations of using nanoparticles in water disinfection.

2.3 Limitations of nanomaterials for water treatment

There are still knowledge gaps in the technical and safety aspects of using nanomaterials in water treatment (Hossain *et al*., 2014). Rigorous, long-term research into this technology is necessary before nanomaterials can be used in applications for water disinfection.

2.3.1 Retention of nanomaterials

The application of nanomaterials in water treatment is not without its challenges. The retention of nanomaterials is of two-fold concern: first, losing nanoparticles from the treatment system has cost implications and second, the possible effects on human health and ecosystems (Q. Li *et al*., 2008). Additionally, there is the problem of maintaining long-term efficacy of antibacterial nanomaterials, especially those which rely on the release of ions as these will eventually be depleted (Qu, Alvarez, & Li, 2013). According to Li *et al*. (2008), there is still much critical research that needs to be conducted before nanotechnology can be used for water disinfection on a larger scale than current applications. The key area that the researchers identified requires improvement is treatment technologies that can better retain the nanoparticles; this could include improving surface coatings, impregnating nanoparticles into other materials and minimising the fouling on filtration membranes by using nanoparticle suspensions.

2.3.2 Cost of nanotechnology

Economic analyses would need to be conducted in order to compare the cost of nanotechnology systems with conventional water treatment technologies. This is particularly pertinent in poor, developing counties where the problem of contaminated water is most prevalent. Currently, the cost of antibacterial nanomaterials, with the exception of materials such as nano-TiO_2 and nanoscale iron oxide, is rather high (Qu, Alvarez, & Li, 2013). Evaluating the economic viability of nanotechnology water treatment systems would involve examining the scalability of the processes as well as assessing the suitability of lower cost nanomaterials in water disinfection. A further research consideration is how to develop more effective photocatalytic disinfection technology, which is advantageous because sunlight has no cost implications for those using the devices. The focus should be on improving the water throughput rates which are dependent on incident light wavelength, flux and absorption length in water, contact efficiency of bacterial species on the photocatalysts and other reactor design aspects (Zhang, Li, & Yu, 2010).

2.3.3 Effect on human and environmental health

Concerns have been raised regarding the potential risk nanoparticles pose if emitted into the environment, particularly if taken up by biological organisms. Engineered nanomaterials have been found to be both cytotoxic and genotoxic, but most studies have focused on the interaction of such nanoparticles with singled-celled organisms, i.e. bacteria (You *et al*., 2012). As described in Section 2.1.1, nanoparticles can affect a cell's protective membrane or internal structures such as proteins and

DNA. However, there is limited information regarding the toxicity of nanoparticles against higher organisms made up of more complex cells. Additionally, whilst there are no enforceable regulations, the advised maximum concentration of silver (in the form of salts, ions or nanoparticles) in drinking water by the World Health Organisation is 0.1 mg/L (or 0.6 µM).

It is known that chronic doses of colloidal silver can cause argyria, which, in severe causes, can cause the skin, mucous membranes or eyes to turn a purple-grey colour because of an accumulation of silver-sulphides. This is not life-threatening but is seen as aesthetically undesirable. Whilst medical studies have found favourable results when applying silver nanoparticles in laboratory settings, for example in the treatment of burns, the inhibition of cancerous tumour growth, and the prevention of HIV viral replication, the potential of cytotoxicity towards humans cannot be ignored and investigation into the safety of the nanoparticles is critical (You *et al*., 2012).

As will be explored in Section 2.4.1, evidence suggests that the toxicity of particulate silver is mediated via silver ions released from the particle surface (Hadrup & Lam, 2014). Because of this, the toxicity of silver nanoparticles cannot be separated from that of silver ions. Therefore, when the effects of silver nanoparticles on biological species are discussed, this is inclusive of the effects of released silver ions.

In addition to being toxic to many strains of bacteria, silver nanoparticles have also been found to inactivate viruses, fungi and algae (Marambio-Jones & Hoek, 2010). Some evidence has also been presented showing the toxicity of these nanoparticles to higher organisms. In laboratory conditions (i.e. *in vitro*), silver nanoparticles (15 and 30 nm in size) were shown to cause cell leakage and reduce mitochondrial function of rat liver-derived cells and mouse spermatogonial stem cell lines at concentrations starting at 5 ppm (Cioffi & Rai, 2012). At concentrations above 50 ppm, zebrafish embryos were found to be severely affected by silver nanoparticles (Asharani, Lian Wu, Gong, & Valiyaveettil, 2008). A lowered heart rate, hatching delays and high mortality were observed and TEM images revealed that Ag nanoparticles accumulated in the cell nucleus. These results indicate the deleterious effect silver nanoparticles can have on aquatic species and highlight the need for restrictions on the emission of nanoparticle waste into the environment.

In an investigation that reviewed literature on the *in vivo* toxicity of silver ions and nanoparticles, Hadrup & Lam (2014) state that silver ions and nanoparticles have limited genotoxicity towards lymphatic cells of mice, with effects only being observed at high concentrations. Deleterious effects on the gastrointestinal tracts of mice were observed following oral administration of silver nanoparticles (5 – 20 nm) with a dosage of 20 mg/kg of bodyweight (bw) per day over 21 days (Hadrup & Lam, 2014). Liver toxicity and a dose-dependent accumulation of silver in organ tissues of rats was observed following daily doses of 56 nm Ag nanoparticles at concentrations of 30, 125 and 500 mg/kg of bw over 90 days (Y. S. Kim *et al*., 2010). Subsequently, the NOAEL (no observable adverse effect level) of 30 mg/kg and LOAEL (lowest observable adverse effect level) of 125 mg/kg were proposed (Y. S. Kim *et al*., 2010).

An *in vivo* study looking at the effects of orally dosed silver nanoparticles on humans was performed by Munger *et al*. (2014). This appears to be the first study that performed such an assessment on humans. Silver nanoparticles of either 10 nm or 32 nm were systematically administered to 60 healthy volunteers at an unspecified concentration (presumed to be between 5 and 50 ppm) over a maximum of 14 days. No changes were detected in any of the systems studied. The metabolic, hematologic and urinalysis measures were unaffected, and the lungs, heart, and abdominal organs did not show any morphological

changes. It was, however, noted that further studies that increase the time exposure and dosage of silver nanoparticles and observe more organ systems are essential for understanding the toxicity against humans (Munger *et al*., 2014).

Mitochondria, the powerhouses of the cell, are believed to have evolved from bacteria and share many characteristics (Kutschera, 2009). Whilst the more complex eukaryotic cells (found in humans, plants etc.) are very different from simple prokaryotic cells (bacteria), understanding how silver nanoparticles affect bacteria can aid in the understanding of their effect on important organelles found in the cells of higher organisms such as mitochondria. Because of the structural and functional similarities between bacteria and mitochondria in higher organisms, Marambio-Jones & Hoek (2010) hypothesise that, assuming they can be taken up by the cell, nanoparticles will affect their systems similarly.

If released into the environment, silver nanoparticles may adversely affect several different organism types, including algae, bacteria, vertebrates and invertebrates (Le Ouay & Stellacci, 2015). It is difficult to ascertain exactly what effect silver nanoparticles will have on environmental health and what their environmental persistence may be, because various environmental systems will present different specificities. For example, the presence of natural organic matter (NOM) affects the rate of silver ion release (as shown in Section 2.4.2), most likely because the nanoparticle surface chemistry may be altered (Le Ouay & Stellacci, 2015). Additionally, the presence of salts and living organisms can affect the stability, distribution and speciation of silver.

Further research is clearly necessary to safely make use of the antimicrobial properties of silver nanoparticles without causing adverse effects to human health and the environment. In-vitro, in-vivo and environmental studies should assess the effects of particularly aquatic chemistry on the transport, persistence and toxicity of silver nanoparticles (Marambio-Jones & Hoek, 2010).

2.4 Silver nanoparticles as a disinfectant

Since before the discovery of bacteria and the realisation that they were disease-causing agents, silver has been used for its antimicrobial properties by ancient civilizations, including by the Egyptians, Romans and Greeks (Azócar, Tamayo, Vargas, Vejar, & Páez, 2016). Silver was used in various medical applications for the treatment of infections until the invention of antibiotics (Alexander, 2009; Azócar *et al*., 2016; Becker, 1999). In the face of nanoscale developments, as well as some bacteria developing immunities to antibiotics due to their intensive use, there has been a resurgence in the use of silver as an antibacterial agent (Azócar, Tamayo, Vargas, Vejar, & Páez, 2016). Some current commercial applications include fabrics, implant coatings, water filters and wound dressings (Azócar *et al*., 2016; Rai *et al*., 2009). Silver nanoparticles have been shown to have a bactericidal effect against a wide range of Gram-positive and Gram-negative bacteria strains, including *Escherichia coli*, *Staphylococcus aureus*, *Bacillus subtilis*, *Pseudomonas aeruginosa*, *Enterococcus faecium*, and *Staphylococcus epidermidis.*

Numerous other nanoparticles, including copper, titanium dioxide and gold, have been found to be bactericidally active. Silver was chosen for this study because it is the most commonly used antibacterial nanomaterial, has been cited as one of the most toxic nanoparticles towards bacteria and has a high bactericidal activity and broad antibacterial spectrum (Foldbjerg, Jiang, Miclăuş, *et al*., 2015; Kim *et al*., 2007; Q. Li *et al*., 2008; Qu, Alvarez, & Li, 2013).

2.4.1 Antibacterial mechanism of silver nanoparticles

There is some debate regarding the antibacterial mechanisms of particularly silver (Foldbjerg, Jiang, Miclăuş, *et al*., 2015). Most literature that focuses on silver as an antibacterial agent also considers what mechanisms might be responsible for the inactivation and killing of bacteria in the tests conducted.

Ruparelia *et al*. (2008) state that it is difficult to distinguish between the antibacterial activity of the nanoparticles and that of the silver ions released from the nanoparticles. Some studies have reported that silver nanoparticles are effective as antibacterial agents at lower concentrations than that of the ions, indicating that they are more bactericidally efficient (Choi *et al*., 2008; Lok *et al*., 2006). Xiu *et al*. (2012), however, performed an experiment to determine whether silver nanoparticles exert direct "particle-specific" antibacterial effect in conjunction with the known antibacterial activity of silver ions and produced results that contradict this. The researchers drew the conclusion that, whilst the role of Ag nanoparticles cannot be excluded entirely, Ag^+ is the definitive source of the nanoparticles' antibacterial activity by testing Ag nanoparticles against *E. coli* in anaerobic conditions. This prevented the oxidation of Ag^0 and, subsequently, the release of Ag^+. In anaerobic conditions, Ag nanoparticles showed no statistically significant toxicity towards *E. coli* whilst in aerobic conditions, when exposed to the same nanoparticles, *E. coli* was killed (Xiu, Zhang, Puppala, Colvin, & Alvarez, 2012).

Some of the antibacterial mechanisms of silver nanoparticles and ions suggested in literature include nanoparticles attaching themselves to the bacteria surface, thereby causing an increase in membrane permeability (Dizaj *et al*., 2014; Hajipour *et al*., 2012; Q. Li *et al*., 2008; Morones *et al*., 2005), and possibly penetrating the bacteria thus further disturbing its proper function (Morones *et al*., 2005), Ag^+ interaction with proteins leading to respiratory enzyme inactivation (Dizaj *et al*., 2014; Hajipour *et al*., 2012; Q. Li *et al*., 2008), and Ag^+ preventing the replication of cellular DNA and inhibiting growth (Hajipour *et al*., 2012; Q. Li *et al*., 2008; Qu *et al*., 2013). The fact that a variety of pathways for silver nanoparticles and ions to disrupt bacterial function have been identified may be why silver is such a broad-spectrum antimicrobial agent.

In a review that considers the antibacterial activity of silver nanoparticles from a surface science perspective, Le Ouay & Stellacci (2015) suggest that reactive oxygen species (ROS) action against bacteria may be the main method of bacterial deactivation in the presence of Ag^+. It is believed that Ag^+ disrupt the antioxidant systems within the cells (Carlson *et al*., 2008). Whilst the generation of ROS can be catalysed by silver nanoparticles, particularly in the presence of UV-radiation, ROS are also produced by cells during normal function (Matés, 2000). Silver ions have a strong affinity to thiols and selenols, which are present in several biological molecules. The role of intracellular glutathione, a thiol that is present in plants, animal tissues, and microorganisms, is to protect cells from the effects of reactive oxygen species (Meister, 1988). The Ag^+ interaction with glutathione reductase enzymes will result in the loss of the ROS-regulation system which will cause a build-up of ROS (Le Ouay and Stellacci, 2015). The increase in concentration of the ROS induces a high oxidative stress in the cells causing inactivated proteins, damaged membranes and cellular mutation, ultimately resulting in cell death (Deponte, 2013).

The role of the silver nanoparticles in the bactericidal process cannot be entirely excluded, although most studies indicate that the critical step for the antibacterial effect is the oxidative dissolution to silver ions. Experimental investigations in the field have found that the antibacterial activity of silver nanoparticles increases with a decrease in nanoparticle size (Foldbjerg, Jiang, Miclăuş, *et al*., 2015; Le

Ouay & Stellacci, 2015; Panacek *et al*., 2006; Xiu *et al*., 2012). Because the surface area per unit mass scales at a rate of $\frac{1}{r}$ (with the surface area scaling at r^2 and the mass scaling at r^3 where r is the radius), smaller nanoparticles have a higher specific surface area, and thus a higher surface activity and a higher dissolution rate (Le Ouay & Stellacci, 2015).

In contradiction to this, Sotiriou & Pratsnis (2010) produced Figure 2-3 after investigating the toxicity of Ag^+ ions against E. coli in the presence and absence of silver nanoparticles. The material used in these experiments was nanosilver on nanostructured silica synthesised via one-step flame spray pyrolysis (FSP). The Ag/SiO_2 particles were separated from the released Ag^+ ions after centrifugation so as to isolate the antibacterial effect of the ions, and the Ag^+ concentration was measured using an ion selective electrode. The *E. coli* fluorescence (expressed on the *y*-axis) is equivalent to the surviving *E. coli* population, with 100% fluorescence corresponding to approximately 10^7 cells/ml, and was measured over a period of 330 minutes.

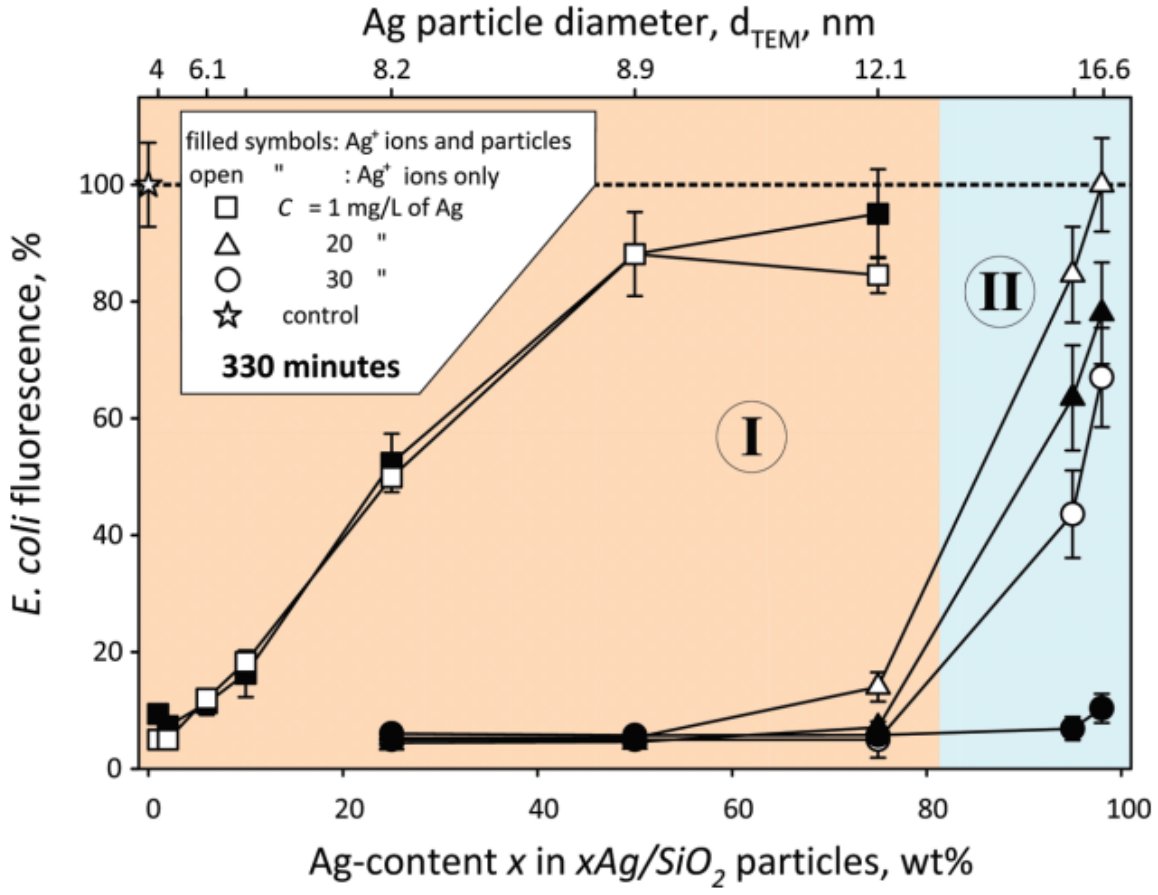

Figure 2-3: E. coli population after 330 min in the presence of Ag^+ ions and Ag nanoparticles of different sizes and concentrations. Zone I (orange) indicates the particle size range in which the antibacterial activity is dominated by ions whilst zone II (blue) indicates the tested size range in which the particles play a role in the antibacterial activity. Reprinted, with permission, from Sotiriou & Pratsinis (2010).

Very small particles, present in the low Ag-content particles, were found to dissolve almost completely, thus dominating the toxicity of the silver nanoparticles and preventing the particles alone from playing a role in the bactericidal action against *E. coli*. Additionally, it was found that at low concentrations of

1 mg/L of Ag, the suspensions of larger particles (in the size range of 8 – 12 nm) did not demonstrate much bactericidal activity and the concentration of Ag in the bacterial suspension needed to be increased. At higher concentrations of Ag, the aforementioned particle size range exhibited strong antibacterial activity and at the highest tested Ag-content (30 mg/L) all particle suspensions (up to sizes of 16.6 nm) demonstrated strong antibacterial activity. However, when the Ag/SiO_2 particles were removed there was a significantly lower antibacterial effect exhibited at particles sizes of greater than 12 nm (approximately 80 wt% of Ag in Ag/SiO_2 particles). These results indicate that the antibacterial activity of Ag nanoparticles is dependent on particle size. Therefore, the graph presented in Figure 2-3 is divided into two areas based on particle size. For smaller particles with a high release rate of Ag^+ ions, the antibacterial activity is dominated by the ions rather the particles (orange area I). However, when larger nanosilver particles (with an average particle size of greater than 10 nm) were tested, the particles themselves also seemed to influence the antibacterial activity of nanosilver (blue area II). This could explain contradictory studies of the antibacterial mechanism of silver nanoparticles that support either the Ag^+ ions or the Ag particles as the main source of toxicity. Sotiriou & Pratsinis (2010) believe that the dispute in literature regarding the antibacterial mechanism of silver nanoparticles may be due to the inadequate size control and characterisation of the nanoparticles, or their state of agglomeration or flocculation. Because of the results presented above, an aim of the current study is to synthesise and test silver nanoparticles of smaller than 10 nm to isolate the antibacterial effect of just the silver ions. It is also important to note that the surfactant used will likely have an impact on the antibacterial efficacy of the silver nanoparticles because it will have an effect on the silver ion release.

In addition to causing bacterial death, Ag is said to have a lower human toxicity than a number of other disinfectants (Dizaj *et al.*, 2014; Qu *et al.*, 2013). However, Marambio-Jones & Hoek (2009) report that there is evidence that Ag nanoparticles have cytotoxic and genotoxic effects on higher organisms. This raises concerns regarding the potential implications on human health and the environment. It is thus important for further research to be conducted so as to develop silver-containing nanoparticles with high antibacterial activity and minimal toxicity.

Xiu *et al*. (2012) also produced results which suggest that doses of Ag^+ lower than lethal concentrations enhanced the survival rate of *E. coli*. It is believed that low doses of bactericides may stimulate repair mechanisms of the cells thus, hindering any further antibacterial action against the bacteria. This effect has also been seen in other studies with different nanomaterials such as carbon nanotubes, quantum dots, and metal nanoparticles, but the phenomenon is poorly understood which indicates the need for further research in this regard (Xiu, Zhang, Puppala, Colvin, & Alvarez, 2012).

2.4.2 Silver ion release

Because the main source of the bactericidal activity of silver has been shown to be silver ions, a key step for this antibacterial effect is the oxidative dissolution mechanism. Understanding what affects the rate of silver ion release from silver nanoparticles is important for understanding the biocidal effect nanoparticles may have, how the nanoparticles may be tailored for specific antimicrobial use, and how these nanomaterials can be implemented into antibacterial applications.

$$Ag^0 + \frac{1}{4}O_2 + H^+ \rightleftharpoons Ag^+ + \frac{1}{2}H_2O \qquad \textit{Equation 2-2}$$

From Equation 2-2 it can be seen that the release of silver ions in water is dependent on the concentration of dissolved oxygen and the pH (availability of H^+). Thus, when testing the antibacterial

activity of silver nanoparticles, it is important to keep parameters that affect the O_2 and H^+ concentrations constant.

Liu and Hurt (2010) sought to investigate the time-dependent release of dissolved silver from citrate-stabilised nanoparticles, which requires the presences of both dissolved oxygen and protons. The proposed oxidation stoichiometry is seen in Equation 2-3.

$$O_{2(aq)} + H^+_{(aq)} \xrightarrow{Ag^0\ (slow)} Ag^+_{(aq)} + peroxide\ intermediates \xrightarrow{Ag^0\ (fast)} Ag^+_{(aq)} + H_2O_{(l)} \quad \textit{Equation 2-3}$$

It was found that the oxidation reaction produces peroxide intermediates, including hydrogen peroxide, and can even proceed to complete dissolution. Also considered was the effect of pH, natural organic matter and temperature on the kinetics of the silver ion release. However, only one size of silver colloid was investigated (4.8 ± 1.6 nm), and the effect of size on the kinetics was not emphasised. This is despite it being well known that smaller nanoparticles have a faster Ag^+ release because of their higher specific surface area.

The rate of Ag^+ release was found to decrease with argon-stripping of dissolved O_2, the addition of natural organic matter (humic or fulvic acids), the addition of excess citrate, temperature reduction or pH increase. (Liu & Hurt, 2010). As a result of their investigation, an empirical kinetic law was proposed for low silver concentrations that takes these factors into consideration. Naturally, it is expected that release rates will vary with different systems, particularly if different capping agents are used.

$$-\frac{1}{m}\frac{dm}{dt} = Ae^{-\frac{E}{RT}}\left(\frac{[H^+]}{10^{-7}M}\right)^{0.18} e^{-a[NOM]} \quad \textit{Equation 2-4}$$

with $E = 77\ kJ/mol$, $A = 2.5 \times 10^{13} day^{-1}$ and $a = 0.083 \frac{L}{mg}$. NOM = natural organic matter (mg/L), *m* = mass, *t* = time, *T* = temperature

For use with nanosilver particles of a very different size, the law was renormalized to a particle area basis. This was done by using the size distribution data from their TEM analysis to give an alternative value of *A*, where $A_{alt} = 7.6 \times 10^{16} \frac{\mu g\ released}{day.\ m^2 particle\ surface\ area}$. The accuracy of the resulting kinetic law produced using this renormalized value was, however, not established because no comparison against experimental results using different sized particles was performed.

Zhang *et al*. (2011) considered the ion release from silver nanoparticles because of its relevance in understanding the silver NPs effect on the environment, biological impact and transport. Ion release kinetics of three different sized, citrate-coated nanoparticles (20, 40 and 80 nm) were studied, each at two different concentrations (300 and 600 µg/L). The ion release experiments were performed in Hoagland medium, which is a hydroponic medium for growing plants. The medium was chosen because its electrolyte nutrients simulate relevant ionic conditions in soils, sediments and groundwater systems that Ag nanoparticles are likely to enter (Zhang *et al*., 2011). The researchers found that the release rates depended on the particle size and concentration when other environmental factors (for example, dissolved oxygen and protons) were kept constant. The focus of the study was primarily on the particle size and concentration effects on the ion release kinetics because previous research had investigated environmental factors like dissolved oxygen, pH, salinity, and temperature.

In order to describe the Ag^+ release rate (γ_{Ag^+} in $\frac{mol}{L.h}$), a kinetic model was developed based on the hard sphere theory using the Arrhenius equation (Zhang *et al*., 2011).

$$\gamma_{Ag^+} = \frac{3}{4}\left(\frac{8\pi k_B T}{m_B}\right)^{\frac{1}{2}} \rho^{-1} \exp\left(-\frac{E_a}{k_B T}\right)[Ag] r^{-1} [O_2]^{0.5} [H^+]^2 \qquad \text{Equation 2-5}$$

With k_B $(Boltzmann\ constant) = 1.38 \times 10^{-23}\ J/K$, $E_a = 77\ kJ/mol$ and m_B being the molecular mass of either oxygen or protons, T = temperature, r = particle radius, ρ = particle density

The model was derived with respect to time and fitted the experimental data well, with correlation coefficients of between 0.97 and 0.99 (shown in Figure 2-4). Unsurprisingly, the smallest particles have the highest silver ion release rate, demonstrated both by the model and by experimental results. Overall, the scientists believe the model they developed provides insight into the ion release kinetics of silver nanoparticles in aqueous environments which will allow for better understanding and prediction of the toxicity of silver nanoparticles. The results of this study by Zhang *et al.* (2011) were found to correspond well to those of Liu & Hurt (2010).

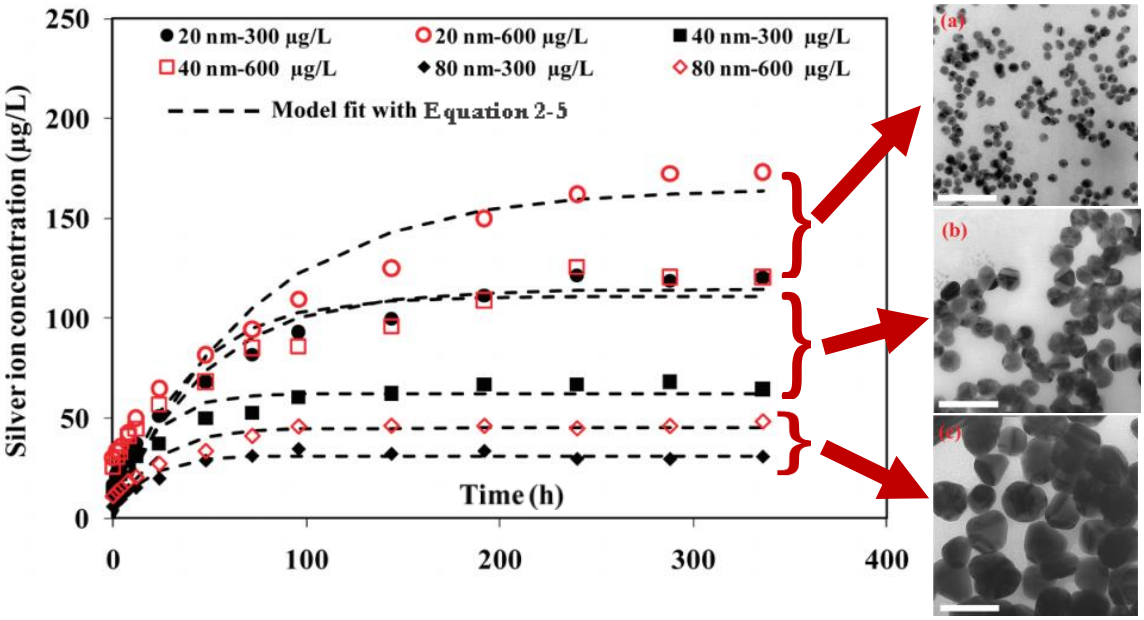

Figure 2-4: Ag^+ experimental (markers) and modelled (dashed line) release kinetics from different sizes and concentrations of citrate-coated Ag nanoparticles. The white bar on the bottom left of the TEM images is equivalent to 100 nm. Reprinted, with permission, from Zhang et al. (2011).

Although estimating the ion release rates of the silver nanoparticles prepared for this study lies beyond the scope of this research, it is important to consider the factors that may influence the toxicity of the nanoparticles. The kinetic studies described provide some insight into what the major factors that affect total silver ion release are, thus allowing a better understanding of what factors should be kept constant in antibacterial efficacy experiments and what factors will affect the results thereof.

2.5 Silver nanoparticle synthesis

There are two general approaches to nanoparticle synthesis – "top-down" and "bottom-up". The top-down approach starts with a bulk-scale material and reduces this to the nanoscale via high-energy processes. Examples of this include ball milling and spark discharge. The bottom-up approach grows or precipitates nanoparticles from the atomic or molecular level via chemical reactions. Examples include chemical reduction, the sol-gel technique and chemical vapour deposition (CVD). A bottom-up approach will be used for the synthesis of nanoparticles in this study because it is a cheaper and simpler

method to apply in small scale experiments such as this (Cunningham & Bürgi, 2013). Naturally, different synthesis methods may result in differences in chemical composition, crystallinity and morphology due to varying synthesis kinetics (Cao, 2004). This may result in the same material exhibiting different physical properties, which should be kept in mind when comparing the performance of similar nanomaterials. Ideally, a nanoparticle preparation method should result in the formation of nanoparticles with the identical size, morphology, crystal structure and chemical composition (Cao, 2004). Brief descriptions of some methods that have been used for silver nanoparticle synthesis follow.

2.5.1 Physical methods

Evaporation-condensation and spark ablation (which is further explored in Section 4.3) are some of the more common physical synthesis approaches. Such methods are advantageous because no solvents or surfactants are involved in the synthesis, thus contamination of the nanoparticles is unlikely (Iravani, Korbekandi, Mirmohammadi, & Zolfaghari, 2014). However, in the case of the evaporation-condensation approach, the use of a tube furnace is energy intensive, requires a lot of space for operation and needs time to achieve thermal stability (Iravani, Korbekandi, Mirmohammadi, & Zolfaghari, 2014; Tran, Nguyen, & Le, 2013).

2.5.2 Photo-induced methods

Photo-induced synthesis of silver nanoparticles can either be done by following a photophysical (top-down) or photochemical (bottom-up) approach. Nanoparticle formation results from either the direct subdivision of bulk metal or from the reduction of metal ions through interactions with photo-chemically produced intermediates, respectively (Tran, Nguyen, & Le, 2013). An interesting study investigated the photoreduction of $AgNO_3$ in the presence of sodium citrate using different light sources (UV, white, blue, cyan, green and orange) and found that the wavelength of light employed affected the size and shape of the nanoparticles and that higher wavelengths of light result in lower yields (Sato-Berŕu, Redón, Vázquez-Olmos, & Saniger, 2009).

2.5.3 Biological methods

Microorganisms and plant extracts have been used for the biosynthesis of silver nanoparticles (Sau & Rogach, 2012). Compounds present in biomass, such as reducing sugars, proteins, enzymes, and peptides, can reduce metal ions thereby resulting in the formation of metal nanoparticles. For example, silver nanoparticles of 5.3 ± 2.6 nm have been prepared using starch as a capping agent and glucose as a reducing agent (Raveendran, Fu, & Scott, 2003). Such biosynthesis methods are viewed favourably because they are cost-effective and 'green'. However, often the actual species involved in the reduction and capping processes are not well understood which makes optimisation of such synthesis methods difficult (Sau & Rogach, 2012)

2.5.4 Chemical methods

Wet chemical reduction of a silver salt is the most common silver nanoparticle synthesis method (Panacek *et al.*, 2006). This nanoparticle synthesis process usually involves three main components: metal precursors, reducing agents and surfactants/capping agents (Tran, Nguyen, & Le, 2013). Nanoparticles are formed from the reduction of silver salts (Ag^+ to Ag^0) following a nucleation and growth process. Template-directed synthesis, seed-mediated synthesis and polyol synthesis procedures are all chemical reduction methods (Sau & Rogach, 2012). It is important to use capping agents to stabilise the silver nanoparticles and prevent agglomeration during synthesis when using such methods (Iravani, Korbekandi, Mirmohammadi, & Zolfaghari, 2014). The wet chemical reduction

method will be used in this study, and the kinetics of silver nanoparticle formation using this approach will be further explored.

2.6 Nucleation and growth of nanoparticles

The formation of nanoparticles via chemical reduction involves the nucleation of primary particles and the subsequent nanoparticle growth. To prepare monodisperse, uniformly sized silver nanoparticles, the initial nuclei must form at the same time (Tran, Nguyen, & Le, 2013). This nanoparticle nucleation and growth can be controlled by adjusting reaction conditions such as the reducing agent, stabilising agent, and reaction temperature (Tran, Nguyen, & Le, 2013).

Polte (2015) states that the classical nucleation theory, seen as the basic model for colloidal formation, does not adequately describe nanoparticle growth and that no theory or model that is comprehensively able to describe or predict the particle size and particle size distribution currently exists. Despite this, the classical nucleation theory (CNT) will be described here as it can be used to explain the nucleation of nanoparticles whilst other theories can be applied to their growth process. The focus will be on homogeneous nucleation since it is the relevant process in this study.

2.6.1 Nucleation

The nucleation of a metal nanoparticle describes the formation of a new phase, the nucleus, typically through the decomposition or reduction of a metal precursor into zero-valent atoms (Xia, Xiong, Lim, & Skrabalak, 2009). Heterogenous nucleation results from formation on inhomogeneities such as seeds, container surfaces and impurities whilst homogeneous nucleation, resulting in uniform nuclei throughout the parent phase, occurs randomly but requires a supercritical state such as supersaturation (Polte, 2015; Thanh, Maclean, & Mahiddine, 2014). Homogeneous nucleation can be considered thermodynamically through the reduction of the overall Gibbs free energy of a supersaturated solution by the formation of a solid phase whilst equilibrium concentration in the solution is maintained (Cao, 2004). The driving force for nucleation and growth is this reduction of this Gibbs free energy (Cao, 2004). The total free energy of a spherical nanoparticle is defined as the sum of the surface free energy (γ) and the bulk free energy (G_v) as shown by Equation 2-6 (Polte, 2015; Sau & Rogach, 2012; Thanh, Maclean, & Mahiddine, 2014).

$$\Delta G = 4\pi r^2\gamma + \frac{4}{3}\pi r^3 \Delta G_v \qquad \textit{Equation 2-6}$$

The Gibbs free energy of the crystal itself depends on the temperature (*T*), solution supersaturation (*S*), and its molar volume (*v*).

$$\Delta G_v = \frac{-k_B T \ln(S)}{v} \qquad \textit{Equation 2-7}$$

Because the surface Gibbs free energy is always positive, and the crystal Gibbs free energy is always negative, it is possible to find the maximum free energy that a stable nucleus will pass through. This is calculated by differentiating the total Gibbs free energy with respect to the nucleus radius and equating this to zero, $\frac{d\Delta G}{dr} = 0$, which leads to the calculation of the critical radius (Equation 2-8) and critical Gibbs free energy (Equation 2-9).

$$r_{crit} = -\frac{2\gamma}{\Delta G_v} = \frac{2\gamma v}{-k_B T \ln(S)} \qquad \textit{Equation 2-8}$$

$$\Delta G_{crit} = \frac{4}{3}\pi\gamma r_{crit}^2 \qquad \textit{Equation 2-9}$$

This can be represented by plotting the Gibbs free energy as a function of particle radius (Figure 2-5). The critical radius corresponds to the minimum size at which a nucleus can survive, and growth is favoured, without dissolving (Thanh, Maclean, & Mahiddine, 2014).

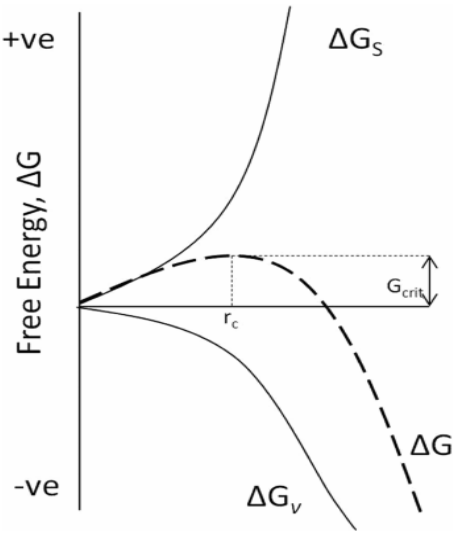

Figure 2-5: The dependence of the Gibbs free energy of a formed nucleus on the radius thereof according to the CNT. Reprinted, with permission, from Thanh, Maclean, & Mahiddine (2014).

An Arrhenius-type equation can be used to express the rate of nucleation (of *N* particles over time *t*) within a system (Equation 2-10).

$$\frac{dN}{dt} = A\exp\left(\frac{16\pi\gamma^3 v^2}{3k_B^3 T^3\, ln(S)^2}\right) \qquad \textit{Equation 2-10}$$

Equation 2-10 shows that the rate of nucleation can be controlled by varying three experimental parameters: supersaturation, temperature and surface energy (Sau & Rogach, 2012). Using this equation, each of these parameters were varied to determine their effect on the rate of nucleation of CdSe nuclei, and this is shown in Figure 2-6 (Thanh, Maclean, & Mahiddine, 2014).

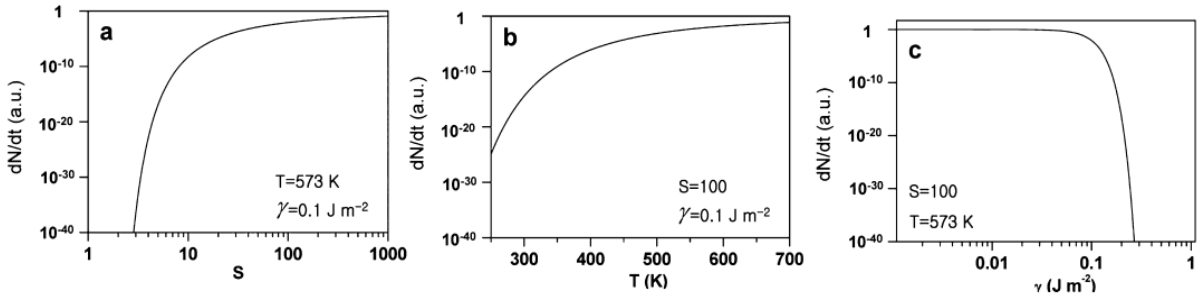

Figure 2-6: Nucleation rate of CdSe nuclei as a function of a) supersaturation, b) temperature, and c) surface energy. Reprinted, with permission, from Thanh, Maclean, & Mahiddine (2014).

Changes in the solution temperature have significantly less of an effect than varying either the supersaturation or the surface energy whilst keeping the other parameters constant (Thanh, Maclean, & Mahiddine, 2014). Of course, this is only a theoretical experiment since both supersaturation and nanoparticle surface energy are affected by temperature (Cao, 2004). A high surface energy (γ) slows the nucleation rate, however the addition of a surfactant to the system can reduce the surface energy (Sau & Rogach, 2012). High supersaturation and temperatures accelerate the nucleation rate. It is favoured to have a fast nucleation rate as this means the nucleation and growth steps will be separate, thus resulting in the formation of more uniform nanoparticles. This concept is termed 'burst nucleation' and is the theory put forward by LaMer (LaMer, 1952; LaMer & Dinegar, 1950). Figure 2-7 aids in describing this phenomenon.

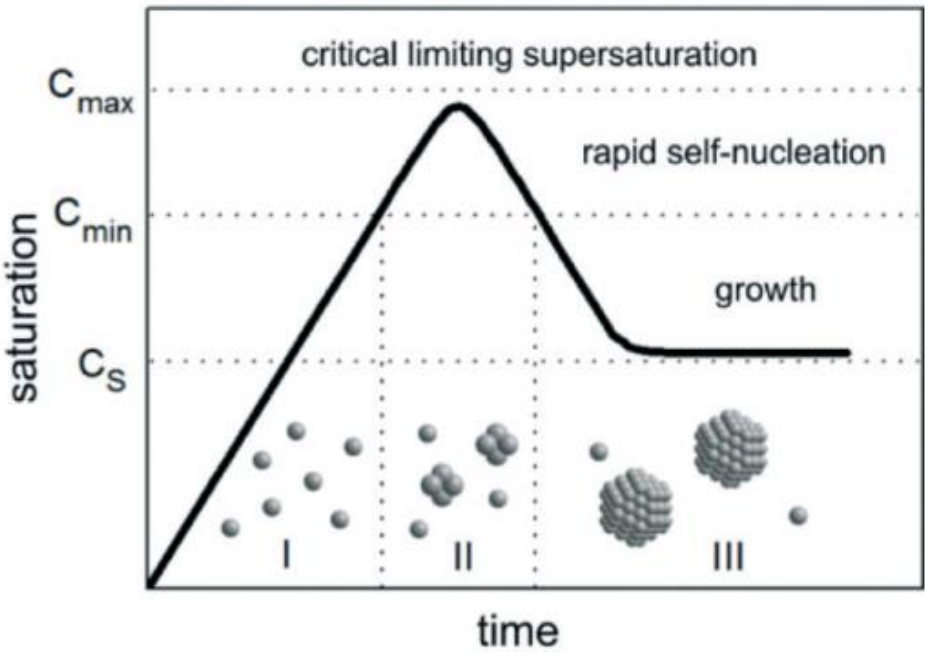

Figure 2-7: A typical plot showing the LaMer model, illustrating the generation of atoms, nucleation, and subsequent growth. Reprinted from Polte (2015).

In the context of metal nanoparticle synthesis via wet chemical reduction, the concentration of metal atoms increases steadily (stage I: induction period) as the metal salt precursor is reduced. The zone below the saturation concentration (C_S) is called the stable zone and nucleation is impossible here because the saturation is too low. The zone between the saturation concentration and the minimum critical supersaturation (C_{min}) is termed the metastable (supersaturated) zone. In this zone, homogeneous nucleation is improbable although seed-mediated growth is possible. The width of the metastable zone can be affected by temperature, agitation rate, the presence of impurities of additives, and the rate of supersaturation generation. At C_{min} (the supersaturation curve), the activation energy for nucleation can be overcome which leads to rapid, spontaneous self-nucleation i.e. burst nucleation through the aggregation of atoms. The zone in which this occurs is called the labile (unstable) zone. The concentration of metal atoms in the solution drops as more nuclei form. If this drops quickly enough below the C_{min}, no further nucleation will occur, and the growth and nucleation steps will happen completely separately. Growth occurs in stage III as metal atoms diffuse from the solution towards particle surfaces. The metallic atoms continuously deposit on the nuclei surfaces, resulting in an

increase in particle size and decrease in atom concentration in the solution until an equilibrium between the nanoparticle surface atoms and solution atoms is reached (Cao, 2004; Polte, 2015; Sau & Rogach, 2012; Tao, Habas, & Yang, 2008; Thanh *et al*., 2014; Xia *et al*., 2009).

2.6.2 Growth

One theoretical approach states that growth is dependent on two factors, the surface process and the diffusion of the metallic atoms to the nanoparticle surface (Thanh *et al*., 2014). The size distribution of nanoparticles depends on the growth process that follows nucleation (Cao, 2004). If the growth of nanoparticles is diffusion-limited, the formation of uniformly sized particles is likely. The growth rate in this instance is given by Equation 2-11.

$$\frac{dr}{dt} = D(C - C_i)\frac{V_m}{r} \qquad \textit{Equation 2-11}$$

where r is the radius of a spherical nucleus, D is the diffusion coefficient of the metallic atoms through the reaction medium, C is the bulk concentration, C_i is the concentration on the interface of the liquid/solid nanoparticles, and V_m is the molar volume of the nucleus.

If the diffusion rate is very rapid, the growth is controlled by the surface processes (Cao, 2004). The surface growth process can follow either a mononuclear growth or a polynuclear growth mechanism. Mononuclear growth occurs layer by layer, with further layer growth only proceeding after the previous layer is complete, and does not favour the formation of uniformly sized particles (Cao, 2004). The growth rate in this instance is proportional to the particle surface area. Polynuclear growth occurs very rapidly and the second layer begins growing before growth of the first layer is complete. The polynuclear growth rate is constant (i.e. independent of particle size and time), depends on the solution temperature, and favours the formation of uniformly sized nanoparticles (Cao, 2004).

It has been suggested that nanoparticle growth can involve all three of these mechanisms; mononuclear growth when the particles are small, polynuclear growth as the particles become larger and diffusion-controlled growth for large particles (Cao, 2004).

There are several other growth mechanisms that have been observed that are not described by the above theory. Ostwald ripening occurs as a result of small particles, which are highly soluble and have a high surface energy, dissolving and redepositing on larger particles (Thanh, Maclean, & Mahiddine, 2014). Coalescent (or aggregative) growth is the phenomenon whereby smaller particles (or nuclei) aggregate and subsequently coalesce to form larger particles, often resulting in a bimodal size distribution (Polte, 2015; Richards, Rath, & Buhro, 2010; Thanh, Maclean, & Mahiddine, 2014). These nanoparticles are capable of further growth via aggregation. Shields, Richards, & Buhro (2010) suggest that this aggregation can be viewed as a second nucleation step following the classical nucleation and growth that precede aggregation. The bimodality often observed is because of the formation of a population of aggregated particles that are larger than the primary particles. Additionally, it has been observed that Ostwald ripening can increase the separation between the two modes (Shields, Richards, & Buhro, 2010).

2.6.3 Size control

The control of nanoparticle sizes can be achieved through thermodynamic, kinetic or stoichiometric methods (Polte, 2015). However, Polte (2015) also cynically states that size control of nanoparticles is usually based on extensive trial-and-error experimentation strategies rather than through the design of a synthesis process. Additionally, Thanh *et* al. (2014) do not believe that predictions regarding the

mechanism of nanoparticle formation for a given system can be made because small variations in the reaction conditions can result in unforeseen changes. It has been found that numerous parameters, including solvent, pH, impurities, temperature, metal precursor, reducing agent, surfactant and agitation, can affect particle size. Some of these are explored below. More than one factor plays a role in the particle synthesis which, unfortunately, makes it difficult to isolate their individual effect on particle size.

2.6.3.1 Effect of metal precursor

The metal precursor can significantly affect particle formation. The critical nucleus size (r_{crit}) has been found to depend on the difference between the redox potential of the reducing agent and metal precursor used (Sau & Rogach, 2012). Additionally, the ions and molecules produced as a by-product of the metal precursor decomposition/oxidation have the potential to influence the pH and ionic strength of the solution in which nanoparticles form, which can subsequently affect particle size (Sau & Rogach, 2012).

2.6.3.2 Effect of reducing agents

The size and size distribution of synthesised metallic colloids can vary significantly with the reducing agent used. Generally, a strong reducing agent results in a rapid reaction rate which favours the formation of smaller nanoparticles whilst using a weak reducing agent results in the formation of larger particles due to slower reaction kinetics (Cao, 2004). Reducing agents have also been found to affect the morphology of nanoparticles (Sau & Rogach, 2012).

2.6.3.3 Effect of surfactant

Using a surfactant that adsorbs onto the nanocrystal surface thus forming a thermodynamically stable nanoparticle/stabiliser entity is often the approach used in controlling the size of nanoparticles (Polte, 2015). Varying either the surfactant type or concentration can be used to vary the particle size. The use of surfactants to stabilise nanoparticles can, however, be detrimental if difficult to remove as they can inhibit nanoparticle activity (Cao, 2004). Surfactants can affect the nucleation and growth kinetics, as well as the reduction of nancompounds and may even act as reactants (Samiey, Cheng, & Wu, 2014). Micelles have also been observed to impact the electron rate transfer, and this is explained by them acting as a strongly hydrating background electrolyte with a high electric charge (Samiey, Cheng, & Wu, 2014).

2.6.3.4 Effect of synthesis temperature

As seen from Equation 2-10, temperature significantly affects the rate of nucleation, which in turn affects the particle size. Based only on LaMer's theory, synthesis at higher temperature will produce smaller nanoparticles. However, silver nanoparticles synthesised following a procedure based on the Tollens process were found to increase in size when the reaction temperature increased slightly, with particles of ~20, ~30 and ~40 nm forming at 27 °C, 30 °C and 35 °C, respectively (Yin *et al*., 2002). It is believed that, in this instance, higher temperature resulted in an increase in the collision frequency of small particles thus leading to the formation of larger particles. Clearly, it is difficult to predict the effect parameter variation may have because of the complexity of chemical reduction systems.

2.6.3.5 Effect of manner of reactant addition

The order of addition of reactants as well as the rate of reactant addition (in portions or all at once) can affect the particle size and morphology (Sau & Rogach, 2012). For example, the hot injection method can be used to induce burst nucleation (Zacharaki, Kalyva, Fjellvåg, & Sjåstad, 2016). This hot injection method is used to synthesise monodisperse nanoparticles, usually in organic solutions.

Chapter 3: Research motivation

The overarching objective of this research is to synthesise silver nanoparticles for water disinfection and antibacterial purposes.

One of the sustainable development goals (SDGs) of the United Nations is to achieve universal access to safe and affordable drinking water for all. The main aim of this research is directly related to this particular SDG but improving the access to clean drinking water will also assist in reaching SDGs related to health and gender equality. Achieving this goal is essential to enhancing the quality of life of the 844 million people who do not have access to a basic drinking-water service (WHO/UNICEF Joint Monitoring Programme for Water Supply and Sanitation, 2017). Preventable diarrhoeal diseases, mainly caused by poor-water quality and sanitation, are still the second leading cause of death among children under the age of five (WHO/UNICEF Joint Monitoring Programme for Water Supply and Sanitation, 2017). There is an undeniable need for change so that the lives of these many millions of people may be improved.

3.1 Scope of the study

The reviewed literature outlines the antibacterial capabilities of silver nanoparticles, as well as the difficulties in using them for disinfection purposes. Numerous studies describe the effectiveness of silver in killing a range of different microbes (Kim *et al*., 2007; Panacek *et al*., 2006; Rai, Yadav, & Gade, 2009; Xiu, Zhang, Puppala, Colvin, & Alvarez, 2012). The physiochemical properties and biological activity of silver nanoparticles can be optimised to improve antimicrobial efficiency and to target specific bacterial strains (Cioffi & Rai, 2012). Although widely debated, it is generally accepted that the bactericidal activity of silver nanoparticles is mainly due to the release of silver ions. In this light, the size, shape, level of agglomeration and dispersity of the nanoparticles will have a significant impact on their antibacterial efficacy. The application of nanomaterials, such as silver nanoparticles, in water treatment technology shows promise. Not only could they be used for improving current technologies, but also in implementing new, efficient, state-of-the-art technology (Hossain, Perales-Perez, Hwang, & Román, 2014). There are, of course, many practical aspects to consider before using silver nanoparticles in water disinfection and other commercial applications, including their toxicity to humans and their effect on the environment. This study seeks to understand the basics of using silver as an antibacterial agent, with a large focus on the synthesis of silver nanoparticles for this purpose.

Two different aqueous chemical reduction methods for the synthesis of silver nanoparticles will be investigated. The chemical reduction method was chosen as it is one of the most commonly used, with these specific preparation procedures being chosen because of the literature indicating the formation of spherical, monodisperse silver nanoparticles of smaller than 10 nm (AL-Thabaiti *et al*, 2008; Cioffi & Rai, 2012; Yang *et al*., 2011). A narrow size distribution is desired because it allows for easier interpretation of the results of antibacterial efficacy studies using silver nanoparticles. The aim of producing small nanoparticles is to isolate the effect of just the ions on the bacteria. This is based on a study by Sotiriou and Pratsinis (2010) that isolated the antibacterial effect of ions released by silver nanoparticles of different sizes and compared this to the *combined* bactericidal effect of the ions and nanoparticles. Particles of smaller than 10 nm had a negligible antibacterial effect in comparison to their released ions, however particles of larger sizes interacted with the bacteria which resulted in a

bactericidal effect from both the nanoparticles and their released ions. Additionally, small particles are desired because they have been found to be more effective antibacterial agents due to their higher rate of dissolution into Ag^+ resulting from their larger specific surface area.

This research will look at optimising the synthesis of silver nanoparticles to produce the desired particle size by changing various reaction conditions, including surfactant concentration, mixing speed, synthesis temperature and method of chemical addition. Additionally, investigation into how to separate the nanoparticles from their colloidal dispersion without affecting the nanoparticle size distribution will be performed.

There is a lack of consistency in published research that studies the antibacterial activity of various nanomaterials, thus making it difficult to compare results and use published results as baselines for further studies (Hajipour *et al.*, 2012; Nature Nanotechnology, 2012). Countless studies on the antibacterial efficacy of particularly silver nanoparticles have been undertaken; however, there seems to be little evidence of a systematic approach and, therefore, a lack of relevant and valuable information pertaining to their bactericidal activity. It is for this reason that a fundamental study of silver nanoparticles, rather than an application-based investigation, will be pursued. Separating the particles from the reaction solution proved difficult, thus antibacterial efficacy studies involving the synthesised silver nanoparticles could not be performed.

A collaboration with Manju Bhamidipati, a master's student in Chemical Engineering at Delft University of Technology, was established with the assistance of Professor Patricia Kooyman[2] and Professor Andreas Schmidt-Ott[3]. The aim of this collaboration is to determine the antibacterial activity of quartz fibre filters that have been loaded with silver nanoparticles (or silver/copper nanoalloys) via spark ablation. The preparation of the filters is done at Delft University of Technology by varying the conditions of the silver nanoparticle aerosol formation. Analysis of how the different spark ablation conditions affect the size, shape and concentration of the nanoparticles deposited on the filters does not form part of the scope of this research. However, the antibacterial efficacy of the different filters against *Escherichia coli* will be studied and related back to the size of the deposited nanoparticles. Although only a fundamental study of the bactericidal capabilities of these filters will be performed, it allows for some insight into how to improve such application-based water disinfection methods. Prior to studying the antibacterial efficacy of the filters, baseline studies using silver ions at different concentrations against *E. coli* will be performed.

[2] Department of Chemical Engineering, University of Cape Town
[3] Department of Chemical Engineering, Delft University of Technology

3.2 Research objectives and key questions

The objectives of this study are to synthesise silver nanoparticles suitable for use in water disinfection applications by exploring how preparation conditions affect the particle size and distribution, and to study the antibacterial efficacy of silver-loaded quartz fibre filters and compare this to the efficacy of known concentrations of silver ions.

These objectives will be explored by focusing on the following key questions:

- Can the synthesis methods be optimised to produce uniform, spherical silver nanoparticles of smaller than 10 nm?
- Which synthesis method will produce the most suitable silver nanoparticles for antibacterial efficacy studies?
    - Suitability to antibacterial applications will be assessed on: size (the smallest produced nanoparticles of less than 10 nm) and monodispersity
- Do the silver nanoparticle-loaded quartz-fibre filters demonstrate antibacterial activity?
- How does their antibacterial activity compare to that of different concentrations of silver ions?

Chapter 4: Methodology

This chapter details the materials and experimental methods used in this study to achieve the objectives outlined in Section 3.2. The experimental approach that follows includes investigation into the effect of surfactant concentration and other synthesis variations on the size and stability of silver nanoparticles as well as into methods used for the assessment of the antibacterial efficacy of silver ions and silver nanoparticle-loaded fibre filters.

4.1 Silver nanoparticle synthesis

Two different chemical reduction methods were used for the synthesis of silver nanoparticles. The chemical reduction approach was used as it is the most common technique for silver nanoparticle synthesis presented in the studied literature (Cioffi & Rai, 2012). The methods were chosen because the literature from which each experimental scheme was sourced reported the formation of spherical, fairly monodisperse particles with an average diameter of approximately 10 nm. As mentioned in Section 2.4.1., the focus is on particles of 10 nm or less because this eliminates the effect of the nanoparticles against the bacteria thereby isolating the effect of the silver ions. For each synthesis method, three different surfactant concentrations (the original concentration described in literature, half the original concentration and double the original concentration) were used to determine the effect thereof on the nanoparticles produced. The surfactant is important as it stabilises the nanoparticles during synthesis, however it needs to be removed if collecting a dry powder. Other variations of the synthesis conditions included the mixing speed, and the concentration and rate of addition of the reducing agent. Both synthesis methods are aqueous reactions and use silver nitrate ($AgNO_3$) as the metal precursor. Because $AgNO_3$ is water-soluble, the salt dissociates into ions (Ag^+ and NO_3^-) when added to the reaction solution as shown in *Equation 4-1.*

$$AgNO_{3(s)} \rightleftharpoons Ag^{+}_{(aq)} + NO^{-}_{3\ (aq)} \qquad \textit{Equation 4-1}$$

This means that subsequent reactions to form metallic silver from silver nitrate involve the reduction of ionic silver.

4.1.1 Method One

The original method presented by AL-Thabaiti *et al.* (2008) was scaled up by a factor of 10. All reagents were combined in a 600-ml beaker using a heating plate and magnetic stirrer set at 25 °C and 1000 rpm. The beaker was suspended in a water bath to maintain the reaction temperature and the probe of a thermocouple connected to the heating plate was inserted into the water bath. The reaction vessel was wrapped in foil to prevent light affecting the synthesis of the nanoparticles. The volume of deionised water required to make a total volume of 500 cm^3 was added first (420 cm^3) and the stirrer was switched on. Then 30 cm^3 of 0.01 mol/dm^3 silver nitrate (≥ 99%, Sigma-Aldrich; $AgNO_3$) and 30 cm^3 of 0.1 mol/dm^3 sodium dodecyl sulphate (≥98.5%, Sigma-Aldrich; SDS) were added. The system was allowed to equilibrate to the required temperature (25 °C) over 15 minutes. The ascorbic acid (≥98%, Sigma-Aldrich), which needs to be prepared freshly to mitigate its oxidation, is added last because it is the reducing agent and causes the reaction to begin. 20 cm^3 of 0.01 mol/dm^3 ascorbic acid was added. The mixture was kept under stirring for three hours. TEM grids were prepared by dripping working

solution onto the carbon-coated copper grids and kept covered (away from light exposure) whilst drying in air at room temperature.

The reaction between ascorbic acid and Ag^+ can be simplified to the balanced equation seen in *Equation 4-2*. For every mole of ascorbic acid reacted, two moles of metallic silver and one mole of dehydroascorbic acid are produced. In the reaction performed for this synthesis, ascorbic acid was in 33.3% excess with respect to Ag^+.

$$2Ag^{+}_{(aq)} + C_6H_8O_{6(aq)} \longrightarrow 2Ag^{0}_{(s)} + C_6H_6O_{6(aq)} + 2H^+ \qquad \textit{Equation 4-2}$$

The possible mechanism of the redox reaction of L-ascorbic acid and silver ions is presented in *Scheme 4-1*. The mechanism is based on schemes presented by Kall (2003), Mushran, Agrawal, Mehrotra, & Sanehi (1974) and Patra *et al*. (2014).

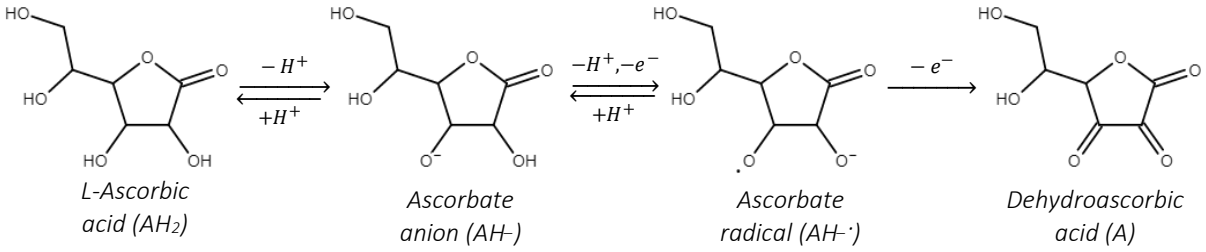

L-Ascorbic acid (AH_2) — *Ascorbate anion (AH^-)* — *Ascorbate radical ($AH^{-\cdot}$)* — *Dehydroascorbic acid (A)*

$$2Ag^+ + 2e^- \longrightarrow 2Ag^0$$

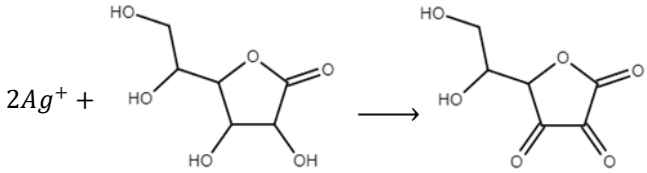

L-ascorbic acid (AH_2) — *Dehydroascorbic acid (A)*

Scheme 4-1: The reduction-oxidation reaction scheme and balanced stoichiometric equation for the formation of Ag nanoparticles using L-ascorbic acid

L-ascorbic acid is strongly polar and highly water-soluble (Patra *et al*., 2014; Xiong, Wang, Xue, & Wu, 2011). The compound acts as a vinylogous carboxylic acid in which a conjugated system is formed by the carbonyl double bond, the double bond of the ring structure and the lone pair of electrons on the hydroxyl group (Patra *et al*., 2014; Xiong *et al*., 2011). The 1,2,3-tricarbonyl on the dehydroascorbic acid structure is highly electrophilic and is not stable in aqueous solutions. The dehydroascorbic acid rapidly, irreversibly hydrolyses and thus does not act as a capping agent for the Ag nanoparticles (Xiong *et al*., 2011).

4.1.1.1 Variations of Method One

Because difficulty was experienced in synthesising silver nanoparticles to the desired specifications using the above method and the original surfactant concentration, variations on the described synthesis

were performed to determine whether smaller particles with a narrower size distribution could be produced by optimising the process. The experiments performed are described below.

Surfactant concentration

As previously mentioned, three different surfactant concentrations (the original concentration described in literature, half the original concentration and double the original concentration) were used to determine the effect thereof on the nanoparticles produced. Table 4-1 details the volumes/masses of the reactants added to each surfactant concentration variation.

Table 4-1: Chemical additions for synthesis Method One when varying surfactant concentration

Chemicals	*Half surfactant concentration*	*Original surfactant concentration*	*Double surfactant concentration*
Deionised water	435 cm^3	420 cm^3	390 cm^3
Silver nitrate	0.0510 g	0.0510 g	0.0510 g
Sodium dodecyl	15 cm^3	30 cm^3	60 cm^3
sulphate	0.4326 g	0.8651 g	1.7302 g
Ascorbic acid	0.0352 g	0.0352 g	0.0352 g

Vessel shape and mixing speed

Neither the mixing speed nor the vessel used by AL-Thabaiti *et al*. (2008) in their experiments was specified in their article. The shape of the vessel in which the synthesis reaction occurs can affect the relative mixing speed of the liquid. For this reason, a 1000 ml round bottomed flask and a 600 ml beaker were used in the original surfactant concentration syntheses at two different mixing speeds, 500 and 1000 rpm.

Synthesis temperature

AL-Thabaiti *et al*. (2008) synthesised their Ag nanoparticles at 25 °C. Since an increase in temperature can increase the rate of nucleation, thus increasing the number of particles and reducing the extent of particle growth, higher temperature synthesis was considered. Increasing the temperature may also decrease the induction period of the formation of the silver nanoparticles that was described by the authors. A 1000 ml round bottomed-flask was suspended in a silicone oil bath and the same procedure as previously described was followed. Syntheses at 40 °C and 90 °C were performed.

Dropwise ascorbic acid addition

A slower addition rate of the reducing agent would mean the creation of a more homogenous reaction environment, thus potentially resulting in slower nucleation and a more uniform particle size. The 20 cm^3 of 0.01 mol/dm^3 ascorbic acid was added dropwise at a rate of approximately one drop per second over 513 seconds (8 minutes 33 seconds). This equates to a drop being approximately 39 µl.

Reducing agent concentration

Halved ascorbic acid concentration

The concentration of the ascorbic acid added to the reaction system was halved by doubling the volume of water (and halving the initial concentration) of the ascorbic acid stock solution added to the system. The total volume of the reaction system was kept at 500 cm^3. This means the total amount of ascorbic acid in the system is maintained. Lowering the concentration of the reagent added means there is not as steep a concentration gradient between the initial and final concentrations, thus maintaining a more

homogenous environment and potentially leading to the formation of more monodisperse particles. For this variation, 40 cm^3 of 0.005 mol/dm^3 (0.0352 g) of ascorbic acid was added.

Excess ascorbic acid

The amount of ascorbic acid added to the reaction system was increased from being in 33.3% excess to being in 50% excess with respect to the silver ions present. This was done to increase the rate of reaction, which could possibly result in the formation of more particles and reduce particle growth, thus producing smaller more monodisperse nanoparticles. To keep the concentration of the added ascorbic acid at a constant 0.01 mol/dm^3, an increased volume of 22.5 cm^3 was added (0.0396 g).

Order of chemical addition

The order of addition of the chemicals to the system was changed to see what effect adding silver nitrate to a solution already containing the reducing agent. Method One was followed exactly except that silver nitrate was added *after* ascorbic acid.

4.1.2 Method Two

The method presented by Yang *et al.* (2011) was followed exactly. To prevent light affecting the silver nanoparticle nucleation and growth, the 250-ml round-bottomed flask used for synthesis was wrapped in aluminium foil. The reaction was performed at 90 °C by placing a silica oil bath on a heating plate, connecting a thermocouple to the heater and positioning the probe in the oil bath. Before heating, 10 mmol of dodecylbenzenesulfonic acid (70 wt.% DBSA in isopropanol, Sigma-Aldrich) was dissolved in 85.30 cm^3 of deionised water to make up 90 cm^3 and the stirrer was switched on at 1000 rpm. Following this, 2 mmol aniline (99%, Sigma-Aldrich) was added and a transparent solution formed. Next, 10 cm^3 of 0.02 mol/dm^3 $AgNO_3$ was added to the solution and the mixture was stirred for 15 minutes to form a DBSA-aniline-$AgNO_3$ aqueous system (DAA system), yielding an overall Ag concentration of 0.4 $mmol/dm^3$. The heating plate was set to heat the silica oil to approximately 105 °C which allowed for some loss of heat between the bath and the reaction vessel. The temperature of the reaction solution was checked regularly using a glass thermometer. The sodium hydroxide is added last because it activates the reaction system by increasing the pH. 4.5 cm^3 of 3 mol/dm^3 NaOH (Sigma-Aldrich) was added to the DAA mixture once it reached 90 °C and this was kept under stirring for one hour. TEM grids were prepared by dripping working solution onto the carbon-coated copper grids and drying in air at room temperature.

The reaction between aniline and Ag^+ in water can be simplified to the balanced equation seen in Equation 4-3. The reaction occurs in a basic environment and is activated through the addition of NaOH to the system. For every two moles of aniline reacted, four moles of metallic silver and one mole of azobenzene are produced.

$$4Ag^+_{(aq)} + 2C_6H_5NH_{2(aq)} \longrightarrow 4Ag^0_{(s)} + C_{12}H_{10}N_{2(aq)} + 4H^+ \qquad \textit{Equation 4-3}$$

The possible mechanism of the oxidation of aniline by silver ions in water is presented in *Scheme 4-2*. The mechanism is based on schemes presented by Z. Khan, AL-Thabaiti, Obaid, & Al-Youbi (2011) and Z. Khan, Hussain, Hashmi, & AL-Thabaiti (2017).

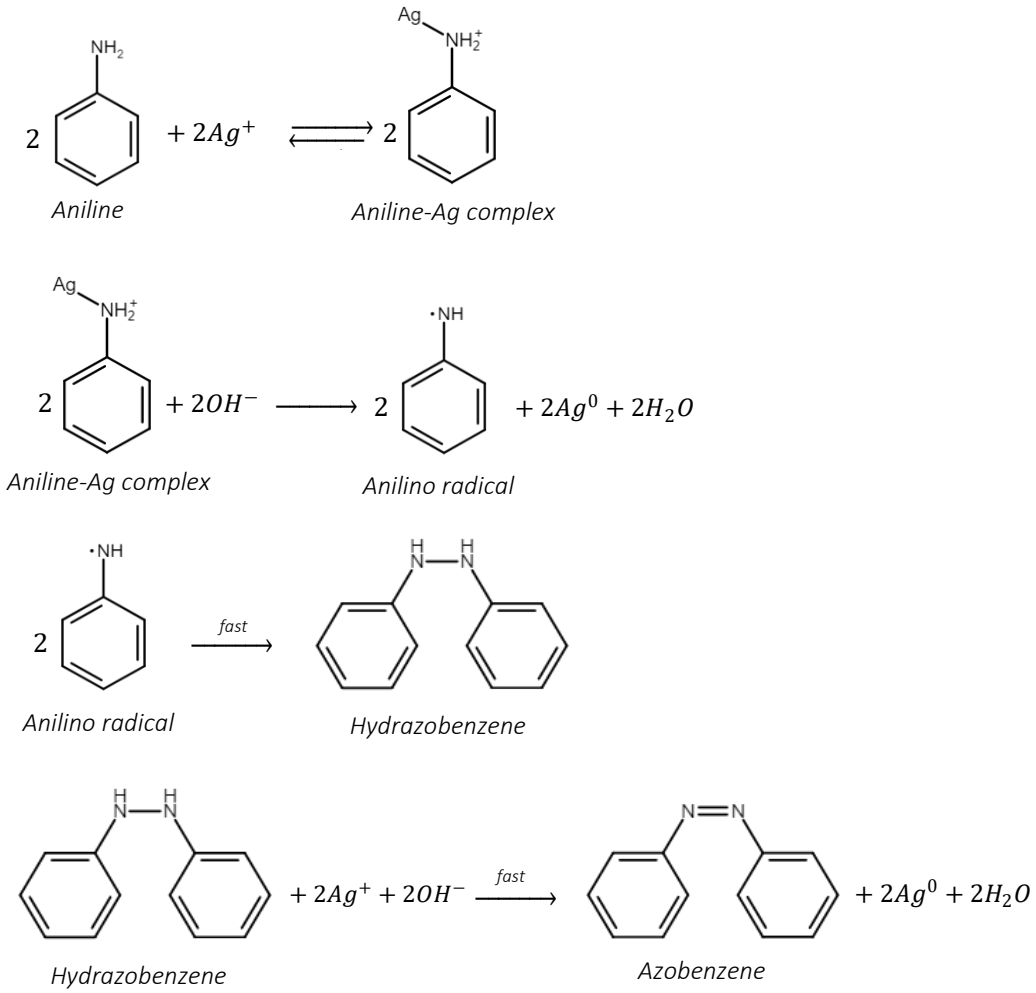

Scheme 4-2: The reaction scheme for the formation of Ag nanoparticles using aniline

Ag^+ ions strongly binds to the nucleophilic -NH_2 group on the aniline to form an aniline-Ag complex. The subsequent oxidation-reduction reaction, the rate-determining step, involves one electron and results in the formation of Ag^0 and an anilino radical. The radical undergoes rapid dimerization to form hydrazobenzene, which, in turn, rapidly oxidizes to azobenzene and causes the reduction of Ag^+ to Ag^0 (Z. Khan, AL-Thabaiti, Obaid, & Al-Youbi, 2011). Azobenzene has been used as a capping agent previously, thus it may have a further stabilising effect on the Ag nanoparticles (Zhou, Ralston, Sedev, & Beattie, 2009).

4.1.2.1 Variations of Method Two

As with Method One, variations of the synthesis using the original surfactant concentration were performed in an attempt to produce smaller particles with a narrow size distribution. The same variations as for Method One were performed, except for synthesis at different temperatures. Because the solvent used is water, nanoparticle synthesis must be performed at temperatures below 100 °C to avoid boiling. The authors of Method Two, Yang *et al.* (2011), experimented with temperature and found that room temperature synthesis produced particles that were bigger, aggregated and had a larger size distribution than particles synthesised at 90 °C.

The variations in the synthesis are described below. In total, including the variations on surfactant concentration, 12 different syntheses variations for Method Two were performed.

Surfactant concentration

As with Method One, three different surfactant concentrations in order to understand the effect the surfactant concentration may have on the synthesised nanoparticles. The masses of each chemical reactant added for this variation are presented in Table 4-2.

Table 4-2: Chemical additions for synthesis Method Two

Chemicals	*Half surfactant concentration*	*Original surfactant concentration*	*Double surfactant concentration*
DBSA in isopropanol	5 mmol	10 mmol	20 mmol
	2.3321 g	4.6641 g	9.3283 g
	87.65 cm^3 DI water	85.30 cm^3 DI water	80.60 cm^3 DI water
Aniline	0.1863 g	0.1863 g	0.1863 g
Silver nitrate	0.0340 g	0.0340 g	0.0340 g
Sodium hydroxide	0.5400 g	0.5400 g	0.5400 g

Vessel size and mixing speed

Changing the size of the vessel used for nanoparticle synthesis essentially changes the effective mixing speed of the system. In a bigger flask, the mixing speed in the centre of the vessel will be faster than the speed on the edge. The effect of the vessel size and mixing speed on the particle size was examined by performing syntheses in 250-ml and 1000-ml round-bottomed flasks at mixing speeds of 500 rpm and 1000 rpm.

Method of NaOH addition

Hot injection

Because a double peak in the PSD graphs was seen, a 'hot' injection method (at 90 °C) was used (Zacharaki, Kalyva, Fjellvåg, & Sjåstad, 2016). The aim was to achieve a smaller mean particle size and particle size distribution than had been produced by inducing a very rapid increase in pH and thus rapid nucleation of Ag aggregates. Method Two was followed exactly with the exception of the addition of NaOH, which was quickly injected into the system when it reached the desired temperature.

Dropwise

Adding the NaOH slowly would mean a slower rate of change in the pH of the mixture thus creating a more homogenous environment and a slower rate of nucleation. This could potentially result in particles of a more uniform size. NaOH was added dropwise at a steady rate over a period of 3.5 minutes (where each drop is approximately 30 µl) when it reached 90 °C.

Reduced aniline concentration

The amount of aniline added to the system was halved to 0.0932 g. The same method as described previously was followed, with a lower mass of aniline making up the DAA system. This was done to see what effect lowering the concentration of the reducing agent had on the particle size.

Order of chemical addition

The order of addition of the chemicals to the system was changed to see what effect adding aniline, the reducing agent, to an already basic solution would have on the particle size. This also meant that

the previously described DAA system was not formed, which could possibly result in a less uniform particle size. Method Two was followed exactly except that aniline was added *after* NaOH.

Increased Ag concentration

Discrepancies in the starting Ag concentration were noted in the paper published by Yang *et al*. (2008). Starting concentrations of both 0.02 mol/dm^3 and 0.2 mol/dm^3 $AgNO_3$ are mentioned throughout the paper. Because using a concentration of 0.02 mol/dm^3 $AgNO_3$ did not reproduce the published results, a concentration ten times higher was used. The same procedure outlined above was followed except a mass of 0.3400 g of $AgNO_3$ was dissolved in 10 cm^3 of deionised water, to yield a concentration of 0.2 mol/dm^3. Once added to the system, the total Ag concentration was 4 mmol/dm^3.

4.1.3 Particle separation and purification

Different methods (physical and chemical) were used in an attempt to separate the silver nanoparticles, in the form of a colloidal dispersion, from the reaction system.

4.1.3.1 Evaporation

To evaporate large volumes of liquid from the dispersion, a rotary evaporator (Büchi Rotavapor® R-205) was used. The evaporation flask containing the sample is rotated in a heated water bath at a user-specified speed under reduced pressure. The vapour is condensed by a cooling coil and the condensate is collected in a flask below the condenser. Because the reaction systems for both methods are mostly aqueous, the rotary evaporator was set at a rotation speed of 150 rpm and a pressure of 72 mbar, and the heating bath at a temperature of 40 °C as advised by the manufacturer.

The difficulty with using such a method is that nanoparticles remain coated in excess surfactant because it is mainly water that evaporates from the sample. It is also a concern that this process may result in particle size changes from Ostwald ripening, exposure to light and/or further reaction.

4.1.3.2 Centrifugation

Samples were centrifuged in a Beckman & Coulter Avanti J-E using a JA-20 fixed angle rotor at rotational speeds of up to 20,000 rpm for two hours at a time. This resulted in some particles settling but the colloidal dispersion remained yellow, indicating the presence of smaller nanoparticles in the supernatant. Subsequent centrifugation of the supernatant had little effect on the smaller particles still suspended in the dispersion. These smaller particles are critical for the antibacterial testing of the synthesised silver nanoparticles, thus centrifuging alone is not sufficient for the separation of the particles from the reaction system.

4.1.3.3 Phase extraction and centrifugation

A range of different organic solvents (Table 4-3) were investigated for use in phase extraction separation with the aim of extracting either the excess surfactant or the silver nanoparticles from the reaction system. These solvents were selected based on their use in literature for separations of nanoparticles from dispersions, as well as their availability within the laboratory.

Table 4-3: Properties of solvents used in phase-extraction experiments

Solvent	*Dipole moment (D)*	*Density (kg/m^2)*	*Solvent type*
Acetic acid	1.74	1049	Polar protic

Acetone	2.88	786	Polar aprotic
Benzene	0	879	Non-polar
Chloroform	1.04	1498	Non-polar
Cyclohexane	0	779	Non-polar
Dichloromethane (DCM)	1.60	1327	Non-polar
Diisopropyl ether	1.13	725	Non-polar
Dimethyl sulfoxide (DMSO)	3.96	1092	Polar aprotic
Ethanol	1.69	789	Polar protic
Hexane	0	655	Non-polar
Isopropanol	1.66	785	Polar protic
Methanol	1.70	791	Polar protic
Toluene	0.36	867	Non-polar
Water	1.85	1000	Polar protic

The dipole moment of a solvent is an important factor to consider in separation as it can essentially be used for the qualitative understanding of the strength of the intermolecular interaction between the extractant and the solvent (Bailey & Mahi, 1987; Kuipa & Hughes, 2002).

As a first step, the surfactants from Method One and Method Two, SDS and DBSA, respectively, were combined with each of these solvents to assess their solubility. Once this was ascertained, 1:1 mixtures (total volume of 1 ml) of the synthesised nanoparticle dispersion and each of the solvents were prepared in microcentrifuge tubes. These tubes were centrifuged three times for 15 minutes each at 13,000 rpm using a *Hiraeus Biofuge Pico* microcentrifuge. Between each centrifugation cycle, the tubes were rotated 180° in the centrifuge. Performing this separation study on a small scale meant that the effectiveness of the solvents as phase extraction diluents could be determined rapidly and inexpensively (i.e. only using small volumes of synthesised Ag dispersions and solvents). Once the best solvents for effecting the separation of the solid nanoparticles from the reaction liquid were confirmed, studies using the best identified solvents were pursued.

Mixtures of the Ag dispersion (15 ml) that was found to have the smallest mean particle size (for each of Method One and Method Two) with the best solvents (15 ml) were made in 50-ml centrifuge tubes. The tubes were centrifuged at 20,000 rpm for 45 minutes, rotated 180° and centrifuged for a further 30 minutes at the same speed. The resulting supernatant (termed the first supernatant) from each of the dispersion/solvent mixtures was collected for UV-Vis, pH and silver ion concentration analysis. The centrifuge tubes were then refilled with 30 ml (plus an additional amount to ensure each tube had the same mass) of the respective solvents and then sonicated to loosen and redisperse the particles. The tubes were centrifuged at 12,000 rpm for 30 minutes, rotated 180° and centrifuged for another 30 minutes. The supernatants formed following this centrifugation cycle (termed the second supernatants) were collected. The particles were redispersed in solvent and were left in the fume hood overnight so as to evaporate off the excess solvent. It was found that, after two washes, the particles were still coated in surfactant thus three further washing and centrifugation cycles were undertaken. The complete description of these cycles are as follows:

1. Centrifuge at 20,000 rpm for 1 hour 15 minutes, pour off supernatant (first supernatant) and collect, add fresh solvent and redisperse

2. Centrifuge at 12,000 rpm for 1 hour, pour off supernatant (second supernatant) and collect, add fresh solvent and redisperse
3. Centrifuge at 10,000 rpm for 1 hour, pour off supernatant, add fresh solvent and redisperse
4. Centrifuge at 10,000 rpm for 30 minutes, pour off supernatant, add fresh solvent and redisperse
5. Centrifuge at 10,000 rpm for 30 minutes, pour off half the supernatant and pour the nanoparticles in solvent into a beaker for overnight evaporation in the fume hood

Different rotation speeds were used because of the availability of centrifuges, which each have different rotational speed capabilities, within the laboratory. After evaporation of the solvents, attempts to collect the dry particles were made by scraping the nanoparticles from the bottom of the beakers. Based on how easily the particles formed a dry powder, the best solvents for separating out the nanoparticles from their dispersions were chosen.

4.2 Characterisation of silver nanoparticles

The main method of characterisation used on the silver nanoparticles was transmission electron microscopy (TEM) imaging. This was performed largely to determine the particle size distribution of the synthesised nanoparticles. As previously highlighted in Section 2.4.1, monodisperse particles of 10 nm or less are desired to isolate the effect on silver ions on the antibacterial mechanism of silver nanoparticles. Therefore, it is important to determine the size of the particles in a particular sample.

4.2.1 Transmission electron microscopy

All the TEM images presented in this work were taken using an FEI Tecnai F20 transmission electron microscope equipped with a field emission gun (FEG) and operated at 200 kV. Briefly, high-energy electrons, emitted after heating a zirconia-coated tungsten crystal to approximately 2100 °C, are focused into a beam using an electromagnetic condenser lens. The electron beam is passed through the specimen to be studied and interacts with it. Some electrons pass through the sample and others are scattered, depending on the thickness and density of the materials present. The subsequent beam is focused by electromagnetic lenses and is projected onto a screen or camera. For bright field TEM, used in this study, the darker areas in the projected 2D image show where the sample is thickest or contains denser materials.

4.2.1.1 Sample preparation

The reaction solution, containing silver nanoparticles and excess reagent/surfactant chemicals, was dripped onto a carbon-coated copper TEM grid using a pipette. The grid, which was placed on a piece of filter paper, was dried at ambient conditions to remove excess liquid and leave behind solid silver nanoparticles. Unless the sample was specifically aged, the TEM grids were prepared on the day of nanoparticle synthesis to limit the change in size or other properties of the nanoparticles over time. Although simpler, using the reaction solution meant that some carbon-containing chemicals were left on the grid which may cause some contamination to occur when the sample is under the electron beam in the TEM. Where possible, at least 500 nanoparticles were counted.

4.2.1.2 Characterisation software

The TEM images (in TIFF format) were studied using ImageJ, open-source image processing software. Once an image is open within the software, characterisation of the particles can be done. The method

of measuring the nanoparticle sizes is described here in detail because the results thereof are integral to this study.

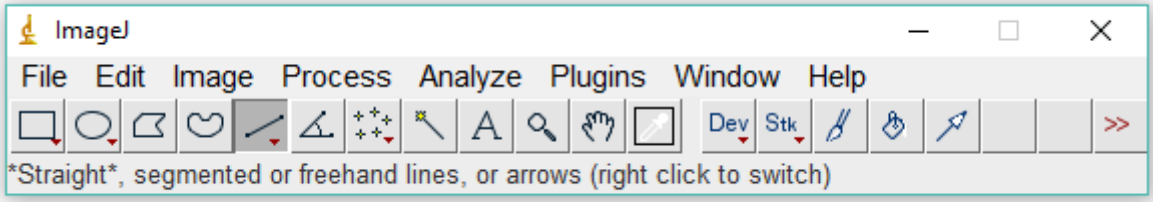

Figure 4-1: ImageJ menu bar with "straight" line tool selected

The scale of the image was set using the scale bar on the TEM images. A straight line was drawn (using the tool selected in *Figure 4-1*) along the scale bar and the 'Set Scale' option under 'Analyze' on the menu bar. This option brings up a window in which the pixels measured using the scale bar can be described according to the scale of the image.

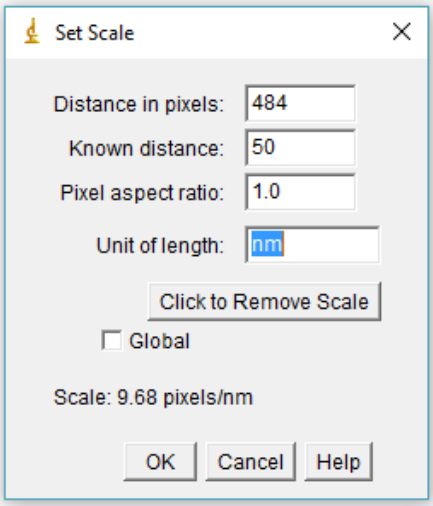

Figure 4-2: The 'Set Scale' window in ImageJ

Using the straight-line tool, the particles were measured by drawing a line across the diameter and pressing 't' on the keyboard to record the measurement. This action brings up the 'Region of Interest (ROI)' Manager window in which the 'Show All' and 'Labels' options, seen in *Figure 4-3*, can be selected to ensure each particle is only measured once. When all the particles on a single image were measured, the 'Measure' button on the ROI Manager window was selected which allows for measurements to be saved in *csv* format.

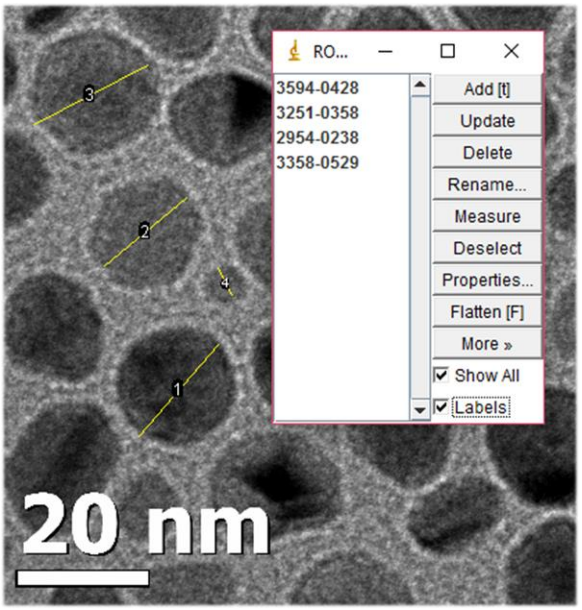

Figure 4-3: Particle measurements and the 'ROI Manager' window

4.2.1.3 Particle size analysis

Particle size distributions were generated from the measurements produced using ImageJ. Particles were classified into size classes with an interval size of 1 nm, starting with the interval $0 \leq x < 1$, for the purposes of constructing bar graphs to show the particle size distributions. To allow for easy comparison of samples, the median, sample mean, and standard deviation of each data set was calculated for the raw data. Calculating these statistical values indicates whether the desired particle size has been attained and how monodisperse the synthesised particles are. The mean particle size and associated standard deviation were determined both for the number-based and volume-based size distributions. The number-based distribution gives an idea of the range of sizes of each of the formed particles, however the volume-based distribution essentially shows the distribution of the mass of silver within the system and relates this to a particle size.

The mean particle size is not entirely indicative of the characteristics of a sample. For example, in a data set with outliers, the mean may be skewed thus giving an inaccurate summary of the data. Therefore, to more accurately describe the sample, the median was also calculated.

The number-based sample mean ($\bar{x}_{\mathrm{N}}$) is the arithmetic average of the data set and is calculated by summing the particle sizes (x) and dividing by the number of particles (n), as per Equation 4-4. The number-based sample standard deviation (s_N), calculated by Equation 4-5, is used to quantify the amount of variation within the particle sizes. A lower value of the standard deviation indicates a more monodisperse sample. The median value is determined by finding the 'middle' number in a data set arranged in numerical order (i.e. $\frac{n}{2}$); if there is an even number of data points in the set then the median value is the average of the two middle numbers.

$$\bar{x}_{\mathrm{N}} = \frac{\sum_{i=1}^{n} x_i}{n} \qquad \textit{Equation 4-4}$$

$$s_N = \sqrt{\frac{\sum_{i=1}^{n}(x_i - \bar{x}_N)^2}{(n-1)}} \qquad \textit{Equation 4-5}$$

The measured particle sizes were translated into volume using the assumption that each particle is spherical (Equation 4-6). The volume-based mean particle size ($\bar{x}_V$) was calculated using Equation 4-7 and the volume-based standard deviation (s_V) was calculated using Equation 4-8.

$$V_{particle} = \frac{4}{3}\pi\left(\frac{d_{particle}}{2}\right)^3 \qquad \textit{Equation 4-6}$$

$$\bar{x}_V = \frac{\sum_{i=1}^{n} n_i x_i^4}{\sum_{i=1}^{n} n_i x_i^3} \qquad \textit{Equation 4-7}$$

$$s_V = \sqrt{\frac{\sum_{i=1}^{n} n_i x_i^3 \left(x_i - \bar{x}_V\right)^2}{\frac{n-1}{n}\sum_{i=1}^{n} n_i x_i^3}} \qquad \textit{Equation 4-8}$$

4.2.2 Ultraviolet visible spectroscopy

The colloidal dispersions of silver were analysed using ultraviolet-visible (UV-Vis) spectroscopy prior to TEM analysis. This was done to give an initial indication of whether the different syntheses methods produced nanoparticles of different sizes or shapes (Baser *et al.*, 2011; Haiss *et al*., 2007). The SPR (surface plasmon resonance) peak of spherical silver nanoparticles is generally positioned between 380 nm and 430 nm and strongly depends on the shape, size, structure, and assembly of the nanoparticles (Amendola, Bakr, & Stellacci, 2010). It has been reported that there is a blue or red shift in this SPR peak with a decrease or increase in particle size, respectively (Martinez-Castanon, Niño-Martínez, Martínez-Gutierrez, Martínez-Mendoza, & Ruiz, 2008). Bhui *et al.* (2009) also state that the absorption efficiency of a spherical metallic nanoparticle is affected by the dielectric constant of both the metal and the medium, and by the particle size. For non-spherical (or irregularly-shaped) particles, more than one plasmon band is expected which may result in the appearance of a broad peak as each of these bands combine (Martinez-Castanon, Niño-Martínez, Martínez-Gutierrez, Martínez-Mendoza, & Ruiz, 2008). Broad peaks also result from wide particle size distributions.

For this study, a Thermo Scientific™ GENESYS 10S UV-Vis spectrophotometer was used. Using the associated software, VISIONlite™ (version 5.2), a scan of each of the analysed samples was performed from 200 nm to 900 nm. The baseline used in each case was deionised water, however, for the synthesised dispersion, scans of the reaction solutions were performed too.

4.2.3 Silver ion concentration measurement

A Mettler Toledo perfectION™ combined Ag^+/S^{2-} ion selective electrode (ISE) was used to determine the concentration of silver ions (in ppm) in the Ag NP dispersions. The electrode is an attachment to the Mettler Toledo SevenCompact™ pH/ion meter S220 and is operated similarly to a pH meter. Before operation, the ISE is filled with the reference electrolyte solution Ion Electrolyte B (Mettler Toledo, composition not specified) and is calibrated using 100 ppm and 1000 ppm Ag^+ solutions. To measure the ion concentration of a sample, the electrode probe tip is fully immersed in the sample. Note that the sensor is made of epoxy resin and therefore cannot be used with acetone.

4.3 Silver nanoparticles on fibre filters

The silver nanoparticles were deposited on quartz fibre filter discs using the spark discharge method. This synthesis was performed by Manju Bhamidipati within the Department of Chemical Engineering at the Delft University of Technology in The Netherlands. Nanoparticles are most often deposited on textiles via wet-chemistry techniques, such as the pad-dry-cure process or the cold pad-batch method (Ki, Kim, Kwon, & Jeong, 2007; Lim & Hudson, 2004). Such methods often result in the production of toxic liquid wastes and the presence of impurities within the synthesised material. A gas phase synthesis method was thus chosen as a more environmentally friendly synthesis and deposition process, leading to pure nanoparticles. Low loadings of silver nanoparticles were used on the fibre discs to ensure that, after disposal, they are harmless to humans and the environment (Bhamidipati, 2017; Feng *et al*, 2016).

4.3.1 Synthesis and deposition process

A schematic of the spark ablation process is shown in Figure 4-4. Pure, room-temperature nitrogen gas (N_2), acting as the carrier gas, is passed through the spark generator via a mass flow controller. The spark generator produced a high voltage spark with a spark frequency of 1000 Hz and a capacitor potential difference of 1000 V. The carrier gas quenches the vapours produced from the metal electrodes (made of silver, in this instance) by the spark, producing particles via condensation. A supersaturated cloud, comprising electrode material vapours and carrier gas, is formed between the gap of the electrodes ($\sim$1 mm) within the spark generator. Alloyed nanoparticles can be made by using electrodes of two different metals (e.g. silver and copper).

The extremely high supersaturations in the rapidly quenched vapour cloud results in the critical nucleus size being of the atomic scale and the growth of the particles can thus be modelled as a consequence of particle-particle collisions (Feng, Biskos & Schmidt-Ott, 2015). The aerosol stream, consisting of the formed silver nanoparticles and the inert carrier gas. This is fed into a tube oven, maintained at the melting point of silver (961 °C), where heat-induced coalescence (i.e. sintering) is used to produce spherical nanoparticles from agglomerates that formed (Bhamidipati, 2017).

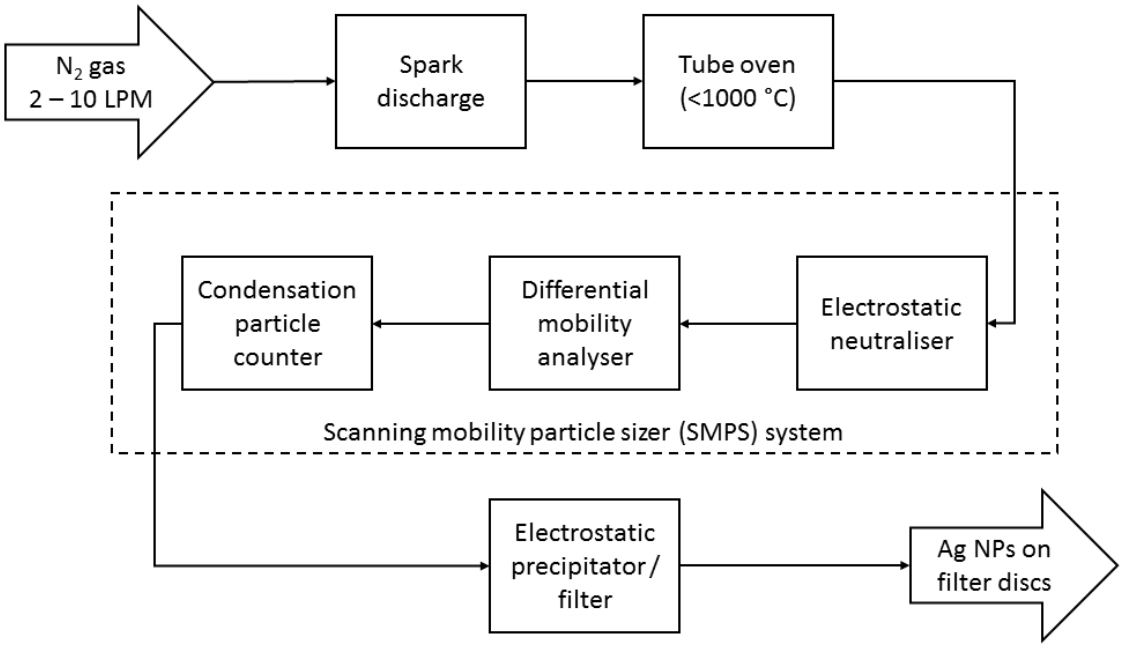

Figure 4-4: Schematic of the generation of aerosol flow using silver nanoparticles

The size distribution of the charged nanoparticles is measured using a scanning mobility particle sizer (SMPS) system. The electrostatic neutraliser (also called a bipolar charger) is used to bring the particle charge distributions to Boltzman Equilibrium, a stationary charging state (Bhamidipati, 2017). The neutraliser was, however, not used in this setup because it increases the residence time of the nanoparticles in the system before reaching the differential mobility analyser (DMA) by approximately seven seconds which leads to undesired agglomerate formation (Bhamidipati, 2017; Feng, Biskos & Schmidt-Ott, 2015). The DMA separates charged particles based on their electrical mobility, which is a function of particle size, thus allowing for size selection and the production of monodisperse particles. The aerosol is saturated with water or 1-Butanol in the condensation particle counter (CPC). The supersaturation of the vapour and subsequent condensing of vapour on the particle surface results in the production of optically detectable particles. A laser beam assists in counting the number of particles present in the stream per cubic centimetre whilst the intensity of scattered light from the beam is used to measure particle size (Bhamidipati, 2017).

The resulting monodisperse particle stream is collected on a fibre filter disc by securing a filter holder perpendicular to the particle flow at the end of the CPC or on a TEM grid by placing the grid on an electrostatic precipitator (Bhamidipati, 2017). The fibres of the quartz fibre filter discs are woven in a criss-cross mat fashion, equivalent to a series of thin filters placed on top of each other, to ensure maximum contact with the particles. The filter discs have a diameter of 47 mm, a thickness of 430 µm and weigh approximately 0.1475 g (85 g/m^2)

4.3.2 Characterisation of deposited silver nanoparticles

Scanning electron microscopy (SEM) was used to image the nanoparticles on the quartz fibre filters. TEM could not be used without performing ultramicrotomy because of the thickness of the filters. An FEI Nova NanoSEM 230 was used for this study. It is a high-resolution field emission SEM that combines microanalytical capabilities (high voltage) and high-resolution imaging (low voltage) whilst under low vacuum operation. The SEM was operated using both a backscatter and a secondary detector. The secondary electrons (SE), produced through inelastic scattering, originate from the surface or near-surface layer of the specimen and allow for topographical analysis (Goldstein *et al.*, 2017). The backscattered electrons (BSE) originate from a wide region within the specimen being analysed. They are generated by elastic collisions of electrons with atoms that reverse their initial trajectory. The BSE signal can provide information on the composition, topography and crystallography of a specimen (Goldstein *et al.*, 2017). Larger atoms (i.e. those with a higher atomic number) scatter electrons more strongly; thus, the differences in BSE intensity can be used to identify differences in composition (Goldstein *et al.*, 2017). SPIDER (System for Processing Image Data from Electron microscopy and Related fields), an image processing software package, was used to view, analyse and record SEM images.

Pieces of the quartz fibre filters were carbon-coated to inhibit charging, reduce potential thermal damage and improve the secondary electron signal necessary for the topographical SEM examination. Images of each filter piece were recorded at 5 kV and 200,000x magnification using the secondary electron detector. In instances where there was uncertainty surrounding the presence of impurities or the composition of the nanoparticles, the backscatter detector was used to confirm that the analysed nanoparticles were of the desired metal (i.e. silver or copper).

Where possible, 300 particles were measured using ImageJ following the previously described procedure. In some cases, the nanoparticle deposition was very low thus fewer particles were

measured. Since it was found that the particles on the filters are *not* perfectly spherical, but rather spheroidal, a pair of perpendicular 'diameter' measurements (*a* and *c*) were made for each particle and the spheroidal volume was calculated using Equation 4-9. Since the image is 2D, only two of the particles' dimensions could be measured. An assumption was thus made that (for a spheroid with dimensions *a*, *b*, and *c) a = b* and *a > c*. Because most of the particles visible in the SEM images did not appear elongated, the volumes of the particles were estimated using an equation for an oblate (flattened) spheroid ($V_{o.s.}$). This volume was then related back to an equivalent spherical particle diameter (D_e) by Equation 4-10.

$$V_{o.s.} = \frac{\pi}{6} a^2 c \qquad \textit{Equation 4-9}$$

$$D_e = 2\left(\frac{3}{4\pi} V_{o.s.}\right)^{\frac{1}{3}} \qquad \textit{Equation 4-10}$$

Statistical values (both number-based and volume-based) for the equivalent particle diameters measured for each sample were determined using Equation 4-4 to Equation 4-8.

4.4 Antibacterial efficacy studies

Basic investigations were performed to determine antibacterial efficacy of the silver-loaded fibre filters. Studies were also performed using $AgNO_3$ for comparison. *Escherichia coli* (*E. coli*) was chosen as the indicative bacterium because it is common, is often found in water sources, and has been used in numerous nanotoxicology studies thus making it easier for comparison. Unfortunately, because difficulty was experienced in separating the synthesised silver nanoparticles from the liquid dispersion without affecting the particle size, antibacterial efficacy studies were not performed on the Ag nanoparticles.

4.4.1 Time-kill curve development

A laboratory-type *Escherichia coli* strain (*DH5α*) was used for the initial $AgNO_3$ bactericidal studies (at 6 µM and 12 µM Ag^+) and then a wild-type *E. coli (ATCC ® 25922 ™)* was used for the remaining studies. This was due to the availability of *E. coli* strains within the laboratory. An *E. coli* colony was grown on a lysogeny broth (LB) agar plate (LB medium supplemented with 15 g/L bacteriological agar) and used to make a starting inoculum in LB (10 g/L Tryptone, 5 g/L yeast extract, 5 g/L NaCl). The starting inoculum was left to grow overnight on a shaker (at 120 rpm) in an incubator set at 37 °C. The following day, a colony count of this inoculum was performed using a counting chamber (hemocytometer) under a microscope. The required amount of *E. coli* to produce a count of 10^6 cells/ml was then spun down at 3000 rpm for 5 minutes using a *Hiraeus Biofuge Pico* microcentrifuge. This allowed the LB medium, in which the bacteria were grown, to be poured off and the bacteria were subsequently resuspended in the desired volume of phosphate-buffered saline (PBS). PBS (137 mM NaCl, 2.7 mM KCl, 10 mM Na_2HPO_4, 2 mM KH_2PO_4; pH of 7.4) was used as the bacteria medium for the antibacterial studies because it does not provide a suitable environment for bacterial growth (unlike LB) but does allow for bacterial survival. For an experiment with the aim of establishing antibacterial activity, it is best not to have the bacteria colonies both growing and being killed off as this may produce contradictory results.

Once the silver ($AgNO_3$ or filters) had been added to flasks containing the PBS/*E. coli* mixture, timing of the experiment began. It was important to note the precise times sampling takes place so that an accurate time-kill curve could be developed. The table below shows the time intervals that the

experiments were based on. These times were not always exactly met, but attempts were made to stick as close as possible to them.

Table 4-4: Time intervals for sampling of silver/E. coli solutions

Time interval	*Elapsed time (hours)*	*Elapsed time (minutes)*
T_0	0	0
T_1	0.5	30
T_2	1	60
T_3	1.5	90
T_4	2	120
T_5	4	240
T_6	6	360
T_7	9	540
T_8	15	900
T_9	28.5	1710

At every time interval, 100 µL of the solution from each flask was spread on LB agar plates at predetermined dilutions. The LB agar provides nutrients for the bacteria to grow big enough to be visible (and thus big enough to count). A range of different dilutions was used as it was unclear what the cell count would be at each time interval; too high a dilution would mean one would not see cells on the plates whilst too low a dilution would mean there would be too many cells on the plates to count (i.e. too numerous to count, TNTC). In the interim period between sampling, the flasks were placed on a shaker operating at 120 rpm in a 37 °C incubator. Plates were left in the 37 °C until such a time that bacteria colonies had grown big enough to count manually.

Figure 4-5 shows an example of an LB agar plate with a countable number of bacterial colonies and an example with cells that are TNTC.

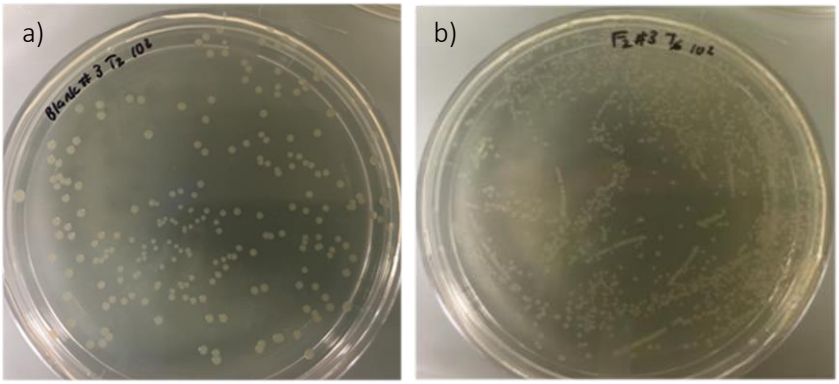

Figure 4-5: LB agar plates with bacteria colonies that are a) easily countable and b) "too numerous to count"

To calculate the bacteria concentration from the plate counts, the following equation is used:

$$Cell\ concentration\ \left(\frac{cells}{ml}\right) = cell\ count\ \times\ dilution\ factor \div vol.liquid\ on\ plate\ (ml) \qquad Equation\ 4\text{-}11$$

4.4.1.1 Silver nitrate studies

Initial experiments with three different concentrations of $AgNO_3$, 0 µM (control), 6 µM and 12 µM, were performed in triplicate using *E. coli* (DH5α). Following the results of this initial experiment, studies were performed at lower $AgNO_3$ concentrations (1.5 µM and 3 µM) using *E. coli* (ATCC® 25922™). A master mix of PBS with an *E. coli* concentration of 10^6 cells/ml was made, and 50 ml was dispensed into nine flasks. A 10 mM $AgNO_3$ stock solution was prepared and used to make solutions in the flasks to the desired $AgNO_3$ concentration.

The experiments were performed as previously described. For the control experiment, a dilution factor of 10^3 was used when plating. The dilution factors used for each time interval for the silver nitrate experiments are presented below. The sampling was stopped at interval T_8 because the bacteria count had reached zero before T_4.

Table 4-5: Dilution factors used for the antibacterial study of $AgNO_3$

Time interval	*Dilution factors*
T_1	10^3, 10^2, 10,1
T_2	10^3, 10^2, 10,1
T_3	10^3, 10^2, 10,1
T_4	10^3, 10^2, 10,1
T_5	10^2, 10,1
T_6	10^2, 10,1
T_7	10^2, 10,1
T_8	10^2, 10,1

Between taking each sample, the flasks were put on a shaker set at 120 rpm in a 37 °C incubator. A cotton wool bung is inserted into the neck of the flask and the flask is covered with foil to prevent contamination and evaporation.

4.4.1.2 Silver-loaded filter studies

To test the antibacterial activity of the silver nanoparticle loaded filters in triplicate, a punch was used to make circular discs of the same size from the filters (Figure 4-6a). Figure 4-6b shows the silver nanoparticle coating on a filter alongside discs that have been in the PBS/*E. coli* solution.

Based on the mass loading, filter size and disc size, the concentration of silver in the flasks could be estimated. The diameter of the actual coating on the filters was measured as they weren't completely coated in silver nanoparticles. The small, punched discs were also measured and found to be 0.6 cm in diameter (an area of 0.28 cm^2). This allowed for an estimation of the mass of silver deposited on each disc, assuming an even distribution of silver across the filter, and, subsequently, the estimation of the mass concentration per surface area of each filter. It can be seen from Figure 4-6b that the silver nanoparticles were not evenly distributed over the filters. To mitigate the effect this may have on the study, the punched discs were taken from areas on the filter that appeared to have a similar silver nanoparticle concentration. This means that, although the concentration of silver in the flasks may not be exactly the value estimated, the concentrations across the different flasks should be very similar. It

must, again, be emphasised that the concentration of silver in the flasks is a best estimate based on the available information. The same experimental procedure, as previously described, was followed. 50 ml of PBS with an *E. coli* (ATCC® 25922™) count of 10^6 cells/ml was dispensed into each flask and two filter discs were added.

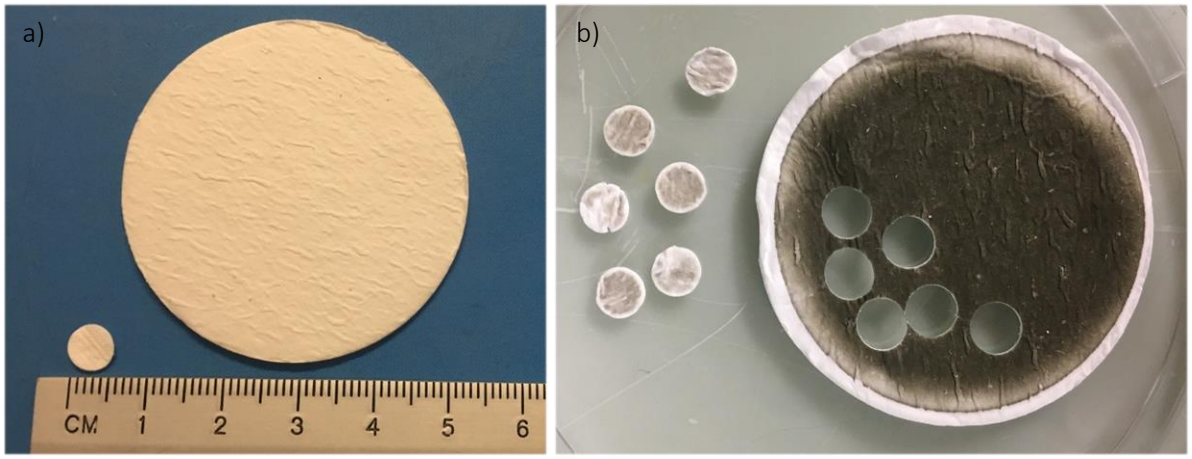

Figure 4-6: a) Comparison of disc and filter size and b) a silver nanoparticle loaded filter alongside used discs

Table 4-6: Estimations of silver concentration on each quartz fibre filter

Filter	*Mass deposited on filter (g)**	*Concentration (µg/cm²)*	*Mass per filter disc (µg)*	*Ag concentration in PBS (µM)*
A1	0.0001	7.96	2.25	0.83
A3	0.0004	37.54	7.79	2.81
A4	0.0005	41.86	11.83	4.39
B3	0.0004	33.48	9.47	3.51
S6	0.0005	32.88	9.30	3.45
F1	0.0002	14.44	4.08	1.51
F2	0.0002	14.44	4.08	1.51
F3	0.0002	14.44	4.08	1.51
F4 [Ag(+) Cu(-)]	0.0004	28.87	8.16	-
F5 [Ag(-) Cu(+)]	0.0002	14.44	4.08	-

* measured by Bhamidipati (2017)

The dilution factors used at each of the sampling time intervals are presented below. For the negative control (blank filter), a dilution of 10^3 was used. Timing of the experiment began once the silver-loaded filter discs were added to the flasks. The large number of experiments that had to be performed (3 x 11 loaded filter discs) meant they were done in four batches, with a blank filter being used as a control study for each batch.

Table 4-7: Dilution factors used for the antibacterial study of Ag loaded filters

Time interval	Dilution factors
T_1	10^3, 10^2
T_2	10^3, 10^2
T_3	10^3, 10^2, 10
T_4	10^3, 10^2, 10
T_5	10^3, 10^2, 10, 1
T_6	10^3, 10^2, 10, 1
T_7	10^3, 10^2, 10, 1
T_8	10^3, 10^2, 10, 1
T_9	10^3, 10^2, 10, 1
T_{10}	10^3, 10^2, 10, 1

As previously mentioned, between taking each sample, the flasks were put on a shaker set at 120 rpm in a 37 °C incubator. The main reason for this was to ensure that the filter discs circulated freely through the solution, instead of remaining stagnant. Figure 4-7 demonstrates how the discs were placed in the flasks, and also shows how a cotton wool bung and foil were used to inhibit outside contamination.

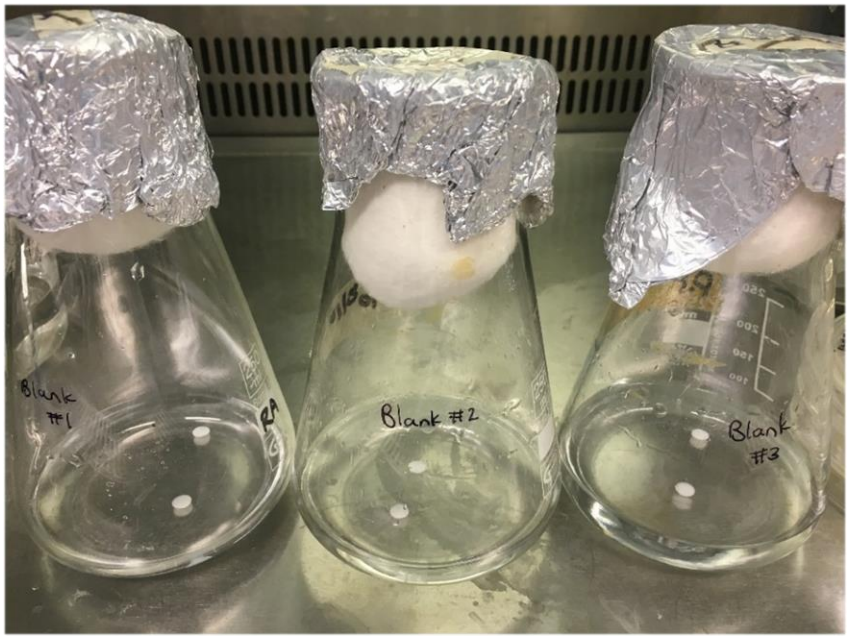

Figure 4-7: Filter discs in flasks

4.4.2 Additional antibacterial activity measurement techniques

4.4.2.1 Fluorescein diacetate assays

The processes of making serial dilutions, plate spreading and manual colony counting that are required for the development of time-kill curves are very labour intensive and time consuming. For this reason, the fluorescein diacetate assay was investigated as a method for determining the number of viable *E. coli* cells more rapidly. Fluorescein diacetate (FDA) readily penetrates the cell membrane and is cleaved within the cell by nonspecific esterases produced by metabolically active bacteria (Wanandy *et al.*,

2004). This cleavage results in the accumulation of fluorescein, a green fluorescent compound that can be detected at excitation/emission wavelengths of 485/520 nm. Because some bacterial media have been found to cleave FDA, thus reducing the reliability of the assay, Wanandy *et al.* (2004) performed a study to determine what the optimal buffer for use with FDA is. MOPS (4-morpholinepropanesulfonic acid) was found to be one of the most suitable buffers (because it produced low background fluorescence) and was therefore used in this investigation.

Following a method described by Dorsey, Yentsch, Mayo & McKenna (1989), a stock solution of 480 µM FDA in DMSO was made. *E. coli* (ATCC® 25922™) in MOPS solutions of 10^8, 10^7 and 10^6 cells/ml were prepared. Five different studies, performed in triplicate at the three different *E. coli* concentrations, were performed using a 96-well microplate. These studies were:

- 200 µl MOPS/*E. coli* mixture without FDA
- 200 µl MOPS/*E. coli* mixture with DMSO (12.5 µl) but without FDA
- 200 µl MOPS/*E. coli* mixture with FDA + DMSO (12.5 µl stock solution)
- 200 µl MOPS/*E. coli* mixture with FDA + DMSO (12.5 µl stock solution) with 6 µM $AgNO_3$
- 200 µl MOPS/*E. coli* mixture with DMSO (12.5 µl) without FDA and with 6 µM $AgNO_3$

The reason so many studies were performed was to account for any background fluorescence contributed by the MOPS, DMSO or $AgNO_3$. To allow time for the absorption of the FDA by the *E. coli* cells, the microplate was placed in 37 °C incubator in the dark for 1 hour before fluorescence measurements were made.

Fluorescence was measured at an excitation wavelength of 485 nm and an emission wavelength of 520 nm using a BMG Labtech FLUOstar Omega plate reader.

4.4.2.2 Disc diffusion tests

Lawns of *E. coli* (ATCC® 25922™ were grown on LB agar plates by spreading 100 µl of PBS containing 10^6 cells/ml onto the plates. Two filter discs from each of the silver-loaded filters tested were placed on each plate. 5 µl of PBS was dripped onto the filters to moisten them, ensuring that the Ag nanoparticles were able to dissolve into Ag^+ on the plates and diffuse into the bacteria on the agar plates.

The idea behind a disc diffusion test is that the antibacterial agent will diffuse from the disc and into the agar, killing the bacteria surrounding the disc in what is termed a 'zone of inhibition'. This zone is easily identifiable as no bacteria grows in the area. The wider the zone, the more potent the antibacterial agent. This test provides qualitative data, rather than quantitative, but allows for easy comparison of the effectiveness of the toxicity of the agent by studying the diameter of the inhibition zone (Hudzicki, 2009). The discs were left on the lawn of *E. coli* for 72 hours, and the zone of inhibition was checked every 24 hours. In the interim, the agar plates were placed in an incubator at 37 °C (the optimum temperature for *E. coli* growth) to ensure that only the Ag^+ diffusion into the bacteria affected their health rather than any other external factor (such as temperature).

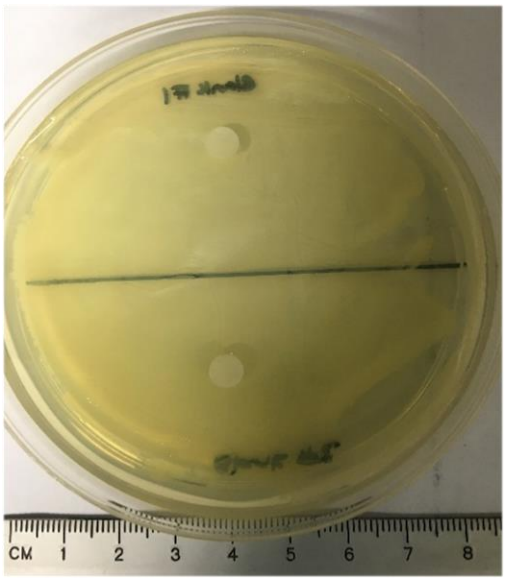

Figure 4-8: Filter discs on a lawn of E. coli for a disc diffusion test

4.4.2.3 Silver ion release measurements

One disc from each of the silver-loaded filters studied, and a disc from a blank filter for the control experiment, were placed into individual vials each containing 10 ml of PBS, and the investigation was performed in duplicate. The same protocol as described for use of the *Mettler Toledo* perfectION™ combined Ag^+/S^{2-} ion selective electrode (ISE) in Section 4.2.3 was adopted. The silver ion concentration in the PBS solution was measured for each of the filter discs after 0 hours, 3 hours, 6 hours, 12 hours and 24 hours of contact. In the interim period, between measuring the Ag^+ concentration, the vials were placed on a shaker set at 120 rpm in a 37 °C incubator (to maintain consistency with the experiments performed for the time-kill curves). The same experiment was repeated using deionised water instead of PBS.

Chapter 5: Silver nanoparticle synthesis and characterisation results

5.1 Method One

This method, outlined by AL-Thabaiti, Al-Nowaiser, Obaid, Al-Youbi, & Khan (2008), uses silver nitrate as the silver precursor, ascorbic acid as the reducing agent and sodium dodecyl sulphate as the surfactant. Initially, their method was followed exactly, however, after numerous attempts, their results could not be reproduced. They claim that spherical, uniformly sized silver nanoparticles approximately 10 nm in diameter were synthesised. A TEM image was provided to demonstrate this and is shown in Figure 5-1, along with a particle size analysis that was performed on the image.

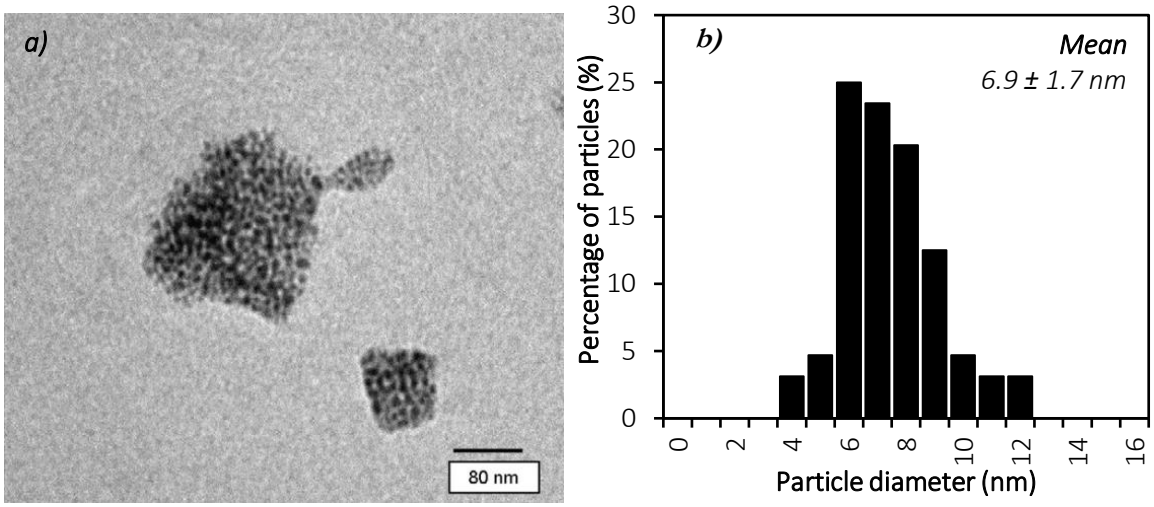

Figure 5-1: a) TEM image of Ag NPs produced by AL-Thabaiti et al. (2008), reprinted with permission, and b) the particle size distribution thereof

As seen from the above figure, the particles are monodisperse and smaller than 10 nm. No particle size analysis was presented by AL-Thabaiti *et al.* (2008), thus comparison of the results produced in this study to those given by the researchers is limited to the data shown in Figure 5-1 and the description provided in their paper. Figure 5-1b was generated for this study for comparative purposes from the image provided by the researchers (Figure 5-1a).

A TEM image and the particle size distribution of the Ag NP dispersion produced by following the original method outlined by AL-Thabaiti *et al.* (2008) are given in Figure 5-2. The TEM image (Figure 5-2a) shows that the nanoparticles produced are not monodisperse, with particles in the same cluster ranging in size from 3 to 20 nm. The particle size distribution graph (Figure 5-2b) further demonstrates this polydispersity and shows a bimodal size distribution which may indicate two separate nucleation and growth steps. Additionally, with a mean particle size of 9.73 ± 7.02 nm and almost half the counted particles larger than 10 nm, the particles are bigger than desired.

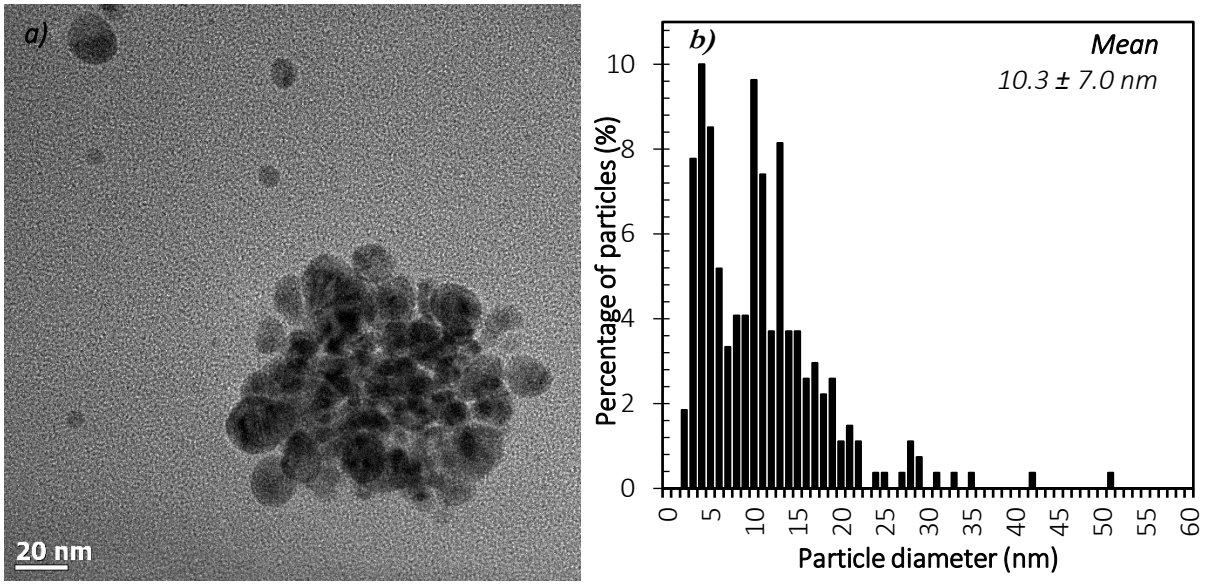

Figure 5-2: a) TEM image of the Ag NPs produced in this study by following Method One in light conditions and b) the number-based particle size distribution of the dispersion

The above synthesis was repeated numerous times so as to rule out the possibility of experimental error. Similar results were found upon each repetition, however, the dispersions produced were slightly different colours, ranging from yellow to pale orange, and seemed to change colour over time. Colloidal dispersions of spherical silver nanoparticles within this size range are expected to be yellow due to their localised surface plasmon resonance spectra which are highly size and shape dependent (Huang & Xu, 2010). This led to the idea that slight synthesis variations may have a significant effect on the particle size. Several variations of this synthesis method were thus performed; these included changing the surfactant concentration, increasing the reaction temperature and adding the reducing agent dropwise. None of these synthesis variations, the complete results of which can be found in Appendix A.1.2, produced stable, uniformly-sized nanoparticles with a diameter of 10 nm or less, as desired. However, the variation in reaction conditions did produce particles of slightly different sizes. These particle sizes are presented in Table 5-1.

Table 5-1: Summary of the sizes of particles produced whilst exposed to light using Method One

Synthesis variation	*Mean particle size (nm)*	*Median particle size (nm)*
Original method (no variation)	10.3 ± 7.0	9.7
Halved surfactant concentration	8.2 ± 14.6	5.5
Doubled surfactant concentration	21.6 ± 22.6	17.6
Higher temperature: 40 °C	6.3 ± 8.7	4.5
Higher temperature: 90 °C	11.9 ± 18.1	6.8
Halved reducing agent concentration	6.3 ± 5.6	4.5
Dropwise reducing agent addition	3.9 ± 2.4	3.2

Two different measures of central tendency have been provided in Table 5-1: the mean particle size with the standard deviation of the mean and the median particle size. A median value that is lower than

the mean value, as is the case with all the synthesis variations shown above, indicates data skewed to the right. In other words, whilst there were many smaller particles measured, larger particles are also present in the dispersions (most likely resulting from agglomeration and inhomogeneous growth) and this leads to a high value of standard deviation in the data. Here, standard deviation is used to show the uniformity of the particles, with a low value showing greater monodispersity. Both the temperature and surfactant concentration variations resulted in dispersions with large particle size ranges which are not favourable. Additionally, these dispersions were opaque, and sedimentation occurred over time.

The particles produced by halving the reducing agent concentration, and adding the reducing agent dropwise appear to be within the desired size range and are fairly uniform. It was, however, observed that the colour of these two colloidal dispersions changed over time, revealing an instability in the system. After being left at ambient conditions for a week, the particles were again measured using TEM and were found to have changed in size thus explaining the colour change of the dispersion. Ostwald ripening may be the cause of this change, however, because silver is a photocatalyst and because the measured particle size of the particles produced using a lower concentration of ascorbic acid *decreased* over time, it is believed that exposure to light was affecting the size of the particles. Bhaduri *et al*. (2013) used SDS and sunlight to reduce Ag^{+} to Ag nanoparticles whilst Prathna, Raichur, Chandrasekaran, & Mukherjee (2014) used a combination of citric acid and ascorbic acid in the presence of solar radiation to produce Ag nanoparticles. These studies, therefore, show that it is possible for ambient light to affect the growth and nucleation of the silver nanoparticles produced.

Because light appears to affect the Ag nanoparticles, the synthesis was performed in dark conditions. Additionally, because it was found that slightly different synthesis conditions result in different particle sizes, 11 variations of the original synthesis method were performed.

5.1.1 Synthesis variations of Method One in dark conditions

Preparing the silver nanoparticles in dark conditions produced results different to those produced when the dispersion was prepared in ambient light conditions, further supporting the theory that light exposure was influencing the formation and growth of the nanoparticles. It should be noted that the colour of the dispersions produced in light conditions have a much more intense yellow colour than those prepared in darkness. The original preparation method is performed at 25 °C in a beaker at a mixing speed of 1000 rpm using the reactant amounts given in Table 4-1.

5.1.1.1 UV-Vis analysis

UV-Vis absorption spectra may be used to estimate the particle size and concentration of uniformly sized nanoparticles in a dispersion (Baset, Akbari, Zeynali, & Shafie, 2011; Haiss, Thanh, Aveyard, & Fernig, 2007). Before analysing the silver dispersions, the reaction solution without $AgNO_3$ was analysed to find the baseline spectra which is given in Appendix A.1.2. The reaction solution (water, SDS and ascorbic acid) has a peak at 285 nm and no registered noise after approximately 320 nm. This shows that the spectra from the other component chemicals did not interfere with the expected spectrum of the silver nanoparticles, with the SPR peak usually appearing between 380 nm and 430 nm.

The UV-vis spectra of each of the differently prepared dispersions are shown in Figure 5-3. They were not diluted because each was pale enough not to cause noise in the spectra. The spectra were produced using a wavelength range of 200 nm to 900 nm, however, Figure 5-3 shows the spectra from 350 nm to 850 nm to eliminate the reaction solution peak and allow for easier reading of the spectra, whilst the inset shows the spectra from 350 nm to 650 nm.

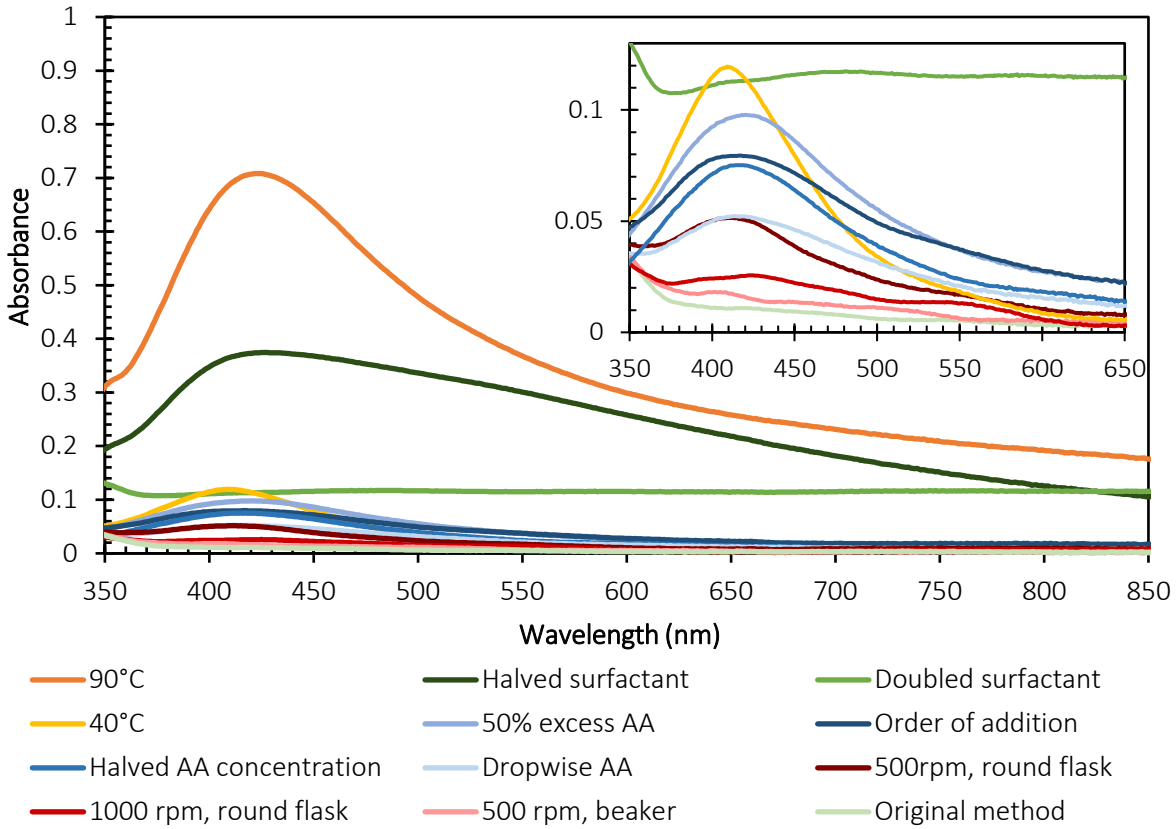

Figure 5-3: Absorption spectra of the Ag dispersions produced using variations of Method One in dark conditions. The inset shows the same data, with the low-absorbance peaks showing more clearly because of a smaller y-axis scale.

AL-Thabaiti *et al*. (2008) report the SPR peak of their synthesised dispersion as 410 nm. For this study, the SPR peaks for the different preparation variations are in the range of 410 to 425 nm. The dispersion prepared in dark conditions exhibited little visible colour which is seen on the UV-Vis spectra (Figure 5-3) as very low intensity absorbance. This low absorbance does not necessarily mean that the dispersion is very dilute (i.e. not all the Ag^+ reacted) and may be a result of the particle size and shape. Bhui *et al*. (2009) performed a theoretical study that calculated the absorption spectra of silver nanoparticles based on Mie's theory and showed that an increase in particle size results in an increase in the absorption efficiency and a decrease in the FWHM (full width at half maximum) of the SPR peak. Peak broadening may also be caused by the particle size distribution and/or the presence of agglomerates and aggregates, however, it is difficult to estimate the particle size from the absorbance spectra if the sample is not monodisperse (Mulfinger *et al*., 2007; Tomaszewska *et al*., 2013; Zook, Rastogi, Maccuspie, Keene, & Fagan, 2011). Tomaszewska *et al*. (2013) found, when studying monodisperse and polydisperse silver nanoparticles, that there is no separation of absorption peaks for nanoparticles of different sizes and that the SPR peak is shifted when the dispersion is polydisperse.

The results of these UV-vis scans are ambiguous. It is difficult to draw any meaningful conclusions from the absorption spectra of these colloidal dispersions other than that the particle sizes will be different for the different syntheses variations and that the dispersions are likely to be polydisperse. TEM is, therefore, very important in this study as it is a more reliable technique for determining the particle size distribution.

5.1.1.2 Particle size from TEM

Transmission electron microscopy (TEM) was used to determine the size distribution of each of the nanoparticle dispersions produced. TEM grids were prepared by dripping the dispersion onto the grid *immediately* after synthesis. Using ImageJ freeware, at least 500 nanoparticles were measured from the obtained micrographs. This was, however, difficult in some more dilute systems where particles were extremely dispersed and, in these few instances, 200 – 500 particles were measured.

Most nanoparticles exhibit spherical morphology with some slight deviation. The micrographs shown in Figure 5-4 were chosen as the images which best represented the size distribution of each dispersion. The TEM micrographs of the other synthesis variations are in Appendix A.1.2.

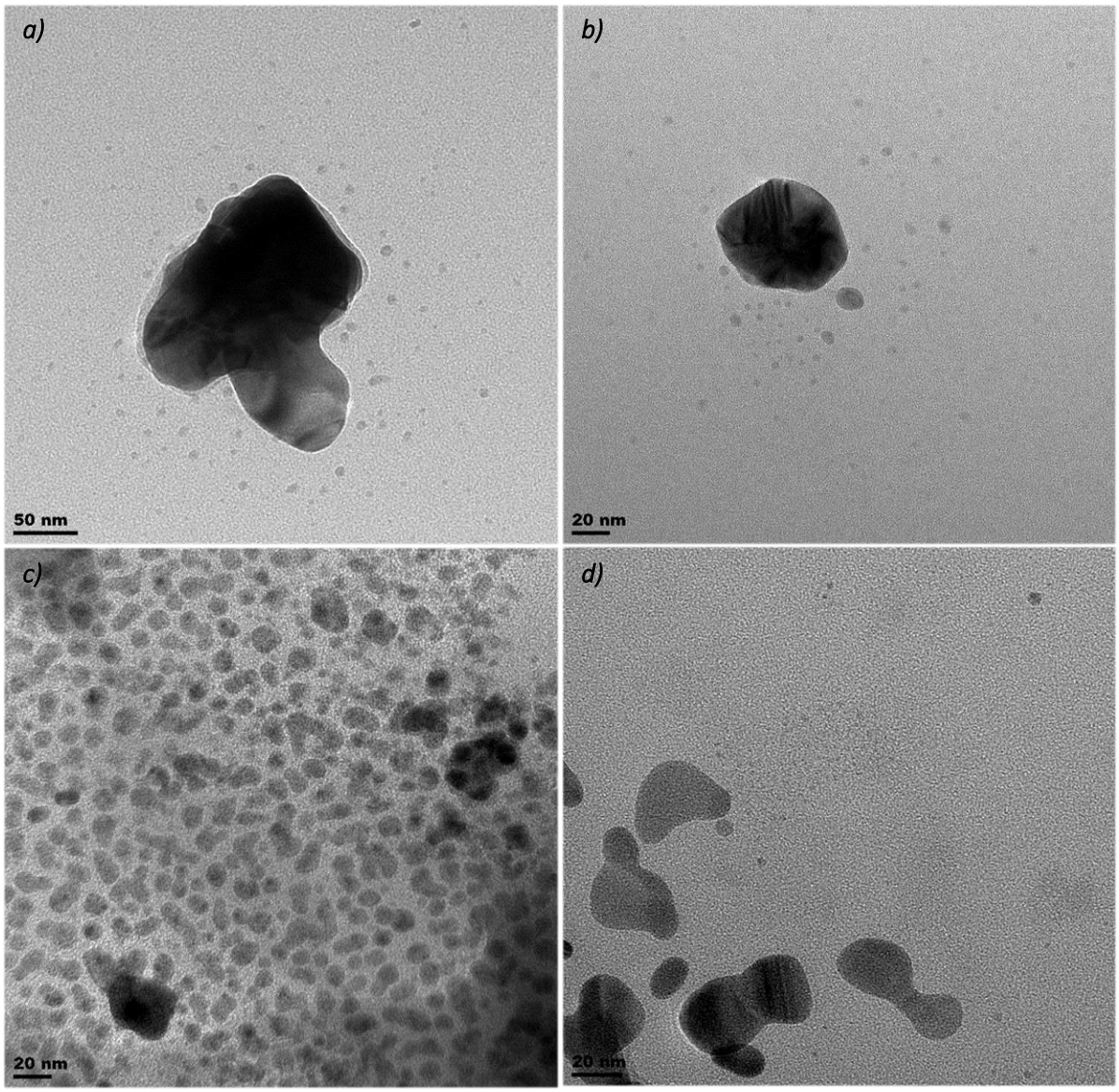

Figure 5-4: TEM micrographs of Method One Ag dispersions prepared in dark conditions using synthesis variation a) halved surfactant concentration, b) round flask at 1000 rpm, c) 40 °C and d) dropwise reducing agent addition

In each of the images shown in Figure 5-4, a wide size distribution is evident with both large aggregates and smaller particles present. Even amongst the smaller particles there is a fairly wide size distribution

which can be seen particularly in Figure 5-4b and d. These differences may suggest two separate nucleation phases which will yield a double peak in the number-based particle size distribution graphs.

Figure 5-5 shows a TEM image of the particles produced following Method One in dark conditions alongside the particle size distribution of the sample.

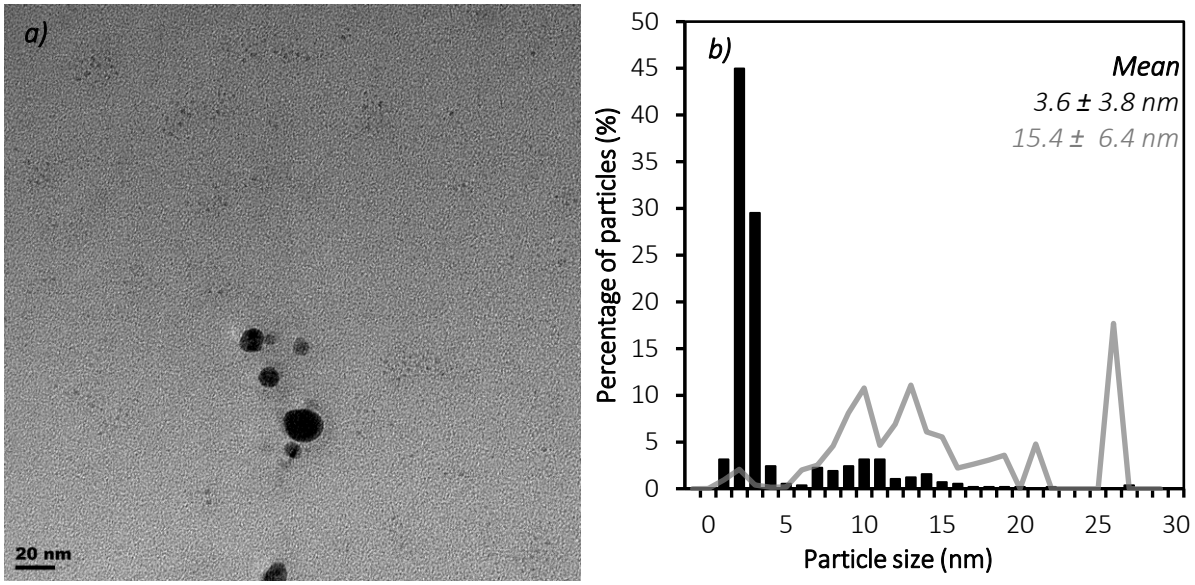

Figure 5-5: a) TEM image of the Ag NPs produced in this study by following the original Method One in dark conditions and b) the number-based (black bars) and volume-based (grey line) particle size distribution of the dispersion

In Figure 5-5a, larger particles of 7 nm to 17 nm can be seen surrounded by many smaller particles of 1 nm to 3 nm. This was the case throughout the sample and is reflected in the number-based particle size distribution shown in Figure 5-5b. This phenomenon may be caused by two separate nucleation phases, with the older particles having a longer growth period. Alternatively, these larger particles may be the result of aggregation. To study the possible formation of aggregates over time, samples of the dispersion could be taken during the reaction and examined using TEM. The particles produced using the original Method One procedure in dark conditions are the smallest of all the particles produced using the different synthesis variations, as evidenced by Table 5-2 and Figure 5-6. By considering only the number-based mean, it could be said that the aim of producing particles smaller than 10 nm has been achieved. However, the volume-based particle size distribution shows that, although more than 90% of the particles in the sample are *smaller* than 10 nm, almost 80% of the mass of silver in the dispersion is from particles of *larger* than 10 nm. This means that, in measuring the antibacterial activity of these particles, there would be uncertainty regarding whether the bactericidal action is mostly due to the release of silver ions (because the majority of particles are smaller than 10 nm) or if there is an interaction between the bacteria and the actual nanoparticles (as has been shown to be the case in particles of larger than ~10 nm, (Sotiriou & Pratsinis, 2010)). It would still be possible to assess the effectiveness of these nanoparticles as antibacterial agents but understanding the mechanism behind the action would be difficult.

Table 5-2: Number-based and volume-based mean particle size and median particle size for each synthesis variation of Method One in dark conditions

Synthesis variation	*Number-based mean particle size (nm)*	*Volume-based mean particle size (nm)*	*Median particle size (nm)*
Original method (no variation)	3.6 ± 3.8	15.4 ± 6.4	2.1
Halved surfactant concentration	4.9 ± 8.6	71.7 ± 15.3	3.5
Doubled surfactant concentration	65.5 ± 117.4	330.3 ± 69.9	2.7
Agitation rate: 500 rpm	5.5 ± 7.5	35.6 ± 13.8	2.3
Agitation rate: 500 rpm, round flask	4.4 ± 5.8	19.9 ± 7.3	4.4
Agitation rate: 1000 rpm, round flask	8.0 ± 13.8	110.3 ± 39.5	3.8
Higher temperature: 40 °C	9.5 ± 8.1	47.3 ± 22.6	8.2
Higher temperature: 90 °C	4.0 ± 6.1	39.6 ± 15.8	2.2
Dropwise reducing agent addition	9.6 ± 11.1	53.0 ± 25.3	5.6
50% excess reducing agent	13.4 ± 18.4	66.9 ± 16.8	6.0
Halved reducing agent concentration	3.8 ± 9.5	73.4 ± 17.6	1.8
Order of addition	10.5 ± 14.5	80.9 ± 42.1	3.5

Studying Table 5-2 and Figure 5-6, one can make a number of conclusions about the effect each of the synthesis variations has on the size of the particles formed.

Surfactants are used to stabilise nanoparticle dispersions and limit aggregation, which is particularly important in the case of silver where aggregation reduces the antibacterial activity of nanoparticles (Kvítek *et al*., 2008). Generally, an increase in surfactant concentration leads to the formation of smaller particles, however, some studies have found that an optimum surfactant concentration exists for the formation of small particles for each system (Dang, Le, Fribourg-Blanc, & Dang, 2012; Patakfalvi, Virányi, & Dékány, 2004). Because of the observation of an optimum surfactant concentration, the surfactant concentration used in the present work was varied. It was found that both halving and doubling the surfactant to silver molar ratio resulted in an increase in size of the particles formed which indicates that the surfactant concentration used for the original preparation method, and the remaining synthesis variations, is the best of the three surfactant concentrations tested. The effect of the SDS on particle size is especially evident at the higher concentration where particles with a diameter of over 400 nm were observed. Samiey, Cheng, & Wu (2014) state that surfactants can influence the nucleation and growth kinetics and reduction of nanomaterials and can even act as reactants. The researchers also describe how micelles can affect electron transfer rates. It is thus suggested that, at this high concentration, the surfactant may affect the reaction rate of the formation of silver nanoparticles, resulting in large particles.

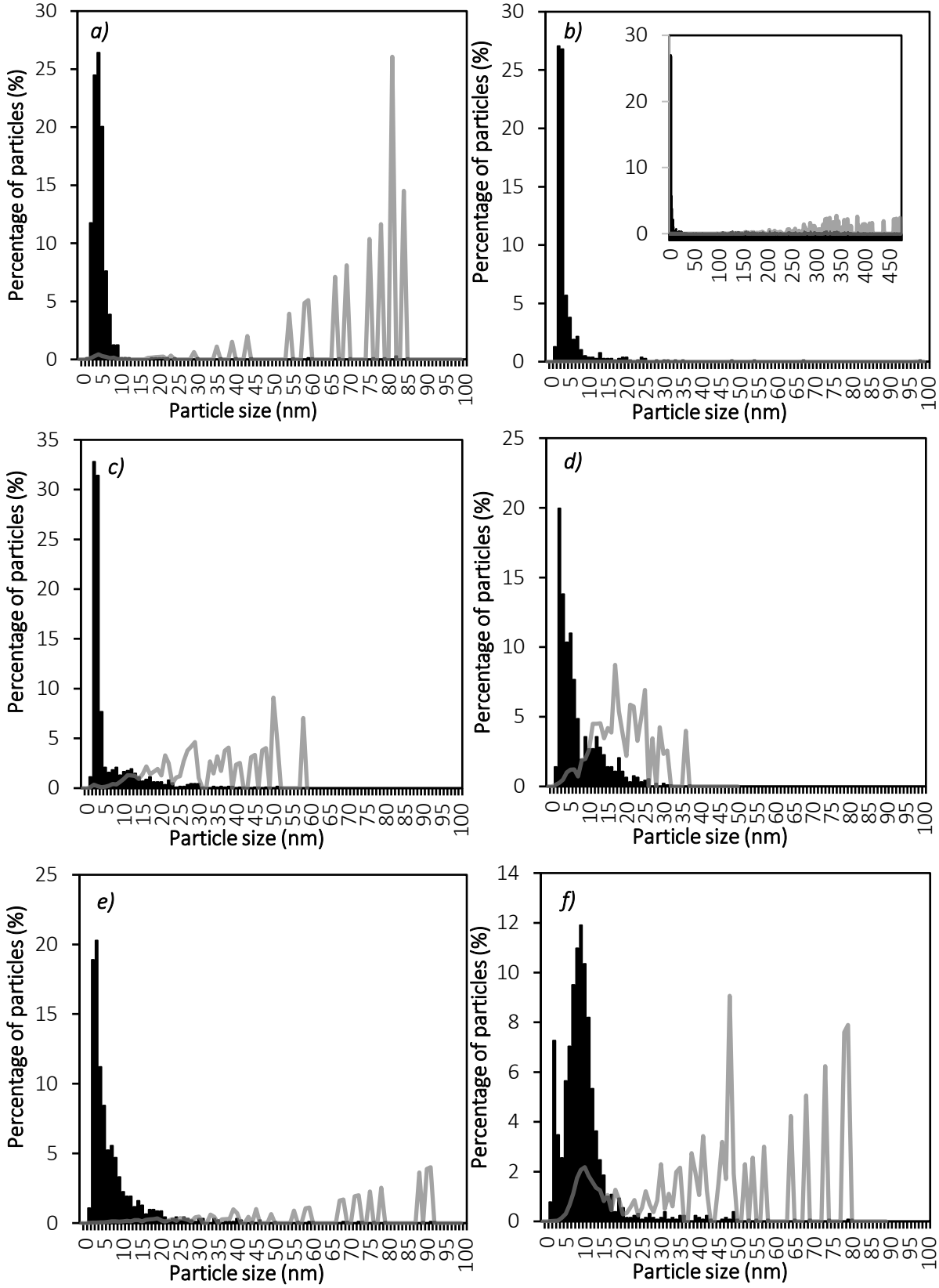

Figure 5-6: Number-based (black bars) and volume-based (grey lines) particle size distribution for the synthesis variation of Method One in dark conditions at a) halved surfactant concentration, b) doubled surfactant concentration with inset showing the size distribution on a larger scale, c) 500 rpm, d) round flask at 500 rpm, e) round flask at 1000 rpm and f) 40 °C

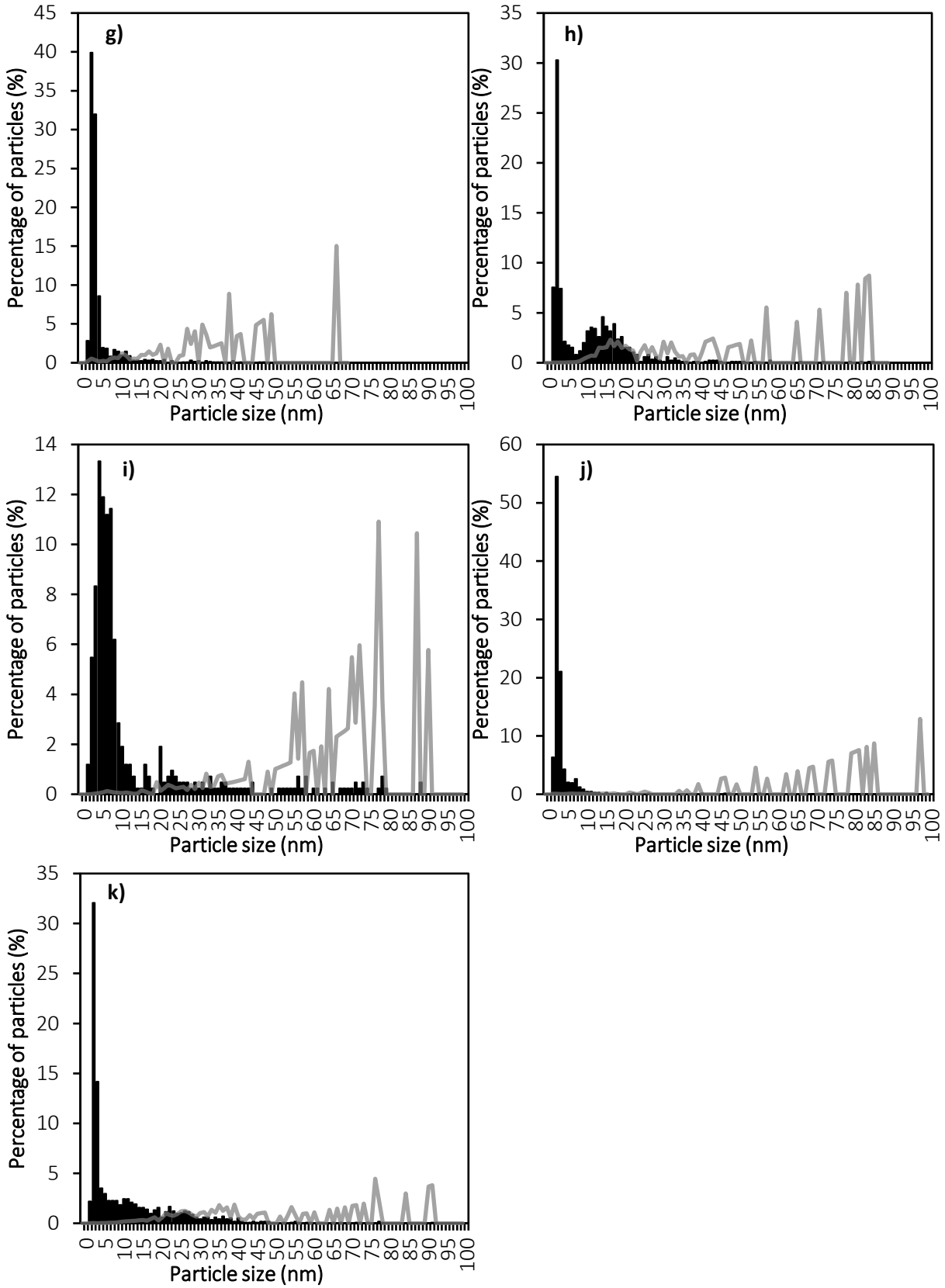

Figure 5-6 continued: Number-based (black bars) and volume-based (grey lines) particle size distribution for the synthesis variation of Method One in dark conditions at g) 90 °C, h) dropwise reducing agent addition, i) 50% excess reducing agent, j) halved concentration reducing agent and k) order of addition

It was expected that a higher agitation rate would lead to the formation of smaller particles because of the creation of a more homogeneous reaction environment. It therefore makes sense that the synthesis at 500 rpm formed larger particles than the original synthesis method, which is performed in a beaker at 1000 rpm. However, the opposite trend was found following the use of a round-bottomed flask; synthesis at 500 rpm produced particles smaller than at 1000 rpm. It appears that the shape of the reaction vessel has a definitive effect on particle size distribution too. Sau & Rogach (2012) state that the agitation rate can affect the metastable zone width, which affects the rate of nucleation and growth. This may be the reason for the differently sized nanoparticles resulting from a change in mixing speed.

The nanoparticles were synthesised at higher temperatures because it was thought this may reduce the induction period of nucleation, described by AL-Thabaithi *et al.* (2008), and produce smaller particles. Instead, performing the synthesis at 40 °C and 90 °C appears to have caused the formation of a turbid dispersion containing unstable particles with a tendency to clump and settle. This contrasts with the stable, transparent, yellow colloidal dispersion that forms at room temperature. The particles formed at these temperatures have a wider size distribution and it seems that the ability of the surfactant to stabilise the nanoparticles is reduced. Higher temperature synthesis is clearly unsuitable for this preparation method. The higher temperatures may have caused the hydrolysis of the SDS, resulting in its decomposition into fatty alcohols and sodium sulphate (Sigma-Aldrich, 2017b). This would explain the observed instability of the colloidal dispersion – the nanoparticles would not have been surrounded by the surfactant and the system's chemistry would be different.

The way in which the reducing agent, ascorbic acid, was added to the reaction solution was varied so as to influence the nucleation of the Ag nanoparticles. Adding the ascorbic acid dropwise means that there is only a small concentration change in the reaction solution with each drop added, meaning the system maintains homogeneity. It was thought this homogeneity would lead to the formation of monodisperse nanoparticles. However, the bimodal size distribution of Figure 5-6h suggests two separate nucleation phases or, alternatively, an aggregative growth mechanism (Shields, Richards, & Buhro, 2010).

Changing the concentration of the reducing agent could affect the rate of reaction and, in this instance, has widened the size distribution range of the particles. More than a quarter of the counted particles formed by adding ascorbic acid in 50% excess are bigger than 10 nm, whilst adding 2x diluted ascorbic acid leads to the formation of very small particles (with over 80% smaller than 4 nm) and a few large particles. From these results, it is evident that adding the original amount of ascorbic acid (in 33% excess) all at once is best to produce small particles with a narrow size distribution.

The final synthesis variation performed was to add $AgNO_3$ to the reaction solution last (i.e. after both the surfactant and reducing agent were mixed together). From the particle size distribution of this synthesis, it is clear that adding the reducing agent last is important for the synthesis of small, monodisperse nanoparticles. This could be because mixing the $AgNO_3$ and surfactant first ensures that the Ag^+ ions are surrounded by the stabilising surfactant before Ag nucleation.

In comparing the size of the particles produced in light conditions (Table 5-1) to those produced in dark conditions (Table 5-2), it is observed that the synthesis variations affect the particle size differently in the two different light conditions. For example, adding the reducing agent dropwise in light conditions produces very small nanoparticles whilst much larger particles are produced using the same variation

in dark conditions. As mentioned, previous studies (e.g. Bhaduri *et al.*, 2013, and Prathna *et al.*, 2014) have shown that sunlight can be used in the synthesis of silver nanoparticles and therefore has an impact on their growth and nucleation. The exact effect of sunlight on particle size is not clear but understanding this is beyond the scope of the current study.

The interplanar spacing (d-spacing) of the particles synthesised using Method One was analysed to determine their crystal structure and to confirm that they are pure silver (and not a silver compound like silver oxide). Figure 5-7 shows an example of the interplanar spacing used to identify the surface structure of the nanoparticles. The measured d-spacings (which were approximately 2.35 Å and 2.05 Å) were compared to that of Ag, Ag_2O and Ag_2S found in the International Centre for Diffraction Data PDF-2 2008 database (PDF 00-001-1167, PDF 00-001-1041, and PDF 00-001-1151, respectively). Table 5-3 lists some of the relevant d-spacings and the associated lattice planes of the considered Ag compounds.

Table 5-3: Some d-spacing measurements and the respective lattice planes of Ag, Ag_2O, and Ag_2S

D-spacing (Å)	*Silver compound*	*hkl lattice plane*
2.72	Ag_2O	111
2.43	Ag_2S	200
2.36*	Ag	111
2.36*	Ag_2O	200
2.04*	Ag	200
1.98	Ag_2S	211

*d-spacing measurements relevant to this study

Silver and silver oxide are naturally found in the cubic crystalline form, thus only the lattice spacings of cubic silver were used in this comparison (Eberhart & Horner, 2010; Hofmeister, 2004; M. Y. Li *et al.*, 2016; Molleman & Hiemstra, 2015; Vitos, Ruban, Skriver, & Kollár, 1998). The (111) lattice spacing of fcc (face-centred cubic) Ag and the (200) lattice spacing of cubic Ag_2O are both 2.36 Å. However, the measurement of a d-spacing of 2.05 Å indicates that these are indeed metallic silver nanoparticles.

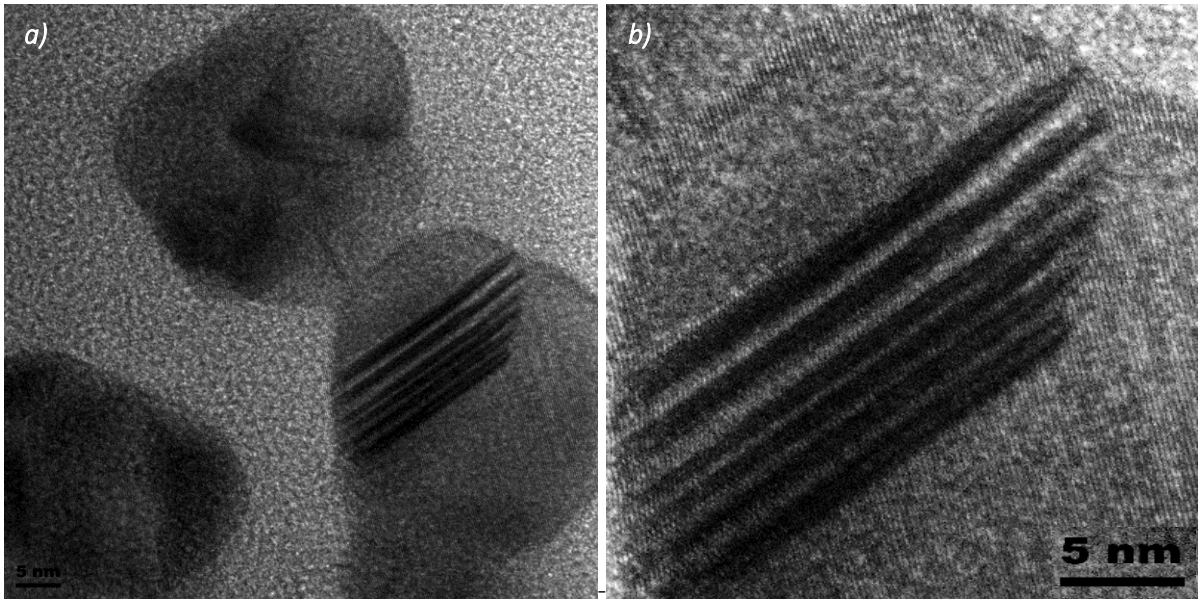

Figure 5-7: a) TEM image of Ag NPs produced in this study by following the original Method One in dark conditions and b) an enhanced view of this image to show more clearly the interplanar spacing

Numerous measurements of the lattice spacing were made. From this, two different lattice planes of metallic Ag were identified: (111) with an associated d-spacing of 2.36 Å and (200) with an associated d-spacing of 2.04 Å.

5.1.1.3 pH and Ag^+ concentration measurements

There is no identifiable correlation between the final pH of the reaction solution, the final Ag^+ concentration nor the particle size distribution. The initial concentration of Ag^+ is 64.6 ppm.

Table 5-4 shows the measured pH and Ag^+ concentration after the synthesis of each dispersion. The pH of each of the systems seems to be fairly consistent, at between 3.55 and 3.65 except in the case of different surfactant concentrations being used and for the dispersion prepared at 90 °C. The slightly lower pH of the dispersion prepared at 90 °C suggests that the reactants were affected by the higher temperature which may explain why the dispersion was not stable, as previously described.

Table 5-4: Final pH and Ag^+ concentration for each synthesis variation of Method One in dark conditions

Synthesis variation	*pH*	*Ag^+ concentration (ppm)*	*Number-based mean particle size (nm)*
Original method (no variation)	3.65	19.67	3.6 ± 3.8
Halved surfactant concentration	3.16	0.16	4.9 ± 8.6
Doubled surfactant concentration	3.34	0.09	65.5 ± 117.4
Agitation rate: 500 rpm	3.60	45.30	5.5 ± 7.5
Agitation rate: 500 rpm, round flask	3.60	44.02	4.4 ± 5.8
Agitation rate: 1000 rpm, round flask	3.69	47.45	8.0 ± 13.8
Higher temperature: 40 °C	3.67	52.44	9.5 ± 8.1
Higher temperature: 90 °C	3.33	0.46	4.0 ± 6.1
Dropwise reducing agent addition	3.59	0.16	9.6 ± 11.1
50% excess reducing agent	3.57	43.95	13.4 ± 18.4
Halved reducing agent concentration	3.65	48.41	3.8 ± 9.5
Order of addition	3.59	49.86	10.5 ± 14.5

It is difficult to interpret the meaning of the measured Ag^+ concentration without doing further studies, however the concentration does indicate how much of the added silver is in particle form. For most of the synthesis variations, the silver present in the nanoparticles is only 20 – 30% of the total added silver. The Ag ions in the dispersion could be from unreacted Ag^+, but it is more likely that the measured Ag^+ is the equilibrium ion concentration of each dispersion. One could investigate this by separating the solid nanoparticles from the liquid in which they are suspended, re-dispersing the particles in water and, after allowing time for the particles to achieve equilibrium in the dispersion, measuring the Ag^+ concentration. Unfortunately, the separation process was a lot more difficult than expected, as is outlined in Section 5.1.2, and this experiment could not be performed.

5.1.1.4 Summary of the characterisation of Ag NPs synthesised using Method One

Following difficulty in reproducing the results reported by AL-Thabaiti *et al*. (2008) in light conditions, the Ag nanoparticle synthesis was performed in darkness. Synthesis conditions were varied to establish whether changing the surfactant concentration, agitation speed, synthesis temperature, reducing agent concentration or method of chemical addition would result in the production of smaller, more monodisperse nanoparticles. Unfortunately, none of these variations improved the particle size distribution and it was found that the original synthesis method produced the best particles for the purposes of this study.

UV-Vis spectroscopy was used as a preliminary characterisation technique to determine whether the dispersions differed from each other. Theoretically, UV-Vis can be used to estimate particle size, however, because the produced dispersions are polydisperse, size estimation based on these absorption spectra could not be performed. Bhui *et al*. (2009) indicate that smaller particles have wider FWHM and less intense absorption peaks. The smallest particles produced were those using the original synthesis method. The absorption spectrum of this dispersion is also the least intense and does not exhibit an SPR peak, which correlates to the aforementioned findings. However, the spectra of the other Ag dispersions do not follow this same trend which is most likely due to the effect of a wide particle size distribution on absorption spectra.

TEM analysis was used to determine the particle size distribution of the dispersions. This analysis revealed that, at 3.6 ± 3.8 nm, the original synthesis method produced the smallest particles with the narrowest size distribution and that, using a number-based mean, the particles are smaller than the desired 10 nm. However, the volume-based particle size distribution is far wider because of the presence of large particles in the sample. This will result in discrepancies if these particles are tested for antibacterial activity and thus results may not be reliable. Lattice spacing measurements were used to confirm that the synthesised nanoparticles are fcc metallic silver and showed them to have (111) and (200) crystallographic planes.

pH and Ag^+ concentration measurements were performed to try explain the size results of the different synthesis variations. Unfortunately, no correlation between the data was found.

5.1.2 Separation of Ag nanoparticles synthesised using Method One

Washing and drying the silver nanoparticles allow for the collection of a powder which could be more easily used in antibacterial studies. It also means that excess surfactant and reducing agent present in the dispersion liquid are removed, which would allow for the nanoparticles to dissolve and act on bacteria without being affected by other chemicals. It is, however, difficult to separate solids from a stable colloidal dispersion.

Centrifugation of the dispersion proved unsuccessful. The sample prepared in darkness using the original, unvaried method was initially centrifuged for 30 minutes at 10,000 rpm, however this was ineffectual, and the nanoparticles barely settled. The sample was then centrifuged at 20,000 rpm, the maximum rotational speed the available facilities can achieve, for 60 minutes. Judging by the colour of the supernatant, more particles settled out of the dispersion but these still easily re-dispersed.

To better facilitate the separation of particles, various solvents, listed in Table 5-5, were tested for use in a phase extraction/centrifugation process. Before this was studied, SDS was combined with each of these organic solvents to determine which it is soluble in, and therefore which is a feasible option for

use in cleaning the silver nanoparticles of excess surfactant. SDS is an anionic surfactant that is soluble in water and slightly soluble in alcohols.

Table 5-5: Solvents used in phase-extraction experiments for Method One

Solvent	*Dipole moment (D)*	*Solvent type*	*SDS solubility*
a) Acetic acid	1.74	Protic	Soluble
b) Acetone	2.88	Aprotic	Insoluble
c) Chloroform	1.04	Non-polar	Sparingly soluble
d) Cyclohexane	0	Non-polar	Sparingly soluble
e) Dichloromethane (DCM)	1.60	Non-polar	Sparingly soluble
f) Diisopropyl ether	1.13	Non-polar	Insoluble
g) Dimethyl sulfoxide (DMSO)	3.96	Aprotic	Soluble
h) Ethanol	1.69	Protic	Sparingly soluble
i) Hexane	0	Non-polar	Insoluble
j) Isopropanol	1.66	Protic	Sparingly soluble
k) Methanol	1.70	Protic	Soluble
l) Toluene	0.36	Non-polar	Insoluble
m) Water	1.85	Protic	Soluble

30 mg of SDS was combined with 5 ml of each of the solvents listed in Table 5-5. The surfactant is soluble in only a few of the solvents. The white hue at the base of the vials shown in Figure 5-8 is the undissolved SDS powder. The solubility of SDS in the solvents was labelled as “sparingly soluble” when the powder only partially dissolved and was judged by the naked eye.

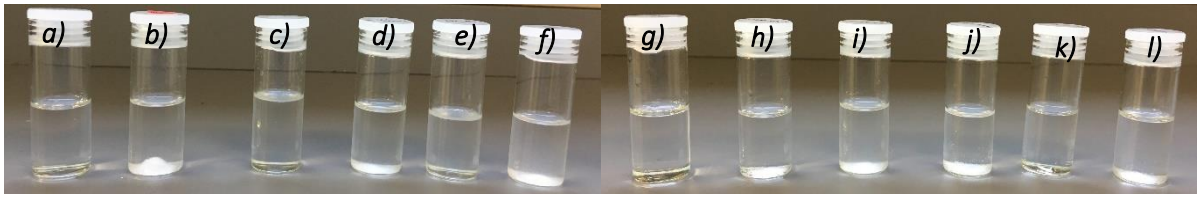

Figure 5-8: The solutions of SDS mixed with a) acetic acid, b) acetone, c) chloroform, d) cyclohexane, e) dichloromethane, f) diisopropyl ether, g) dimethyl sulfoxide, h) ethanol, i) hexane, j) isopropanol, k) methanol and l) toluene for evaluation of phase extraction viability

SDS was found to be insoluble in acetone, diisopropyl ether, hexane and toluene, sparingly soluble in chloroform, cyclohexane, dichloromethane, ethanol and isopropanol, and soluble in acetic acid, dimethyl sulfoxide (DMSO) and methanol. This is indicated in Table 5-5. Other than water, the surfactant most easily dissolved in the DMSO. Following this, the solvents were combined in a 1:1 ratio with the aqueous Ag dispersion prepared in darkness using the original synthesis method in microreaction tubes. The tubes were centrifuged three times for 15 minutes at 14 000 rpm. The resulting separations are shown in Figure 5-9. Because the starting system is very dilute in silver nanoparticles, the colour is not very evident in photographs. Observations of the effectiveness of the phase extraction separations will thus be described.

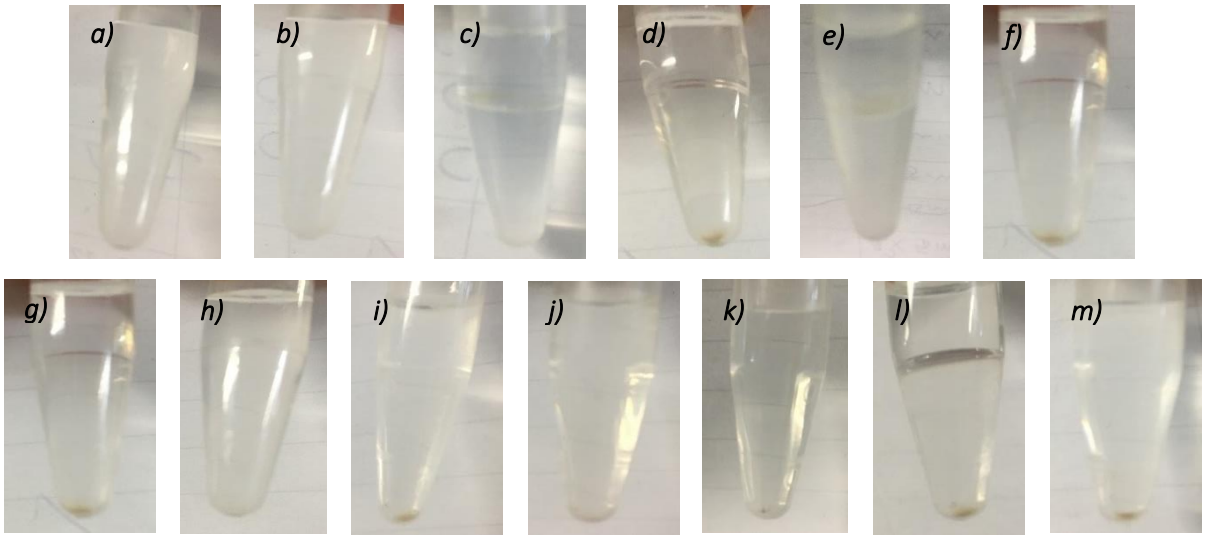

Figure 5-9: Centrifuged microtubes containing 50% synthesised silver nanoparticles and 50% a) acetic acid, b) acetone, c) chloroform, d) cyclohexane, e) dichloromethane, f) diisopropyl ether, g) dimethyl sulfoxide, h) ethanol, i) hexane, j) isopropanol, k) methanol, l) toluene and m) water

The samples centrifuged with acetic acid, ethanol and isopropanol did not present visible separation of nanoparticles (Figure 5-8a, h and j). This may be because of the very dilute system. It would be interesting to see if this is still the case in a more concentrated silver dispersion. In the experiments using chloroform and dichloromethane, the nanoparticles collected on the interface between the heavier, immiscible organic solvents and water. This makes it difficult to separate the nanoparticles efficiently from the resulting solution. A pale orange/brown precipitate settled out to the bottom of the tube for the cyclohexane, diisopropyl ether, hexane, toluene and water experiments, but was easily redispersed thus preventing effective separation. The acetone, DMSO and methanol experiments resulted in grey solid settling out and were the effective in separating the nanoparticles from the liquid. Of these, DMSO is the most promising solvent as it easily dissolves SDS and effects good separation.

Unfortunately, there was limited DMSO available for use and the replacement order had not arrived at the time of writing, thus no further experiments using the solvent could be performed. It was decided that, because DMSO is the most promising solvent for the purposes of this separation, there is little point in further pursuing this experiment without it. Interesting to note is that the acetone did not dissolve the SDS but effected nanoparticle separation. This insolubility could be the reason separation of the nanoparticles, which are surrounded by SDS molecules, is achieved. There may also be an interaction the Ag nanoparticles themselves, and subsequent studies on the potential effect of the solvent on the particle size would be necessary.

Had this particular investigation into separation continued, acetic acid, acetone, DMSO, methanol, ethanol, isopropanol, and water (as a control) would have been used in larger scale experiments. This would have involved the washing of nanoparticles, using the aforementioned solvents, via centrifugation at 20,000 rpm. The resulting supernatants would have been poured off and collected, and several washing cycles would have followed. The separated particles would have been analysed using TEM to examine the effect this washing process had on the particle size, as this is the most important property of silver nanoparticles used for antibacterial purposes. This procedure was followed when separating the particles prepared using Method Two and is fully described in Section 5.2.2.

5.2 Method Two

This synthesis procedure follows the method presented by Yang, Yin, Jia, & Wei (2011) and uses silver nitrate ($AgNO_3$) as the silver precursor, aniline as the reducing agent, dodecylbenzenesulfonic acid (DBSA) as the surfactant and sodium hydroxide (NaOH) to activate the reaction at 90 °C. As with Method One, this preparation method was repeated numerous times, however, their results could not be reproduced. The researchers call this a "facile" silver nanoparticle preparation method and claim that the mean particle size of the resulting dispersion is 8.9 ± 1.1 nm. A TEM image and a histogram were provided to demonstrate this and can be seen in Figure 5-10.

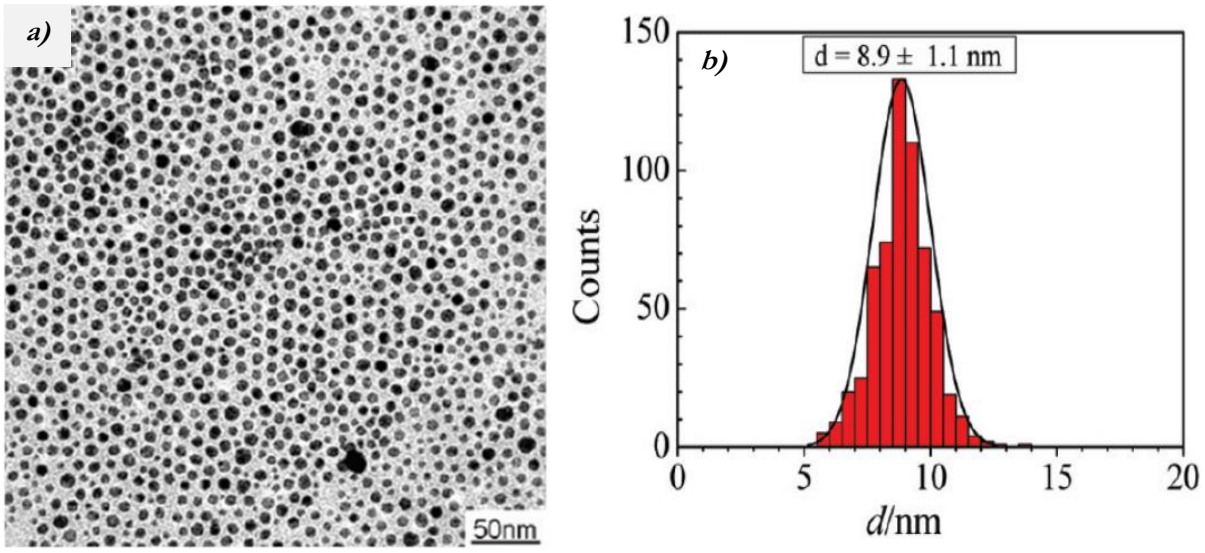

Figure 5-10: a) TEM image of Ag NPs produced by Yang et al. (2011) and b) the particle size distribution of the dispersion determined by Yang et al. (2011). Reprinted with permission.

As seen from Figure 5-10a, the spherical nanoparticles assemble into 2D arrays on the TEM grid and are a lot more concentrated than those prepared using Method One. Figure 5-10b shows the symmetrical, narrow size distribution of the system. There are two inherent advantages that Method Two has over Method One: there is no induction period for the formation of the nanoparticles, thus less time is required for the synthesis, and the concentration of silver in the dispersion is over 30x more concentrated.

Figure 5-11 shows a TEM image and the number-based particle size distribution of the colloidal dispersion prepared by following the original method presented by Yang *et al.* (2011). The TEM image (Figure 5-11a) shows many small particles and a larger, non-spherical particle. There was a significant number of larger particles in the dispersion, and this is shown by the bimodal size distribution in Figure 5-11b which, as previously stated, may indicate two separate nucleation steps. With a mean particle size of 12.57 ± 8.37 nm and more than 65% of the particles larger than 10 nm, the aim of the synthesis was clearly not achieved.

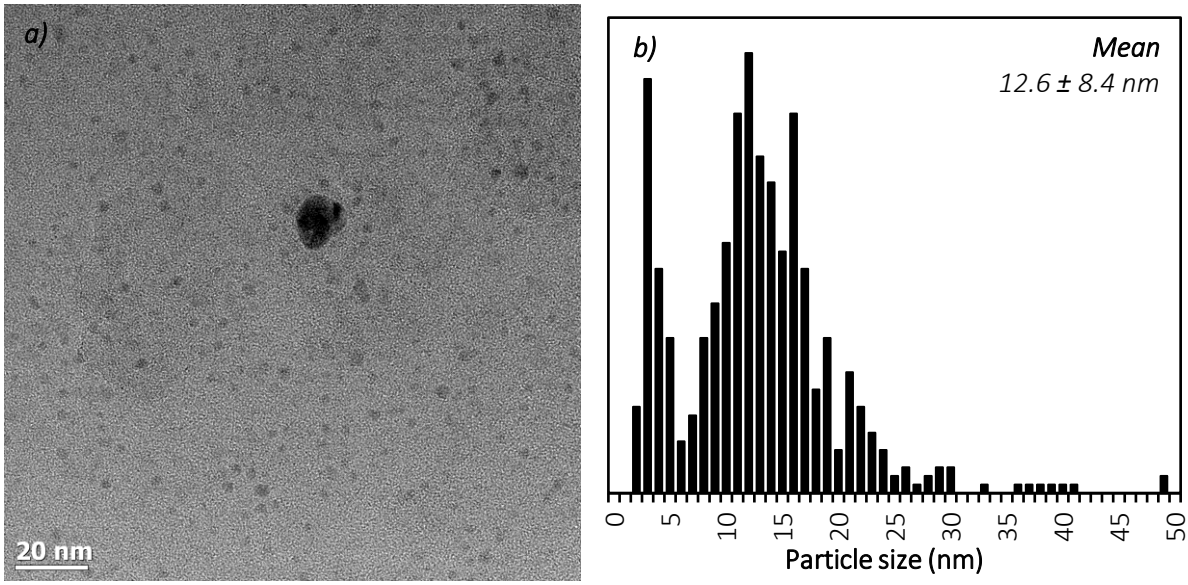

Figure 5-11: a) TEM image of the Ag NPs produced in this study by following Method Two in light conditions and b) the number-based particle size distribution of the dispersion

Only two variations of this synthesis were performed because of the knowledge that light may be affecting the result: halving the surfactant and injecting the NaOH into the system. Once again, these variations were done to investigate the impact on the particle size of the dispersion. Although usually carried out at higher temperatures (above 150 °C), a 'hot injection' method at 90 °C was used to induce burst nucleation (Kwon & Hyeon, 2011; Timonen, Seppälä, Ikkala, & Ras, 2011; Zacharaki, Kalyva, Fjellvåg, & Sjåstad, 2016). The creation of a supersaturated environment by rapid addition (injection) of the activating chemical should result in a short burst of nucleation followed by diffusional growth, thus leading to the formation of monodisperse particles (LaMer & Dinegar, 1950). A more in-depth explanation was provided in Section 2.6.3.5. This variation was thought to be the most likely to result in the production of smaller, more monodisperse nanoparticles.

Table 5-6 below shows the particle size produced for each of the three synthesis variations performed in light conditions. The hot injection of NaOH has a positive effect on the particle size distribution, forming particles with a mean size of less than 10 nm. The complete results of these variations can be found in Appendix A.2.1.

Table 5-6: Summary of the sizes of particles produced whilst exposed to light using Method Two

Synthesis variation	*Mean particle size (nm)*	*Median particle size (nm)*
Original method (no variation)	12.6 ± 8.4	11.4
Halved surfactant concentration	26.3 ± 16.4	28.7
NaOH hot injection	9.7 ± 6.6	7.8

For both the original synthesis method and the NaOH injection variation, the median particle size is lower than the mean particle size. This indicates the presence of large particles (outliers) that skew the mean to the right and lead to a larger standard deviation value, which is used to indicate particle size uniformity. None of the produced dispersions are monodisperse. Halving the surfactant concentration

produced an opaque dispersion and evidently meant that particles were not stabilised enough, resulting in the formation of large particles.

Because neither the original preparation method nor the hot injection method produced results similar to those of Yang *et al*. (2011), synthesis was performed in the dark. Similar variations to those performed for Method One were followed.

5.2.1 Synthesis variations of Method Two in dark conditions

As before, preparing the Ag nanoparticles in dark conditions produced differently sized nanoparticles in comparison to preparation in light conditions. The original preparation method is performed at 90 °C (heated by an oil bath) in a 250-ml round-bottomed flask at a mixing speed of 1000 rpm using the reactant amounts given in Table 4-2. The large flask used in the experimental variations is a 1000-ml round bottomed flask.

5.2.1.1 UV-Vis analysis

The absorption spectra of the various Ag dispersions were produced to provide preliminary insight into the particle size and concentration of the nanoparticles (Baser *et al*., 2011; Haiss *et al*., 2007). The reaction solution without $AgNO_3$ (containing water, DBSA, aniline and NaOH) was analysed using UV-Vis and found to have a peak at 300 nm. When diluted 10 times, this peak is at 287 nm. These baseline spectra can be found in Appendix A.2.1. Yang *et al*. (2011), authors of the method being followed, reported an SPR peak for the produced Ag nanoparticles at 420 nm. Thus, one can be sure that the spectra from the reactants will not interfere with the expected spectrum of the silver nanoparticles.

The absorption spectra of each of the synthesis variations appear in Figure 5-12. Spectra across a wavelength range of 200 nm to 900 nm were collected, however Figure 5-12 shows the area of interest which is between 300 nm and 700 nm. Because of the intense colour of the dispersions, dilutions had to be made to produce interpretable data. Most of the spectra shown in Figure 5-12 are from dispersions diluted 10x with deionised water, which means the absorbance intensity may be compared. For the 10x Ag variation, the dispersion had to be diluted 100x because the data was noisy at high concentrations, as is to be expected because of the higher concentration of Ag nanoparticles present. For the doubled surfactant concentration and changed order of addition variations, no dilution was necessary. This was because the dispersions were so pale in colour that further dilution resulted in very low intensity absorption.

The absorption spectra of these dispersions are a lot more intense than those of Method One. This is an indication of the much higher concentration of silver nanoparticles present in the Method Two dispersions. Most of the dispersions exhibit an SPR peak at approximately 415 nm. In comparing the spectra in Figure 5-12 to each other, it must be noted that smaller particles are expected to have a lower absorption intensity and an increased FWHM of the SPR peak (Bhui *et al.*, 2009). Using the original synthesis method as a means of comparison, it may be expected that the particles formed using all other variations (excluding the 10x Ag, doubled surfactant concentration, and changed order of addition variations because of their different dilutions and the halved surfactant concentration variation because it was an unstable, turbid dispersion) are larger than those produced using the original synthesis method. The spectra for the dropwise and injected addition of NaOH are very similar, which is surprising because these very different methods of addition were expected to result in different particle sizes. It is not, however, easy to predict particle size trends from these absorption spectra because of the effect that particle shape and polydispersity have. It is thus necessary to use

TEM to confirm the particle size distribution and verify whether this follows the trends that were estimated from these absorption spectra.

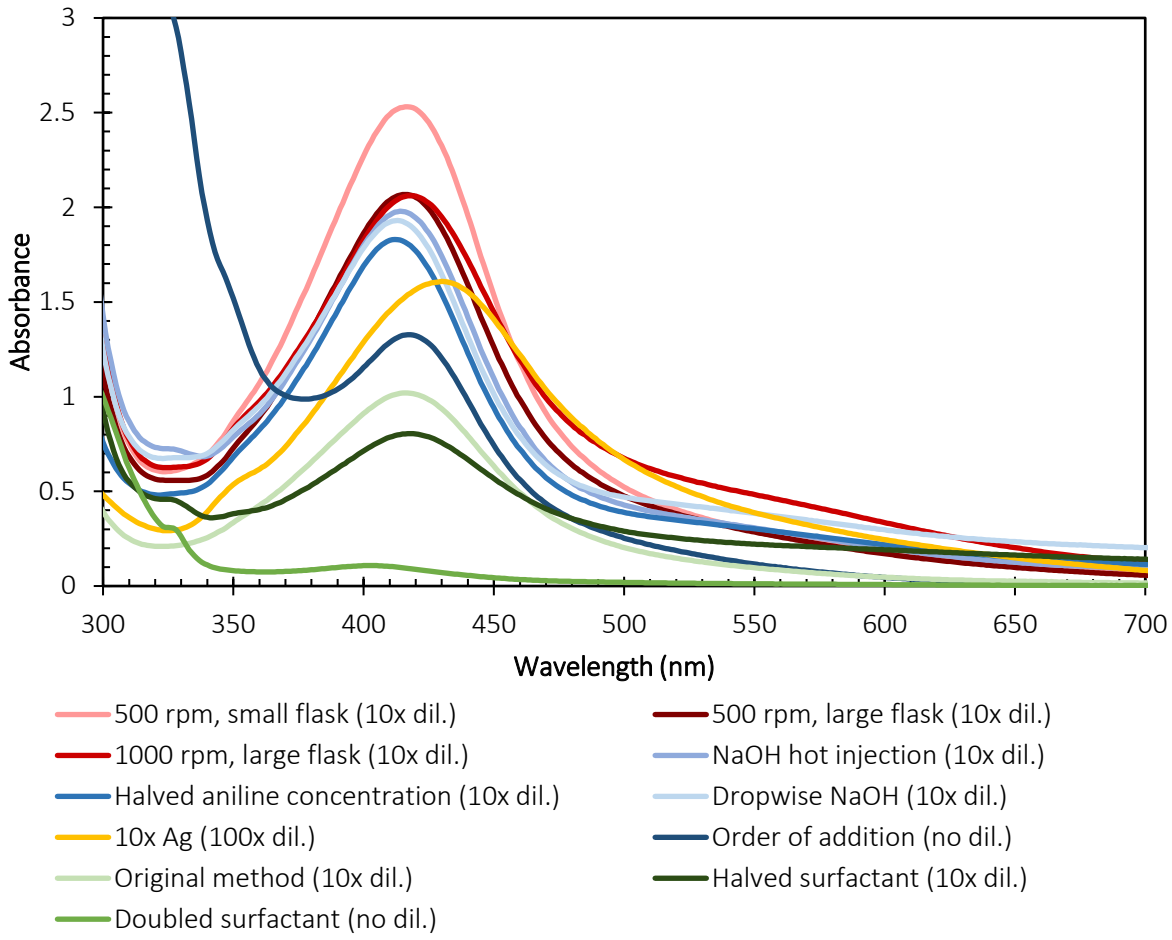

Figure 5-12: Absorption spectra of the Ag dispersions produced using variations of Method Two in dark conditions

5.2.1.2 Particle size from TEM

The particle size distribution of each dispersion was determined using TEM. At least 500 particles were measured for each sample, with some distributions including more than 1000 particles.

The nanoparticles synthesised using this method were mostly spherical across the variations, as can be seen from Figure 5-13. Each of these images was selected because it best represents the size distribution of their respective synthesis variation. Interestingly, the 10x Ag variation (seen in Figure 5-13c) contains spheroidal and triangular particles, with hybrids of the two shapes also present. The higher silver concentration evidently has a significant effect on particle shape as this is the only variation that contains triangular nanoparticles. The TEM micrographs of the other synthesis variations can be found in Appendix A.2.1.

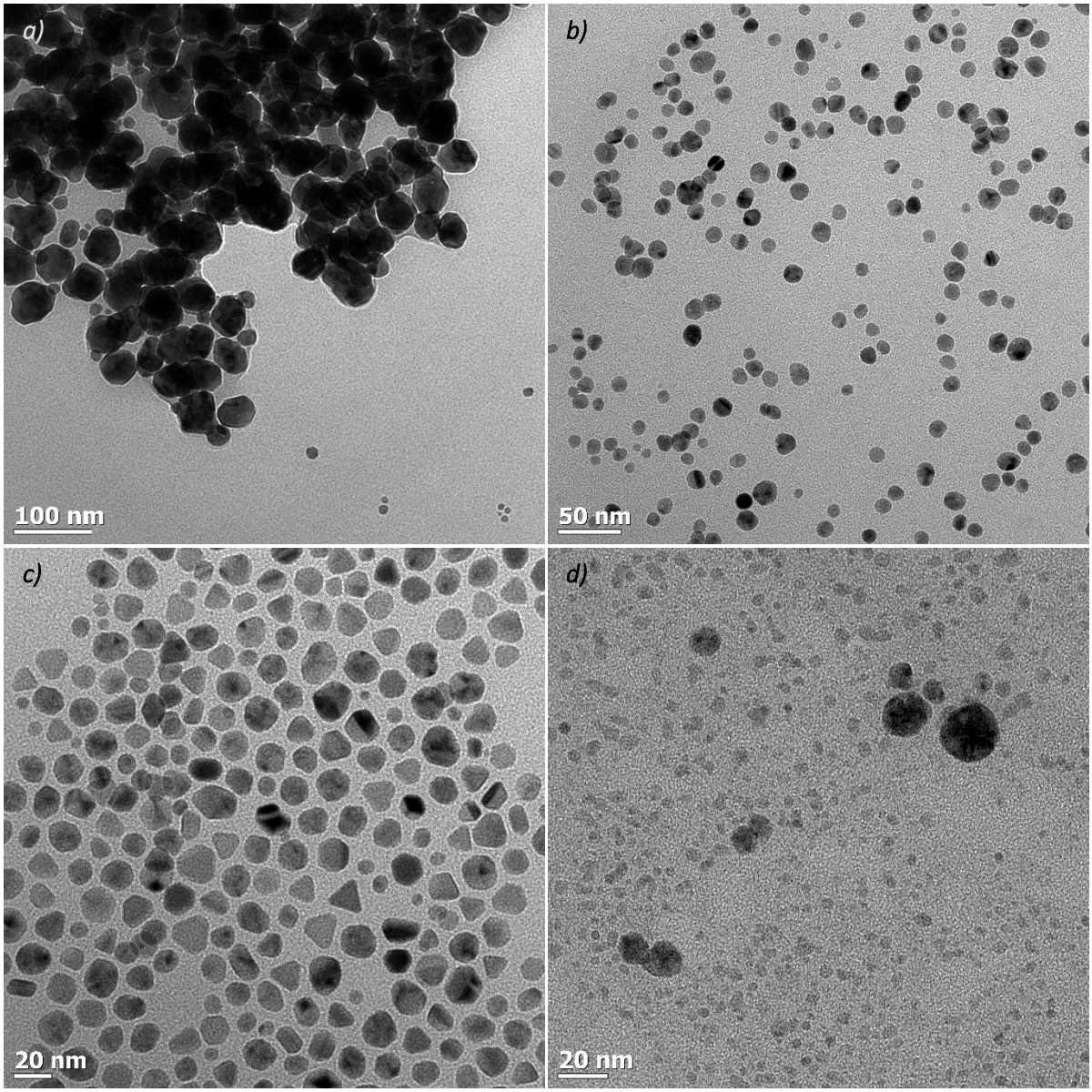

Figure 5-13: TEM micrographs of Method Two Ag dispersions prepared in dark conditions using synthesis variation a) halved surfactant concentration, b) large flask at 500 rpm, c) 10x Ag concentration and d) NaOH hot injection

The agglomeration seen in Figure 5-13a may have resulted from using a lower surfactant concentration, however it could also have taken place upon drying on the grid. TEM analysis alone cannot determine whether the sample was agglomerated in the dispersion.

A TEM image and particle size distribution of particles produced using Method Two in dark conditions are shown in Figure 5-14.

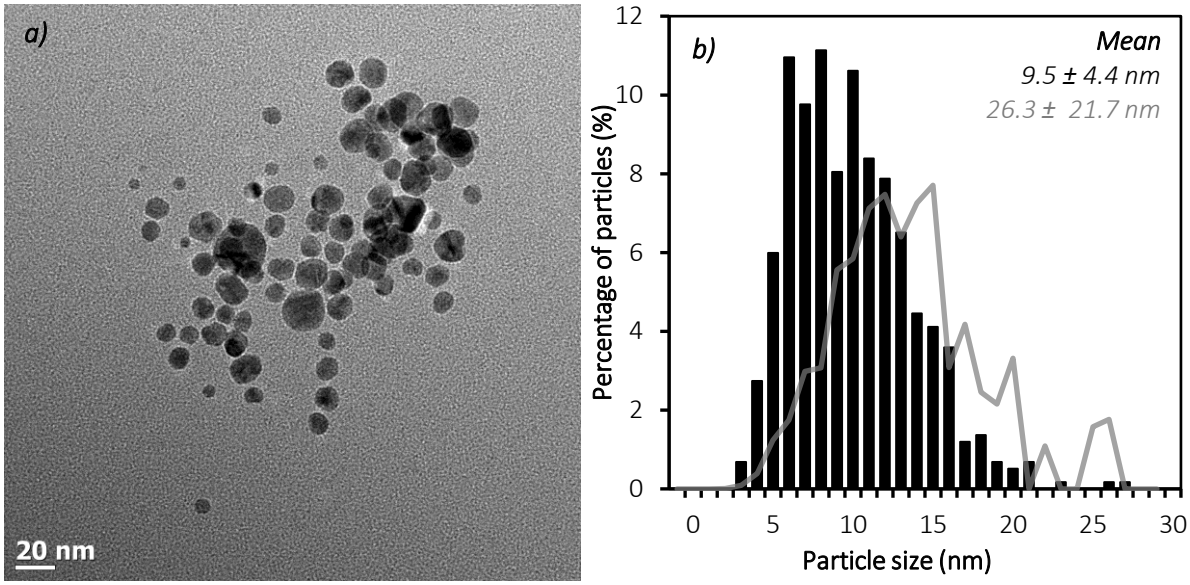

Figure 5-14: a) TEM image of the Ag NPs produced in this study by following the original Method Two in dark conditions and b) the number-based (black bars) and volume-based (grey line) particle size distribution of the dispersion

The particles produced in darkness are more uniform than those produced in the light. The size distribution is, however, still fairly wide as can be seen from the provided image (Figure 5-14a) which shows particles ranging in size from 5 nm to 25 nm. Additionally, the size distribution is not within the desired range; only 60% of particles are smaller than 10 nm and more than 80% of the silver mass is contained in particles bigger than 10 nm. Nevertheless, based on the lack of bimodality in the particle size distribution, the dark conditions appear to have prevented the occurrence of two separate nucleation events.

The original synthesis method did not yield the smallest particles; the best synthesis variation of Method Two was found to be the injection of NaOH. This can be seen in Table 5-7 and Figure 5-15 when comparing the measures of central tendency for each of the variations. For each of the dispersions, the median value is lower than the number-based mean value, indicating that the mean particle sizes have been skewed to the right because of the presence of very large particles. The clearest example of how these large particles can affect the data collected is found in Figure 5-15c. Two particles of over 100 nm were measured and collectively contribute to over 30% of the mass of the measured particles, reflected as two peaks in the volume-based size distribution. These outliers significantly affect the volume-based mean, highlighting that, although TEM analysis produces the most accurate particle size distribution, there is still some associated error. This error is minimised by taking images across a wide area of the TEM grid and by measuring over 500 particles.

Table 5-7: Number-based and volume-based mean particle size and median particle size for each synthesis variation of Method Two in dark conditions

Synthesis variation	*Number-based mean particle size (nm)*	*Volume-based mean particle size (nm)*	*Median particle size (nm)*
Original method (no variation)	9.5 ± 4.4	26.3 ± 21.7	9.0
Halved surfactant concentration	30.0 ± 15.2	45.0 ± 8.8	30.0
Doubled surfactant concentration	12.3 ± 7.0	32.1 ± 16.1	11.1
Agitation rate: 500 rpm	14.5 ± 13.9	86.2 ± 53.2	9.7
Agitation rate: 500 rpm, large flask	12.9 ± 5.4	28.0 ± 17.5	12.3
Agitation rate: 1000 rpm, large flask	14.1 ± 9.8	32.4 ± 11.0	11.2
10x Ag concentration	12.0 ± 4.9	20.8 ± 10.6	11.3
Dropwise NaOH addition	18.0 ± 21.9	120.9 ± 34.3	14.1
NaOH hot injection	6.7 ± 5.4	22.3 ± 10.9	4.4
Halved reducing agent concentration	14.4 ± 12.5	37.5 ± 12.3	7.5
Order of addition	30.0 ± 25.5	82.3 ± 31.6	28.5

In examining Table 5-7 and Figure 5-15, several observations on the effect of each variation can be made. As expected, reducing the surfactant concentration resulted in an increase in average particle size and produced an unstable, turbid dispersion. It also led to a wide, bimodal size distribution which may be due to two separate nucleation events or an aggregative growth process (Richards, Rath, & Buhro, 2010). Aggregative growth involves the aggregation and coalescence of primary nanoparticles and may be a nucleation-driven process. In fact, Richards, Rath, & Buhro (2010) refer to the aggregative-nucleation process as a second nucleation event because a critical aggregate constituting primary nanoparticles (produced from classical nucleation and growth) must form to cause further aggregative growth. Polycrystallinity is consistent with aggregative growth, thus a way to assess whether these large particles were formed via aggregation would be to examine their crystallinity (Richards, Rath, & Buhro, 2010). Doubling the surfactant concentration also led to a wider size distribution, confirming that the original surfactant concentration is the optimum tested concentration. Again, the higher concentration of surfactant in the system may have affected the reaction rate for the silver nanoparticle formation.

The varied agitation rates led to wider particle size distributions. A stirring speed of 1000 rpm in the smaller (250-ml) flask used in the original synthesis method produced smaller particles than at 500 rpm in the same sized flask. Generally, one would expect a higher agitation rate to form smaller particles because the homogeneity of the reaction system is better maintained. Interestingly, stirring at 500 rpm in the large (1000-ml) flask produced smaller particles than both stirring at 500 rpm in the small flask and stirring at 1000 rpm in the large flask. Again, this may be a result of the effect the agitation rate has on the metastable zone width (Sau & Rogach, 2012).

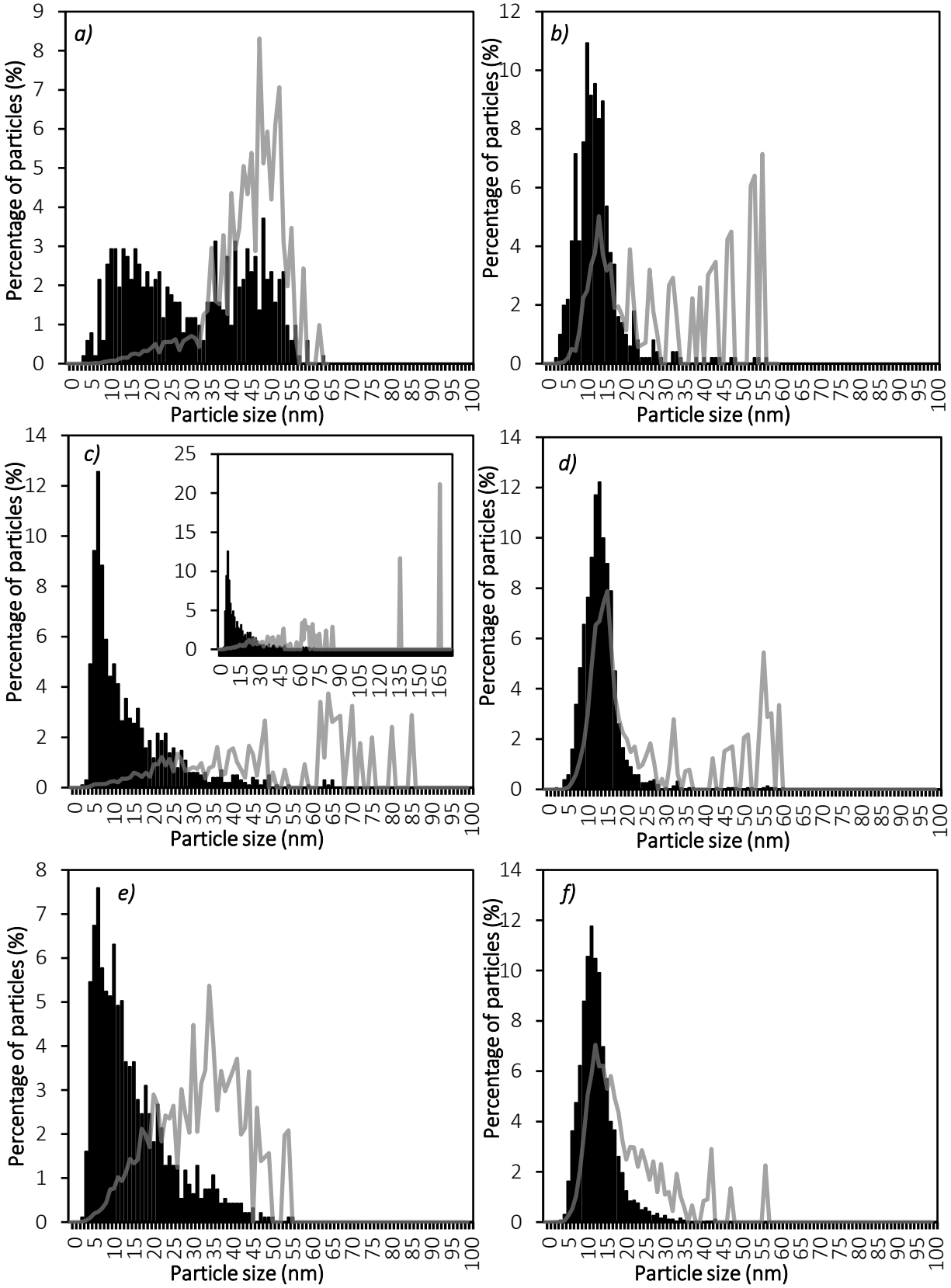

Figure 5-15: Number-based (black bars) and volume-based (grey lines) particle size distribution for the synthesis variation of Method Two in dark conditions at a) halved surfactant concentration, b) doubled surfactant concentration, c) 500 rpm with inset showing the size distribution on a larger scale, d) large flask at 500 rpm, e) large flask at 1000 rpm and f) 10x Ag concentration

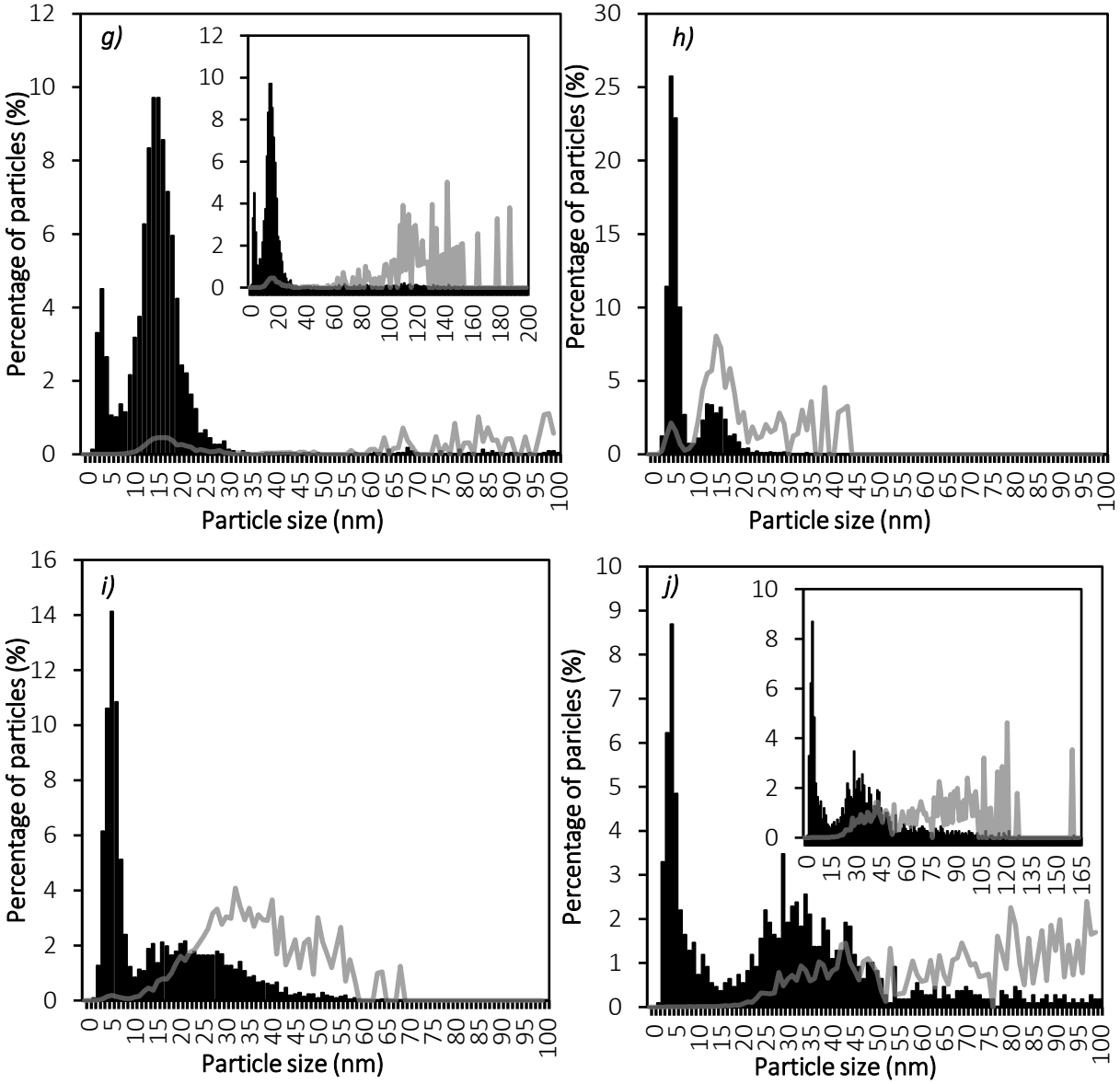

Figure 5-15 continued: Number-based (black bars) and volume-based (grey lines) particle size distribution for the synthesis variation of Method Two in dark conditions at g) dropwise NaOH addition with inset showing the size distribution on a larger scale, h) NaOH hot injection, i) halved reducing agent concentration and j) changed order of addition with inset showing the size distribution on a larger scale

Synthesising the silver nanoparticles at a concentration 10x higher than the original concentration produced a dispersion with a relatively narrow, although skewed, size distribution. Despite the increase in concentration, at 12.0 ± 4.9 nm, the nanoparticles formed in this dispersion are not much larger than those formed at a lower silver concentration. Synthesis at higher silver concentrations is attractive, particularly at larger scales of production. Although the particles are bigger than desired, the resulting particle size shows potential for use in antibacterial applications. Further optimisation of this synthesis variation could be done by combining this increased Ag concentration with the injection of NaOH, which was found to produce the smallest particles.

NaOH activates the reaction system for this synthesis. The rapid addition of NaOH via injection at 90 °C produced a dispersion with a bimodal particle size distribution and an average particle diameter of 6.7

± 5.4 nm. This is the smallest particle size achieved using the Method Two procedure. The data are, however, skewed by the presence of large particles within the dispersion. This can clearly be seen in the volume-based size distribution shown in Figure 5-15h: only 7.4% of the silver mass in the dispersion is contained in particles smaller than 10 nm. The data set is bimodal, however the larger particles (possibly formed because of the previously mentioned aggregative growth phenomenon) are much less frequent than the smaller particles. The 'hot injection' method is used to produce monodisperse nanoparticles through inducing burst nucleation, so this bimodality was surprising (Zacharaki, Kalyva, Fjellvåg, & Sjåstad, 2016). A possible reason that other syntheses using this technique have produced more uniform dispersions is that synthesis usually takes place at higher temperatures (> 150 °C) than Method Two specifies. A higher temperature would result in a faster rate of reaction and thus a faster nucleation rate, which may form smaller particles. However, because this is an aqueous synthesis (an organic solvent is often used in syntheses that make use of the hot injection technique), one cannot heat the system much above 90 °C.

In contrast to this, adding NaOH dropwise resulted in the formation of some very large particles (> 100 nm). The slow addition of NaOH clearly produces a wide particle size distribution. This was anticipated because Yang *et al*. (2011) state that the system lacks the induction period that is common in silver nuclei. This was discovered by measuring the UV-Vis absorbance of the dispersion during the reaction and finding that after 2 minutes approximately 94% of the silver nanoparticles had formed. Because of this very fast nucleation, adding the NaOH slowly would mean that the growth period of the first silver nuclei formed would be extended which would result in the formation of large particles.

In lowering the reducing agent concentration, only 53% of the particles produced are smaller than 10 nm. The polydisperse sample has a broad size distribution, possibly caused by the slower reaction rate resulting from a lower reducing agent concentration. The slower formation allows for more particle growth, which would explain the broad, Gaussian size distribution seen after the initial peak between 3 nm and 10 nm in Figure 5-15i.

Finally, the $AgNO_3$ solution was added to the reaction system *after* the NaOH. Some small particles were formed, however 70% of the produced particles are larger than 10 nm (Figure 5-12j). Evidently, the order of addition is very important in this synthesis for the formation of monodisperse nanoparticles. As with Method One, this is most likely because adding the reaction activating chemical *after* the silver ensures that the silver ions are well mixed and surrounded by surfactant molecules, thus better stabilising the nanoparticles.

The expected particle size trend from the UV-Vis spectra does not correspond to the actual particle sizes. This is likely a result of the effect particle size and polydispersity have on produced spectra. Unless nanoparticles are of uniform size and shape, size predictions from absorption spectra are difficult.

TEM images were used to measure the lattice spacing of nanoparticles synthesised in dark conditions using Method Two. These measured d-spacings were compared to those of metallic Ag, Ag_2O and Ag_2S found in the International Centre for Diffraction Data PDF-2 2008 database (PDF 00-001-1167, PDF 00-001-1041, and PDF 00-001-1151, respectively). An example of the lattice spacing seen on the TEM images of these nanoparticles is shown in Figure 5-16. As with Method One, the produced particles appear to be metallic and the measured lattice spacings correspond with the (111) and (200) crystallographic planes of fcc metallic Ag which have d-spacings of 2.36 Å and 2.04 Å, respectively (as indicated in Table 5-3). The lattice spacings thus confirm that metallic Ag nanoparticles were produced.

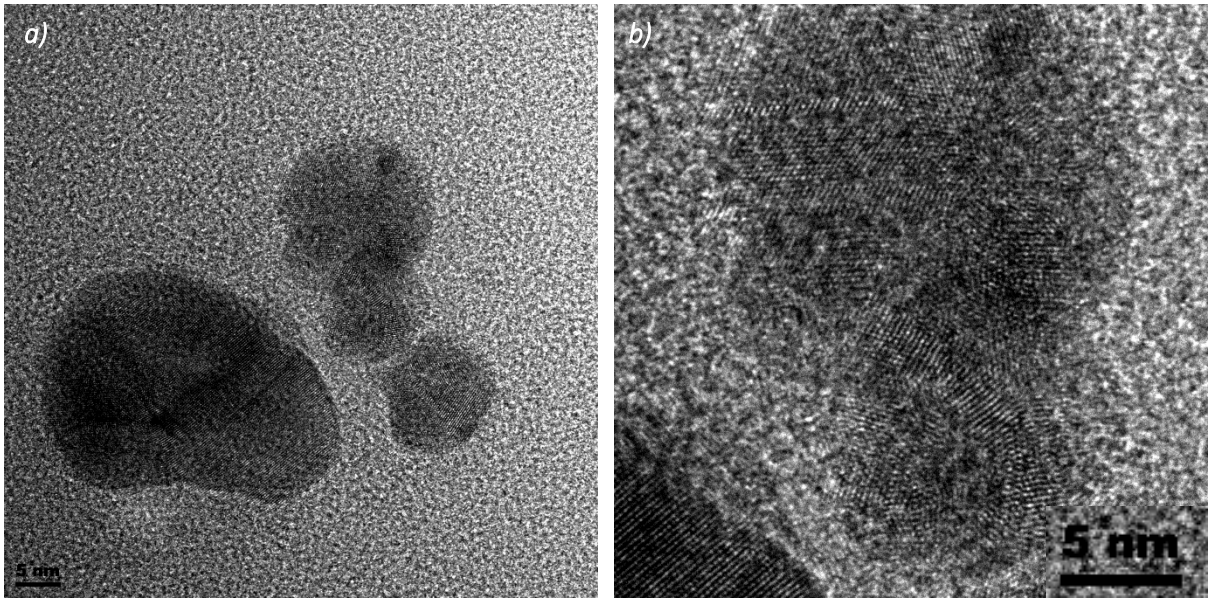

Figure 5-16: a) TEM image of Ag NPs produced in this study by following the NaOH hot injection variation of Method Two in dark conditions and b) an enhanced view of this image to show more clearly the interplanar spacing

5.2.1.3 pH and Ag^+ concentration measurements

The pH and equilibrated Ag^+ concentration were determined for each of the synthesis variations to investigate whether a relationship between these factors and the particle size is evident. No correlation between these factors was found. The starting concentration of Ag^+ in the 10x Ag variation is 2040 ppm whilst for all other synthesis variations it is 204.6 ppm.

Table 5-8: Final pH and Ag^+ concentration for each synthesis variation of Method Two in dark conditions

Synthesis variation	*pH*	*Ag^+ concentration (ppm)*	*Number-based mean particle size (nm)*
Original method (no variation)	11.27	0.020	9.5 ± 4.4
Halved surfactant concentration	12.62	0.003	30.0 ± 15.2
Doubled surfactant concentration	1.77	90.320	12.3 ± 7.0
Agitation rate: 500 rpm	11.31	0.010	14.5 ± 13.9
Agitation rate: 500 rpm, large flask	11.92	0.001	12.9 ± 5.4
Agitation rate: 1000 rpm, large flask	11.87	0.003	14.1 ± 9.8
10x Ag concentration	6.09	6.031	12.0 ± 4.9
Dropwise NaOH addition	12.21	0.005	18.0 ± 21.9
NaOH hot injection	12.26	0.001	6.7 ± 5.4
Halved reducing agent concentration	12.03	0.001	14.4 ± 12.5
Order of addition	12.25	0.003	30.0 ± 25.5

Table 5-8 presents the measured pH and Ag^+ concentration of each dispersion. Except for the syntheses where the amount of chemicals added was different (i.e. halved surfactant, doubled surfactant and 10x Ag concentration variations), the pH is fairly consistent and ranges between 11.25 and 12.25. The low pH of the doubled surfactant variation is from the higher concentration of dodecylbenzenesulfonic acid and *vice versa* for the halved surfactant variation.

The very low silver ion concentrations measured in all but the doubled surfactant variation indicate that, in the reaction solution, there is very little dissolution of the nanoparticles and that nearly 100% of the silver added during synthesis is in solid form. These near-zero measurements must, however, be interpreted with caution because such low values are near the measurement threshold of the Ag^+ Ion Selective Electrode. The high Ag^+ concentration in the doubled surfactant variation explains why the absorbance of the dispersion measured using UV-Vis is so low; 44% of the silver is still in solution, rather than in the form of nanoparticles thus very little colour is exhibited. The higher surfactant concentration appears to hinder the formation of silver nuclei.

5.2.1.4 Summary of the characterisation of Ag NPs synthesised using Method Two

As with Method One, light appears to have a significant impact on the size of particles formed using the procedure described by Yang *et al.* (2011). Their results could not be reproduced following synthesis in light conditions, thus prompting the investigation of different synthesis conditions. In darkness, the surfactant concentration, agitation speed, reducing agent concentration and method of chemical addition were varied, and the effect of this on the particle size was analysed. The variation that resulted in the most suitable particle size for the assessment of antibacterial activity (i.e. < 10 nm) is the injection of NaOH. The 10x Ag variation also showed promise, thus it is recommended that further studies combine these two variations to try produce small, concentrated, monodisperse silver nanoparticles.

The UV-Vis spectra seem to indicate that the original synthesis method produced the smallest particles. This was based on the phenomenon of smaller particles exhibiting a lower absorption intensity and an increased FWHM of the SPR peak (Bhui *et al.*, 2009). However, TEM analysis showed that this is not the case and that the NaOH hot injection variation produced smaller particles. Interestingly, the dropwise NaOH addition dispersion has a similar absorption spectrum as that of the hot injection method, but the particle sizes are very different. This main reason for the discrepancy between the TEM and UV-Vis results is that the polydispersity (in both size and shape) of the nanoparticles in the samples affect the absorption spectra, thus making it difficult to determine particle size.

The particle size distribution for each dispersion was determined following TEM imaging. The NaOH hot injection variation was found to produce the smallest particles but, with a number-based mean particle size of 6.7 ± 5.4 nm, it does not have the narrowest size distribution. This, paired with the fact that most of the silver mass is present in particles greater than 10 nm (revealed by the volume-based mean particle size), would make interpreting the results of any antibacterial efficacy studies difficult. The reason for aiming to produce small nanoparticles was to isolate the effect of just the ions on the bacteria but, since there are many particles bigger than 10 nm, this would not be possible. The lattice spacing determined from the TEM images allowed for the crystal structure of the metallic Ag nanoparticles to be identified as fcc, with d-spacings correlating to (111) and (200) lattice planes.

The measurement of the Ag^+ concentration in the dispersions showed that almost all the silver is contained in the solid nanoparticles. However, neither the Ag^+ concentration nor the pH of the samples provided any insight into the size results of this study.

5.2.2 Separation of Ag Nanoparticles synthesised using Method Two

In order to perform characterisation techniques such as XRD (X-ray diffraction), a dry powder form of the silver nanoparticles is required. Having the nanoparticles in powder form would also allow for easier assessment of their antibacterial efficacy as they could simply be re-dispersed in water at a desired concentration without the presence of other chemicals that may affect the bacteria. However, the formation of a stable dispersion means it is difficult to collect solid nanoparticles by separating them from the reaction solution.

The author of the method being followed suggests using centrifugation to collect the silver nanoparticles in powder form (J. Yang, personal communication, 14 March 2017). The dispersion that was prepared using the original synthesis method was centrifuged at 20 000 rpm for 60 minutes. These parameters were selected because difficulty had previously been experienced in separating the solid particles from the liquid. After 30 minutes, the particles started separating out of the reaction solution, however the supernatant was still clearly orange which indicates the presence of nanoparticles. Nothing improved after another 30 minutes, and the nanoparticles re-dispersed easily back into the liquid.

The use of both ultracentrifugation (at speeds of over 35 000 rpm) and freeze drying for separation was considered, however, due to the availability of equipment, neither could be performed. Phase extraction in conjunction with centrifugation was thus performed to remove the excess dodecylbenzenesulfonic acid (DBSA) from the dispersion and allow cleaning of the silver nanoparticles.

DBSA is soluble in water, alcohols, glycols, glycol ethers, esters, ketones, and aromatic and aliphatic hydrocarbons (Sigma-Aldrich, 2017a). The surfactant is ionic, has a large dipole moment of 4.5 D and has a strong association to toluene (Goual & Firoozabadi, 2004; León, Rogel, Urbina, Andújar, & Lucas, 1999). The polar and non-polar solvents that were selected for the phase extraction experiments are shown in Table 5-9. A short description of the effectiveness of these solvents in separating the Ag nanoparticles from the dispersion is also provided in the table.

Table 5-9: Solvents used in phase-extraction experiments for Method Two

Solvent	*Dipole moment (D)*	*Solvent type*	*Ag separation effectiveness*
a) Acetic acid	1.74	Protic	Grey precipitate settles
b) Acetone	2.88	Aprotic	Brown precipitate settles
c) Benzene	0	Non-polar	Ag NPS easily redispersed
d) Chloroform	1.04	Non-polar	Ag NPS easily redispersed
e) Cyclohexane	0	Non-polar	Ag NPS easily redispersed
f) Dichloromethane (DCM)	1.60	Non-polar	Ag NPS easily redispersed
g) Diisopropyl ether	1.13	Non-polar	Ag NPS easily redispersed
h) Dimethyl sulfoxide (DMSO)	3.96	Aprotic	Ag NPS easily redispersed
i) Ethanol	1.69	Protic	Brown precipitate settles
j) Hexane	0	Non-polar	Ag NPS easily redispersed
k) Isopropanol	1.66	Protic	Brown precipitate settles
l) Methanol	1.70	Protic	Brown precipitate settles
m) Toluene	0.36	Non-polar	Ag NPS easily redispersed
n) Water	1.85	Protic	Ag NPS easily redispersed

The 70% DBSA in isopropanol solution was combined with each of the solvents listed in Table 5-9 in a 1:1 ratio. The DBSA was soluble in all of the tested solvents, thus making them suitable for use in phase extraction where they are used to wash the nanoparticles of excess DBSA. Interestingly, it was found that adding acetone to DBSA results in an amber-coloured solution as seen in Figure 5-17. It is believed that this colour is a result of acetone breaking down the surfactant.

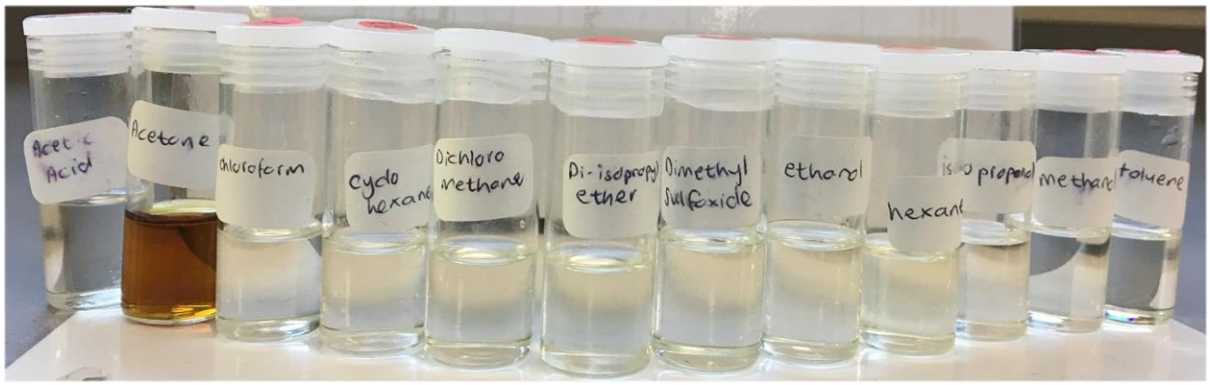

Figure 5-17: The solutions of DBSA mixed with various solvents for evaluation of phase extraction viability

Each of these solvents were subsequently used for small-scale testing of their effectiveness in causing synthesised silver nanoparticles to settle out of dispersion. This was done by centrifuging micro-reaction tubes containing a mixture of 50% synthesised silver nanoparticles and 50% solvent. The micro-tubes were centrifuged 3 times for 15 minutes at 14,000 rpm. The results of this series of centrifugations are shown in Figure 5-18.

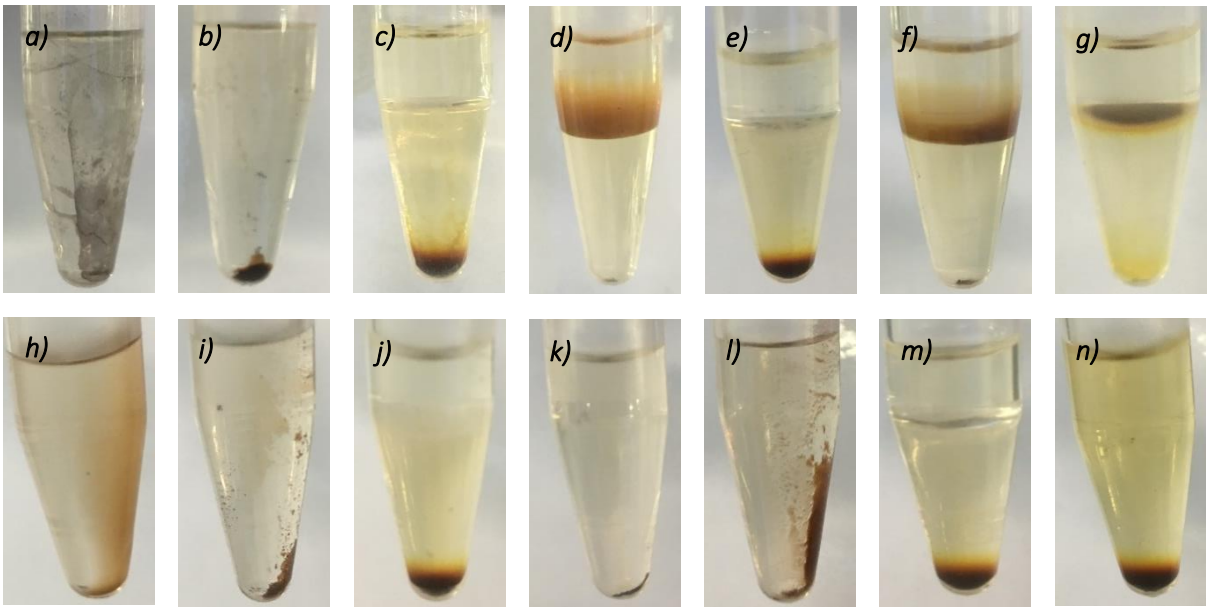

Figure 5-18: Centrifuged microtubes containing 50% synthesised silver nanoparticles and 50% a) acetic acid, b) acetone, c) benzene, d) chloroform, e) cyclohexane, f) dichloromethane, g) diisopropyl ether, h) dimethyl sulfoxide, i) ethanol, j) hexane, k) isopropanol, l) methanol, m) toluene and n) water

Examining the above images, one can immediately eliminate benzene, chloroform, cyclohexane, dichloromethane, diisopropyl ether, dimethyl sulfoxide, hexane and toluene as solvents to be used in further phase extraction experiments (Figure 5-18c, d, e, f, g, h, j and m). This is because colour is clearly still evident in each of these solvent mixtures, little to no settling of the particles has taken place, and the particles can be easily redispersed in solution. Although water is clearly not suitable either (Figure 5-18n), it is used as a control when scaling up the separation attempts. Acetic acid (Figure 5-18a) causes a grey precipitate to come out of solution, possibly because of the significant change in pH the system undergoes. Acetone (Figure 5-18b) seems to break down the DBSA and some brown solid settles to the bottom. Ethanol and methanol (Figure 5-18i and l) cause the particles to settle against the side of the tube. Isopropanol (Figure 5-18k) appears to induce the best settling, most likely because the DBSA used is 70 wt% in isopropanol. Each of these solvents (acetic acid, acetone, ethanol, isopropanol, methanol and water) will be used in phase separation experiments in centrifugation tubes.

A mixture of 50% solvent (15 ml) and 50% silver nanoparticle dispersion (15 ml) was added to centrifugation tubes and topped up with deionised water to ensure the masses of each tube were equal. The dispersion prepared in darkness by injection NaOH into the system was used as this contains the smallest particles. The tubes were centrifuged for 45 minutes at 20,000 rpm, rotated 180° and centrifuged again for 30 minutes at 20,000 rpm. The result of this first centrifugation is shown in Figure 5-19. Each of the chosen solvent, except for water which was used as a control, led to particle settling on the centrifuge tube walls. Again, the best separation was induced by isopropanol as the particles neatly stuck to the bottom of the tube. The particles in the silver dispersion/water mixture did not settle out but rather tended towards the bottom of the tube (Figure 5-19f). The yellow colour is strongly evident, indicating that there is still a high concentration of silver nanoparticles in the 'supernatant'. Upon shaking, the nanoparticles immediately redispersed into the liquid.

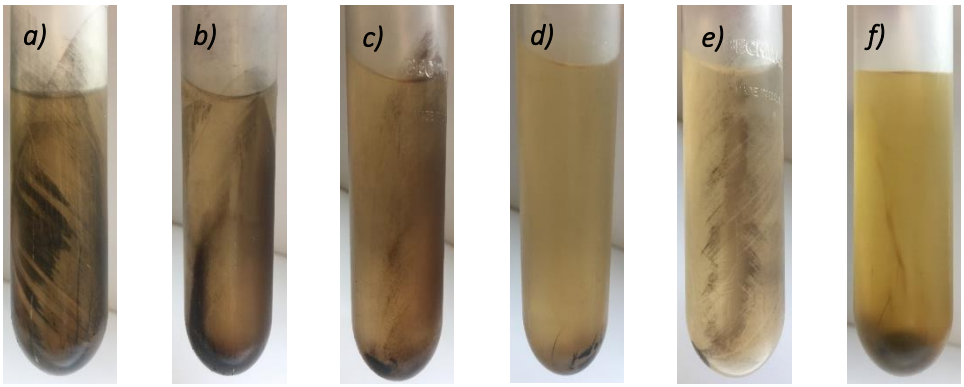

Figure 5-19: Centrifuge tubes containing a silver nanoparticle dispersion and a) acetic acid, b) acetone, c) ethanol, d) isopropanol, e) methanol an f) water mixture following the first centrifugation

The supernatant of each of these solvent mixtures following this first centrifugation, henceforth called the first supernatant, was poured off and collected (except for the water sample which could not be poured off without significant loss of particles). Each of the first supernatants had a slight orange colour, indicating the presence of silver nanoparticles. Obviously, it is impossible not to lose some nanoparticles in this separation process, however it is desired to minimise this loss.

Following this, 30 ml of solvent was added to the respective centrifuge tubes which were then centrifuged at 12,000 rpm for 60 minutes. The supernatants formed following this second centrifugation, henceforth called the second supernatants, were poured off and collected. Each was absent of colour, except for the sample centrifuged with water. The particles were subsequently redispersed and the samples were left overnight in the fume hood to evaporate off the remaining solvent. Following the evaporation, the particles were difficult to scrape off the glassware and were not in the expected powder form because they were still well-coated in DBSA.

A further three cycles of redispersion, centrifugation and removal of the supernatant were undertaken at 10,000 rpm for an hour and then twice at 30 minutes. The solvents were then evaporated overnight. All samples, except for those centrifuged with acetic acid and isopropanol, were difficult to remove from the glassware and stuck to the spatula which indicates the presence of surfactant. The particles washed with acetic acid could easily be collected and formed a grey, shiny powder. The particles washed with isopropanol were more difficult to remove but left a brown powder; one more wash cycle may have been enough to completely clean this sample of excess DBSA. Therefore, the most suitable solvents (investigated in this study) to separate the synthesised silver nanoparticles from their reaction media are acetic acid and isopropanol.

Because this was just a preliminary experiment to understand what separation method might work best for these particles, instead of collecting the dried powder, the particles were redispersed and TEM grids were prepared to analyse the effect the solvents had on the particle size.

The first and second supernatants were analysed in the UV-Vis to determine whether synthesised nanoparticles had been discarded during the separation process (Figure 5-20). Because the second supernatant of the acetone phase extraction experiment contained highly concentrated acetone, a UV-Vis measurement could not be performed as plastic cuvettes were used.

Figure 5-20 shows that adding a solvent other than water is imperative in preventing the loss of particles to the supernatant. Both the first (water 1) and second (water 2) supernatants collected following centrifugation with water as solvent contain silver nanoparticles, as indicated by the SPR peak which correlates with that of the NaOH hot injection dispersion. The first supernatants resulting from the use of the organic solvents do not contain much silver, evidenced by the low absorption registered for each experiment. Acetic acid, which was one of the best performing solvents for this study, led to the greatest loss of nanoparticles in comparison to the other organic solvents (as determined by the absorbance reading). This loss, however, is not viewed as significant. The second supernatants are effectively silver-nanoparticle free which means that the particles settle well during the centrifugation. This does not, unfortunately, give any indication of how successful the washing of excess DBSA from the particles is.

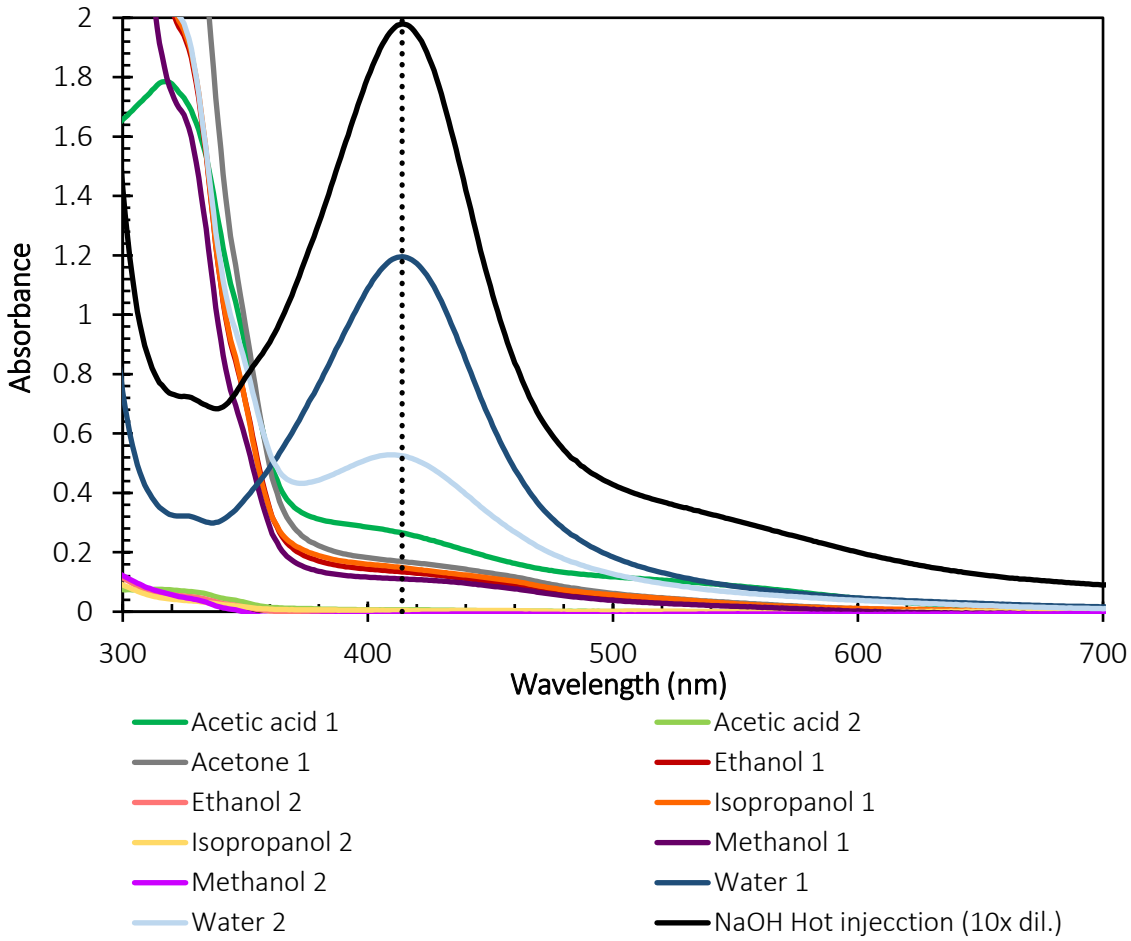

Figure 5-20: Absorption spectra of the first (1) and second (2) supernatants resulting from the phase extraction separation experiments performed on the NaOH hot injection variation of Method Two

The pH and Ag^+ concentration of each of the supernatants were also measured and compared to the original measurements taken for the NaOH injection variation of this synthesis. Again, because the Ag^+ ion selective electrode is made from epoxy resin, measurements of the Ag^+ concentration for the acetone sample were not performed to prevent damage to the probe. The initial pH and Ag^+ concentration measurements of the NaOH hot injection dispersion were 12.26 and 0.001 ppm, respectively.

Table 5-10: The pH and Ag+ concentration for the first and second supernatants resulting from the phase extraction separation experiments performed on the NaOH hot injection variation of Method Two

Solvent	*First supernatant pH*	*Second supernatant pH*	*First supernatant Ag^+ concentration (ppm)*	*Second supernatant Ag^+ concentration (ppm)*
Acetic acid	1.75	1.00	0.102	0.003
Acetone	12.93	8.90	-	-
Ethanol	12.52	8.76	0.002	0.001
Isopropanol	12.83	7.72	0.001	0
Methanol	11.90	7.15	0.001	0
Water	11.81	10.53	0.013	0.023

From Table 5-10, the low Ag^+ concentrations confirm that little to no silver was dissolved during the washing process which makes the use of these solvents in the separating process, particularly acetic acid and isopropanol, quite promising.

The next important thing to consider is how the addition of organic solvents, and the centrifugation and washing process, may have affected the size of the particles. Following the five washing cycles described, TEM analysis was done on the resulting particles of each of the samples. The number-based and volume-based particle sizes are presented in Table 5-11. The particle size of the dispersion before separation is also provided.

Table 5-11: Number-based and volume-based mean particle size and median particle size resulting from the phase extraction separation experiments performed on the NaOH hot injection variation of Method Two

Solvent	*Number-based mean particle size (nm)*	*Volume-based mean particle size (nm)*	*Median particle size (nm)*
NaOH hot injection (before separation)	6.7 ± 5.4	22.3 ± 10.9	4.4
Acetic acid	12.5 ± 14.9	58.5 ± 26.2	5.5
Acetone	12.3 ± 8.9	29.8 ± 11.5	11.3
Ethanol	9.1 ± 10.2	44.7 ± 22.4	4.1
Isopropanol	9.4 ± 9.1	28.3 ± 9.8	4.5
Methanol	12.0 ± 11.2	49.3 ± 31.3	9.7
Water	13.5 ± 8.7	29.6 ± 13.3	11.9

Each of the different solvents used in the washing experiments led to a particle size increase. This is most likely due to the removal of excess surfactant that stabilised the particles thus limiting agglomeration and further growth. Except for the experiments using ethanol and isopropanol, the number-based mean particle sizes for the separated particles are greater than 10 nm. The volume-based size distributions also indicate the presence of much larger particles. Even if particles are separated using isopropanol as the solvent (which seems to be the most promising), the large particle size range means that using these separated particles in antibacterial studies will result in discrepancies and make it difficult to understand the antibacterial mechanism (Sotiriou & Pratsinis, 2010).

5.3 Characterisation of purchased Ag nanoparticles

Two different spherical silver nanoparticle dispersions, each containing particles with an average size of 10 nm at a concentration of 0.02 mg/ml, were purchased from Sigma-Aldrich for comparative purposes against the particles synthesised in this study. One dispersion uses sodium citrate as the stabilising surfactant, whilst the other is PVP (polyvinylpyrrolidone) functionalised. Despite containing different surfactants, the same absorption spectra and TEM image is provided by Sigma-Aldrich for the dispersions (Sigma-Aldrich, 2018a, 2018b). These are shown in Figure 5-21.

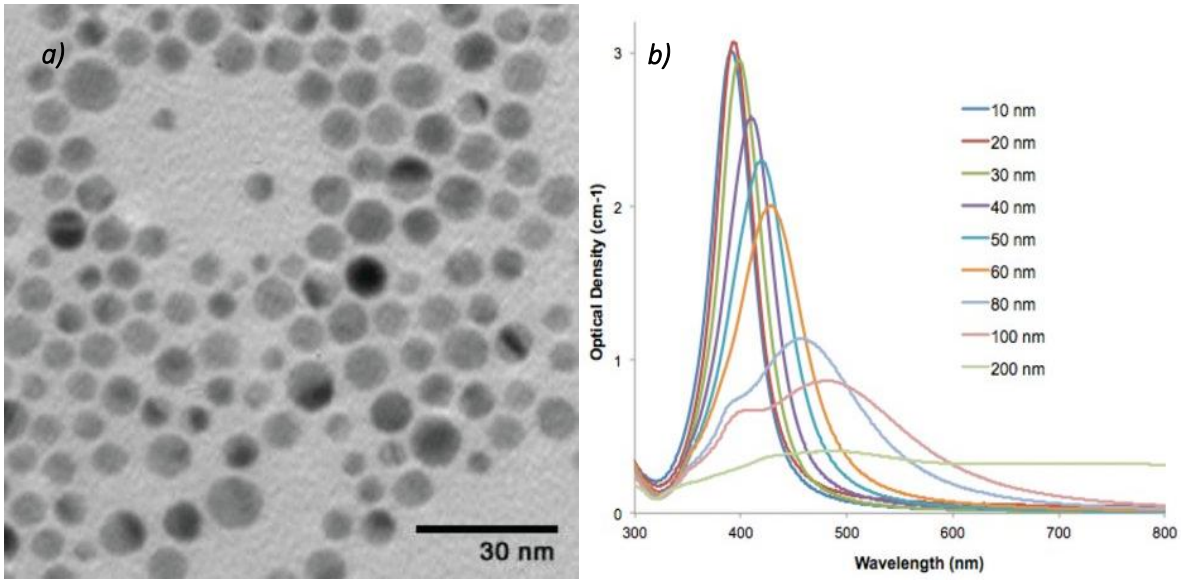

Figure 5-21: a) TEM image and b) absorption spectra at 0.02 mg/ml provided by Sigma-Aldrich for the purchased Ag nanoparticle dispersions from Sigma-Aldrich (2018a, 2018b)

The TEM image in Figure 5-21a shows particles ranging in size from 3 nm to 12 nm. It is interesting to note that, even when prepared by a world-renowned chemical company, the particles shown are not monodisperse. Figure 5-21b reveals that the expected SPR peak is at approximately 390 nm.

Analysis of both dispersions using TEM and UV-Vis was performed. The TEM characterisation results are shown in Figure 5-22 below.

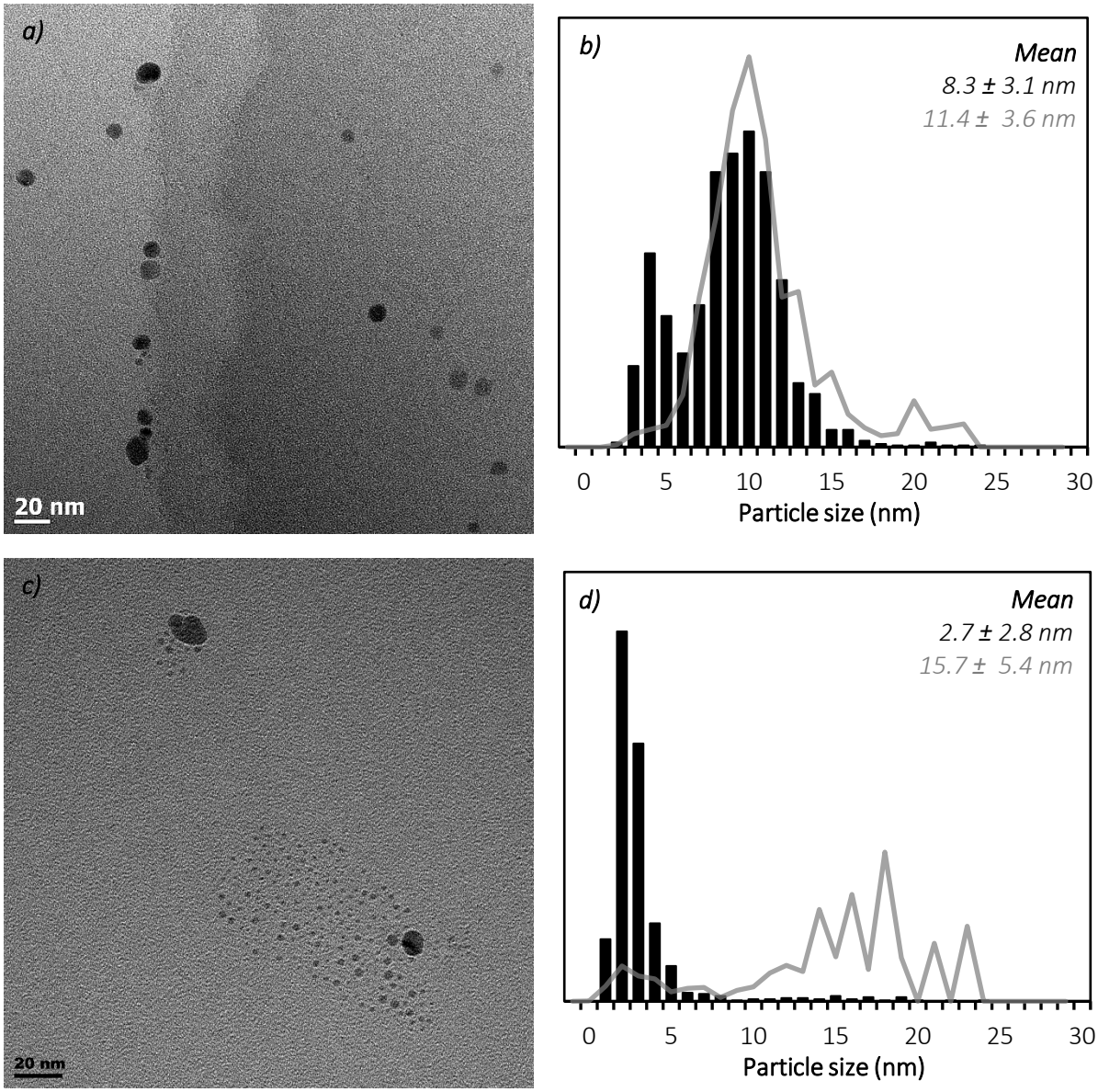

Figure 5-22: a) TEM image of the citrate stabilised Ag NPs purchased from Sigma Aldrich, b) the number-based (black bars) and volume-based (grey line) particle size distribution of the citrate stabilised Ag NPs purchased from Sigma Aldrich, c) TEM image of the PVP functionalised Ag NPs purchased from Sigma Aldrich and d) the number-based (black bars) and volume-based (grey line) particle size distribution of the PVP functionalised Ag NPs purchased from Sigma Aldrich

Figure 5-22 shows more uniformly sized particles than those synthesised in this study. Although some contamination on the TEM grid is evident for the citrate stabilised Ag NPs (Figure 5-22a), spherical particles of between 3 nm and 13 nm can clearly be seen. From Figure 5-22b, one can see that the volume-based size distribution of the citrate-stabilised nanoparticles matches well with the number-based size distribution. This is because the biggest particle measured was 23 nm, thus there is no outlier skewing the data. The citrate-stabilised particles are less than 10 nm in size, with a volume-based mean of 11.4 ± 3.6 nm, making them ideal for antibacterial assessments involving the release of silver ions. This means that, in future, antibacterial studies can be performed using these purchased silver nanoparticles. Alternatively, investigation into silver nanoparticle preparation methods that use sodium

citrate as a surfactant could be undertaken. Sigma-Aldrich did not provide information regarding the concentration of sodium citrate in the silver dispersion, however ICP-OES (inductively coupled plasma optical emission spectrometry) was performed and it was determined that the sodium concentration is 0.13 g/l. If one assumes that all the sodium present in the dispersion is from the added sodium citrate, the sodium citrate concentration can be calculated to be 0.48 g/l. Despite being made for commercial purposes (presumably following optimisation of synthesis methods), the purchased silver nanoparticles are not monodisperse. This suggests that synthesis of uniformly sized silver nanoparticles may be challenging even for chemical companies.

Figure 5-22c shows the presence of many very small nanoparticles in the PVP functionalised Ag NPs, most measuring less than 5 nm in diameter. The sample has a number-based mean particle size much smaller than 10 nm and a narrow size distribution. There are, however, some larger nanoparticles present in the dispersion that shift the volume-based size distribution to a mean of 15.7 ± 5.4 nm. This would create some uncertainty as to the mechanism of the antibacterial action of the nanoparticles, should their bactericidal activity be tested. It would, however, be interesting to compare the antibacterial activity of the PVP functionalised nanoparticles to the citrate stabilised nanoparticles.

This particle size analysis reveals that, due to their higher degree of size uniformity, the purchased nanoparticles would be better suited to antibacterial efficacy assessments than the particles synthesised in this study. It also shows that investigation into synthesising Ag nanoparticles (intended for use in bactericidal applications) using sodium citrate or PVP would be valuable.

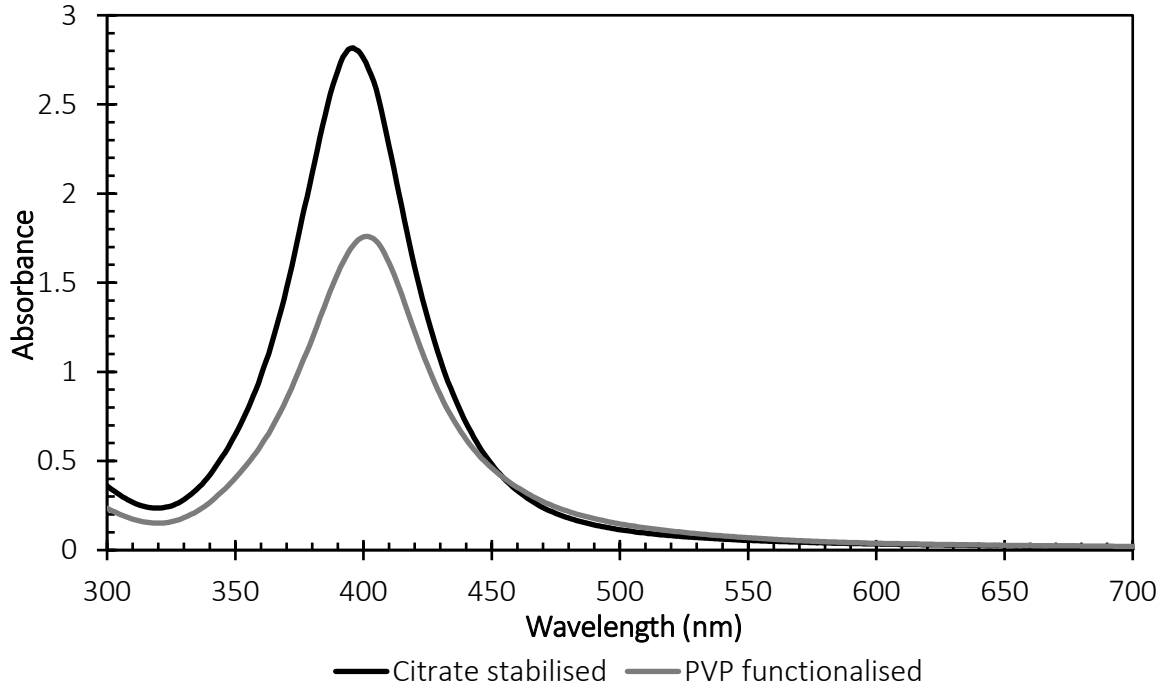

Figure 5-23: Absorption spectra of the Ag dispersions purchased from Sigma-Aldrich

UV-Vis analysis was performed for both Sigma-Aldrich samples and their absorption spectra are shown in Figure 5-23. The SPR peak for the citrate stabilised sample is at 396 nm and for the PVP functionalised sample it is at 400 nm. This is slightly different to the information supplied. It also shows that the

particles of each dispersion are different sizes, as was confirmed by studying the TEM images taken. Interestingly, the PVP functionalised nanoparticles exhibit an SPR peak at a higher wavelength than the citrate stabilised particles, despite being smaller. As is seen in Figure 5-21b, larger particles are expected to have SPR peaks at higher wavelengths (a blue-shift). However, it has previously been observed that as the size of highly uniform Ag nanoparticles decrease below a diameter of 12 nm, there is a strong red shift in the SPR absorption band (Peng, McMahon, Schatz, Gray, & Sun, 2010). The researchers found a multilayer Mie theory model to be in agreement with their observations. They state that the surface- and size-related effects become more important as the nanoparticle diameter decreases. The smaller the particle, the more pronounced the chemical interactions with the surfactant and surrounding medium. The red-shift is caused by chemical interactions which lower the conductivity in the outer metallic layer of the nanoparticles. It is believed that this, in conjunction with the difference in surrounding medium of the two purchased Ag nanoparticle dispersion, is the reason for the observed red-shift of the smaller nanoparticles.

Table 5-12 provides the measured pH and Ag^+ concentration for both purchased dispersions. Whilst the pH is just a point of interest, the low Ag^+ concentration values demonstrate the stability of the nanoparticles in the dispersion. The presence of the excess surfactant clearly inhibits the dissolution of the nanoparticles.

Table 5-12: pH and Ag+ concentrations for the Ag dispersions purchased from Sigma-Aldrich

Sigma-Aldrich sample	*pH*	*Ag^+ concentration (ppm)*
Citrate stabilised	8.12	0.749
PVP functionalised	8.96	0.622

Although not done in this study, to investigate the viability of these purchased nanoparticles in antibacterial applications, the dispersions could be diluted with water and a study on the Ag^+ concentration over time could be performed. Performing this preliminary experimental work would ensure that resources and time are not wasted by immediately assessing the nanoparticles against bacteria.

The ease of separation of these particles from the dispersion liquid would also need to be investigated, as this has already been identified as an issue through the synthesis of silver nanoparticles for this study.

Chapter 6: Antibacterial efficacy studies for silver

6.1 Antibacterial efficacy of silver ions

Silver ions are believed to be the main source of the antibacterial activity of silver nanoparticles. For this reason, the antibacterial efficacy of silver ions was assessed before any further studies on silver were performed. $AgNO_3$ was used for this study because it readily dissolves in water into the required Ag^+ ions and a time-kill curve against *Escherichia coli* (*E. coli*) was developed as described in Section 4.4.1.

Initially, a laboratory-strain of *E. coli* (*DH5α)* was used for the antibacterial efficacy assessment due to the availability of bacterial strains within the laboratory. DH5*α* is used to maximise the efficiency of transformations (the process in which bacteria take up foreign DNA) (Chan, Verma, Lane, & Gan, 2013). Experiments with three different concentrations of Ag^+, 0 µM (control), 6 µM (0.65 ppm Ag^+) and 12 µM,(1.29 ppm Ag^+) were performed in triplicate using phosphate buffered solution (PBS). PBS was used as the bacteria medium because it allows for bacteria survival but does not provide a suitable, nutrient-rich environment for bacterial growth (unlike other media such as lysogeny broth). For an experiment with the aim of establishing antibacterial activity, it is best not to have the bacteria colonies both growing and being killed off as this may produce contradictory results. Both concentrations of Ag^+ killed off the *E. coli* (DH5α) colonies in less than 2.5 hours, demonstrating how efficient silver ions are as an antibacterial agent. Concentrations of 12 µM Ag^+ had a slightly faster initial kill rate of bacteria, with 99.99% of bacteria killed in the first hour of contact in comparison 97.98% of the bacteria killed in the first hour at 6 µM Ag^+.

These results, which can be found in Appendix B.1, give a preliminary indication of the antibacterial effectiveness of silver ions against *E. coli* in PBS. However, it was desired to develop a time-kill curve with a longer period of cell death to better understand the rate at which silver ions kill *E. coli*. For this reason, lower concentrations of Ag^+ were used in antibacterial efficacy studies.

A wild-type *Escherichia coli* (ATCC® 25922™), which is a recommended strain for antimicrobial susceptibility testing, was used for all subsequent antibacterial studies (American Type Culture Collection, 2017). Ag^+ concentrations of 0 µM, 1.5 µM (0.16 ppm) and 3 µM (0.32 ppm Ag^+) were combined with *E. coli* (ATCC® 25922™) at 10^6 cells/ml in PBS in triplicate and the viable cells were counted over time. The time-kill curve developed from the counting of *E. coli* (ATCC® 25922™) colonies 24 hours after being treated with Ag^+ is presented in Figure 6-1. The starting colony count was approximately 10^6 cells/ml. This is much higher than the *E. coli* concentration that would be found in natural water sources, even if contaminated. Such high bacterial counts are often used in bacterial susceptibility studies and therefore this study did the same to allow for easy comparison of these results to other investigations.

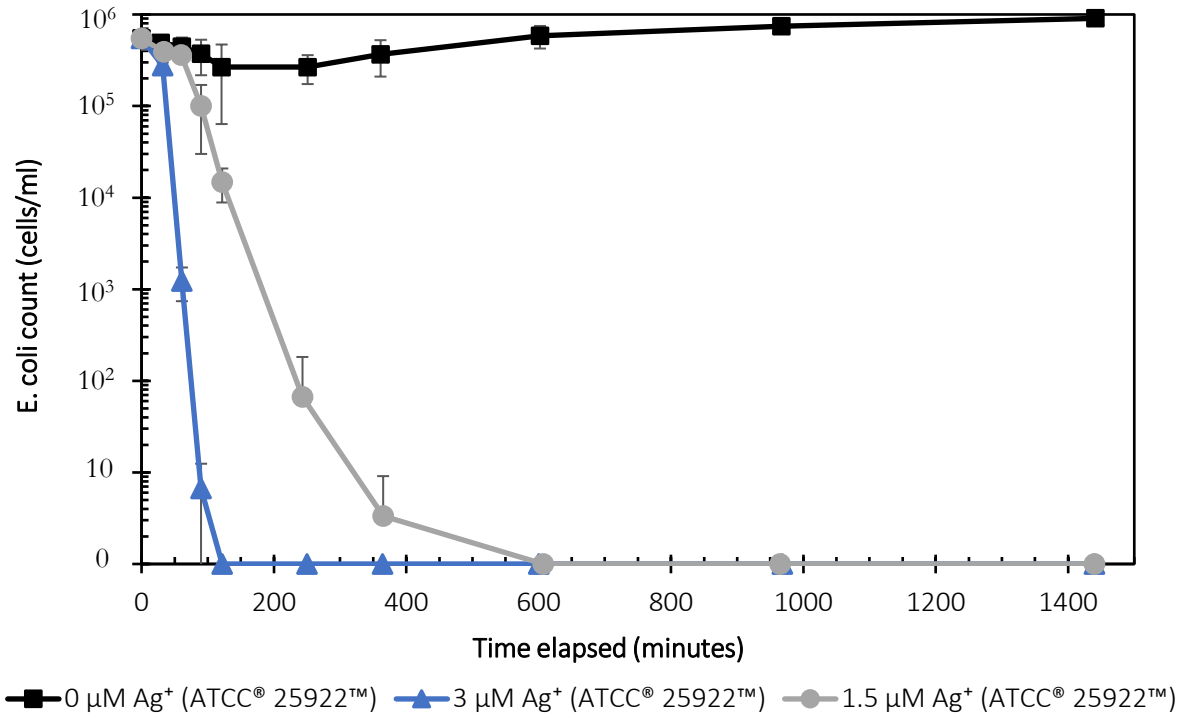

Figure 6-1: Time-kill curve of E. coli (ATCC® 25922™) after treatment with Ag^+

Figure 6-1 shows that 1.5 µM Ag^+ kills off the *E. coli* (ATCC® 25922™) at a much slower rate than 3 µM Ag^+, as was expected. Interestingly, the kill-curve of the 3 µM Ag^+ against ATCC® 25922™ is very similar to that of the 6 and 12 µM Ag^+ kill-curves against DH5α. There might be a slight difference between the susceptibility of the two *E. coli* strains to silver ions, which would explain this result. Alternatively, these concentrations may be well above the threshold minimum bactericidal concentration (MBC, the lowest concentration of an antimicrobial agent that will kill a particular bacterium in 24 hours). The 1.5 µM Ag^+ kill-curve very clearly shows a rapid decrease in the number of viable cells initially, and then a slower rate of cell death as the cell-count reaches zero. Shorter time intervals between sampling would have given a clearer picture of the rate at of cell death. Unfortunately, manual sampling and spreading of plates (a very laborious process) every 30 minutes over 24 hours is not feasible, therefore other methods of developing the time-kill curves should be investigated.

Some preliminary studies using fluorescein diacetate (FDA), a substrate used for rapid, high-throughput antibacterial screening, to develop time-kill curves of *E. coli* were performed (Wanandy *et al.*, 2005). Once absorbed by the cell, esterase cleaves (hydrolyses) the FDA to produce fluorescein which collects in viable cell walls and fluoresces green under UV light (Oukarroum, Bras, Perreault, & Popovic, 2012). The intensity of this fluorescence, and therefore the number of viable cells, can be quantified using a fluorometer. Measuring the fluorescence of bacteria is far less labour intensive than plate spreading and cell counting, and results are collected instantly, rather than having to wait for cells to grow on agar before counting them. Some bacteria media have been known to cause the cleavage FDA, most likely because of the presence of nucleophiles, resulting in fluorescence which thus convolutes the results.

Wanandy *et* al. (2005) studied which of Good's buffers[4] were most suitable for use with FDA. Based on their conclusions, MOPS (morpholonepropanesulfonic acid) was chosen above the previously used phosphate buffer.

Experiments using FDA, following the method explained in Section 4.4.2.1 at different cell dilutions in microtitre plates, were performed to ascertain whether it could be used in the assessment of cell viability. Unfortunately, difficulty was experienced in correlating the fluorescence to a known number of cells in the samples. After two hours of contact between *E. coli* cells and FDA, the fluorescence of 10^6 cells/ml was not registered by the spectrofluorometer. It was hypothesised that not enough FDA had been taken up by the cells, however, after overnight contact the cells were still not fluorescing. Additionally, the FDA crystallised out of solution when added to the MOPS buffer. Using a fluorescent microscope with a green-light filter, the cells were still not visible and only crystal structures (most likely the precipitated FDA) were seen. Due to time constraints, this experimental method could not be optimised, and therefore the original plate-spreading and cell-counting techniques were used for all other antibacterial experiments within this study.

Important to consider is the maximum allowable concentration of silver in drinking water. Although no enforceable regulations are in place, the advised maximum concentration of silver in drinking water by the World Health Organisation is 0.1 mg/L (or 0.6 µM)[5]. This value relates particularly to cases where silver is used as a bactericide in drinking water and yields a total dose of half the human No Observable Adverse Effect Level (NOAEL) of 10 g over 70 years. A more in-depth description of the potential health effects of silver is given in Section 2.3.3. Concentrations much higher than this advised maximum concentration were used in the current study for the Ag^+ control experiments. In follow-up studies, lower Ag^+ concentrations should be investigated.

It is relevant to note that the bacterial medium PBS contains chloride ions from NaCl and KCl. Most natural water sources will also contain Cl^-. Chloride ions form the water-insoluble salt AgCl with silver, which has the potential to affect the measured antibacterial activity. Choi *et al*. (2008) found that AgCl colloids of ca. 0.25 µm in size could inhibit nitrification and *E. coli* growth almost as effectively as Ag^+. On the other hand, Le Ouay & Stellacci (2015) state in their review paper on the antibacterial activity of silver nanoparticles that the presence of ions such as chloride (Cl^-), phosphate ($PO4^{3-}$) and sulphide (S^{2-}) in solutions may result in the reduction of the toxicity of Ag^+ because of the formation of insoluble silver salts. The formation of these salts lowers the bioavailability of silver, thus lowering their biocidal activity. Studies have found, however, that the dissolution of Ag nanoparticles and the antibacterial effect of Ag^+ in the presence of Cl^- is highly dependent on the Cl/Ag ratio (Chambers *et al*., 2014; Levard *et al*., 2013). At high Cl/Ag ratios, soluble silver polychloride species $AgCl_x^{(x-1)-}$ are formed. These species do not have a significant impact on Ag^+ antibacterial activity and may even enhance the dissolution of Ag nanoparticles thus increasing the nanoparticle toxicity towards bacteria (Levard *et al*., 2013).

To ascertain what species of Ag would be present in the PBS solution (and in water sources containing Cl^-), the ion component concentrations of the solution (found in Appendix B.1) were entered into the

[4] Buffers investigated and described by Norman Good and colleagues in 1966.

[5] The South African Water Quality Guidelines, presented by the Department of Water Affairs and Forestry, does not mention the maximum allowable concentration of silver in drinking water (Department of Water Affairs and Forestry, 1996).

chemical equilibrium speciation modelling freeware Visual MINTEQ (Gustafsson, 2018). This software, a Windows version of MINTEQA2 which is published by the United States Environmental Protection Agency, uses multicomponent thermodynamic equilibrium speciation models for aqueous systems (Van Briesen, Small, Weber, & Wilson, 2010). The speciation of Ag in PBS solution across a range of concentrations relevant to this study, of between 0 and 15 µM, is presented in Figure 6-2. Higher concentrations of Ag^+, of between 0 and 100 mM, were also investigated to better understand the speciation in the presence of chloride and this is shown in Figure 6-3. The results showing the speciation of non-Ag species at relevant concentrations of Ag^+ can be found in Appendix B.1.

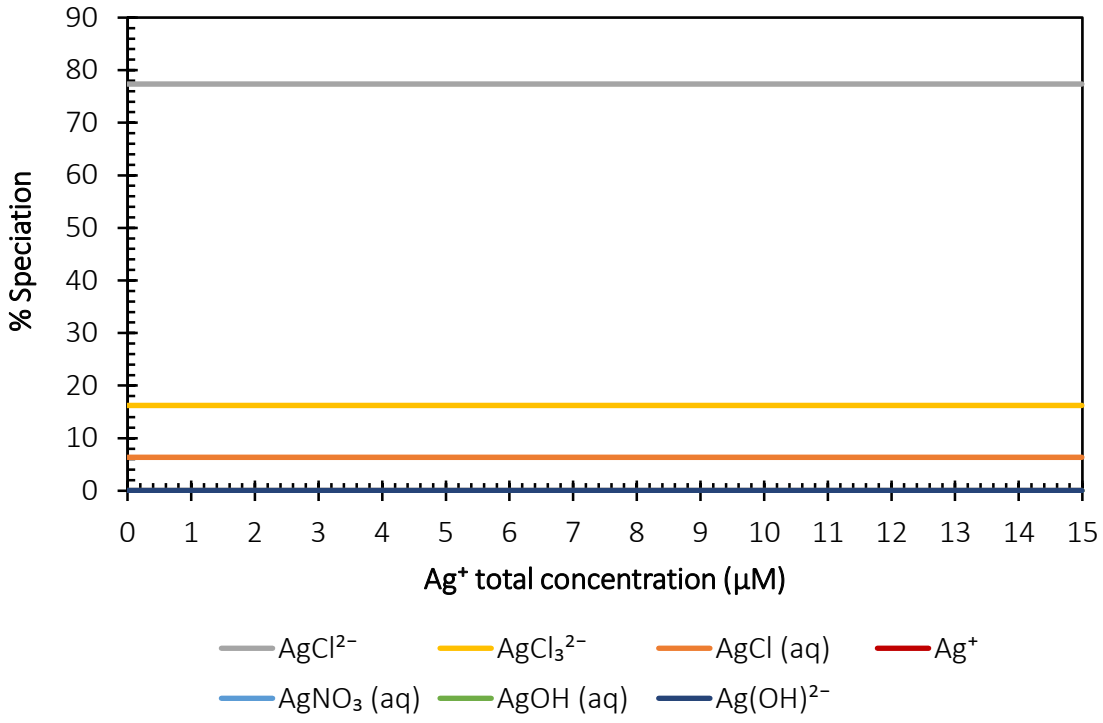

Figure 6-2: The Ag species distribution in PBS solution in the presence of 0 to 12 µM of Ag^+ determined using Visual MINTEQ

Figure 6-2 shows that less than 7% of the added silver forms AgCl across the range of Ag^+ concentrations applicable to this study. This means that, in the experiments performed to study the antibacterial efficacy of $AgNO_3$, at least 93% of the added silver is bioavailable. The low concentration of free Ag^+ in the solution may mean that the Ag^+ ion-selective electrode will not register the presence of Ag because of its formation of polychloride species. This formation has not prevented the antibacterial effect of Ag^+, as clearly shown by the results presented in Figure 6-2 and Figure 6-3..

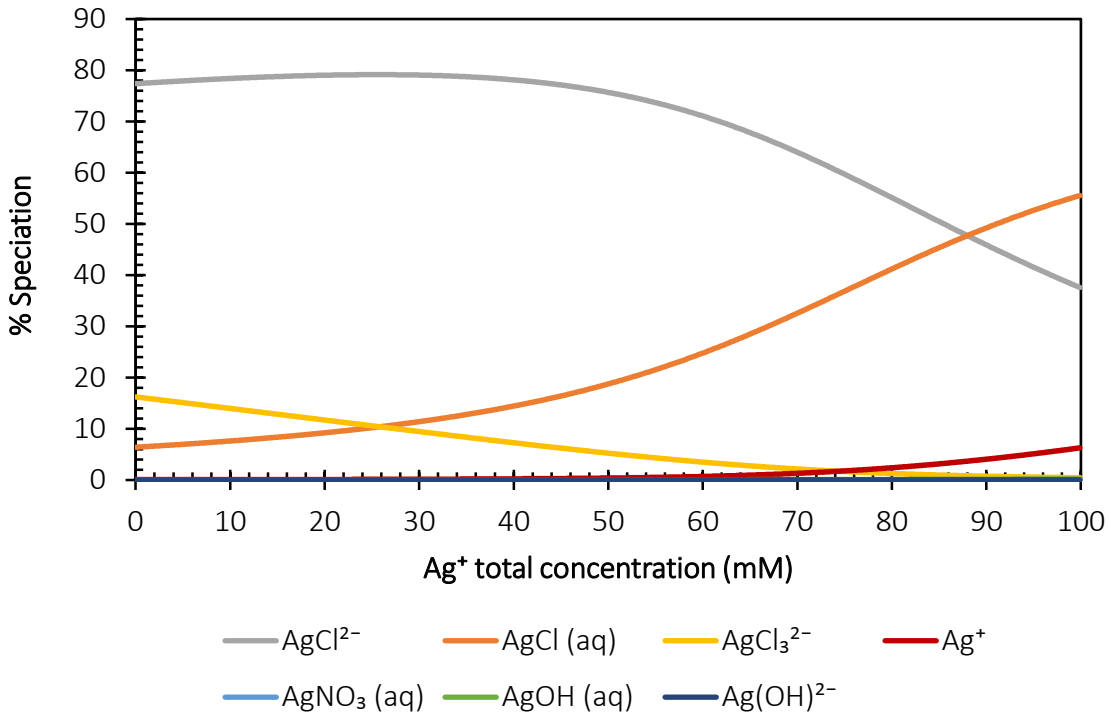

Figure 6-3: The Ag species distribution in PBS solution in the presence of 0 to 100 mM of Ag^+ determined using Visual MINTEQ

From Figure 6-3 one can see that the percentage of Ag present as non-bioavailable AgCl reaches 10% only at total Ag concentrations of approximately 24 mM. The results of this simulation also assist in understanding the chloride concentration at which silver ions and nanoparticles can be used for water disinfection. There are no enforceable regulations regarding the maximum allowable concentration of chloride in drinking water, however the World Health Organisation recommends lower than 250 mg/l (approximately 7 mM) due to the salty taste. At this recommended concentration or lower, less than 10% of the added silver is present as AgCl. This means that silver can be used for the disinfection of natural, fresh water without there being an issue of antibacterial efficacy inhibition through interaction with chloride ions.

6.2 Antibacterial efficacy of silver nanoparticle-loaded filters

Quartz fibre filters loaded with silver nanoparticles were studied for their antibacterial efficacy. Silver was deposited on these filters by Bhamidipati (2017) at Delft University of Technology using a spark ablation method, which is described in Section 4.3.1. The filters allow for the study of a more application-based method of water disinfection using silver nanoparticles, rather than the fundamental, proof-of-concept investigation using silver ions.

The various spark ablation conditions used for the formation of the Ag nanoparticles that were deposited on the quartz fibre filters are presented in Table 6-1. The spark ablation frequency used to produce the silver nanoparticles was 1000 Hz. For filters F4 and F5, alloys of silver and copper were made by using the two metals as the cathode (+) and anode (-). This alloy was investigated because copper also has antibacterial properties but is cheaper than silver. Therefore, if the bactericidal activity of the alloy is similar to that of the silver nanoparticles, the alloy would be the better option for use in water disinfection in the communities of poor, developing countries.

Table 6-1: Spark ablation conditions used for the preparation of silver nanoparticles deposited on quartz fibre filters

Deposition variation	*Carrier gas flowrate (L/min)*	*Loading time (min)*	*DMA Voltage (V)*	*Oven at 961 °C*
A1	5	7.5	120	No
A3	5	30	120	No
A4	5	60	120	No
B3	5	30	50	Yes
S6	7	60	83	No
F1	7	90	165	No
F2	7	90	83	No
F3	7	90	120	No
F4 [Ag(+) Cu(-)]	7	90	120	No
F5 [Ag(-) Cu(+)]	7	90	120	No

The silver nanoparticles deposited on the "A-series" filters, on B3 and on S6 were intended to be the same size, and on the TEM grids were found to be in a similar size range (reported in Table 6-2). The A-series differed only in the deposition time, which theoretically only increases the loading on the filters. Filter B3 differs in that it was placed in a tube oven after deposition to coalesce agglomerated particles; a lower DMA (differential mobility analyser) voltage was used to achieve a similar particle size range to the A3 filter. The carrier gas flowrate used for silver deposition on the S6 filter was higher than for the A-series, which leads to the formation of smaller primary particles. The DMA voltage was varied for the "F-series" filters, F1 – F3, which theoretically results in the deposition of size-selected monodisperse particles based on their electrical mobility (a function of particle size). Finally, a copper electrode and a silver electrode were used for the formation of silver/copper alloys. Particles prepared using silver as the cathode and copper as the anode were deposited on filter F4 and *vice versa* for filter F5.

6.2.1 Particle size from SEM

As previously described, to isolate the antibacterial effect of silver ions released from silver nanoparticles, the nanoparticles should be 10 nm or smaller in size (Sotiriou & Pratsinis, 2010). The filters were analysed using Scanning Electron Microscopy (SEM) to determine the particle sizes of the deposited nanoparticles. The spark frequency, the flow rate of the carrier gas and the spark energy all affect the size of the produced particles. Bhamidipati (2017) aimed to produce spherical, uniformly sized silver nanoparticles smaller than 10 nm using spark ablation by varying the time of deposition and the voltage across the DMA. Particles were directly deposited on TEM grids to measure their size distribution, and an image of this is shown in Figure 6-4a alongside a SEM image of silver nanoparticles on filter fibres. Further SEM images of the silver nanoparticles deposited on the filters can be found in Appendix B.2.

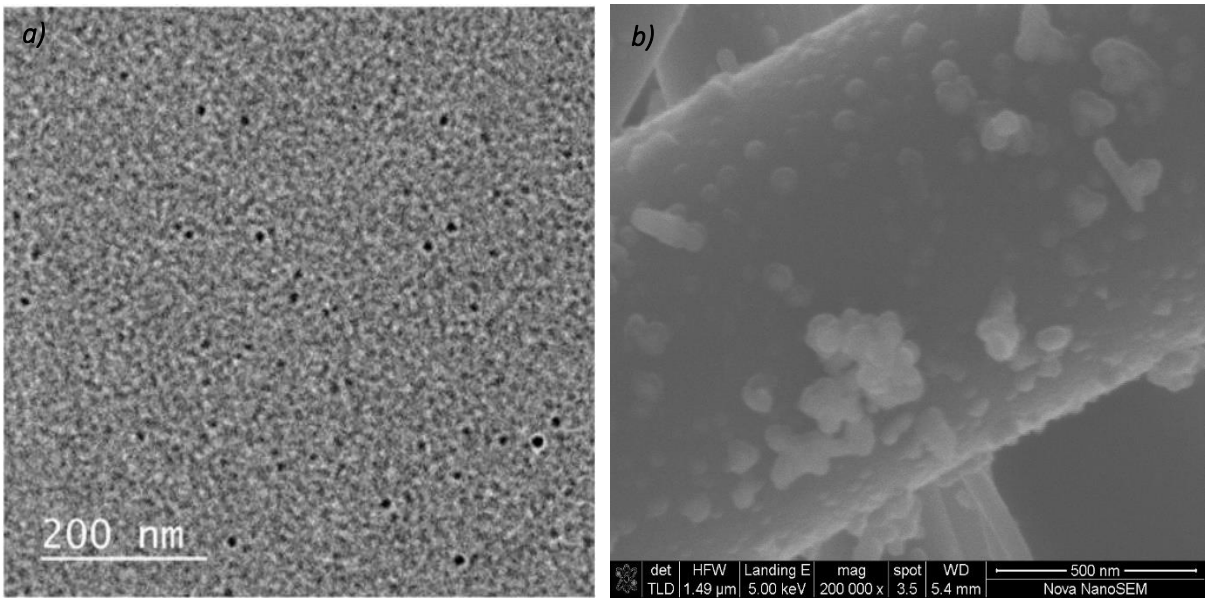

Figure 6-4: Silver nanoparticles produced using spark ablation a) deposited on a TEM grid and shown using a TEM image taken from Bhamidipati (2017) and b) deposited on a quartz fibre filter and shown using a SEM image

There is an observable difference in the appearance of the particles on the TEM grid and on the quartz fibre filter, as seen in Figure 6-4. The particles on the filter are clearly much larger and are also not spherical or uniformly sized like those on the TEM grid. Additionally, there appears to be a lot of agglomeration of the particles on the fibres, appearing almost tentacle-like. The measured particle sizes on the filters using SEM analysis are shown alongside the particle size measured by Bhamidipati (2017) using TEM in Table 6-2.

Table 6-2: Number-based and volume-based mean particle size and median particle size for each quartz fibre filter

Deposition variation	*TEM mean particle size (nm)**	*Number-based mean particle size (nm)*	*Volume-based mean particle size (nm)*	*Median particle size (nm)*
A1	~5-7	57.2 ± 13.0	55.9 ± 13.5	55.9
A3	~5-7	48.5 ± 16.8	64.0 ± 15.8	46.1
A4	~5-7	59.0 ± 16.1	72.3 ± 17.7	57.1
B3	~5-7	56.8 ± 12.0	64.6 ± 13.3	55.4
S6	6	53.2 ± 14.5	64.9 ± 15.6	52.0
F1	9	53.5 ± 16.3	72.6 ± 25.3	51.2
F2	3	33.4 ± 12.4	46.9 ± 14.8	32.7
F3	6	27.0 ± 12.6	44.1 ± 14.7	24.2
F4 [Ag(+) Cu(-)]	-	29.7 ± 11.1	41.8 ± 13.4	29.0
F5 [Ag(-) Cu(+)]	-	24.8 ± 11.1	39.2 ± 13.6	23.6

* from Bhamidipati (2017)

Clearly, both the number-based and volume-based particle sizes are much larger than the desired 10 nm. It is not within the scope of this study to investigate why the silver nanoparticles are different sizes when directly deposited on TEM grids than when deposited on quartz fibre filters under the same spark ablation conditions, nor is it within the scope to study the trends of the particle sizes as the spark ablation conditions are varied. However, it is suggested that the larger particles form *after* deposition on the filter through agglomeration on the fibres. This is further supported by the fact that the silver nanoparticles on the filters are not spherical and appear almost tentacle-like, whilst on the TEM micrographs provided by Bhamidipati (2017), the particles appear round.

The purpose of determining the sizes of the particles on the filters is to relate this to their antibacterial effect. The large particle size means that the antibacterial activity of the filters will be lower than expected because of the slower dissolution rate of large particles. Additionally, because of the wide size distribution, it will be difficult to correlate the antibacterial action of the filters with a particle size. Finally, it was also observed that the nanoparticles are not uniformly distributed on the filters. Because pieces of each filter were used in the antibacterial efficacy studies, there is expected to be variation in the antibacterial activity across each of the experimental replicates using the same filter. The loading on each filter also differed, so it is anticipated that the filters will demonstrate different antibacterial activities because of differing silver concentrations.

6.2.2 Measurements of the antibacterial efficacy

The dissolution of silver in water takes place via the following reaction:

$$Ag^0 + \frac{1}{4}O_2 + H^+ \rightleftharpoons Ag^+ + \frac{1}{2}H_2O \qquad \textit{Equation 6-1}$$

It is evident from Equation 6-1 that the dissolved oxygen concentration and the pH of the solution will affect the release of silver ions from silver nanoparticles and, therefore, the antibacterial efficacy of the silver-loaded quartz fibre filters. Throughout the experiments performed to develop the kill-curves of the filters, the pH of the PBS, which is a buffer solution, is maintained at 7.4. Flasks containing the filters, *E. coli* (ATCC® 25922™) and PBS were kept on a shaker (at 120 rpm) to keep the filter discs circulating, thus ensuring that the oxygen content in the solution did not limit the release of silver ions. The experiments to develop the time-kill curves were performed in triplicate, and the error bars shown are the standard deviation of the data points.

The antibacterial efficacy studies of the filters were done in batches because of the laborious and time-consuming nature of the sampling, plate spreading and manual colony counting. As described in Section 4.4.1.2, a punch was used to ensure filter discs were of the same size throughout the investigation. Based on the size of the discs and the mass of silver deposited on the filters, measured by Bhamidipati (2017), the total concentration of silver in the flasks used for the investigation could be calculated. This is shown in Table 6-3, which is reprinted from Section 4.4.1.2.

Table 6-3: Estimations of silver concentration on each quartz fibre filter

Filter	*Mass deposited on filter (g)**	*Concentration (µg/cm²)*	*Mass per filter disc (µg)*	*Ag concentration in PBS (µM)*
A1	0.0001	7.96	2.25	0.83
A3	0.0004	37.54	7.79	2.81
A4	0.0005	41.86	11.83	4.39
B3	0.0004	33.48	9.47	3.51
S6	0.0005	32.88	9.30	3.45
F1	0.0002	14.44	4.08	1.51
F2	0.0002	14.44	4.08	1.51
F3	0.0002	14.44	4.08	1.51
F4 [Ag(+) Cu(-)]	0.0004	28.87	8.16	-
F5 [Ag(-) Cu(+)]	0.0002	14.44	4.08	-

* measured by Bhamidipati (2017)

In considering concentration alone, filter A4 would be expected to have the highest antibacterial activity, followed by B3 and S6. However, A4 also has the largest mean particle size which subsequently means it will be the filter with the slowest ion release rate per nanoparticle. It is difficult to say whether the concentration or the particle size will have a greater effect on the overall ion release rate without performing thermodynamic calculations that take into consideration the surface energy of the nanoparticles, which is a function of particle size and morphology (van Helden, van Santen, & van Steen, 2009). It is recommended that the estimation of the equilibrium ion concentration of silver nanoparticles of a specific size in water be done in future studies.

The first set of antibacterial efficacy studies was performed on the "A-series" filters, filter B3 and S6. The silver nanoparticles deposited on these filters were intended to be the same size, and on the TEM grids were found to be in a similar size range. For this reason, they have been grouped together. The total silver concentration in the flasks, however, differed vastly across the different filters because of different silver loading and the mean number-based particle size on these filters ranges from 48 nm to 59 nm. The filters were studied for 15 hours whilst in contact with *E. coli*. The bacteria count during this period is shown in Figure 6-4.

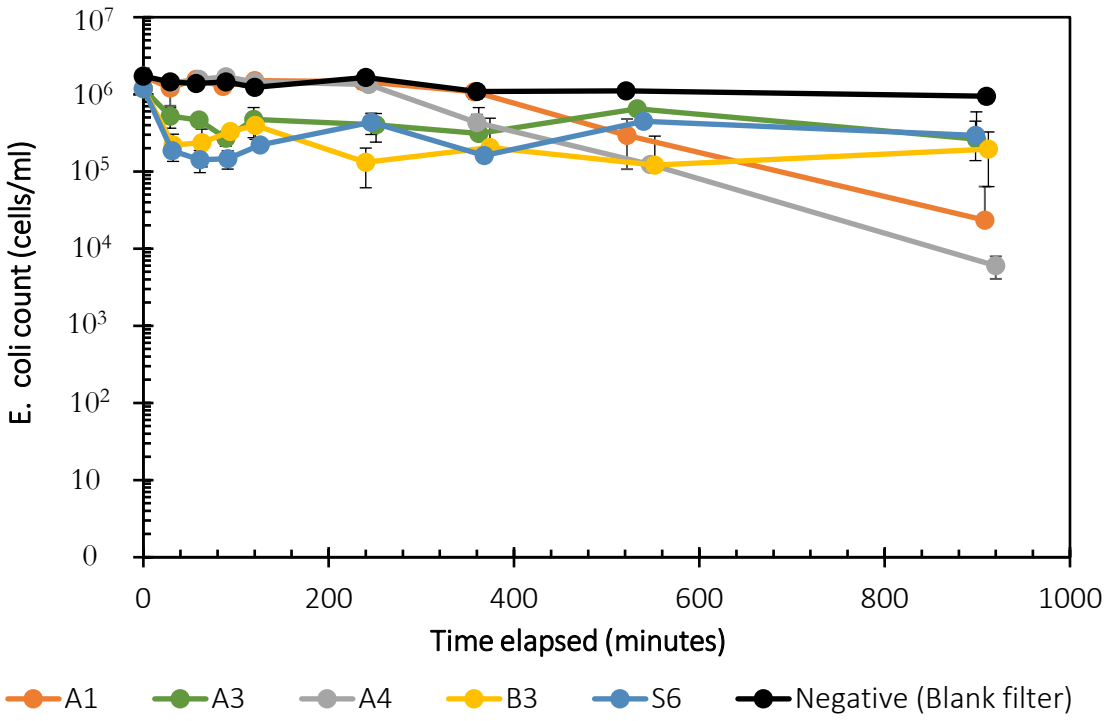

Figure 6-5: Time kill curve of silver nanoparticle-loaded filters, prepared through varying the time of deposition, use of the oven and DMA voltage, against E. coli (ATCC® 25922™)

There is no definitive evidence of antibacterial activity of the filters shown in Figure 6-5. After a slight initial decrease, the bacterial count over the 15-hour period remains fairly constant (and high) for filters A3, B3 and S6. Filters B3 and S6 have similar silver nanoparticle size distributions and mass loadings, which would explain their similar performance against *E. coli*. Filters A1 and A4 show a slight downward trend in bacteria count. This suggests a toxicity towards the bacteria, albeit rather low.

It is difficult to understand why filters A1 and A4 would demonstrate antibacterial activity but A3 would not, particularly because there is a higher mass loading of silver nanoparticles on A3 than on A1. A possible explanation may be found in looking at the volume-based mean particle size of the three filters shown in Table 6-2. Although the number-based mean particle size of A3 is lower than that of A1, the volume-based mean is higher. This indicates that more of the silver mass on A3 is contained in larger particles than for on A1 (since volume is proportional to mass). Thus, although there is a higher concentration of silver present on A3, the silver ion release rate may be slower than for A1 because of the dissolution kinetics relating to larger particles. A lower dissolution rate means a lower bactericidal rate which may be the reason for A3 not demonstrating an antibacterial effect. The silver concentration on A4 is five times higher than that of A1 and, although the deposited silver nanoparticles are larger, it also demonstrates higher antibacterial efficacy.

Important to note is that the bacterial count *cannot* increase in these experiments because there are no nutrients in the PBS solution off which the bacteria can feed. Therefore, any perceived increase in bacteria count is an error, most likely resulting from the inherent inaccuracy of manual plate spreading and colony counting.

The second set of antibacterial studies were performed on the "F-series" (F1 – F3), where silver nanoparticle deposition was varied by changing the DMA voltage. It was estimated that the total silver concentration in the flasks was the same for each filter. This would mean that any difference in antibacterial efficacy between the filters is because of the the difference in size of the deposited silver nanoparticles which will release silver ions at different rates. Filter F1 has the largest particle size (53.5 ± 16.3), whilst F3 has the smallest (27.0 ± 12.6). The filters were in contact with the *E. coli* for over 28 hours and the bacterial count during this period is shown in Figure 6-6.

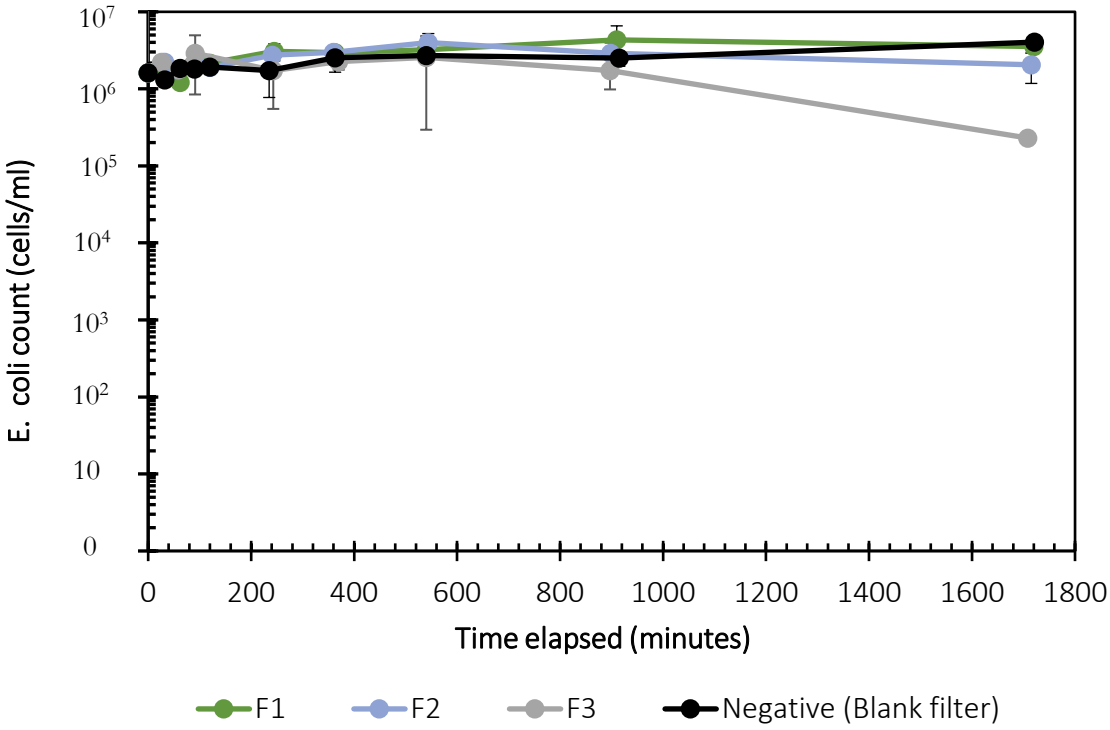

Figure 6-6: Time kill curve of silver nanoparticle-loaded filters, prepared through varying the DMA voltage, against E. coli (ATCC® 25922™)

In studying the results presented in Figure 6-6, there is no clear evidence of antibacterial activity of the filters. The number of surviving bacteria colonies in the flasks containing filter discs from F1 and F2 remains constant and that seen in the control experiment. The number of surviving bacteria for the sample containing F3 filter discs decreases after between 15 and 28 hours of contact time. Because this decrease was seen in each of the three replicates, it is believed this is an indication of low levels of toxicity towards the bacteria. This slow bactericidal action is likely due to the very slow release of silver ions from the filter disc.

Finally, the filters loaded with the silver/copper alloyed nanoparticles (F4 and F5) were studied. It is difficult to estimate the concentrations of silver and copper present on the filter because only the total mass of nanoparticles deposited on each of the filters is known. Filter F4 has twice the mass of deposited nanoparticles than F5. One would therefore expect a stronger antibacterial effect from F4.

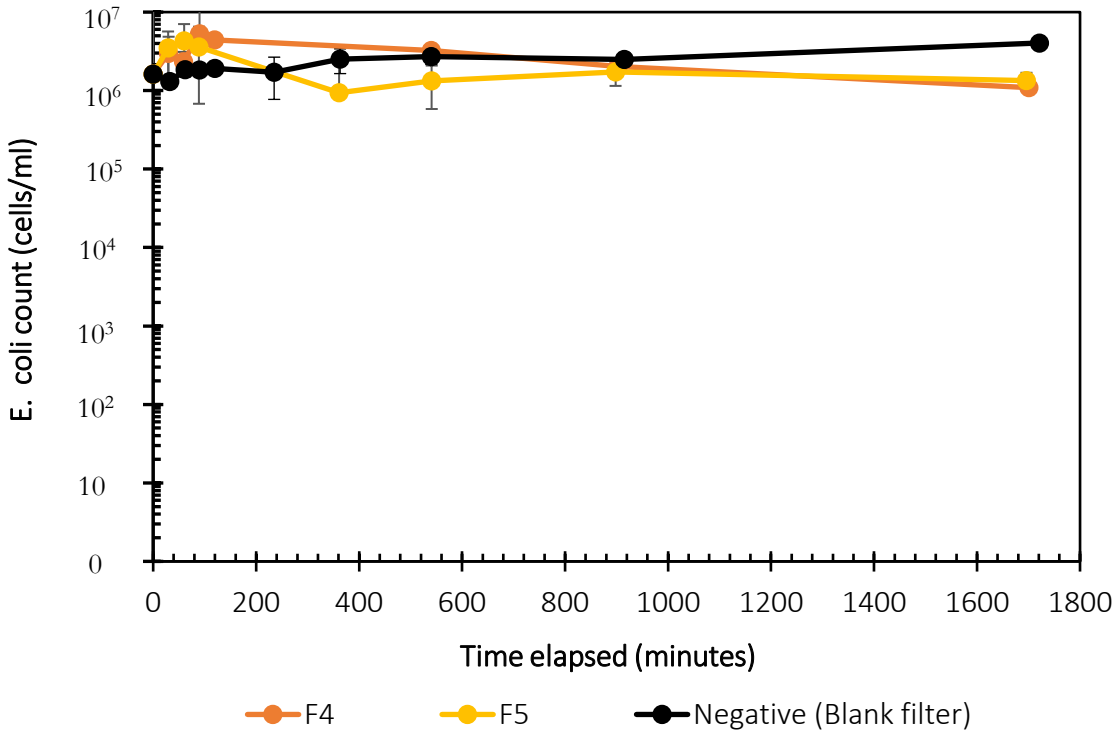

Figure 6-7: Time kill curve of silver/copper alloy nanoparticle-loaded filters against E. coli (ATCC® 25922™)

The data presented in Figure 6-7 shows the number of surviving bacteria is effectively constant over the 28-hour period of contact between the *E. coli* and filters F4 and F5. Once more, this means that neither filter has a demonstrated toxicity at the nanoparticle concentrations present in the solution.

Following the results that showed little to no antibacterial effect demonstrated by the filters in the PBS solution, disc diffusion tests were performed. As described in Section 4.4.2.2, this involves placing the filter disc on a lawn of *E. coli* and observing, over three days, whether a zone of inhibition forms around the discs. The wider the zone of inhibition, the stronger the bactericidal activity of the filter. Unfortunately, no zone of inhibition formed for any of the filters.

There are a number of possible explanations for why the silver-loaded filters show no or very low antibacterial activity. The nanoparticles may be dissolving very slowly, thus only a low concentration of ions, which are the main reason for the antibacterial action of the nanoparticles, will be present in the bacterial solution. Silver nanoparticles are slower-acting antibacterial agents than $AgNO_3$ because the solid first needs to ionise before any bactericidal effect is seen. This ionisation may be hindered because the particle surface is only partially exposed due to the adherence of the nanoparticles to the filter fibres. Additionally, the concentrations present on the filter discs may be too low for any antibacterial effect to be evident. Whole filters, rather than small discs from the filters, may show better antibacterial efficacy because of higher concentrations of silver that would be present. It has already been shown in Figure 6-2 that, at the silver ion concentrations of interest, there will be an interaction with the chloride ions but 93% of the silver in the solution will still be bioavailable therefore the scavenging of the silver ions by chloride is not the reason for the lack of bactericidal activity. However, silver ions may not be dissolving into the solution at all.

In an attempt to better understand the antibacterial activity (or lack thereof) of these filters, ion release studies were performed using an Ag^+ selective electrode. Since silver ion concentration is directly related to antibacterial activity, measuring the ion concentration over time could give an indication as to why there is little to no observed antibacterial effect demonstrated by the filters. Because the kill curve data were collected following contact of the silver-loaded filters with *E. coli* in PBS, the ion concentration measurements were performed by placing a single filter disc from each filter into PBS. A smaller volume of PBS was used for these studies than for the time-kill curve studies such that the total silver concentration in solution is 2.5 times higher. Over a 24-hour period, no silver ion concentration was measured in any solution containing a filter disc. This suggests that the silver nanoparticles are not dissolving, which is the reason for the lack of observed antibacterial activity. However, the measuring limit of the Ag^+ ISE is 0.001 ppm, so the concentrations present may have been much lower than this. Depending on the conditions of the study, the minimum bactericidal concentration (MBC) of silver ions against *E. coli* has been found to be between 0.02 and 3.25 ppm (Berger, Spadaro, Chapin, & Becker, 1976; Chernousova & Epple, 2013; Sintubin *et al.*, 2011; Zhao & Stevens, 1998). If the Ag^+ concentrations in contact with *E. coli* were lower than this, little to no bactericidal effect would be observed.

The formation of silver/chlorine complexes may be the reason that there is no measurable concentration of silver ions in the medium, but this should not have a significant effect on the antibacterial efficacy of the filters. However, precipitation of AgCl on the surface of the silver nanoparticles, and therefore the possible antibacterial activity passivation this results in, is a possibility. To determine whether this phenomenon may be the reason behind the lack of antibacterial activity observed, a filter disc from each of the filters was placed into different vials containing only deionised water with the idea that the silver ion concentration over time would be measured without the presence of chloride. Unfortunately, there was a problem with the Ag^+ ISE where a silver ion concentration of over 0.200 ppm was measured in the control (deionised water) numerous times after instrument recalibration. This Ag^+ concentration measurement was higher than for the samples containing silver-loaded filters, which therefore means the results of this experiment are unreliable. Before this experiment, the ISE performed well so it is believed that all other experimental data collected using the ISE are reliable. Attempts were made to troubleshoot and repair the ISE but, due to time constraints, no further experiments using the instrument could be performed.

6.3 Summary of antibacterial efficacy studies

The potency of Ag^+ against *E. coli* was established, with 12 µM, 6 µM and 3 µM Ag^+ killing off 10^6 cells/ml in less than 3 hours and 1.5 µM Ag^+ killing off the same concentration of *E. coli* in less than 10 hours. These concentrations are equivalent to 0.15 – 1.30 ppm Ag^+ and indicate that, in the conditions of these experiments, the MBC of *E. coli* ATCC® 25922™ is below 0.15 ppm Ag^+. Although, in this study, there is no issue with the formation of AgCl leading to the reduction in toxicity of Ag as a result of high content of Cl^- in the bacteria medium, the concentration of chloride in waters that will be treated with Ag^+ is an important consideration for future studies.

The silver-loaded filters demonstrated little to no antibacterial activity towards *E. coli*. This may be because the filters comprise large silver nanoparticles which have slow Ag^+ dissolution kinetics. The silver dissolution may also be slowed by the interaction between the nanoparticles and the fibres of the filter. Alternatively, there may be no dissolution of ions at all because of passivation of the silver nanoparticles through the precipitation of AgCl on their surface.

The silver ion concentration in PBS after the filters were in contact with the solution for 24 hours registered as 0 ppm. This suggests that there is no dissolution of silver nanoparticles from the silver-loaded filters. Alternatively, there may be concentrations of Ag^{+} that are below the measurement threshold and below the concentration at which a bactericidal effect would be observed.

Chapter 7: Concluding remarks and recommendations for future work

7.1 Summary and concluding remarks

Silver nanoparticles have great potential in being used in water disinfection applications because of their high antibacterial activity and broad antimicrobial spectrum (Qu, Alvarez, & Li, 2013). Development in this area is critical, particularly in advancing technology to allow greater accessibility to clean drinking water for people in poor, rural areas in developing countries. Incorporating nanotechnology into current water disinfection systems, as well as developing new water treatment nanotechnology, shows promise in addressing this issue, however much research needs to be done first before this can become a reality (Q. Li *et al.*, 2008).

This study aimed to synthesise silver nanoparticles suitable for use in water disinfection applications by exploring how preparation conditions affect the particle size and distribution. To do this, two different aqueous chemical reduction preparation methods were performed and reaction conditions such as surfactant concentration, agitation rate, synthesis temperature, and method of chemical addition were varied. This study also aimed to investigate the antibacterial efficacy of silver nanoparticles deposited on quartz fibre filters against *E. coli*.

Synthesis Method One made use of ascorbic acid as the reducing agent and SDS as the surfactant (AL-Thabaiti *et al.*, 2008). Following the discovery that light significantly affected the particle size of the silver nanoparticles, all preparation was done in dark conditions. The surfactant concentration, agitation speed, synthesis temperature, reducing agent concentration or method of chemical addition were varied, but none resulted in the production of smaller, more monodisperse nanoparticles. These parameter changes did, however, have a definitive effect on the particle size, distribution and morphology as evidenced from UV-Vis and TEM studies. The smallest particles had a number-based mean particle size of 3.6 ± 3.8 nm and a volume-based mean particle size of 15.4 ± 6.4 nm. The presence of large particles in the sample means that, in assessing antibacterial activity of the nanoparticles, it will be difficult to interpret whether the bactericidal effect is due to silver ions or because of an interaction between the bacteria and the actual nanoparticles. It was verified, using the d-spacings identified on TEM images, that the nanoparticles were fcc silver with (111) and (200) lattice planes. Removing excess surfactant and collecting these nanoparticles in powder form would facilitate antibacterial efficacy studies, however this proved to be difficult. Centrifugation alone was not successful and, unfortunately, phase extraction using organic solvents in conjunction with centrifugation could not be pursued beyond very small-scale experiments. Bactericidal studies using these nanoparticles could therefore not be performed.

Synthesis Method Two uses aniline as the reducing agent, DBSA as the surfactant and NaOH as the reaction 'activating' chemical (Yang, Yin, Jia, & Wei, 2011). This method produces silver nanoparticles that are 30x more concentrated than Method One and, because of this, is preferred. In dark conditions, the surfactant concentration, agitation speed, reducing agent concentration and method of chemical addition were varied, and the effect of this on the particle size was analysed. The NaOH hot injection

variation was found to produce the smallest particles with a number-based mean particle size of 6.7 ± 5.4 nm. Again, the presence of large particles as evidenced from the mean volume-based particle size of 22.3 ± 10.9 nm means that interpreting the antibacterial efficacy studies would be difficult. Particles were successfully collected in powder form following a phase extraction and centrifugation process using acetic acid, however it was found that this separation process led to the number-based mean particle size increasing to 12.5 ± 14.9 nm. This is highly undesirable since the size of the silver nanoparticle significantly affects its antibacterial activity. No assessment of the bactericidal efficacy was performed for these nanoparticles.

In studying the antibacterial effects that Ag^+ has on *E. coli* (ATCC® 25922™), it was found that concentrations of 12 µM, 6 µM and 3 µM Ag^+ killed off 10^6 cells/ml in less than 2.5 hours. It is believed that these Ag^+ concentrations are well above the threshold minimum bactericidal concentration and therefore the *E. coli* was rapidly deactivated. Ag^+ concentrations of 1.5 µM resulted in complete colony death after 10 hours. Following this investigation, Visual MINTEQ was used to simulate the concentration of Cl^- in the bacteria media and Ag^+ from silver nitrate or dissolved silver nanoparticles to determine silver speciation. At such low silver concentrations (0.5 – 15 µM), and such high chloride concentrations (140 mM), no precipitation of AgCl will be observed and over 93% of the silver in the system would be bioavailable. This, in conjunction with the Ag^+ bactericidal studies, confirmed the legitimacy of studying the antibacterial efficacy of silver nanoparticles deposited on quartz fibre filters in a similar system.

The silver nanoparticles on the quartz fibre filters were deposited via spark ablation. The silver nanoparticle size was analysed using SEM, which revealed that particles far larger than 10 nm were present on the filters with mean particles sizes ranging from 25 to 70 nm. This large particle size, together with the low concentrations of silver nanoparticles present on the filters, may have been the reason that little to no antibacterial activity was observed. Additionally, silver nanoparticles are slower-acting antibacterial agents than $AgNO_3$ because the solid first needs to ionise before any bactericidal effect is seen. To better understand the lack of evident antibacterial activity of the filters, ion release studies were performed. Over a 24-hour period, no silver ion concentration was measured in any solution containing a filter disc. This suggests that the silver nanoparticles were not dissolving, which is the reason for the lack of observed antibacterial activity.

The results of this study indicate how small changes in synthesis parameters can significantly affect nanoparticle size and uniformity, morphology, and degree of agglomeration. All of these properties will impact the antibacterial action of the silver nanoparticles because of their effect on the release of silver ions. This reveals the importance in stipulating the exact parameters used in nanoparticle preparation, including vessel size and shape used for the reaction, the agitation rate, and rate of chemical addition. Specifying these factors will aid improve the reproducibility of nanoparticle syntheses methods.

This work also showed the importance of quantifying the silver ion release from silver nanoparticles before performing antibacterial efficacy assessments. Since silver ions are the most important factor in the antibacterial action of silver nanoparticles, understanding their rate of release will allow for improved experimental design thus producing useful results. The use of silver nanoparticles for disinfection shows promise, as evidenced particularly by the antibacterial efficiency of Ag^+ against *E. coli* (ATCC® 25922™), however improvements in both the synthesis of silver nanoparticles and methods of assessing their bactericidal efficacy are clearly necessary.

There is still much critical research that needs to be performed before silver nanoparticles can be safely and efficiently used for water treatment and disinfection. This includes, but is not limited to, studies on the retention, cost and toxicity of nanoparticles. This study has highlighted the challenges that may be faced in pursuit of achieving this goal.

7.2 Recommendations for future work

The recommendations for future studies, following the work performed in this investigation, are grouped into three sections: nanoparticle synthesis, thermodynamic estimations, and antibacterial efficacy studies. There are several suggestions below that will result in a better understanding of the system being considered and may lead to improvements in the application of silver nanoparticles in the disinfection of water.

7.2.1 Silver nanoparticle synthesis

These recommendations include further investigations into synthesis methods, more extensive characterisation of nanoparticles and improvements in separation techniques of nanoparticles.

- Investigate the effects of combining the different synthesis variations on the size distribution of nanoparticles. For example, increasing the concentration of the silver nitrate precursor 10 times *and* injecting the NaOH into the system whilst following the Method Two protocol has the potential to produce a more concentrated system of nanoparticles with a small mean particle size and narrow size distribution.

- To study the growth and potential formation of aggregates during nanoparticle synthesis, samples of the silver dispersions during the reaction could be taken and examined using TEM.

- Consider performing organic, rather than aqueous, syntheses as this may result in the production of silver nanoparticles that are easier to separate. A different option for changing the method of synthesis would be to deposit the silver nanoparticles on a support, such as silica or carbon, which would allow for easier separation but may impact the antibacterial efficacy of the nanoparticles.

- Characterise the produced silver nanoparticles using EDX and XRD to further analyse their composition. XRD analysis will require the particles to be in powder form, therefore the separation process needs to be optimised first. EDX on the silver nanoparticles deposited on the quartz fibre filters should also be performed.

- Investigate the potential of using ultracentrifugation and ultrafiltration, or dialysis, as a means of separating the silver nanoparticles from their reaction medium *without* affecting the particle size. Alternatively, different chemicals to induce the flocculation of the nanoparticles could be sought.

7.2.2 Thermodynamic estimations of silver ion equilibrium concentration

To determine whether the concentration of silver nanoparticles or the actual silver nanoparticle size will have a greater impact on the concentration of dissolved silver, it is suggested that an estimation of the equilibrium ion concentration of silver nanoparticles of a specific size in water be done. This can be determined using the surface energy of the nanoparticles. This equilibrium concentration of Ag^+ ions will vary with particle size because there is an inverse relationship between the surface energy per area and the size of nanoparticles (van Helden, van Santen & van Steen, 2009). To estimate the surface

energy of the silver nanoparticles, one needs to know the crystal structure. The surface energy of a nanoparticle is proportional to the number and arrangement of the surface atoms, which is related to the particle diameter.

Romanowski (1969) and Cyrot-Lackmann (1969) proposed that the surface energy can be related to the number of unsaturated or "broken" bonds on the surface of the crystal. Van Hardeveld & Hartog (1969) determined how the total number of surface atoms and the proportions of the different surface atom types depend on the crystallite size. The researchers describe how surface atoms are different from atoms in the bulk in that they have an incomplete set of so-called nearest neighbours (i.e. unsaturated bonds) and that the number of nearest neighbours varies with the position of the atom on the face. The coordination number gives the total number of bonds an atom has and will be lower for surface atoms than bulk atoms. The statistics produced by van Hardeveld & Hartog (1969) are often used in the estimation of nanoparticle surface energy. For this estimation to be performed, the crystalline structure of the nanoparticle must be known.

Metallic silver has a face-centred cubic (fcc) crystal structure (Eberhart & Horner, 2010; Hofmeister, 2004; Molleman & Hiemstra, 2015; Vitos, Ruban, Skriver, & Kollár, 1998). Fcc lattices are bound by low-index crystal planes such as the (100) and (111) faces that have high atom densities. The (111) face is the most stable face of the Ag metal and has the highest metal density and lowest surface energy. Molleman and Hiemstra (2015) indicate that, because of this low surface energy, the (111) face is expected to be the dominant surface.

Spheroidal Ag nanoparticles have often been reported to have either an icosahedral or cuboctahedral morphology. Cuboctahedra are singly crystalline whereas icosahedral Ag nanoparticles form due to 5-fold twinning which is a common Ag lattice rearrangement (Henglein & Giersig, 1999; Hofmeister, 2004; Molleman & Hiemstra, 2015). The shape of these spheroids can be seen in Figure 7-1.

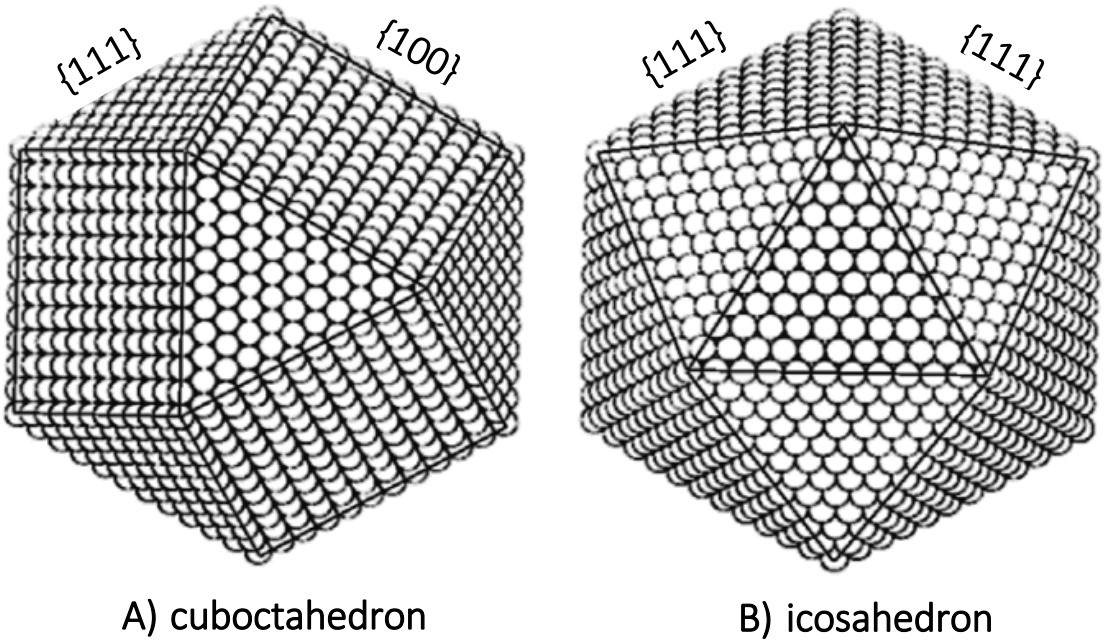

Figure 7-1: The spheroidal, fcc crystal lattice nanoparticle structures showing a) a cuboctahedron and b) an icosahedron from Hofmeister (2004)

These crystal structures were not found when studying the lattice spacings of the synthesised nanoparticles however, for the purposes of this study, this will be suitable as an estimation. Surface statistics determined by Benfield (1992) were used to determine the number of surface atoms at a specific particle diameter which is then used to approximate the surface energy of the particle using Equation 7-1. The surface statistics equations can be found in Appendix C.

$$\gamma_s = \frac{E_{coh}}{N_{low}} \cdot \left[N_{tot} - \sum_{i=0}^{CB} N_i \cdot \left(\frac{CN_i}{CB} \right)^n \right] \qquad \text{Equation 7-1}$$

where E_{coh} is the bulk cohesion energy per bond of silver with a value of 284 kJ/mol, N_{low} is the number of surface atoms (i.e. atoms with low coordination numbers) which is dependent on particle size, N_{tot} is the total number of atoms in a nanoparticle and is also dependent on particle size, N_i is the number of atoms with a specific coordination number CN_i and CB is the bulk coordination number of a shape. n is an arbitrary surface energy correction value that can be approximated as $n = 0.52$ (van Helden, van Santen, & van Steen, 2009).

The calculated surface energy per surface atom for the cuboctahedral and icosahedral structures as a function of particle diameter is presented in Figure 7-2.

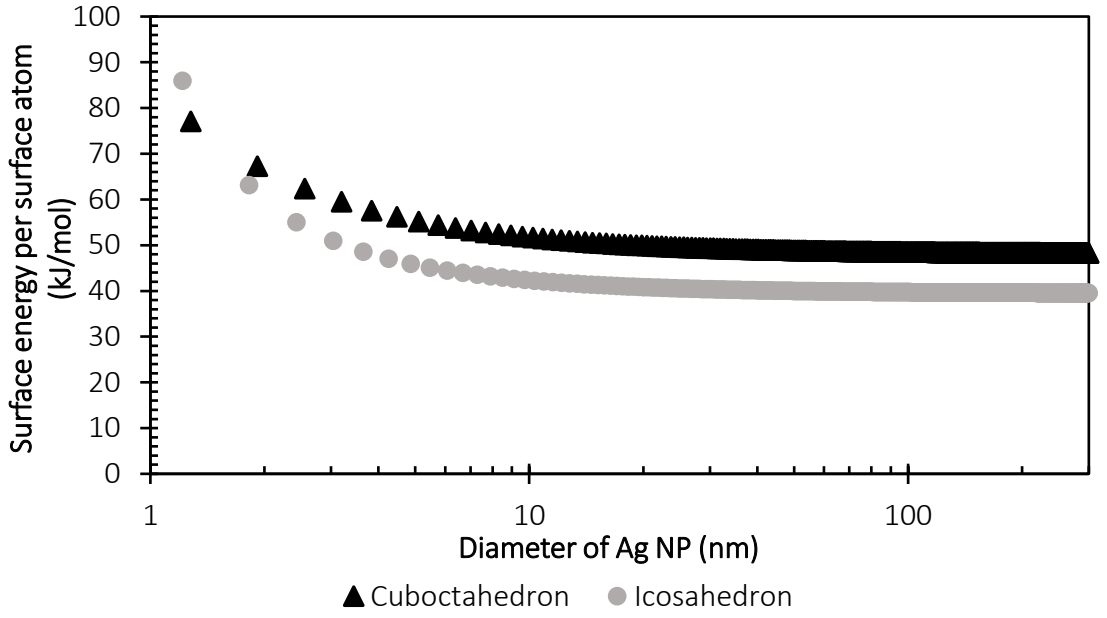

Figure 7-2: Surface energy per surface atom of cuboctahedral and icosahedral silver nanoparticles as a function of particle diameter

Cuboctahedral silver nanoparticles have a higher surface energy per surface atom than icosahedral silver nanoparticles. The cuboctahedral shape tends toward a surface energy of 48.2 kJ/mol whilst the icosahedral shaped nanoparticle tends towards a surface energy of 39.5 kJ/mol.

At equilibrium, the Gibbs free energy of a system is:

$$d\underline{G} = \sum \mu_i dN_i + \gamma dA \qquad \textit{Equation 7-2}$$

The surface energy, shown in Figure 7-2, can also be determined as a function of surface area i.e. as the average surface energy in J/m2. Surface energy is defined as:

$$\gamma = \left(\frac{\partial G}{\partial A}\right)_{T,P} \qquad \textit{Equation 7-3}$$

Using this definition, and the specific relationship that can be developed for the surface energy in relation to the surface area of the two different silver nanoparticle morphologies, the Gibbs free energy equation can then be differentiated, giving:

$$\Delta G_{rxn} = \sum_{i=1}^{i=n} \nu_i \Delta_f G_i^o + RT \ln(K_c) + \gamma f(A) \qquad \textit{Equation 7-4}$$

The Gibbs free energy of reaction at equilibrium is zero. Equation 7-4 is useful for estimating the equilibrium silver ion concentration as a function of particle size when applied in the context of the dissolution of metallic silver in the presence of oxygen, and hydrogen ions. It is thus recommended that these calculations be completed to better understand how the size of silver nanoparticles will affect their antibacterial efficacy in water.

7.2.3 Antibacterial efficacy studies

These recommendations are applicable to studies using both silver nanoparticles and quartz-fibre filters with deposited silver nanoparticles.

- Following successful separation of the silver nanoparticles from the reaction medium (synthesised using Method One and Method Two), antibacterial efficacy studies should be performed. Comparison of the efficacy of the nanoparticles produced using these different synthesis methods will need to consider the effect of the different particle sizes and the presence of different chemical compounds (i.e. residual surfactant and reducing agent).

- Optimisation of the antibacterial efficacy studies using fluorescein diacetate (FDA) would be advantageous because this method is less time consuming than plate spreading and does not rely on manual efforts. These studies would likely produce results with a greater degree of accuracy.

- Higher amounts of silver nanoparticles should be deposited on the quartz fibre filters. Alternatively, whole filters rather than small discs should be used in future antibacterial efficacy studies.

- After treatment with silver ions, nanoparticles and fibre-filters, it is suggested that the bacterial solution be analysed using SEM to investigate how the bacteria cells have been affected by the silver. This will allow one to see how the cells have been damaged and whether the silver has been incorporated into the cells. Performing SEM on the 'used' filter discs could also be considered. Doing this would provide insight into changes in the nanoparticles and filters after treatment.

- The silver ion concentration in the bacterial solutions being treated with silver nanoparticles should be measured over time using an Ag^+ Ion Selective Electrode. This would mean a relationship between the death of bacteria and the measured Ag^+ concentration could be developed.

- More realistic conditions for antibacterial efficacy assessment should be used. This could include using wastewater instead of bacteria media, which would have lower concentrations of Cl^-. Additionally, organic matter could be incorporated into these studies to better simulate conditions of the targeted water sources. Studies across a range of realistic pH values and temperatures would also be interesting as these would affect the kinetics of the silver nanoparticle dissolution and the bacterial growth.

References

AL-Thabaiti, S. A., Al-Nowaiser, F. M., Obaid, A. Y., Al-Youbi, A. O., & Khan, Z. (2008). Formation and characterization of surfactant stabilized silver nanoparticles: A kinetic study. Colloids and Surfaces B: Biointerfaces, 67(2), 230–237. https://doi.org/10.1016/j.colsurfb.2008.08.022

Alexander, J. W. (2009). History of the medical use of silver. Surg Infect (Larchmt), 10(3), 289–292. https://doi.org/10.1089/sur.2008.9941

Amendola, V., Bakr, O. M., & Stellacci, F. (2010). A study of the surface plasmon resonance of silver nanoparticles by the discrete dipole approximation method: Effect of shape, size, structure, and assembly. Plasmonics, 5(1), 85–97. https://doi.org/10.1007/s11468-009-9120-4

American Type Culture Collection. (2017). Escherichia coli (ATCC 25922) Product Sheet.

Asharani, P. V., Wu, Y. L., Gong, Z., & Valiyaveettil, S. (2008). Toxicity of silver nanoparticles in zebrafish models. Nanotechnology, 19(25), 1–8. https://doi.org/10.1088/0957-4484/19/25/255102

Azam, A., Ahmed, A. S., Oves, M., Khan, M. S., Habib, S. S., & Memic, A. (2012). Antimicrobial activity of metal oxide nanoparticles against Gram-positive and Gram-negative bacteria: A comparative study. International Journal of Nanomedicine, 7, 6003–6009.

Azócar, M., Tamayo, L., Vargas, E., Vejar, N., & Páez, M. (2016). Antimicrobial Activity Antibacterial Properties of Silver Nanomaterials. In CRC Concise Encyclopedia of Nanotechnology (pp. 1–8).

Bailey, N. T., & Mahi, P. (1987). The effect of diluents on the metal extracted and phase separation in the extraction of aluminium with mononononyl phosphoric acid. Hydrometallurgy, 18(3), 351–365. https://doi.org/10.1016/0304-386X(87)90075-2

Baset, S., Akbari, H., Zeynali, H., & Shafie, M. (2011). Size Measurement of Metal and Semiconductor Nanoparticles Via UV-Vis Absorption Spectra. Digest Journal of Nanomaterials and Biostructures, 6(2), 709–716.

Becker, R. O. (1999). Silver ions in the treatment of local infections. Metal-Based Drugs, 6(4–5), 311–4. https://doi.org/10.1155/MBD.1999.311

Benfield, R. E. (1992). Mean Coordination Numbers and the Non-metal-Metal Transition in Clusters. Journal of the Chemical Society-Faraday Transactions, 88(8), 1107–1110. https://doi.org/10.1039/ft9928801107

Berger, T. J., Spadaro, J. A., Chapin, S. E., & Becker, R. O. (1976). Electrically generated silver ions: quantitative effects on bacterial and mammalian cells. Antimicrobial Agents and Chemotherapy, 9(2), 357–358. https://doi.org/10.1128/AAC.9.2.357

Bhaduri, G. A., Little, R., Khomane, R. B., Lokhande, S. U., Kulkarni, B. D., Mendis, B. G., & Šiller, L. (2013). Green synthesis of silver nanoparticles using sunlight. Journal of Photochemistry and Photobiology A: Chemistry, 258, 1–9. https://doi.org/10.1016/j.jphotochem.2013.02.015

Bhamidipati, A. S. M. (2017). Industrial Integration of Aerosol Route to Nanofinishing of Highly Effective Antibacterial Textiles. Delft University of Technology.

Bhui, D. K., Bar, H., Sarkar, P., Sahoo, G. P., De, S. P., & Misra, A. (2009). Synthesis and UV-vis spectroscopic study of silver nanoparticles in aqueous SDS solution. Journal of Molecular Liquids, 145(1), 33–37. https://doi.org/10.1016/j.molliq.2008.11.014

Cao, G. (2004). Nanostructures and Nanomaterials - Synthesis, Properties and Applications (1st ed., Vol. 2). London: Imperial College Press. https://doi.org/10.1142/9781860945960

Carlson, C., Hussain, S. M., Schrand, A. M., Braydich-Stolle, L. K., Hess, K. L., Jones, R. L., & Schlager, J. J. (2008). Unique cellular interaction of silver nanoparticles: size dependent generation of reactive oxygen species. J Phys Chem B, 112(43), 13608–13619. https://doi.org/10.1021/jp712087m

Centers for Disease Control and Prevention. (2013). Diarrhea: Common Illness, Global Killer. USA: U.S. Department of Heath and Human Services.

Chambers, B. A., Afrooz, A. R. M. N., Bae, S., Aich, N., Katz, L., Saleh, N. B., & Kirisits, M. J. (2014). Effects of chloride and ionic strength on physical morphology, dissolution, and bacterial toxicity of silver nanoparticles. Environmental Science and Technology, 48(1), 761–769. https://doi.org/10.1021/es403969x

Chan, W., Verma, C. S., Lane, D. P., & Gan, S. K. (2013). A comparison and optimization of methods and factors affecting the transformation of Escherichia coli. Bioscience Reports, 33(6), 931–937. https://doi.org/10.1042/BSR20130098

Chernousova, S., & Epple, M. (2013). Silver as antibacterial agent: Ion, nanoparticle, and metal. Angewandte Chemie - International Edition, 52(6), 1636–1653. https://doi.org/10.1002/anie.201205923

Choi, O., Deng, K. K., Kim, N.-J., Ross, L., Surampalli, R. Y., & Hu, Z. (2008). The inhibitory effects of silver nanoparticles, silver ions, and silver chloride colloids on microbial growth. Water Research, 42(12), 3066–3074. https://doi.org/10.1016/j.watres.2008.02.021

Chudasama, B., Vala, A. K., Andhariya, N., Upadhyay, R. V., & Mehta, R. V. (2009). Enhanced antibacterial activity of bifunctional Fe3O4-Ag core-shell nanostructures. Nano Research, 2(12), 955–965. https://doi.org/10.1007/s12274-009-9098-4

Cioffi, N., & Rai, M. (2012). Nano-Antimicrobials - Progress and Prospects (1st ed.). Heidelberg: Springer. https://doi.org/10.1007/978-3-642-24428-5

Cui, Y., Zhao, Y., Tian, Y., Zhang, W., Lu, X., & Jiang, X. (2012). The molecular mechanism of action of bactericidal gold nanoparticles on Escherichia coli. Biomaterials, 33(7), 2327–2333. https://doi.org/10.1016/j.biomaterials.2011.11.057

Cunningham, A., & Bürgi, T. (2013). Bottom-up Organisaion of Metallic Nanoparticles. In C. Rockstuhl & T. Scharf (Eds.), Amorphous Nanophotonics (1st ed., pp. 1–37). Berlin, Heidelberg: Springer. https://doi.org/10.1007/978-3-642-32475-8_1

Cyrot-Lackmann, F. (1969). On the calculation of surface tension in transition metals. Surface Science, 15(3), 535–548.

Dang, T. M. D., Le, T. T. T., Fribourg-Blanc, E., & Dang, M. C. (2012). Influence of surfactant on the preparation of silver nanoparticles by polyol method. Advances in Natural Sciences: Nanoscience and Nanotechnology, 3(3), 4pp. https://doi.org/10.1088/2043-6262/3/3/035004

Department of Water Affairs and Forestry. (1996). South African Water Quality Guidelines (second edition). Volume 2: Recreational Water Use. (S. Holmes, Ed.). Pretoria: DWAF.

Deponte, M. (2013). Glutathione catalysis and the reaction mechanisms of glutathione-dependent enzymes. Biochimica et Biophysica Acta - General Subjects, 1830(5), 3217–3266. https://doi.org/10.1016/j.bbagen.2012.09.018

Dizaj, S. M., Lotfipour, F., Barzegar-Jalali, M., Zarrintan, M. H., & Adibkia, K. (2014). Antimicrobial activity of the metals and metal oxide nanoparticles. Materials Science and Engineering C, 44, 278–284. https://doi.org/10.1016/j.msec.2014.08.031

Dorsey, J., Yentsch, C. M., Mayo, S., & McKenna, C. (1989). Rapid analytical technique for the assessment of cell metabolic activity in marine microalgae. Cytometry, 10(5), 622–628. https://doi.org/10.1002/cyto.990100518

Eberhart, J. G., & Horner, S. (2010). Bond-energy and surface-energy calculations in metals. Journal of Chemical Education, 87(6), 608–612. https://doi.org/10.1021/ed100189v

Feng, J., Biskos, G., & Schmidt-Ott, A. (2015). Toward industrial scale synthesis of ultrapure singlet nanoparticles with controllable sizes in a continuous gas-phase process. Scientific Reports, 5(15788), 1–9. https://doi.org/10.1038/srep15788

Feng, J., Hontanon, E., Blanes, M., Meyer, J., Guo, X., Santos, L., … Biskos, G. (2016). A Scalable and Environmentally Benign Process for Smart Textile Nanofinishing. Applied Materials and Interfaces, 8(23), 14756–14765. https://doi.org/10.1021/acsami.6b03632

Foldbjerg, R., Jiang, X., Chen, C., Autrup, H., & Beer, C. (2015). Toxicology Research, 4(3), 563–575. https://doi.org/10.1039/c4tx00110a

Foldbjerg, R., Jiang, X., Miclăuş, T., Chen, C., Autrup, H., & Beer, C. (2015). Silver nanoparticles – wolves in sheep's clothing? Toxicol. Res., 4(3), 563–575. https://doi.org/10.1039/C4TX00110A

Goldstein, J. I., Newbury, D. E., Michael, J. R., Ritchie, N. W. M., Scott, J. H. J., & Joy, D. C. (2017). Microscopy and X-Ray Microanalysis (4th ed.). New York: Springer. https://doi.org/10.1007/978-1-4939-6676-9

Goual, L., & Firoozabadi, A. (2004). Effect of Resins and DBSA on Asphaltene Precipitation from Petroleum Fluids. AIChE Journal, 50(2), 470–479. https://doi.org/10.1002/aic.10041

Grass, G., Rensing, C., & Solioz, M. (2011). Metallic copper as an antimicrobial surface. Applied and Environmental Microbiology, 77(5), 1541–1547. https://doi.org/10.1128/AEM.02766-10

Gustafsson, J. P. (2018). Visual Minteq (ver 3.1). Stockholm: Stockholm Royal Institute of Technology (KTH). Retrieved from https://vminteq.lwr.kth.se/

Hadrup, N., & Lam, H. R. (2014). Oral toxicity of silver ions, silver nanoparticles and colloidal silver - A review. Regulatory Toxicology and Pharmacology, 68(1), 1–7. https://doi.org/10.1016/j.yrtph.2013.11.002

Haiss, W., Thanh, N. T. K., Aveyard, J., & Fernig, D. G. (2007). Determination of size and concentration of gold nanoparticles from UV-Vis spectra. Analytical Chemistry, 79(11), 4215–4221. https://doi.org/10.1021/ac0702084

Hajipour, M. J., Fromm, K. M., Akbar Ashkarran, A., Jimenez de Aberasturi, D., Ruiz de Larramendi, I., Rojo, T., … Mahmoudi, M. (2012). Antibacterial properties of nanoparticles. Trends in Biotechnology, 30(10), 499–511. https://doi.org/10.1016/j.tibtech.2012.06.004

Harvey, R. A., Cornelissen, C. N., & Fisher, B. D. (2007). Bacterial Structure, Growth and Metabolism. In R. A. Harvey (Ed.), Lippincott's Illustrated Reviews: Microbiology (3rd ed., pp. 49–58). Baltimore: Lippincott Williams & Wilkins.

Henglein, A., & Giersig, M. (1999). Formation of Colloidal Silver Nanoparticles: Capping Action of Citrate. The Journal of Physical Chemistry B, 103(44), 9533–9539. https://doi.org/10.1021/jp9925334

Hofmeister, H. (2004). Fivefold Twinned Nanoparticles. In H. S. Nalwa (Ed.), Encyclopedia of Nanoscience and Nanotechnology (Vol. 3, pp. 431–452). Stevenson Ranch: American Scientific Publishers. Retrieved from http://www.mpi-halle.de/mpi/publi/pdf/5278_04.pdf

Hossain, F., Perales-Perez, O. J., Hwang, S., & Román, F. (2014). Antimicrobial nanomaterials as water disinfectant: Applications, limitations and future perspectives. Science of the Total Environment, 466–467, 1047–1059. https://doi.org/10.1016/j.scitotenv.2013.08.009

Huang, T., & Xu, X.-H. N. (2010). Synthesis and characterization of tunable rainbow colored colloidal silver nanoparticles using single-nanoparticle plasmonic microscopy and spectroscopy. Journal of Materials Chemistry, 20(44), 9867–9876. https://doi.org/10.1039/c0jm01990a

Hudzicki, J. (2009). Kirby-Bauer disk diffusion susceptibility test protocol. American Society for Microbiology.

Iravani, S., Korbekandi, H., Mirmohammadi, S. V., & Zolfaghari, B. (2014). Synthesis of silver nanoparticles: Chemical, physical and biological methods. Research in Pharmaceutical Sciences, 9(6), 385–406.

Jia, H., Hou, W., Wei, L., Xu, B., & Liu, X. (2008). The structures and antibacterial properties of nano-SiO2 supported silver/zinc-silver materials. Dental Materials, 24(2), 244–249. https://doi.org/10.1016/j.dental.2007.04.015

Kall, M. A. (2003). Ascorbic Acid: Properties and Determination. In B. Caballero (Ed.), Encyclopedia of Food Sciences and Nutrition (2nd ed., pp. 316–324). Oxford: Academic Press. https://doi.org/10.1016/B0-12-227055-X/00068-7

Kedziora, A., Strek, W., Kepinski, L., Bugla-Ploskonska, G., & Doroszkiewicz, W. (2012). Synthesis and antibacterial activity of novel titanium dioxide doped with silver. Journal of Sol-Gel Science and Technology, 62(1), 79–86. https://doi.org/10.1007/s10971-012-2688-8

Keleher, J., Bashant, J., Heldt, N., Johnson, L., & Li, Y. (2002). Photo-catalytic preparation of silver-coated TiO2 particles for antibacterial applications. World Journal of Microbiology and Biotechnology, 18(2), 133–139. https://doi.org/10.1023/A:1014455310342

Khan, H. (2005). Disinfection of Drinking Water. In H. Khan (Ed.), Guidelines for the Design, Construction and Operation of Water and Sewerage Systems (pp. 4-1-4–6). St John's: Government of Newfoundland and Labrador: Department of Environment and Conservation.

Khan, Z., AL-Thabaiti, S. A., Obaid, A. Y., & Al-Youbi, A. O. (2011). Preparation and characterization of silver nanoparticles by chemical reduction method. Colloids and Surfaces B: Biointerfaces, 82(2), 513–517. https://doi.org/10.1016/j.colsurfb.2010.10.008

Khan, Z., Hussain, J. I., Hashmi, A. A., & AL-Thabaiti, S. A. (2017). Preparation and characterization of silver nanoparticles using aniline. Arabian Journal of Chemistry, 10(S2), S1506–S1511. https://doi.org/10.1016/j.arabjc.2013.05.001

Ki, H. Y., Kim, J. H., Kwon, S. C., & Jeong, S. H. (2007). A study on multifunctional wool textiles treated with nano-sized silver. Journal of Materials Science, 42(19), 8020–8024. https://doi.org/10.1007/s10853-007-1572-3

Kim, J. S., Kuk, E., Yu, K. N., Kim, J. H., Park, S. J., Lee, H. J., … Cho, M. H. (2007). Antimicrobial effects of silver nanoparticles. Nanomedicine: Nanotechnology, Biology, and Medicine, 3(1), 95–101. https://doi.org/10.1016/j.nano.2006.12.001

Kim, Y. S., Song, M. Y., Park, J. D., Song, K. S., Ryu, H. R., Chung, Y. H., … Yu, I. J. (2010). Subchronic oral toxicity of silver nanoparticles. Particle and Fibre Toxicology, 7(1), 20. https://doi.org/10.1186/1743-8977-7-20

Kuipa, P. K., & Hughes, M. A. (2002). Diluent effect on the solvent extraction rate of copper. Separation Science and Technology, 37(5), 1135–1152. https://doi.org/10.1081/SS-120002246

Kutschera, U. (2009). Symbiogenesis, natural selection, and the dynamic Earth. Theory in Biosciences, 128(3), 191–203. https://doi.org/10.1007/s12064-009-0065-0

Kvítek, L., Panáček, A., Soukupová, J., Kolář, M., Večeřová, R., Prucek, R., … Zbořil, R. (2008). Effect of surfactants and polymers on stability and antibacterial activity of silver nanoparticles (NPs). Journal of Physical Chemistry C, 112(15), 5825–5834. https://doi.org/10.1021/jp711616v

Kwon, S. G., & Hyeon, T. (2011). Formation mechanisms of uniform nanocrystals via hot-injection and heat-up methods. Small, 7(19), 2685–2702. https://doi.org/10.1002/smll.201002022

LaMer, V. K. (1952). Nucleation in Phase Transitions. Industrial & Engineering Chemistry, 44(6), 1270–1277. https://doi.org/10.1021/ie50510a027

LaMer, V. K., & Dinegar, R. H. (1950). Theory, Production and Mechanism of Formation of Monodispersed Hydrosols. Journal of the American Chemical Society, 72(11), 4847–4854. https://doi.org/10.1021/ja01167a001

Le Ouay, B., & Stellacci, F. (2015). Antibacterial activity of silver nanoparticles : A surface science insight. Nano Today, 10(3), 339–354. https://doi.org/10.1016/j.nantod.2015.04.002

Lee, Y.-J., Kim, J., Oh, J., Bae, S., Lee, S., Hong, I. S., & Kim, S.-H. (2012). Ion-release kinetics and ecotoxicity effects of silver nanoparticles. Environmental Toxicology and Chemistry, 31(1), 155–159. https://doi.org/10.1002/etc.717

León, O., Rogel, E., Urbina, A., Andújar, A., & Lucas, A. (1999). Study of the adsorption of alkyl benzene-derived amphiphiles on asphaltene particles. Langmuir, 15(22), 7653–7657. https://doi.org/10.1021/la9812370

Levard, C., Mitra, S., Yang, T., Jew, A. D., Badireddy, A. R., Lowry, G. V., & Brown, G. E. (2013). Effect of chloride on the dissolution rate of silver nanoparticles and toxicity to E. coli. Environmental Science and Technology, 47(11), 5738–5745. https://doi.org/10.1021/es400396f

Li, M., Noriega-Trevino, M. E., Nino-Martinez, N., Marambio-Jones, C., Wang, J., Damoiseaux, R., … Hoek, E. M. V. (2011). Synergistic Bactericidal Activity Ag-TiO2 Nanoparticles in Both Light and Dark Conditions. Environ. Sci. Technol., 45(20), 8989–8995. https://doi.org/10.1021/es201675m

Li, M. Y., Mao, Y. Q., Yang, S. K., Dai, T. T., Yang, H., Feng, F., … Wu, J. H. (2016). Out-of-Substrate Ag–Ag2O Nanoplates: Surfactantless Photochemical Synthesis, Structural Evolution, and Mechanistic Study. ACS Omega, 1(4), 696–705. https://doi.org/10.1021/acsomega.6b00149

Li, Q., Mahendra, S., Lyon, D. Y., Brunet, L., Liga, M. V, Li, D., & Alvarez, P. J. (2008). Antimicrobial nanomaterials for water disinfection and microbial control: potential applications and implications. Water Research, 42(18), 4591–4602.

Li, R., Zhang, L., & Wang, P. (2015). Rational design of nanomaterials for water treatment. Nanoscale, 7(41), 17167–17194. https://doi.org/10.1039/c5nr04870b

Lim, S. H., & Hudson, S. M. (2004). Application of a fiber-reactive chitosan derivative to cotton fabric as an antimicrobial textile finish. Carbohydrate Polymers, 56(2), 227–234. https://doi.org/10.1016/j.carbpol.2004.02.005

Liu, H., Tang, X., & Liu, Q. (2014). A novel point-of-use water treatment method by antimicrobial nanosilver textile material. Journal of Water and Health, 12(4), 670–677.

Liu, J., & Hurt, R. H. (2010). Ion release kinetics and particle persistence in aqueous nano silver colloids. Environmental Science and Technology, 44(6), 2169–2175.

Lok, C., Ho, C., Chen, R., He, Q., Yu, W.-Y., Sun, H., … Che, C. (2006). Proteomic analysis of the mode of antibacterial action of silver nanoparticles. Journal of Proteome Research, 5(4), 916–924. https://doi.org/10.1021/pr0504079

Marambio-Jones, C., & Hoek, E. M. V. (2010). A review of the antibacterial effects of silver nanomaterials and potential implications for human health and the environment. Journal of Nanoparticle Research, 12(5), 1531–1551. https://doi.org/10.1007/s11051-010-9900-y

Martinez-Castanon, G. A., Niño-Martínez, N., Martínez-Gutierrez, F., Martínez-Mendoza, J. R., & Ruiz, F. (2008). Synthesis and antibacterial activity of silver nanoparticles with different sizes. Journal of Nanoparticle Research, 10(8), 1343–1348. https://doi.org/10.1007/s11051-008-9428-6

Matés, J. M. (2000). Effects of antioxidant enzymes in the molecular control of reactive oxygen species toxicology. Toxicology, 153(1–3), 83–104. https://doi.org/10.1016/S0300-483X(00)00306-1

Mauter, M., & Elimelech, M. (2008). Environmental applications of carbon-based nanomaterials. Environmental Science & Technology, 42(16), 5843–5859. https://doi.org/10.1021/es8006904

Meister, A. (1988). Glutathione metabolism and its selective modification. Journal of Biological Chemistry, 263(33), 17205–17208.

Molleman, B., & Hiemstra, T. (2015). Surface Structure of Silver Nanoparticles as a Model for Understanding the Oxidative Dissolution of Silver Ions. Langmuir, 31(49), 13361–13372. https://doi.org/10.1021/acs.langmuir.5b03686

Moritz, M., & Geszke-Moritz, M. (2013). The newest achievements in synthesis, immobilization and practical applications of antibacterial nanoparticles. Chemical Engineering Journal, 228, 596–613. https://doi.org/10.1016/j.cej.2013.05.046

Morones, J. R., Elechiguerra, J. L., Camacho, A., Holt, K., Kouri, J. B., Ramirez, J. T., & Yacaman, M. J. (2005). The bactericidal effect of silver nanoparticles. Nanotechnology, 16(10), 2346–235353. https://doi.org/10.1088/0957-4484/16/10/059

Mulfinger, L., Solomon, S. D., Bahadory, M., Jeyarajasingam, A. V, Rutkowsky, S. A., & Boritz, C. (2007). Synthesis and Study of Silver Nanoparticles. J. Chem. Educ., 84(2), 322–325. https://doi.org/10.1021/ed084p322

Munger, M. A., Radwanski, P., Hadlock, G. C., Stoddard, G., Shaaban, A., Falconer, J., … Deering-Rice, C. E. (2014). In vivo human time-exposure study of orally dosed commercial silver nanoparticles. Nanomedicine: Nanotechnology, Biology, and Medicine, 10(1), 1–9. https://doi.org/10.1016/j.nano.2013.06.010

Mushran, S. P., Agrawal, M. C., Mehrotra, R. M., & Sanehi, R. (1974). Kinetics and mechanism of reduction of silver(I) by ascorbic acid. Journal of the Chemical Society, Dalton Transactions, (14), 1460–1462. https://doi.org/10.1039/DT9740001460

Nature Nanotechnology. (2012). Editorial: Join the dialogue. Nature Nanotechnology, 7(9), 545. https://doi.org/10.1038/nnano.2012.150

Oukarroum, A., Bras, S., Perreault, F., & Popovic, R. (2012). Inhibitory effects of silver nanoparticles in two green algae, Chlorella vulgaris and Dunaliella tertiolecta. Ecotoxicology and Environmental Safety, 78, 80–85. https://doi.org/10.1016/j.ecoenv.2011.11.012

Panacek, A., Kvitek, L., Prucek, R., Kolar, M., Vecerova, R., Pizurova, N., … Zboril, R. (2006). Silver Colloid Nanoparticles : Synthesis , Characterization , and Their Antibacterial Activity. Journal of Physical Chemistry B, 110(33), 16248–16253. https://doi.org/10.1021/jp063826h

Patakfalvi, R., Virányi, Z., & Dékány, I. (2004). Kinetics of silver nanoparticle growth in aqueous polymer solutions. Colloid and Polymer Science, 283(3), 299–305. https://doi.org/10.1007/s00396-004-1138-8

Patra, S., Sen, D., Pandey, A. K., Bahadur, J., Mazumder, S., Ramagiri, S. V., … Goswami, A. (2014). Time resolved growth of membrane stabilized silver NPs and their catalytic activity. RSC Advances, 4(103), 59379–59386. https://doi.org/10.1039/C4RA10400E

Peng, S., McMahon, J. M., Schatz, G. C., Gray, S. K., & Sun, Y. (2010). Reversing the size-dependence of surface plasmon resonances. Proceedings of the National Academy of Sciences, 107(33), 14530–14534. https://doi.org/10.1073/pnas.1007524107

Pissuwan, D., Cortie, C. H., Valenzuela, S. M., & Cortie, M. B. (2010). Functionalised gold nanoparticles for controlling pathogenic bacteria. Trends in Biotechnology, 28(4), 207–213. https://doi.org/10.1016/j.tibtech.2009.12.004

Polte, J. (2015). Fundamental growth principles of colloidal metal nanoparticles – a new perspective. CrystEngComm, 17(36), 6809–6830. https://doi.org/10.1039/C5CE01014D

Prabhu, S., & Poulose, E. K. (2012). Silver nanoparticles: mechanism of antimicrobial action, synthesis, medical applications, and toxicity effects. International Nano Letters, 2(32), 1–10. https://doi.org/10.1186/2228-5326-2-32

Prathna, T. C., Raichur, A. M., Chandrasekaran, N., & Mukherjee, A. (2014). Sunlight Irradiation Induced Green Synthesis of Stable Silver Nanoparticles Using Citrus limon Extract. Proceedings of the National Academy of Sciences, India Section B: Biological Sciences, 84(1), 65–70. https://doi.org/10.1007/s40011-013-0193-7

Qu, X., Alvarez, P. J. J., & Li, Q. (2013). Applications of nanotechnology in water and wastewater treatment. Water Research, 47(12), 3931–3946. https://doi.org/10.1016/j.watres.2012.09.058

Rai, M., Yadav, A., & Gade, A. (2009). Silver nanoparticles as a new generation of antimicrobials. Biotechnology Advances, 27(1), 76–83. https://doi.org/10.1016/j.biotechadv.2008.09.002

Ren, G., Hu, D., Cheng, E. W. C., Vargas-Reus, M. A., Reip, P., & Allaker, R. P. (2009). Characterisation of copper oxide nanoparticles for antimicrobial applications. International Journal of Antimicrobial Agents, 33(6), 587–590. https://doi.org/10.1016/j.ijantimicag.2008.12.004

Richards, V. N., Rath, N. P., & Buhro, W. E. (2010). Pathway from a molecular precursor to silver nanoparticles: The prominent role of aggregative growth. Chemistry of Materials, 22(11), 3556–3567. https://doi.org/10.1021/cm100871g

Romanowski, W. (1969). Equilibrium forms of very small metallic crystals. Surface Science, 18(2), 373–388.

Ruparelia, J. P., Chatterjee, A. K., Duttagupta, S. P., & Mukherji, S. (2008). Strain specificity in antimicrobial activity of silver and copper nanoparticles. Acta Biomaterialia, 4(3), 707–716. https://doi.org/10.1016/j.actbio.2007.11.006

Salton, M. R. J., & Kim, K.-S. (1996). Bacteriology - Structure. In S. Baron (Ed.), Medical Microbiology (4th ed.). Galveston: University of Texas Medical Branch at Galveston.

Sato-Berŕu, R., Redón, R., Vázquez-Olmos, A., & Saniger, J. M. (2009). Silver nanoparticles synthesized by direct photoreduction of metal salts. Application in surface-enhanced Raman spectroscopy. Journal of Raman Spectroscopy, 40(4), 376–380. https://doi.org/10.1002/jrs.2135

Sau, T. K., & Rogach, A. L. (2012). Complex-shaped Metal Nanoparticles: Bottom-up Syntheses and Applications (1st ed.). Singapore: Wiley-VCH Verlag GmbH & Co. KGaA. https://doi.org/10.1080/714040773

Shields, S. P., Richards, V. N., & Buhro, W. E. (2010). Nucleation control of size and dispersity in aggregative nanoparticle growth. A study of the coarsening kinetics of thiolate-capped gold nanocrystals. Chemistry of Materials, 22(10), 3212–3225. https://doi.org/10.1021/cm100458b

Sigma-Aldrich. (2017a). Dodecylbenzenesulfonic acid solution. Retrieved August 14, 2017, from https://www.sigmaaldrich.com/catalog/product/aldrich/522953?lang=en&region=ZA

Sigma-Aldrich. (2017b). Sodium dodecyl sulfate. Retrieved November 29, 2017, from https://www.sigmaaldrich.com/catalog/product/sigma/l3771?lang=en&region=ZA

Sigma-Aldrich. (2018a). Silver, dispersion (sodium citrate stabilised). Retrieved January 31, 2018, from https://www.sigmaaldrich.com/catalog/product/aldrich/730785?lang=en&region=ZA

Sigma-Aldrich. (2018b). Silver nanospheres (PVP functionalized). Retrieved January 31, 2018, from https://www.sigmaaldrich.com/catalog/product/aldrich/795925?lang=en&region=ZA

Sintubin, L., De Gusseme, B., Van Der Meeren, P., Pycke, B. F. G., Verstraete, W., & Boon, N. (2011). The antibacterial activity of biogenic silver and its mode of action. Applied Microbiology and Biotechnology, 91(1), 153–162. https://doi.org/10.1007/s00253-011-3225-3

Sotiriou, G. A., & Pratsinis, S. E. (2010). Antibacterial activity of nanosilver ions and particles. Environmental Science and Technology, 44(14), 5649–5654. https://doi.org/10.1021/es101072s

Tao, A. R., Habas, S., & Yang, P. (2008). Shape control of colloidal metal nanocrystals. Small, 4(3), 310–325. https://doi.org/10.1002/smll.200701295

Thanh, N. T. K., Maclean, N., & Mahiddine, S. (2014). Mechanisms of nucleation and growth of nanoparticles in solution. Chemical Reviews, 114(15), 7610–7630. https://doi.org/10.1021/cr400544s

Thiel, J., Pakstis, L., Buzby, S., Raffi, M., Ni, C., Pochan, D. J., & Shah, S. I. (2007). Antibacterial properties of silver-doped titania. Small, 3(5), 799–803. https://doi.org/10.1002/smll.200600481

Timonen, J. V. I., Seppälä, E. T., Ikkala, O., & Ras, R. H. A. (2011). From hot-injection synthesis to heating-up synthesis of cobalt nanoparticles: Observation of kinetically controllable nucleation. Angewandte Chemie - International Edition, 50(9), 2080–2084. https://doi.org/10.1002/anie.201005600

Tomaszewska, E., Soliwoda, K., Kadziola, K., Tkacz-Szczesna, B., Celichowski, G., Cichomski, M., … Grobelny, J. (2013). Detection limits of DLS and UV-Vis spectroscopy in characterization of polydisperse nanoparticles colloids. Journal of Nanomaterials, 2013, 10. https://doi.org/10.1155/2013/313081

Tran, Q. H., Nguyen, V. Q., & Le, A.-T. (2013). Silver nanoparticles : synthesis, properties, toxicology, applications and perspectives. Advances in Natural Sciences: Nanoscience and Nanotechnology, 4(3), 033001 (20pp). https://doi.org/10.1088/2043-6262/4/3/033001

UNICEF, & World Health Organisation. (2015). Progress on sanitation and drinking water - 2015 update and MDG assessment. Geneva: WHO Press. Retrieved from http://www.unicef.org/publications/files/Progress_on_Sanitation_and_Drinking_Water_2015_Update_.pdf

United Nations. (2016). United Nations Sustainable Development Goals. Retrieved from http://www.un.org/sustainabledevelopment/water-and-sanitation/

Van Briesen, J. M., Small, M., Weber, C., & Wilson, J. (2010). Modelling Chemical Speciation: Thermodynamics, Kinetics and Uncertainty. In G. Hanrahan (Ed.), Modelling of Pollutants in Complex Environmental Systems, Volume 2 (Vol. 2, pp. 133–149). St Albans: ILM Publications.

van Hardeveld, R., & Hartog, F. (1969). The statistics of surface atoms and surface sites on metal crystals. Surface Science, 15(2), 189–230.

van Helden, P., van Santen, R. A., & van Steen, E. (2009). Nanorod calculations on body-centered cubic iron: A method for estimation of size-dependent surface energies of metal nanocrystals. Journal of Physical Chemistry C, 113(2), 644–649. https://doi.org/10.1021/jp807426f

Vitos, L., Ruban, A. V., Skriver, H. L., & Kollár, J. (1998). The surface energy of metals. Surface Science, 411(1–2), 186–202. https://doi.org/10.1016/S0039-6028(98)00363-X

Vrček, I. V., Žuntar, I., Petlevski, R., Pavičić, I., Sikirić, M. D., Ćurlin, M., & Goessler, W. (2016). Comparison of in vitro toxicity of silver ions and silver nanoparticles on human hepatoma cells. Environmental Toxicology, 31(6), 679–692. https://doi.org/10.1002/tox.22081

Wanandy, S., Brouwer, N., Liu, Q., Mahon, A., Cork, S., Karuso, P., … Jamie, J. (2005). Optimisation of the fluorescein diacetate antibacterial assay. Journal of Microbiological Methods, 60(1), 21–30. https://doi.org/10.1016/j.mimet.2004.08.010

WHO/UNICEF Joint Monitoring Programme for Water Supply and Sanitation. (2017). Progress on drinking water, sanitation and hygiene: 2017 update and SDG baselines. Geneva: World Health Organisation (WHO) and the United Nations Children's Fund (UNICEF).

World Health Organisation. (2017). Guidelines for Drinking-water Quality: Recommendations (4th ed.). Geneva: World Health Organisation. Retrieved from http://www.who.int/water_sanitation_health/publications/drinking-water-quality-guidelines-4-including-1st-addendum/en/

Xia, Y., Xiong, Y., Lim, B., & Skrabalak, S. E. (2009). Shape-controlled synthesis of metal nanocrystals: Simple chemistry meets complex physics? Angewandte Chemie - International Edition, 48(1), 60–103. https://doi.org/10.1002/anie.200802248

Xiong, J., Wang, Y., Xue, Q., & Wu, X. (2011). Synthesis of highly stable dispersions of nanosized copper particles using l-ascorbic acid. Green Chemistry, 13(4), 900–904. https://doi.org/10.1039/c0gc00772b

Xiu, Z., Zhang, Q., Puppala, H. L., Colvin, V. L., & Alvarez, P. J. J. (2012). Negligible Particle-Specific Antibacterial Activity of Silver Nanoparticles. Nano Letters, 12(8), 4271–4275. https://doi.org/dx.doi.org/10.1021/nl301934w

Yang, J., Yin, H., Jia, J., & Wei, Y. (2011). Facile Synthesis of High-Concentration, Stable Aqueous Dispersions of Uniform Silver Nanoparticles Using Aniline as a Reductant. Langmuir, 27(8), 5047–5053. https://doi.org/10.1021/la200013z

Yin, Y., Li, Z.-Y., Zhong, Z., Gates, B., Xia, Y., & Venkateswaran, S. (2002). Synthesis and characterization of stable aqueous dispersions of silver nanoparticles through the Tollens process. Journal of Materials Chemistry, 12(3), 522–527. https://doi.org/10.1039/b107469e

You, C., Han, C., Wang, X., Zheng, Y., Li, Q., Hu, X., & Sun, H. (2012). The progress of silver nanoparticles in the antibacterial mechanism, clinical application and cytotoxicity. Molecular Biology Reports, 39(9), 9193–9201. https://doi.org/10.1007/s11033-012-1792-8

Yu, B., Leung, K. M., Guo, Q., Lau, W. M., & Yang, J. (2011). Synthesis of Ag-TiO2 composite nano thin film for antimicrobial application. Nanotechnology, 22(11), 115603. https://doi.org/10.1088/0957-4484/22/11/115603

Zacharaki, E., Kalyva, M., Fjellvåg, H., & Sjåstad, A. O. (2016). Burst nucleation by hot injection for size controlled synthesis of ε-cobalt nanoparticles. Chemistry Central Journal, 10(1), 10. https://doi.org/10.1186/s13065-016-0156-1

Zain, N. M., Stapley, A. G. F., & Shama, G. (2014). Green synthesis of silver and copper nanoparticles using ascorbic acid and chitosan for antimicrobial applications. Carbohydrate Polymers, 112, 195–202. https://doi.org/10.1016/j.carbpol.2014.05.081

Zhang, D., Li, G., & Yu, J. C. (2010). Inorganic materials for photocatalytic water disinfection. Journal of Materials Chemistry, 20(22), 4529–4536.

Zhang, W., Yao, Y., Sullivan, N., & Chen, Y. (2011). Modeling the primary size effects of citrate-coated silver nanoparticles on their ion release kinetics. Environmental Science and Technology, 45(10), 4422–4428. https://doi.org/10.1021/es104205a

Zhao, G., & Stevens, S. E. (1998). Multiple parameters for the comprehensive evaluation of the susceptibility of Escherichia coli to the silver ion. BioMetals, 11(1), 27–32. https://doi.org/10.1023/A:1009253223055

Zhou, J., Ralston, J., Sedev, R., & Beattie, D. A. (2009). Functionalized gold nanoparticles: Synthesis, structure and colloid stability. Journal of Colloid and Interface Science, 331(2), 251–262. https://doi.org/10.1016/j.jcis.2008.12.002

Zook, J. M., Rastogi, V., Maccuspie, R. I., Keene, A. M., & Fagan, J. (2011). Measuring Agglomerate Size Distribution and Dependence of Localized Surface Plasmon Resonance Absorbance on Gold Nanoparticle Agglomerate Size Using Analytical Ultracentrifugation. ACS Nano, 5(10), 8070–8079.

Appendices

A. Silver nanoparticle synthesis

A.1 Method One

A.1.1 Calculations for excess reagent ascorbic acid

To determine excess amount of ascorbic acid for the reduction of silver ions to silver metal, Equation 4-12 was used.

$$2Ag^{+}_{(aq)} + C_6H_8O_{6(aq)} \longrightarrow 2Ag^{0}_{(s)} + C_6H_6O_{6(aq)} + 2H^{+} \qquad \textit{Equation 4-12}$$

The chemical equation shows that for every mol of ascorbic acid reacted, two moles of silver ions are required.

Table A-1: Amounts of reactants added to original Method One synthesis

Chemicals	*Amount added (mol)*
Silver ions (Ag^+)	0.0003
Ascorbic acid ($C_6H_8O_6$)	0.0002

Table A-1 shows the moles of silver ions and ascorbic acid available for reaction. It is known that the silver nitrate is the limiting reactant. The calculation below was therefore performed to determine how much of the ascorbic acid is consumed in the formation of the silver nanoparticles under the assumption that all the Ag^+ reacts.

$$mol\ C_6H_8O_6\ used = Ag^{+}available\ \times molar\ ratio\ C_6H_8O_6 : Ag^{+} \qquad \textit{Equation A-1}$$

$$mol\ C_6H_8O_6\ used = \ 0.0003\ \cancel{mol\ Ag^{+}} \times \frac{1\ mol\ C_6H_8O_6}{2\ \cancel{mol\ Ag^{+}}}$$

$$mol\ C_6H_8O_6\ used = 0.00015\ mol$$

The result from Equation A-1 show that a maximum of 0.00015 mol ascorbic acid will be consumed in the reaction. The calculation that follows shows the determination of the amount of ascorbic acid in excess.

$$\%\ excess\ C_6H_8O_6 = \frac{C_6H_8O_6\ remaining}{C_6H_8O_6\ consumed} \times 100\% \qquad \textit{Equation A-2}$$

$$\%\ excess\ C_6H_8O_6 = \frac{(C_6H_8O_6\ available - C_6H_8O_6\ consumed)}{C_6H_8O_6\ consumed} \times 100\%$$

$$\%\ excess\ C_6H_8O_6 = \frac{(0.0002 - 0.00015)\ mol\ C_6H_8O_6}{0.00015\ mol\ C_6H_8O_6} \times 100\%$$

$$\%\ excess\ C_6H_8O_6 = 33.33\ \%$$

Thus, for the original synthesis procedure for method one, the ascorbic acid is in 33.33 % excess with respect to the silver nitrate added.

To calculate the amount of ascorbic acid that needs to be added so that it is in 50 % excess of the silver nitrate, the subject of Equation A-2 is changed to be *$C_6H_8O_6$ available*.

$$\% \; excess \; C_6H_8O_6 = \frac{C_6H_8O_6 \; remaining}{C_6H_8O_6 \; available} \times 100\% \qquad \textit{Equation A-3}$$

$$C_6H_8O_6 \; available \; = C_6H_8O_6 \; consumed \left(1 + \frac{\% \; excess \; C_6H_8O_6}{100 \; \%}\right)$$

$$C_6H_8O_6 \; available \; = 0.00015 \; mol \left(1 + \frac{50\%}{100 \; \%}\right)$$

$$C_6H_8O_6 \; available \; = 0.000225 \; mol$$

Therefore, the amount of ascorbic that needs to be added in order to achieve a 50 % excess with respect to water is 0.000225 mol or 0.0396 g.

A.1.2 Results of the Method One synthesis

The complete particle size results of the syntheses variations in light conditions are presented in Table A-2 and Figure A-1.

Table A-2: Summary of the size measurements for particles produced whilst exposed to light using Method One

Synthesis variation	*Mean particle size (nm)*	*Median particle size (nm)*	*Maximum particle size measured (nm)*	*Number of particles counted*
Original method (no variation)	10.3 ± 7.0	9.7	50.9	270
Halved surfactant concentration	8.2 ± 14.6	5.5	171.5	441
Doubled surfactant concentration	21.6 ± 22.6	17.6	210.1	700
Higher temperature: 50 °C	6.3 ± 8.7	4.5	137.9	493
Higher temperature: 90 °C	11.9 ± 18.1	6.8	180.1	660
Halved reducing agent concentration	6.3 ± 5.6	4.5	39.7	584
Dropwise reducing agent addition	3.9 ± 2.4	3.2	14.3	222

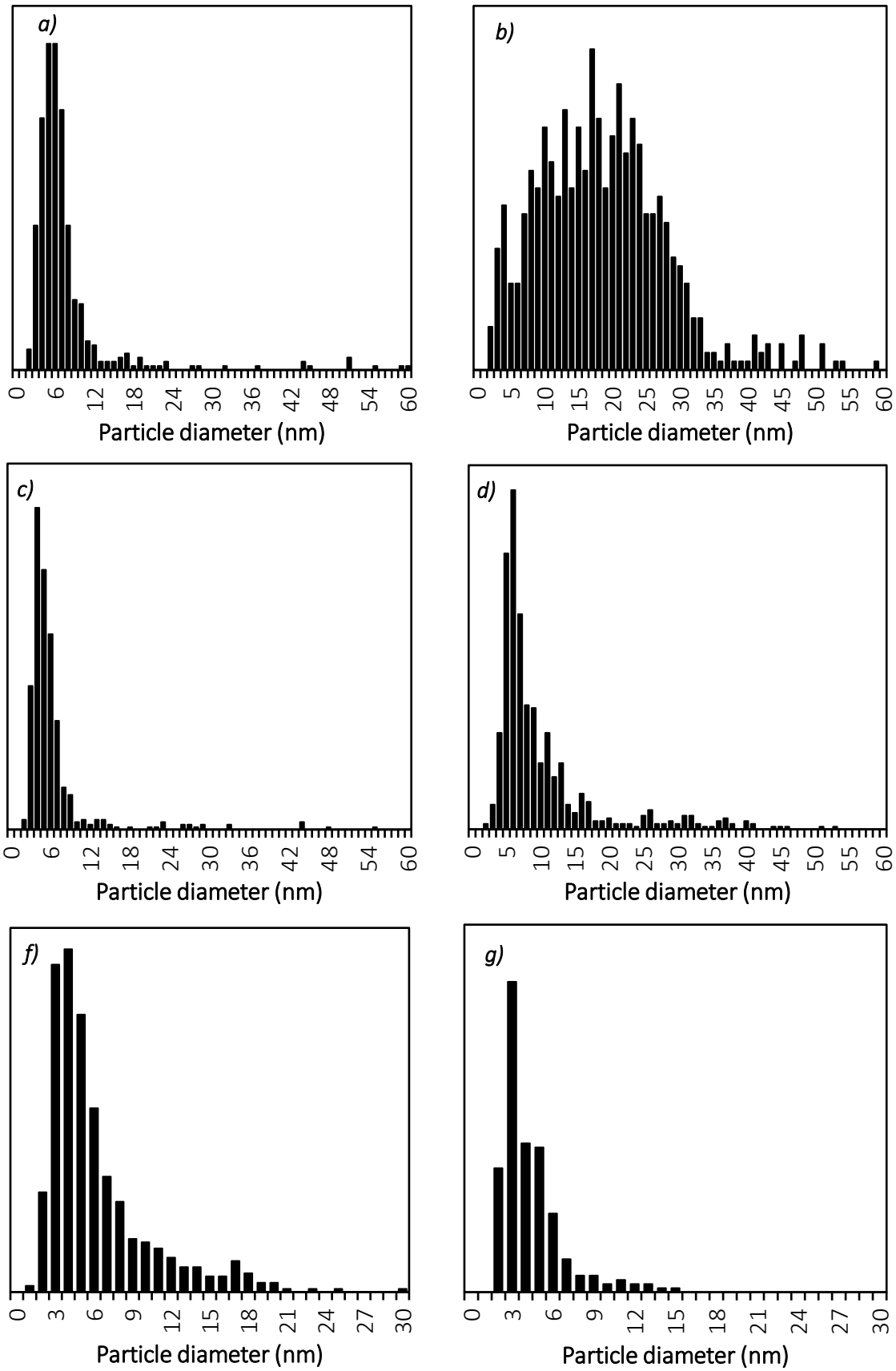

Figure A-1: Number-based particle size distribution for the synthesis variation of Method One in light conditions at a) halved surfactant concentration, b) doubled surfactant concentration, c) 40 °C, d) 90 °C, e) halved concentration reducing agent and f) dropwise reducing agent addition

The UV-Vis absorption spectra of the reaction solution for Method One (SDS, Ascorbic Acid, Water) are shown in Figure A-2. The major peak is at 285 nm, and clearly will not interfere with the spectra of the Method One syntheses variations which have peaks ranging from approximately 380 nm to 420 nm.

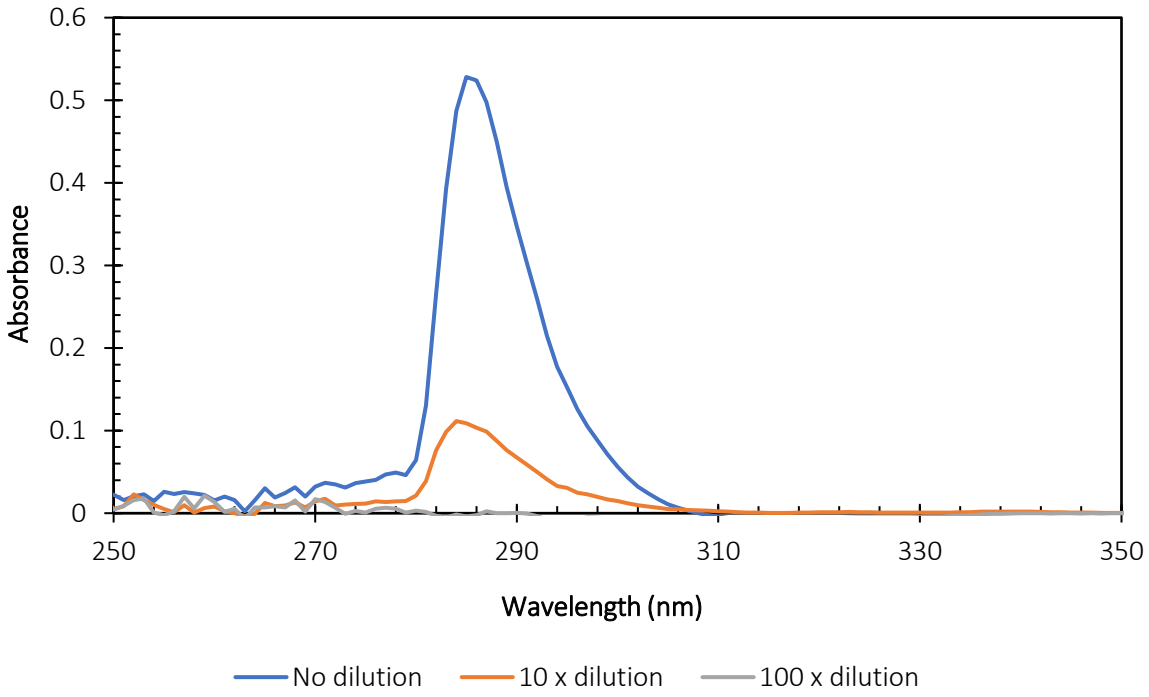

Figure A-2: Absorption spectra of the reaction solution used in Method One

Figure A-3 shows TEM micrographs of the Method One Ag dispersion prepared in dark conditions.

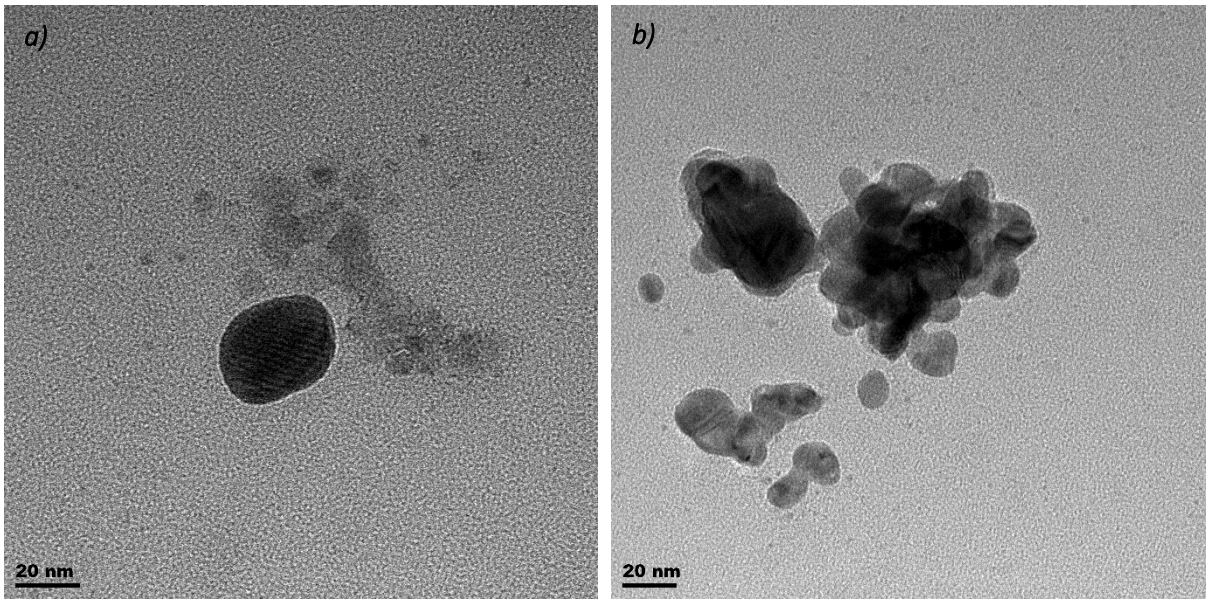

Figure A-3: TEM micrographs of Method One Ag dispersions prepared in dark conditions using synthesis variation a) doubled surfactant concentration and b) 500 rpm

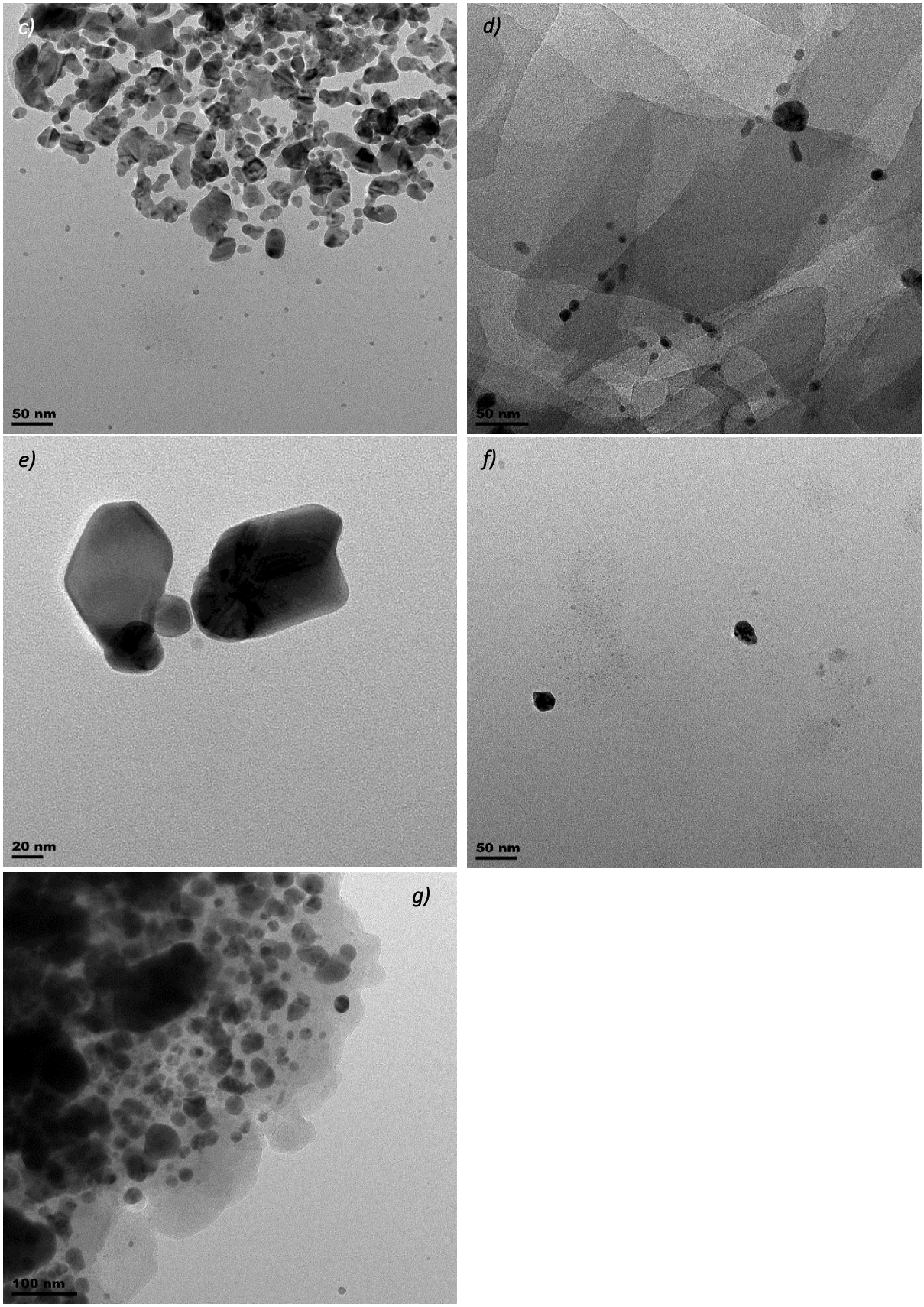

Figure A-3 cont: TEM micrographs of Method One Ag dispersions prepared in dark conditions using synthesis variation c) round flask at 500 rpm, d) 90 °C, e) 50% excess reducing agent, f) halved concentration reducing agent and g) order of addition

A.2 Method Two

A.2.1 Results of the Method Two synthesis

The complete particle size results of the syntheses variations in light conditions are presented in Figure A-3 and Figure A-4.

Table A-3: Summary of the size measurements for particles produced whilst exposed to light using Method Two

Synthesis variation	*Mean particle size (nm)*	*Median particle size (nm)*	*Maximum particle size measured (nm)*	*Number of particles counted*
Original method (no variation)	12.6 ± 8.4	11.4	90.0	551
Halved surfactant concentration	26.3 ± 16.4	28.7	73.8	574
NaOH hot injection	9.7 ± 6.6	7.8	45.9	565

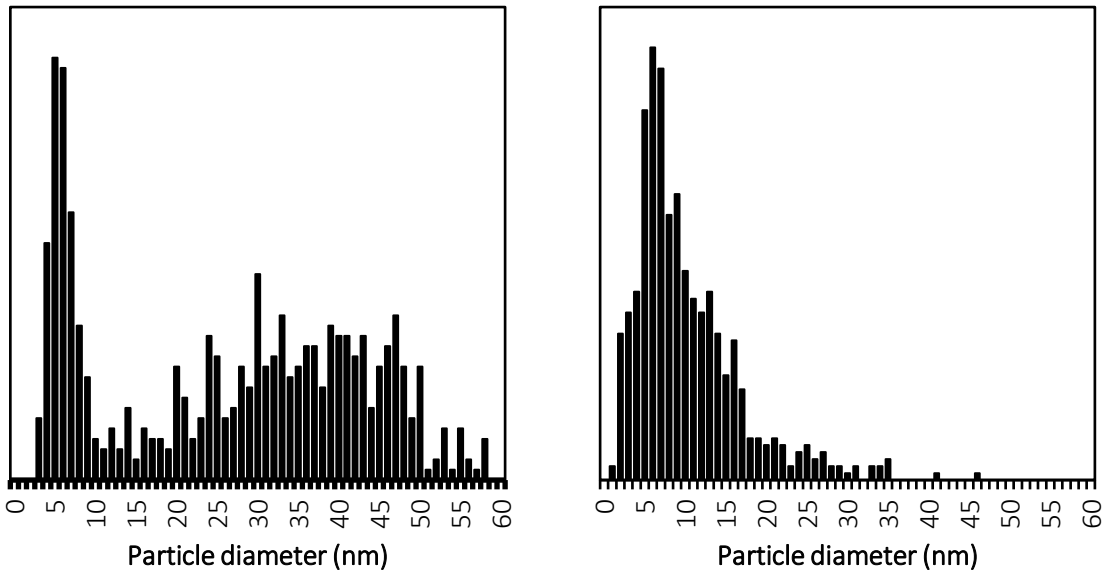

Figure A-4: Number-based particle size distribution for the synthesis variation of Method Two in light conditions at a) halved surfactant concentration and b) NaOH hot injection

The UV-Vis absorption spectra of the reaction solution for Method Two (DBSA, Aniline, NaOH, Water) are shown in Figure A-5. The major peak is at 300 nm, and clearly will not interfere with the spectra of the Method Two syntheses variations which have peaks ranging from approximately 400 nm to 430 nm.

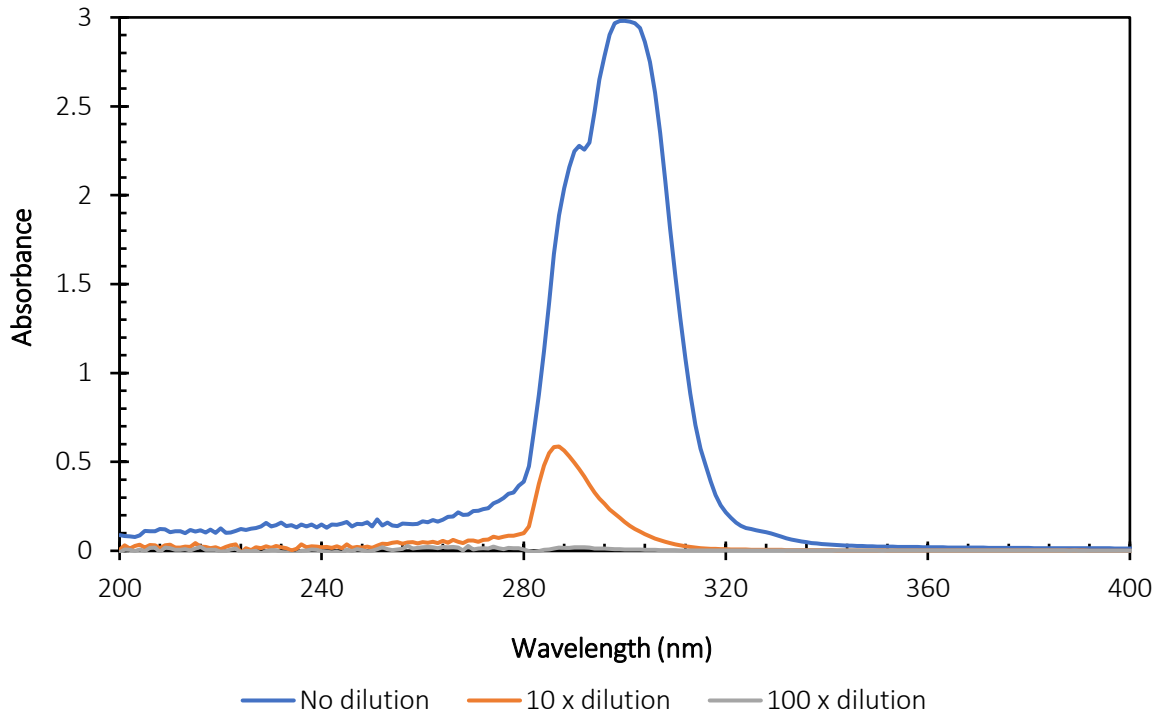

Figure A-5: Absorption spectra of the reaction solution used in Method Two

Figure A-6 shows TEM micrographs of the Method Two Ag dispersion prepared in dark conditions. In Figure A-6a, excess surfactant can be seen surrounding the darker particles. This is to be expected because of the doubled surfactant concentration used in the synthesis. Figure A-6f shows a mixture of large and small particles.

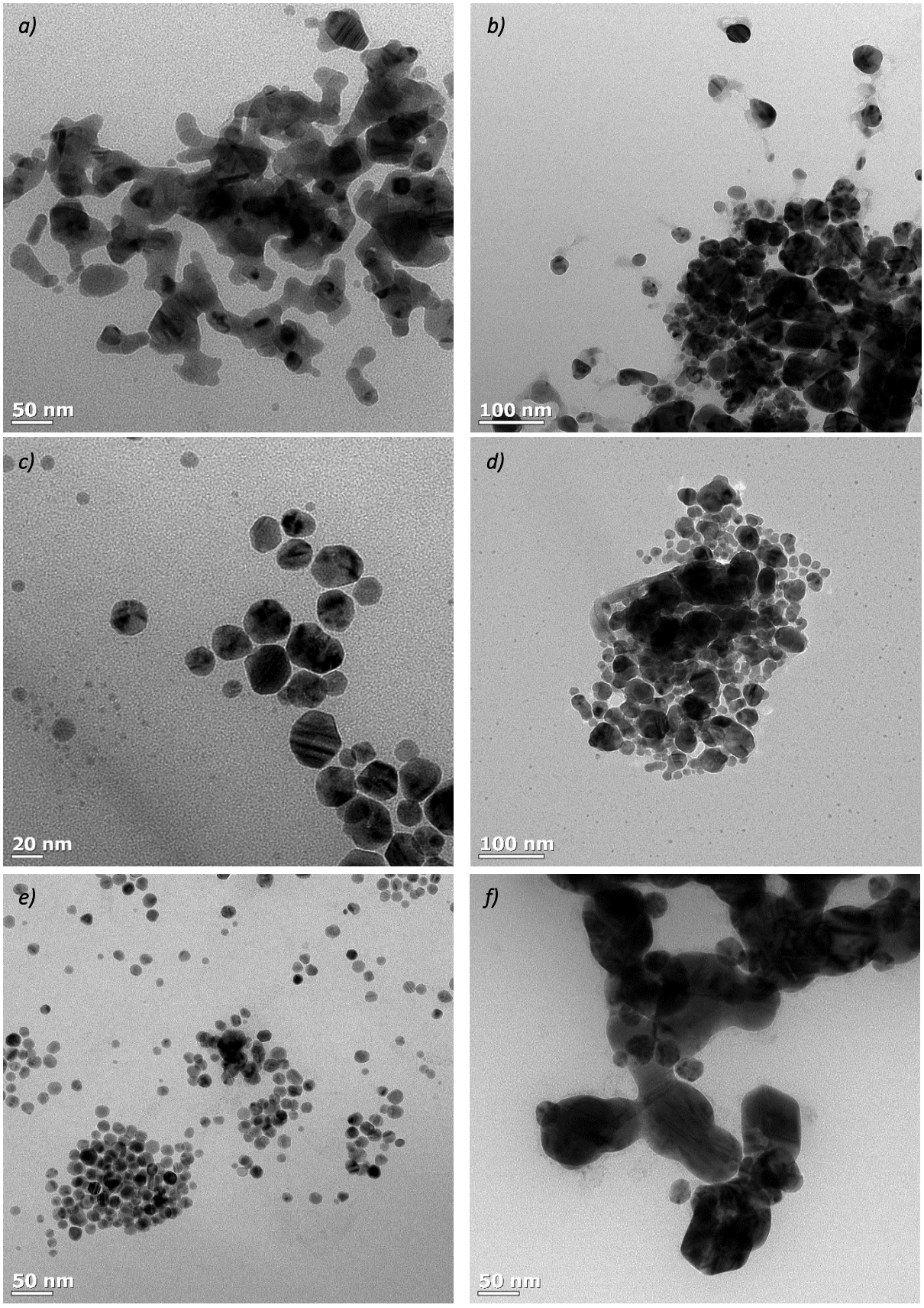

Figure A-6: TEM micrographs of Method Two Ag dispersions prepared in dark conditions using synthesis variation a) doubled surfactant concentration, b) 500 rpm, c) large flask at 1000 rpm, d) dropwise NaOH, e) halved aniline and f) changed order of addition

B. Antibacterial efficacy studies for silver

B.1 Antibacterial efficacy of silver ions

Initially, a laboratory-strain of *E. coli* (*DH5α)* was used for the antibacterial efficacy assessment due to the availability of bacterial strains within the laboratory. Experiments with three different concentrations of Ag^+, 0 µM (control), 6 µM and 12 µM, were performed in triplicate using phosphate buffered solution (PBS). The aforementioned concentrations were chosen based on experimental results presented by Lok *et al*. (2006). There are, however, three major differences between this study and that of Lok *et al*. (2006): the bacteria media, the *E. coli* type and the method of assessing antibacterial activity. In their study, the growth medium M9 was used, a wild-type *E. coli* strain K12 was assessed, and optical density was used to measure the antibacterial activity of $AgNO_3$. The choice of growth media meant that their study aimed to develop a growth inhibition curve rather than a bacteria kill-curve.

The time-kill curve developed from the counting of *E. coli* (DH5α) colonies 24 hours after being treated with Ag^+ is presented in Figure B-1. The starting colony count was approximately 10^6 cells/ml. In this experiment, there seems to be an error with the last data point in the control experiment which is most likely due to an error in diluting or plating the sample. This error does not affect the outcome of the study and is thus insignificant.

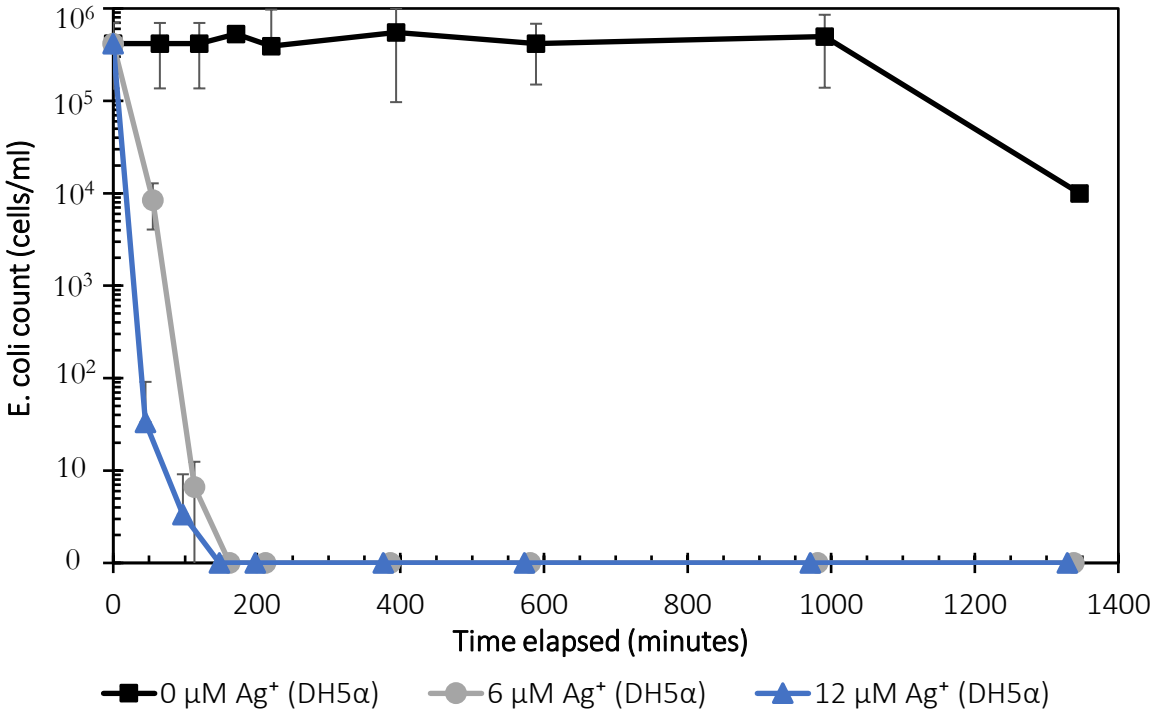

Figure B-1: Time-kill curve of E. coli (DH5α) after treatment with Ag^+

Figure B-1 shows that both concentrations of Ag^+ killed off the *E. coli* (DH5α) colonies in less than 2.5 hours, demonstrating how efficient silver ions are as an antibacterial agent. The time-kill curves for the two concentrations of Ag^+ appear very similar even though it would be expected that the higher concentration of Ag^+ would result in a more rapid bacterial death than the lower concentration. The

difference may have been more evident if shorter time intervals between sampling were used but, due to logistical constraints, 30 minutes is the shortest time interval that could be achieved. Concentrations of 12 µM Ag^+ did, however, have a slightly faster initial kill rate of bacteria, with 99.99% of bacteria killed in the first hour of contact in comparison 97.98% of the bacteria killed in the first hour at 6 µM Ag^+.

To determine the equilibrium species in PBS when $AgNO_3$ of varying concentrations is added, the component ions of PBS (as shown in Table B-1) were entered into the chemical equilibrium software application Visual MINTEQ.

Table B-1: Concentration of component ions in PBS

Component ion	*Concentration in PBS (mM)*
Cl^-	139.7
H^+	10.0
K^+	4.7
Na^+	157.0
PO_4^{3-}	12.0

The concentrations of Ag^+ and NO_3^- used in the Ag^+ antibacterial studies were 12 µM, 6 µM, 3 µM and 1.5 µM, therefore these concentrations were entered into the Visual MINTEQ program with the PBS components for the calculation of the equilibrium speciation of these component ions. The output of the program is shown in Table B-2 and the percentage of the total concentration of each ion is presented in relation to a chemical species. This allows one to see what form the Ag in solution is in.

Table B-2: The species distribution made up from component ions within a PBS/Ag^+ mixture at different Ag^+ concentrations applicablte to the $AgNO_3$ investigations performed in this study, determined using Visual MINTEQ

Component ion	*Species*	*12 µM Ag^+: % of total concentration*	*6 µM Ag^+: % of total concentration*	*3 µM Ag^+: % of total concentration*	*1.5 µM Ag^+: % of total concentration*
Cl:Ag ratio	-	11 642	23 283	46 567	93 133
Ag^+	Ag^+	0.042	0.042	0.042	0.042
	AgCl (aq)	6.383	6.393	6.393	6.393
	$AgCl_2^-$	77.376	77.411	77.411	77.411
	$AgCl_3^{2-}$	16.197	16.153	16.154	16.154
Cl^-	Cl^-	95.991	96.004	96.000	96.007
	$AgCl_2^-$	0.013	0.003	0.004	0.001
	KCl (aq)	0.118	0.118	0.118	0.118
	NaCl (aq)	3.873	3.873	3.873	3.873
K^+	K^+	94.595	94.594	94.594	94.594
	KOH	0.059	0.059	0.059	0.059
	KCl (aq)	3.497	3.498	3.498	3.498
	$KHPO_4^-$	1.562	1.562	1.562	1.562
	K_2HPO_4 (aq)	0.013	0.013	0.013	0.013
	KPO_4^{2-}	0.268	0.268	0.268	0.268
Na^+	Na^+	93.212	93.211	93.212	93.211
	$NaPO_4^{2-}$	0.264	0.264	0.264	0.264
	NaOH (aq)	0.042	0.042	0.042	0.042
	NaCl (aq)	3.446	3.447	3.446	3.447
	$NaHPO_4^-$	2.384	2.384	2.384	2.384
	Na_2HPO_4 (aq)	0.288	0.288	0.288	0.288
	NaH_2PO_4 (aq)	0.364	0.364	0.364	0.364
NO_3^-	NO_3^-	97.631	97.631	97.631	97.631
	KNO_3 (aq)	0.154	0.154	0.154	0.154
	$NaNO_3$ (aq)	2.215	2.215	2.215	2.215
PO_4^{3-}	PO_4^{3-}	4.708	4.707	4.708	4.707
	$NaPO_4^{2-}$	3.451	3.451	3.451	3.451
	HPO_4^{2-}	55.657	55.657	55.657	55.657
	$NaHPO_4^-$	31.193	31.193	31.193	31.193
	$KHPO_4^-$	0.612	0.612	0.612	0.612
	KPO_4^{2-}	0.105	0.105	0.105	0.105
	Na_2HPO_4 (aq)	1.883	1.883	1.883	1.883
	$Na_2PO_4^-$	2.379	2.379	2.379	2.379

B.2 Antibacterial efficacy of silver nanoparticle-loaded filters

Using Visual MINTEQ, the equilibrium species of PBS and the Ag^+ released from the filters were determined and are shown in Table B-3. The same components as in Table B-1 were entered into the software program, along with varying concentrations of Ag^+. These Ag^+ concentrations are estimations of what the ion concentration may be after the dissolution of nanoparticles from the filters, and therefore a wide range was considered so as to confirm that the same speciation occurs at different Ag^+ concentrations.

Table B-3: The species distribution made up from component ions within a PBS/Ag^+ mixture at different Ag^+ concentrations applicable to the silver-loaded filter investigations performed in this study, determined using Visual MINTEQ

Component ion	*Species*	*10 µM Ag^+: % of total concentration*	*1 µM Ag^+: % of total concentration*	*0.1 µM Ag^+: % of total concentration*	*0.01 µM Ag^+: % of total concentration*
Ag^+	Ag^+	0.042	0.042	0.042	0.042
	AgCl (aq)	6.383	6.382	6.382	6.382
	$AgCl_2^-$	77.375	77.374	77.374	77.374
	$AgCl_3^{2-}$	16.198	16.200	16.200	16.200
Cl^-	Cl^-	95.994	96.007	96.009	96.009
	$AgCl_2^-$	0.011	0.002	0.000	0.000
	KCl (aq)	0.118	0.118	0.118	0.118
	NaCl (aq)	3.873	3.873	3.874	3.874
K^+	K^+	94.595	94.594	94.594	94.594
	KOH	0.059	0.059	0.059	0.059
	KCl (aq)	3.497	3.498	3.498	3.498
	$KHPO_4^-$	1.562	1.562	1.562	1.562
	K_2HPO_4 (aq)	0.013	0.013	0.013	0.013
	KPO_4^{2-}	0.268	0.268	0.268	0.268
Na^+	Na^+	93.212	93.211	93.211	93.211
	$NaPO_4^{2-}$	0.264	0.264	0.264	0.264
	NaOH (aq)	0.042	0.042	0.042	0.042
	NaCl (aq)	3.446	3.447	3.447	3.447
	$NaHPO_4^-$	2.384	2.384	2.384	2.384
	Na_2HPO_4 (aq)	0.288	0.288	0.288	0.288
	$Na_2PO_4^-$	0.364	0.364	0.364	0.364
PO_4^{3-}	PO_4^{3-}	4.707	4.707	4.707	4.707
	$NaPO_4^{2-}$	3.451	3.451	3.451	3.451
	HPO_4^{2-}	55.657	55.657	55.657	55.657
	$NaHPO_4^-$	31.193	31.193	31.193	31.193
	$KHPO_4^-$	0.612	0.612	0.612	0.612
	KPO_4^{2-}	0.105	0.105	0.105	0.105
	Na_2HPO_4 (aq)	1.883	1.883	1.883	1.883
	$Na_2PO_4^-$	2.379	2.379	2.379	2.379

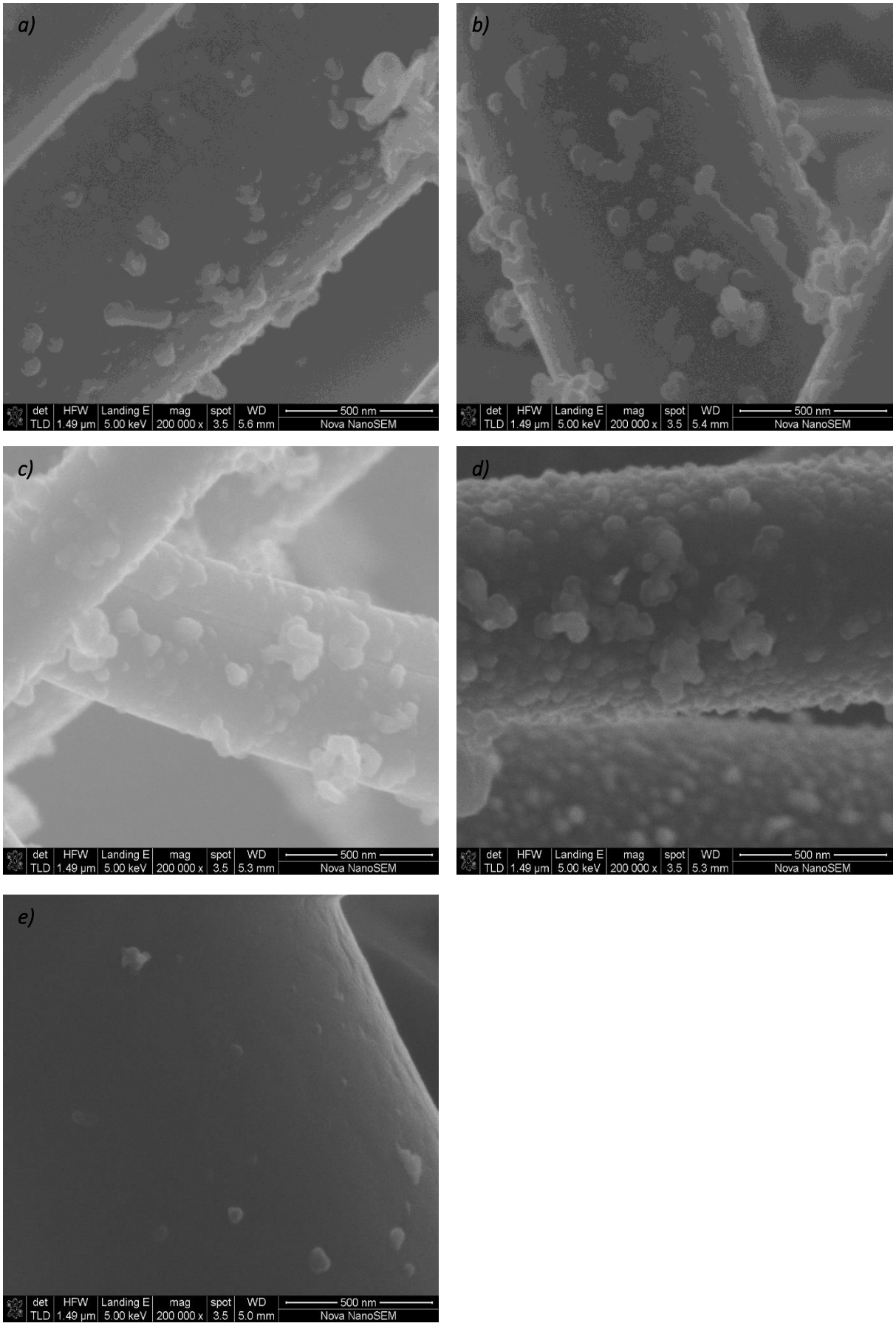

Figure B-2: SEM micrographs the silver-loaded quartz fibre filters of a) A1, b) A3, c) A4, d) B3 and e) S6

C. Thermodynamic estimations of silver ion equilibrium concentration

The surface statistics formulae that can be used for the estimation of the surface energy of icosahedral and cuboctahedral silver nanoparticles are presented. Benfield (1992) sought to calculate the mean coordination number of icosahedral and cuboctahedral clusters as a function of the cluster edge length *m* i.e. the number of atoms along each edge of the crystal. This allows for the determination of the discrete total number of atoms in a cluster at a particular diameter, which, in turn, allows for the approximation of the surface energy of the particle. Presented in the tables below are the formulae provided by Benfield (1992) for cuboctahedra and icosahedra.

Table C-1: Surface statistics for icosahedral-shaped nanoparticles

	Icosahedra
Total number of atoms	$\frac{1}{2}(2m-1)(5m^2-5m+3)$
Number of surface atoms	$10m^2-20m+12$
Bulk atoms (coordination number: 12)	$\frac{1}{3}(2m-3)(5m^2-15m+13)$
Vertex atoms (coordination number: 6)	12
Edge atoms (coordination number: 8)	$30(m-2)$
Face atoms (coordination number: 9)	$10(m-2)(m-3)$

Table C-2: Surface statistics for cuboctahedral-shaped nanoparticles

	Cuboctahedra
Total number of atoms	$\frac{1}{2}(2m-1)(5m^2-5m+3)$
Number of surface atoms	$10m^2-20m+12$
Bulk atoms (coordination number: 12)	$\frac{1}{3}(2m-3)(5m^2-15m+13)$
Vertex atoms (coordination number: 5)	12
Edge atoms (coordination number: 7)	$24(m-2)$
Square face atoms (coordination number: 8)	$6(m-2)^2$
Triangle face atoms (coordination number: 9)	$4(m-2)(m-3)$